THESIS REPORT

Ph.D.

Institute for Systems Research

Kinematic Synthesis and Analysis of a Novel Class of Six-DOF Parallel Minimanipulators

by F. Tahmasebi
Advisor: L-W. Tsai

The Institute for Systems Research is supported by the National Science Foundation Engineering Research Center Program (NSFD CD 8803012), Industry and the University

Ph.D. 93-1

Abstract

Title of Dissertation: Kinematic Synthesis and Analysis of a Novel Class of Six-DOF Parallel Minimanipulators

Farhad Tahmasebi, Doctor of Philosophy, 1992

Dissertation directed by: Professor Lung-Wen Tsai
Department of Mechanical Engineering
and
Institute for Systems Research

A new class of six-degree-of-freedom (six-DOF) parallel minimanipulators is introduced. The minimanipulators are designed to provide high resolution and high stiffness in fine-manipulation operations. Two-DOF planar mechanisms (e.g., five-bar linkages, pantographs) and inextensible limbs are used to improve positional resolution and stiffness of the minimanipulators. The two-DOF mechanisms serve as drivers for the minimanipulators. The minimanipulators require only three inextensible limbs and unlike most of the six-limbed parallel manipulators, their direct kinematics can be reduced to solving a polynomial in a single variable. All of the minimanipulator actuators are base-mounted. As a result, higher payload capacity, smaller actuator sizes, and lower power dissipation can be obtained.

Inverse kinematics of the minimanipulators has been reduced to solving three decoupled quadratic equations, each of which contains only one unknown.

Kinematic inversion is used to reduce the direct kinematics of the minimanipulator to an eighth-degree polynomial in the square of a single variable. Hence, the maximum number of assembly configurations for the minimanipulator is sixteen. It is proved that the sixteen solutions are eight pairs of reflected configurations with respect to the plane passing through the lower ends of the three limbs.

The Jacobian and stiffness matrices of two types of minimanipulators are derived. It is shown that, at a central configuration, the stiffness matrix of the first type minimanipulator (driven by bidirectional linear stepper motors) can be decoupled, if proper design parameters are chosen. It is also shown that the stiffness of the minimanipulators is higher than that of the Stewart platform. Guidelines for obtaining large stiffness values and for designing the drivers of the second type minimanipulator (simplified five-bar linkages) are established.

An algorithm is developed to determine the workspace of the minimanipulators. Given any orientation for the output link, three-dimensional representation of the workspace is obtained. Guidelines for avoiding discontinuities inside of the workspace are established.

Necessary and sufficient conditions for both inverse and direct kinematics singularities of the minimanipulators are obtained. Guidelines for avoiding direct kinematics singularities, which occur within the minimanipulator workspace, are established.

Kinematic Synthesis and Analysis of a Novel Class of Six-DOF Parallel Minimanipulators

by

Farhad Tahmasebi

Dissertation submitted to the Faculty of the Graduate School
of The University of Maryland in partial fulfillment
of the requirements for the degree of
Doctor of Philosophy
1992

Advisory Committee:

Professor Lung-Wen Tsai, Chairman/Advisor
Professor Bruce Berger
Professor P.S. Krishnaprasad
Associate Professor Shapour Azarm
Assistant Professor Uri Tasch

Dedication

To my parents

Acknowledgements

I was lucky to have Dr. Lung-Wen Tsai as my Ph.D. advisor. He is one of the most creative and smartest people that I have ever met. I have learned so much from him. Whenever I was on a wrong track, he helped me find the right approach with his insightful comments. I sincerely thank him for his guidance, encouragement, patience, support, and friendship over the past six years.

Next, I would like to gratefully acknowledge the support of my employer, NASA/Goddard Space Flight Center (GSFC). Without two years of full-time Ph.D. fellowship from NASA/GSFC, completing this study would have been much more difficult. Although, in return, I have to work for NASA during the next six years, I consider myself fortunate to have won the Ph.D. fellowship.

Special thanks to Drs. Bruce Berger, P.S. Krishnaprasad, Shapour Azarm, and Uri Tasch for agreeing to be on my advisory committee, reading this dissertation, and providing helpful comments.

Contents

List of Tables

List of Figures

Nomenclature

a input link length of a simplified five-bar driver

b output link length of a simplified five-bar driver

d circumradius of equilateral triangle $D_1D_2D_3$

e side length of equilateral triangle $D_1D_2D_3$

$f_{i,x}$ X component of actuator force applied at the lower end of the ith limb

$f_{i,y}$ Y component of actuator force applied at the lower end of the ith limb

$\overline{f}$ vector of actuator force components applied at the lower ends of the limbs

i cyclic index (1,2,3)

$\ddot{\imath}$ $\sqrt{-1}$

k constant Z coordinate of point R_i

$\mathbf{k}$ actuator stiffness matrix for the Type 1 minimanipulator (diagonal)

$\widehat{\mathbf{k}}$ actuator stiffness matrix for the Type 2 minimanipulator (diagonal)

l_{i+2} length of vector $\overline{R_iR_{i+1}}$

$\bar{n}_{r,i}$ unit vector in the radial direction at point C_i

$\bar{n}_{t,i}$ unit vector in the tangential direction at point C_i

$\bar{n}_u$ unit vector parallel to the positive U axis

$\bar{n}_v$ unit vector parallel to the positive V axis

$\bar{n}_w$ unit vector parallel to the positive W axis

$\bar{n}_x$ unit vector parallel to the positive X axis

$\bar{n}_y$ unit vector parallel to the positive Y axis

$\bar{n}_z$ unit vector parallel to the positive Z axis

p circumradius of equilateral triangle $P_1P_2P_3$

q	side length of equilateral triangle $P_1P_2P_3$
$\dot{\bar{q}}$	vector of velocity components at the lower ends of the limbs
r	length of each inextensible limb
$\dot{\bar{x}}$	generalized velocity vector of the platform
$\dot{\tilde{x}}$	dimensionally-uniform generalized velocity vector of the platform
$\mathbf{A}$	homogeneous transformation matrix from the moving (UVW) reference frame to the fixed (XYZ) reference frame
A_i	location of the first elbow joint in the ith simplified five-bar linkage
B_i	location of the second elbow joint in the ith simplified five-bar linkage
C_i	output point of the ith simplified five-bar linkage
D_i	actuator location for the ith simplified five-bar linkage
$\mathbf{E}$	orthogonal eigenvector matrix for $\widetilde{\mathbf{K}}$
$\overline{\mathcal{F}}$	vector of generalized force applied to the platform
$\tilde{\mathcal{F}}$	dimensionally-uniform vector of generalized force applied to the platform
$\overline{F}_P$	force applied to the platform
G	centroid of equilateral triangle $P_1P_2P_3$ (origin of the moving reference frame, UVW)
$\mathbf{J}$	Jacobian matrix for the Type 1 minimanipulator
$\tilde{\mathbf{J}}$	dimensionally-uniform Jacobian matrix for the Type 1 minimanipulator
$\mathbf{J}^*$	a matrix related to $\mathbf{J}$ ($\lvert\mathbf{J}^*\rvert = \lvert\mathbf{J}\rvert$)
$\hat{\mathbf{J}}$	Jacobian matrix for the Type 2 minimanipulator
$\grave{\mathbf{J}}$	dimensionally-uniform Jacobian matrix for the Type 2 minimanipulator
$\mathbf{J_d}$	Jacobian matrix for the drivers of the Type 2 minimanipulator

$\mathbf{J_d}^{(i)}$	Jacobian matrix for the ith driver of the Type 2 minimanipulator
$\bar{J}_j$	jth column of $\mathbf{J}$ ($j = 1, 2, \ldots, 6$)
$\bar{J}_j^*$	jth column of $\mathbf{J}^*$ ($j = 1, 2, \ldots, 6$)
$\mathbf{K}$	stiffness matrix for the Type 1 minimanipulator
$\widetilde{\mathbf{K}}$	dimensionally-uniform stiffness matrix for the Type 1 minimanipulator
$\mathbf{K}^+$	central stiffness matrix for the Type 1 minimanipulator
$\mathbf{K}^*$	decoupled central stiffness matrix for the Type 1 minimanipulator
$\widetilde{\mathbf{K}}^*$	dimensionally-uniform decoupled central stiffness matrix for the Type 1 minimanipulator
$\widehat{\mathbf{K}}$	stiffness matrix for the Type 2 minimanipulator
$\grave{\mathbf{K}}$	dimensionally-uniform stiffness matrix for the Type 2 minimanipulator
$\check{\mathbf{K}}$	$\mathbf{K}/\kappa$
$\mathbf{K}^\#$	decoupled central stiffness matrix for the Stewart platform
$\widetilde{\mathbf{K}}^\#$	dimensionally-uniform decoupled central stiffness matrix for the Stewart platform
L	a parameter used in weighting matrices with dimension of length
$\overline{M}_P$	moment applied to the platform
O	centroid of equilateral triangle $D_1D_2D_3$ (origin of the moving reference frame, XYZ)
P_i	upper end of the ith limb
R_i	lower end of the ith limb
$R_{i,c}$	central position of point R_i's operating area
$U_{P,i}$	U coordinate of point P_i

$U_{R,i}$	U coordinate of point R_i
$V_{P,i}$	V coordinate of point P_i
$V_{R,i}$	V coordinate of point R_i
${}^B\overline{V}^{C_i}$	velocity of point C_i in the base reference frame
${}^BV_r^{C_i}$	radial component of ${}^B\overline{V}^{C_i}$
${}^BV_t^{C_i}$	tangential component of ${}^B\overline{V}^{C_i}$
${}^BV_x^{C_i}$	X component of ${}^B\overline{V}^{C_i}$
${}^BV_y^{C_i}$	Y component of ${}^B\overline{V}^{C_i}$
${}^B\overline{V}^{G}$	velocity of point G in the base reference frame
${}^B\overline{V}^{R_i}$	velocity of point R_i in the base reference frame
${}^BV_x^{R_i}$	X component of ${}^B\overline{V}^{R_i}$
${}^BV_y^{R_i}$	Y component of ${}^B\overline{V}^{R_i}$
$W_{R,i}$	W coordinate of point R_i
$\mathbf{W_f}$	$diag(1,\ 1,\ 1,\ L^{-1},\ L^{-1},\ L^{-1})$
$\mathbf{W_v}$	$diag(1,\ 1,\ 1,\ L,\ L,\ L)$
$X_{C,i}$	X coordinate of point C_i
$X_{D,i}$	X coordinate of point D_i
X_G	X coordinate of point G
$X_{P,i}$	X coordinate of point P_i
$X_{R,i}$	X coordinate of point R_i
$Y_{C,i}$	Y coordinate of point C_i
$Y_{D,i}$	Y coordinate of point D_i
Y_G	Y coordinate of point G

$Y_{P,i}$	Y coordinate of point P_i
$Y_{R,i}$	Y coordinate of point R_i
Z_G	Z coordinate of point G
$Z_{P,i}$	Z coordinate of point P_i
$Z_{R,i}$	Z coordinate of point R_i
α_i	$\pi/2 + (i-1)2\pi/3$
β_i	$\pi/2 + (i-1)2\pi/3$
γ_i	angle from the positive X axis to vector $\overline{A_iB_i}$ measured about the positive Z axis
δ_i	angle from vector $\overline{A_iB_i}$ to vector $\overline{A_iC_i}$ measured about the positive Z axis
$\overline{\delta q}$	vector of infinitesimal displacements at the lower ends of the limbs
$\overline{\delta x}$	vector of infinitesimal platform displacement
$\widetilde{\delta x}$	dimensionally-uniform vector of infinitesimal platform displacement
$\overline{\delta \theta}$	vector of infinitesimal displacements of the actuated joints for the Type 2 minimanipulator
ζ	Z_G at the central configuration
η_i	angle between the ith limb and the platform
θ_i	first input angle for the ith simplified five-bar driver
θ_x	yaw of the platform
θ_y	pitch of the platform
θ_z	roll of the platform
$\dot{\overline{\theta}}$	vector of input joint rates for the Type 2 minimanipulator

ϑ_i	angle of line C_iD_i with line C_iA_i or line C_iB_i
κ	diagonal elements of $\mathbf{k}$
λ	a generic symbol for any of the eigenvalues of $\mathbf{K}$
λ_j	jth eigenvalue of $\widetilde{\mathbf{K}}$ $(j = 1, 2, \ldots, 6)$
$\overline{\mu_i}$	$\overline{\Gamma}_i \times \overline{P_iR_i}$
$\mu_{i,x}$	X component of $\overline{\mu_i}$
$\mu_{i,y}$	Y component of $\overline{\mu_i}$
$\mu_{i,z}$	Z component of $\overline{\mu_i}$
$\mu'_{i,x}$	$\mu_{i,x}/\mu_{i,z}$
$\mu'_{i,y}$	$\mu_{i,y}/\mu_{i,z}$
ν	length of vector $\overline{OR_i}$ at the central configuration
ξ_i	angle of line D_iC_i with line D_iA_i or line D_iB_i
ϖ	angle between any limb and the base plane at the central configuration corresponding to $p = \nu/2$
$\overline{\tau}$	vector of input actuator torques (Type 2 minimanipulator)
ϕ_i	second input angle for the ith simplified five-bar driver
ψ_i	angle from the positive X axis to vector $\overline{D_iC_i}$ measured about the positive Z axis
${}^B\overline{\omega}^{L_i}$	angular velocity of the ith limb with respect to the base reference frame
${}^P\overline{\omega}^{L_i}$	angular velocity of the ith limb with respect to the platform reference frame
${}^B\overline{\omega}^{P}$	angular velocity of the platform with respect to the base reference frame

$\overline{\Gamma}_i$ a vector which is collinear with the axis of the topmost revolute joint at point P_i and points in the direction of vector $\overline{P_{i+2}P_{i+1}}$

$\mathbf{\Delta}^{(i)}$ a 2×2 diagonal matrix (see section 5.3)

$\mathbf{\Lambda}$ diagonal eigenvector matrix for $\widetilde{\mathbf{K}}$

Λ_i intersection of the base plane with the Π_i plane

Π_i the plane passing through P_i and perpendicular to vector $\overline{\Gamma_i}$

$\mathbf{\Omega}$ a 3×3 matrix (see section 8.4.1)

Chapter 1

Introduction

1.1 Background

A typical serial manipulator forms an open-loop kinematic chain. Links are joined together serially and the terminal (output) link is connected to only one other link. In contrast, a parallel manipulator is a closed-loop kinematic chain. Every link is connected to at least two other links. In fact, a typical parallel manipulator, with three or more DOF, forms a complex kinematic chain in which its output link is connected to at least three other links (Gosselin and Angeles, 1990).

In general, a serial manipulator provides larger workspace and higher dexterity than a parallel one. However, serial manipulators suffer from low rigidity, due to their cantilever-like structures. In addition, large positioning errors occur at the output link of a serial manipulator because actuator errors accumulate throughout such a mechanism. Furthermore, load-to-weight ratio in a serial manipulator is low because loads are not uniformly distributed between the actuators.

Some researchers have tried to improve the performance of serial manipulators by introducing better control systems for them. Others have tried to accomplish the same by introducing better components (e.g., actuators and sensors) for them. These efforts will not be discussed here.

Another group of researchers have considered parallel manipulators in place of serial ones for applications in which the requirements for accuracy, rigidity, load-to-weight ratio, and load distribution are more important than the need for a large workspace. Another reason for the researchers' interest in parallel manipulators is the following. Unlike a serial manipulator, a parallel one can be designed such that its actuators are mounted on its base (ground link) without using any power transmission devices such as gears and belts. Such devices introduce backlash and friction problems. Note that mounting the actuators on the base results in many benefits such as higher payload capacity, smaller actuator sizes, and lower power dissipation.

The famous Stewart platform (Stewart, 1965) is probably the first six-DOF parallel mechanism which has been studied in the literature. It consists of a moving platform and a base which are connected by means of six independent limbs. At the time of its invention, the Stewart platform was designed as a flight simulator. Hunt (1983) suggested the Stewart platform and other parallel mechanisms as robot manipulators. Other researchers have also studied the Stewart platform as a manipulator (e.g., Fichter and MacDowell, 1980; Yang and Lee, 1984; Premack et al., 1984; Fichter, 1986; Nguyen and Pooran, 1989). Other types of six-DOF parallel manipulators have also been introduced and studied in the literature (e.g., Kohli et al., 1988; Hudgens and Tesar, 1988; Tsai and Tahmasebi, 1991, 1992; Tahmasebi and Tsai, 1992a, 1992b). Hybrid serial-parallel manipulator systems have also been considered for tasks which require both accuracy and large workspace (e.g., Waldron et. al, 1989).

Waldron and Hunt (1987) demonstrated that kinematic behavior of parallel mechanisms has many inverse characteristics to that of serial mechanisms. For example, direct kinematics of a parallel manipulator is much more difficult than its inverse kinematics; whereas, for a serial manipulator, the opposite is true.

1.2 Outline

The objective of this research is to design six-DOF parallel minimanipulators which are capable of providing high resolution and stiffness as well as simpler kinematic characteristics than the existing technology. The term minimanipulator is used because these mechanisms are not designed to provide large platform (output link) displacements. We will concentrate on kinematic issues and will not discuss dynamics of the minimanipulators. The organization of the dissertation is as follows:

In Chapter 2, conceptual design of the minimanipulators is discussed. Topological synthesis methods are used in the design process. Inextensible limbs and two-DOF drivers (e.g., five-bar linkages and pantographs) are used for obtaining high resolution and stiffness. To minimize the number of loops in the structure of a minimanipulator, only three limbs are considered in its design. As a result, the direct kinematics, which is one of the most challenging problems associated with six-DOF parallel manipulators, is simplified. The minimanipulators are designed such that all of the actuators are base-mounted. Therefore, higher payload capacity, smaller actuator sizes, and lower power dissipation can be obtained.

In Chapter 3, inverse kinematics of the minimanipulators is discussed. It is shown that the problem can be reduced to solving three independent quadratic equations, each of which contains only one unknown. A numerical example is also presented.

In Chapter 4, closed-form solution for the direct kinematic problem of the minimanipulators is obtained. Kinematic inversion is used to reduce the problem to solving an eighth-degree polynomial in the square of a variable. Hence, the maximum number of solutions for the direct kinematics problem of a minimanipulator is sixteen. Also, a numerical example is presented and the answers are verified by performing an inverse kinematic analysis using the results obtained in Chapter 3.

In Chapter 5, instantaneous kinematics of the minimanipulators is studied and the expressions for their Jacobian matrices are derived. Results of Chapter 5 are used in Chapter 6 to obtain the stiffness matrices of the minimanipulators. Methods for decoupling the stiffness matrices of some of the minimanipulators, and for increasing stiffness values in different directions[1] are developed. Furthermore, the stiffness of the minimanipulators is compared to that of the Stewart platform.

In Chapter 7, an algorithm is developed to determine the workspace of the minimanipulators. For any given orientation of the platform, three-dimensional representation of the workspace is obtained. Results of Chapter 6 are used to determine minimanipulator dimensions (e.g., limb length and platform size) for the workspace examples. To get an idea about the dexterity of the minimanipulators, different platform roll, pitch, and yaw values are considered in the examples.

In Chapter 8, both inverse kinematics singularities and direct kinematics singularities of the minimanipulators are studied. Necessary and sufficient conditions for both kinds of singularities are obtained. More attention is paid to the direct kinematics singularities, which are much more significant and challenging than the inverse kinematics singularities. Some of the direct kinematics singularity conditions are discussed in detail.

In Chapter 9, results of Chapters 5, 6, 7, and 8 are used to establish design guidelines for dimensional synthesis of the minimanipulators.

Finally, in Chapter 10, summary of the whole dissertation and suggestions

[1]By stiffness we are referring to the relationship between the generalized force applied to the platform and its resulting displacement due to the compliance of the actuators. This is a common definition in the context of robotics (e.g., Asada and Slotine, 1986). We are not referring to structural stiffness.

for future research are presented.

1.3 Contributions

The major contributions of this research can be summarized as follows:

1. Creation of a new class of high-resolution and high-stiffness parallel minimanipulators for high precision operations.

2. Development of inverse kinematics solution for the minimanipulators.

3. Derivation of closed-form direct kinematics solution for the minimanipulators.

4. Derivation of the Jacobian and stiffness matrices for the minimanipulators.

5. Development of an algorithm for determination of the minimanipulators' workspace.

6. Determination of conditions for inverse kinematics singularities as well as direct kinematics singularities.

7. Development of design guidelines for

    - decoupling of the stiffness matrix
    - increasing stiffness values in different directions
    - avoiding discontinuities inside of the workspace
    - avoiding direct kinematics singularities

Chapter 2

Description of the Minimanipulators

2.1 Introduction

A hybrid serial-parallel manipulator system can be an ideal tool for tasks which require both accuracy and large workspace. In such a system, the serial manipulator provides the gross motion. The parallel manipulator, which is mounted between the wrist and the end-effector, can be used for error compensation as well as delicate position and force control. Waldron et. al (1989) studied a hybrid serial-parallel manipulator which includes a three-DOF parallel micro-manipulator. Nguyen and Pooran (1989) suggested the Stewart platform as the parallel portion of a serial-parallel telerobot system. Hudgens and Tesar (1988) introduced a new six-DOF parallel micromanipulator suitable for serial-parallel systems. Their mechanism consists of six inextensible limbs. Spherical joints are used to connect the upper end of each limb to the platform and the lower end of each to an output link of a planar four-bar linkage. The platform motion is obtained by driving the input links of the four-bar linkages, which are used to increase the mechanical advantage and to improve positional resolution of the mechanism. They also presented the inverse kinematics solution and a dynamic model for their system.

In a manipulator with base-mounted actuators, weight of an actuator is not a load for the other actuators. As a result, higher payload capacity, smaller actuator sizes, and lower power dissipation can be achieved (Asada and Youcef-Toumi, 1984; Kohli et al., 1988). In a serial manipulator, mounting the actuators on the base, necessitates the use of power transmission devices such as belts and gear trains. However, due to friction and backlash, power transmission devices introduce flexibility and accuracy problems. On the other hand, in parallel manipulators, it is possible to mount the actuators on the base without using power transmission devices. Asada and Youcef-Toumi (1984) studied a two-DOF parallel manipulator with base-mounted actuators. Hunt (1983) introduced a three-DOF planar parallel manipulator with base-mounted actuators. Kohli et al. (1988) studied six-DOF parallel manipulators which are driven by base-mounted Rotary-Linear actuators. In these six-DOF manipulators, each limb is made up of two links which are connected together by either a revolute or a prismatic joint. Such parallel manipulators are suitable for tasks which require relatively large platform displacements (e.g., motion simulation).

In this work, we introduce a new class of six-DOF parallel minimanipulators which are intended for fine position and force control in hybrid serial-parallel systems, or as stand-alone mechanisms.[1] All of the minimanipulator actuators

[1] A patent application has been filed for the minimanipulators.

are base-mounted. Two-DOF planar linkages as well as inextensible limbs are used to improve the positional resolution and stiffness of the minimanipulators. Unlike the micromanipulator introduced by Hudgens and Tesar (1988), a minimanipulator requires only three limbs. As a result, its direct kinematics can be reduced to solving a polynomial in a single variable (closed-form solution). As mentioned by Griffis and Duffy (1989), a closed-form direct kinematics solution provides much more information on kinematic behavior of a parallel mechanism than an iterative solution. For example, it can predict the exact number of platform configurations, and avoid problems near singularities, which can be experienced by purely numerical solutions. In addition, by using three limbs instead of six, other benefits such as lower possibility of mechanical interference between the limbs and fewer number of parts can be realized.

2.2 Conceptual Design

Many of the six-DOF parallel mechanisms described in the literature contain six limbs. Reducing the number of limbs in a parallel mechanism lowers the number of loops in its structure. As a result, direct kinematics of the mechanism is simplified whereas its inverse kinematics becomes more challenging. Since direct kinematics of a parallel manipulator is much more difficult than its inverse kinematics, the minimanipulators are designed to contain minimum number of limbs. Minimizing the number of limbs results in several additional benefits such as fewer number of links and joints, lower minimanipulator weight, and higher dexterity. Three non-collinear points on a platform of a six-DOF parallel manipulator completely define its location (position and orientation) in space. Therefore, each minimanipulator contains three limbs which connect three non-collinear points on its platform to its base.

For the reasons mentioned earlier, the minimanipulators are designed to have base-mounted actuators and inextensible limbs. In addition, they are symmetric[2]. The latter property is needed for even load distribution. The Lower end of each limb is connected to a two-DOF driver (e.g., a pantograph or a five-bar linkage) which is constrained to move on the base plate. The desired minimanipulator motion is obtained by moving the lower ends of its three limbs on the base plane. Each limb of a symmetric six-DOF parallel manipulator must have six degrees of freedom in its joints (see Appendix A for the proof). Therefore, in addition to the two degrees of freedom provided by a driver, each limb should contain four more degrees of freedom in its joints. To keep the limbs inextensible, joints are placed only at their lower and upper ends. A three-DOF spherical joint at one end and a revolute joint at the other end can be used. However, due to difficulties in their fabrication, spherical joints are not very precise. Hence, they are not used in synthesis of the minimanipulators. Instead, a two-DOF universal joint is placed at each end of a limb, as shown in Figure 2.1. Note that one of the axes of the upper universal joint is collinear with the limb, while the other axis of the upper universal joint as well as one of the axes of the lower universal joint are always perpendicular to the limb. This arrangement is kinematically equivalent to a limb with a spherical joint at its lower end and a revolute joint at

[2]A symmetric parallel manipulator is defined here as having identical joints and links in each limb connecting its base to its platform.

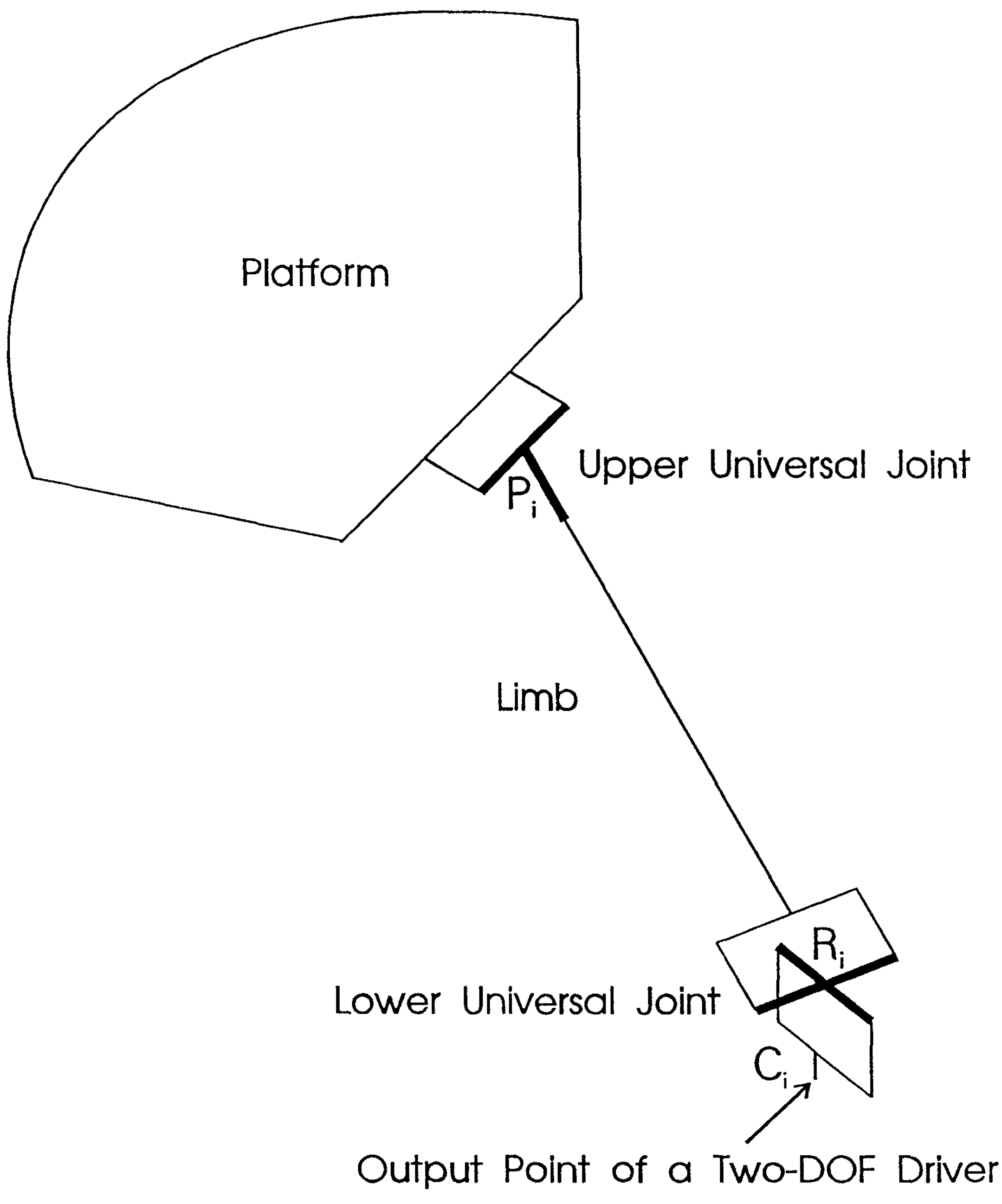

Figure 2.1: Representation of a limb.

its upper end, as shown in Figure 2.2. By using the limb configuration shown in Figure 2.1, kinematics of a minimanipulator is made independent of the output link orientations of its two-DOF drivers. Due to simplicity of its representation, the equivalent limb configuration shown in Figure 2.2 is used in the analysis portion of this work. A representation of a complete minimanipulator is shown in Figure 2.3. Points R_1, R_2, and R_3 are connected to two-DOF drivers and can be moved on the base plate. Points P_1, P_2, and P_3 are on the platform. To keep the minimanipulator geometrically symmetric, axes of the topmost revolute joints at points P_1, P_2, and P_3 are made parallel to lines P_2P_3, P_1P_3, and P_1P_2, respectively.

Two-DOF planar pantographs and five-bar linkages are used as drivers. If properly designed, such mechanisms are capable of increasing the mechanical advantage of a minimanipulator. As a result, better positional resolution and stiffness can be obtained.

2.2.1 Pantographs as Two-DOF Drivers

Pantographs are often used for magnifying displacement and speed (e.g., Song et al., 1985). In this work, we present them as speed-reduction devices. Figure 2.4 shows a possible arrangement of three simple pantographs which can be used to drive a six-DOF parallel minimanipulator. Points C_1, C_2, and C_3 are the output points of the pantographs and are connected to the limbs through universal joints. The desired platform motion is obtained by driving the sliders inside the guides. *Let subscript i in this section and the rest of this work represent*

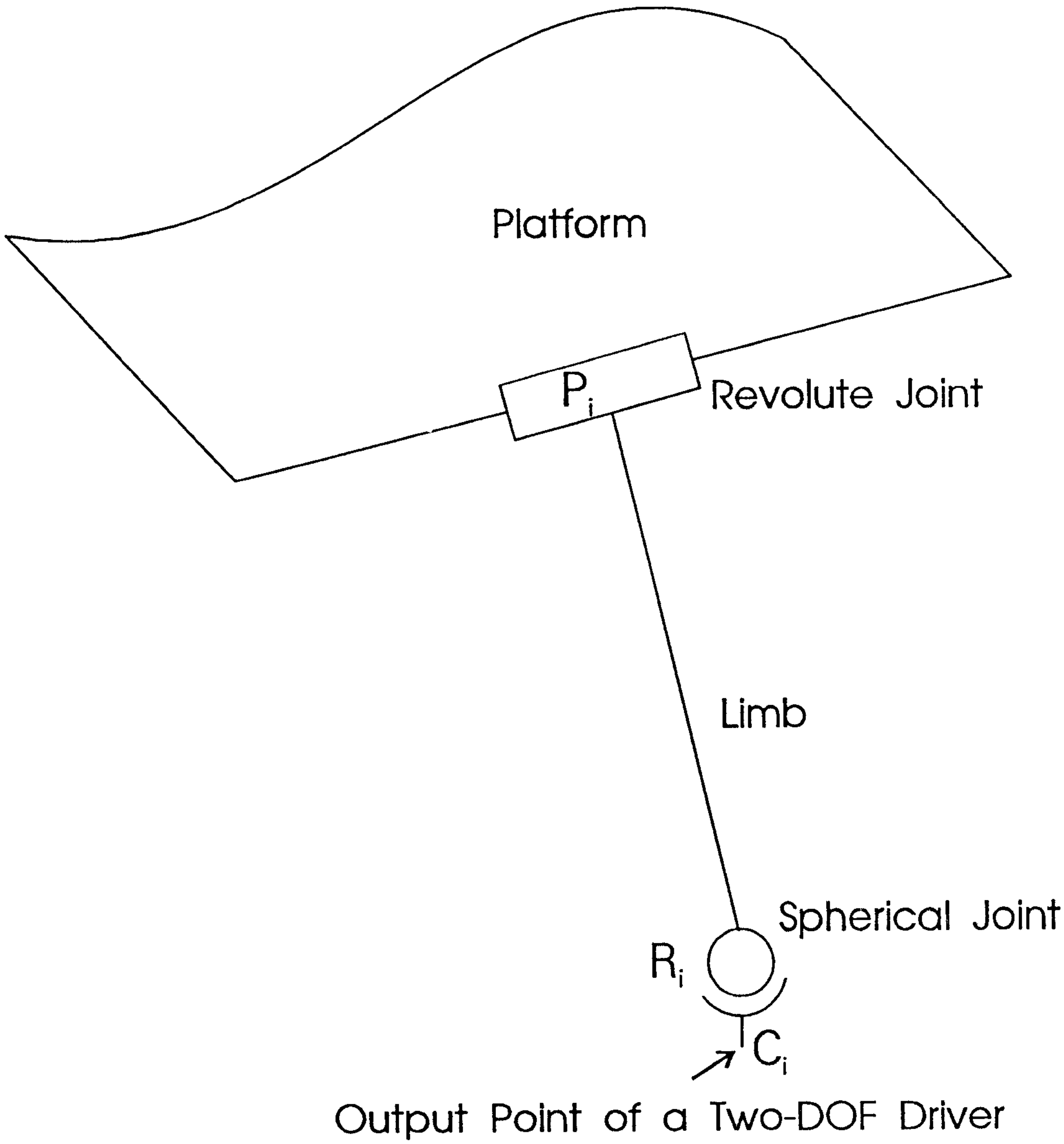

Figure 2.2: Kinematic equivalent of a limb.

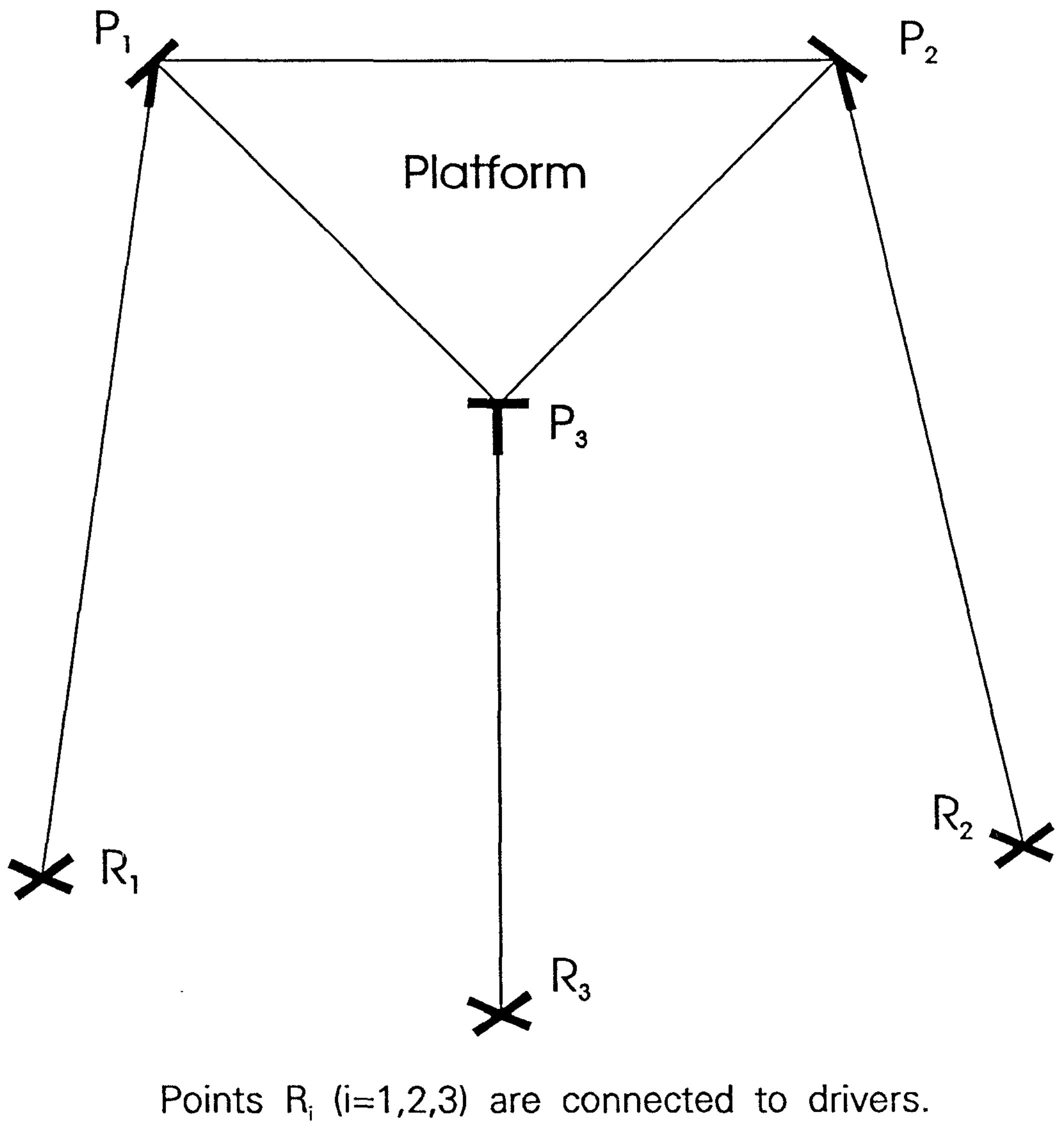

Figure 2.3: Representation of a minimanipulator.

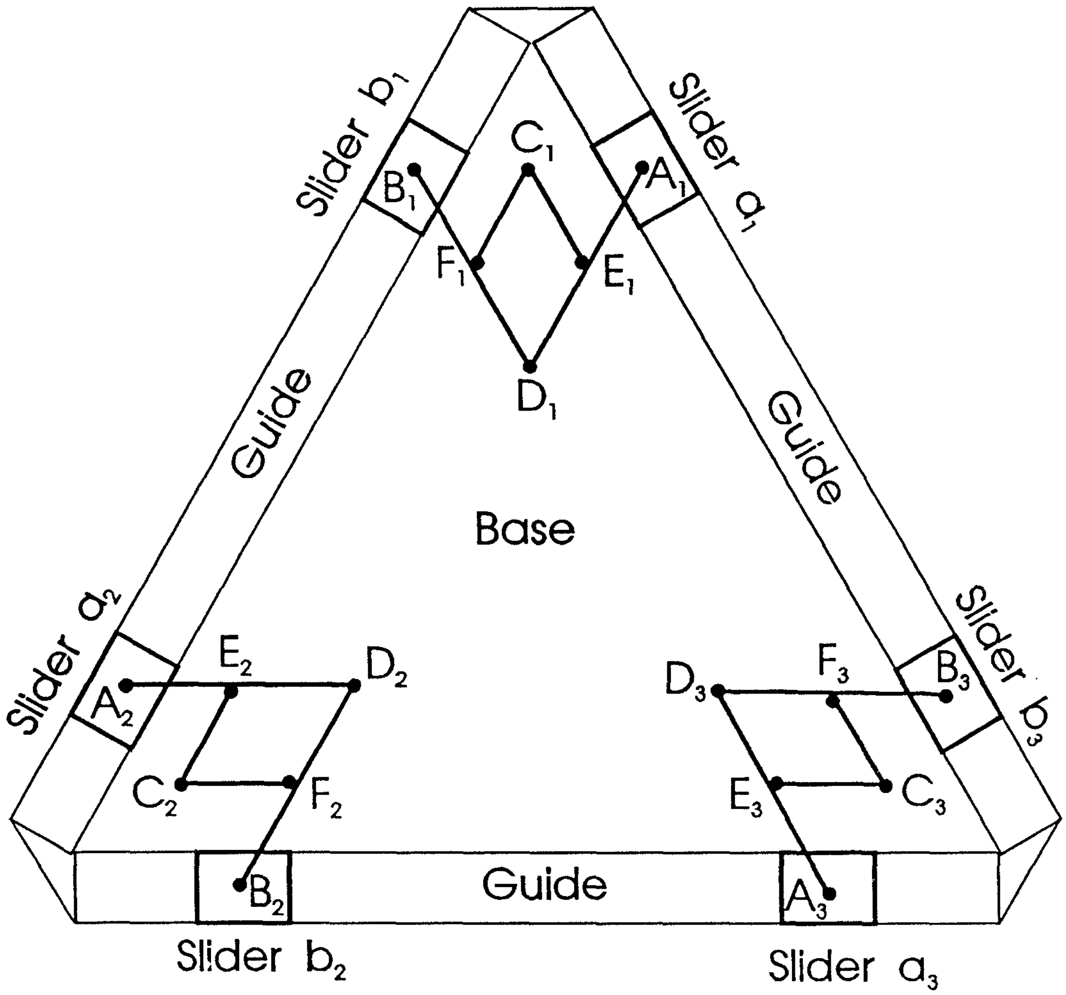

Figure 2.4: Pantographs as two-DOF drivers.

numbers 1, 2, and 3 in a cyclic manner. There are revolute joints at points A_i, B_i, C_i, D_i, E_i, and F_i. Length of link C_iE_i is equal to length of link D_iF_i. Similarly, Length of link C_iF_i is equal to length of link D_iE_i. Prismatic joints connect the sliders to the guides. Point C_i always lies on line A_iB_i. If slider b_i is fixed and slider a_i is moving along its guide, point C_i will move on a straight line with a reduction factor of $R_{a,i}$. Likewise, if slider a_i is fixed and slider b_i is moving along its guide, a parallel straight line path is followed by the output point C_i with a reduction factor of $R_{b,i}$. These reduction factors are equal to the following ratios:

$$R_{a,i} = \frac{B_iC_i}{B_iA_i} = \frac{B_iF_i}{B_iD_i} = \frac{D_iE_i}{D_iA_i} \tag{2.1}$$

$$R_{b,i} = \frac{A_iC_i}{A_iB_i} = \frac{A_iE_i}{A_iD_i} = \frac{D_iF_i}{D_iB_i} \tag{2.2}$$

The above results are based on derivations presented by Song et al. (1985). When both sliders a_i and b_i are moving, the resultant displacement of the output point C_i is the vector sum of the displacements described above. Such a displacement reduction is equivalent to a reduction in speed or an increase in mechanical advantage. As a result, stiffness and positional resolution of the minimanipulator is improved.

Motions generated at the output point C_i by sliders a_i and b_i are decoupled. As mentioned by Song et al. (1985), the decoupling feature of pantographs provides simpler coordination control and better energy efficiency. However, the above equations for the reduction factors show that:

$$R_{a,i} + R_{b,i} = 1 \tag{2.3}$$

Such reduction factors may not be good enough for applications which require very high resolution and stiffness. Therefore, five-bar linkages are also considered for speed reduction in the minimanipulators.

Skew pantographs are not considered because, in an arrangement similar to the one described above, they do not reduce speeds as well as simple pantographs do.[3] In addition, in a skew pantograph, path of the output point is rotated with respect to the slider paths. Such rotations complicate the calculations needed for control of a minimanipulator.

2.2.2 Five-Bar Linkages as Two-DOF Drivers

Five-bar linkages have been used by Asada and Ro (1985) to improve force and speed characteristics of two-DOF direct-drive robot arms. Bajpai and Roth (1986) have studied workspace and mobility of manipulators with structures based on five-bar linkages. Here, we consider two five-bar linkage configurations for improving resolution and stiffness of the minimanipulators. Figure 2.5 shows three identical five-bar linkages which can be used to drive a minimanipulator. Points C_1, C_2, and C_3 are the output points of the five-bar linkages. Base-mounted rotary actuators are placed at points D_i and E_i. Asada and Ro (1985) showed that the larger the speed reduction at the output point of a five-bar linkage, the smaller the workspace which can be generated. They also illustrated that the smaller the input link lengths (E_iA_i and D_iB_i) with respect to the other link lengths (A_iC_i and B_iC_i), the higher the speed reduction at the output point C_i. The lower end of a manipulator limb is not required to move over a large

[3]Sum of the speed reduction factors for a skew pantograph is greater than one.

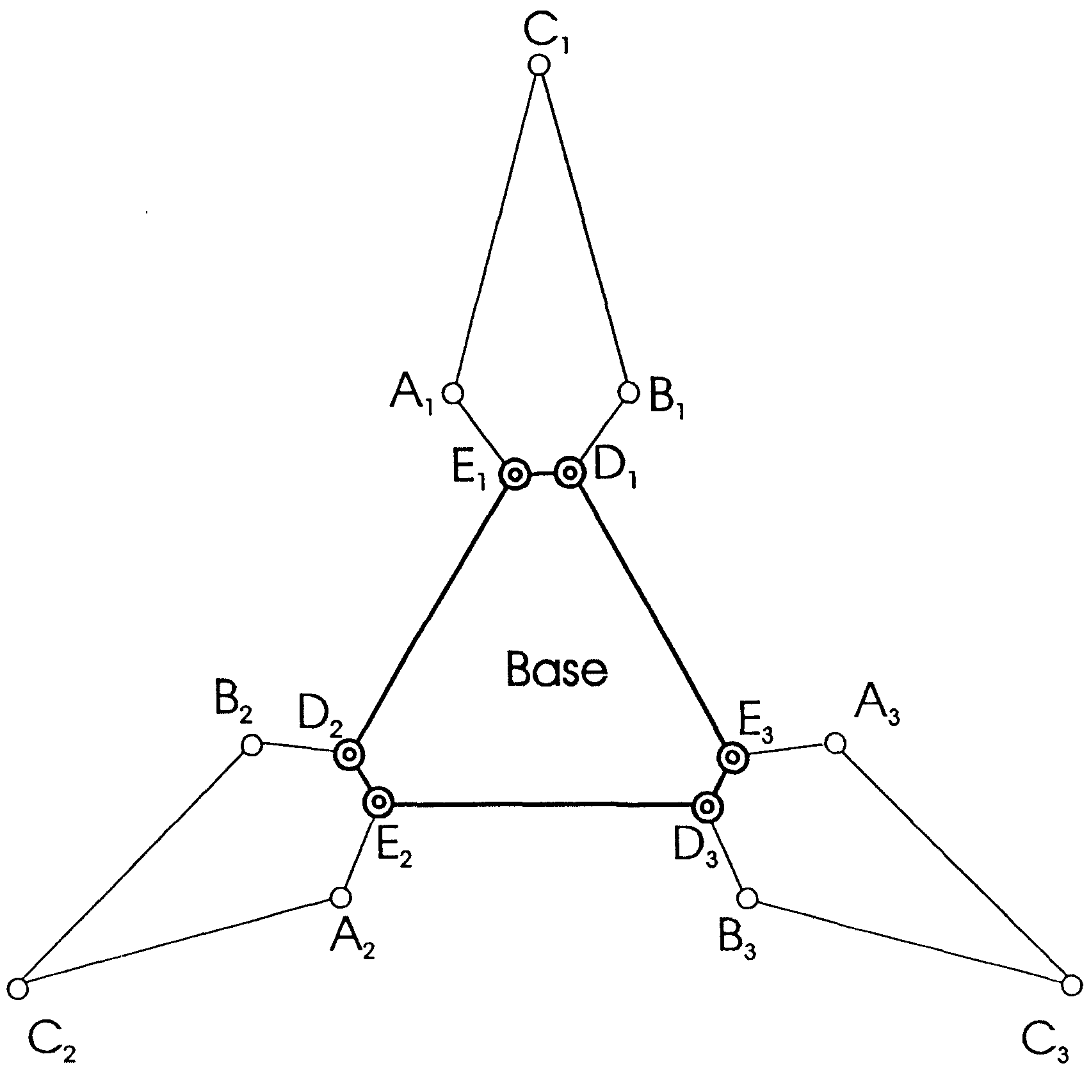

Figure 2.5: Five-bar linkages as two-DOF drivers.

area on a base plate. Hence, the five-bar linkages are designed to provide large speed reductions at their output points (i.e., their input links are made much smaller than their other links).

2.2.3 Simplified Five-Bar Linkages as Two-DOF Drivers

The driving five-bar linkages can be simplified by making the axes of rotary actuators D_i and E_i coincide, as shown in Figure 2.6. At point D_i, there is an actuator on each side of the base plate to drive links D_iA_i and D_iB_i. The simplified five-bar drivers which are considered here are completely symmetric. That is

$$\left|\overline{D_iA_i}\right| = \left|\overline{D_iB_i}\right| = a \tag{2.4}$$

$$\left|\overline{A_iC_i}\right| = \left|\overline{B_iC_i}\right| = b \tag{2.5}$$

As a result, coordination between actuator rotations can be easily accomplished. Namely, angular displacement of an output point C_i is obtained by equal actuator rotations, and its radial displacement is obtained by equal and opposite actuator rotations.

2.2.4 Other Two-DOF Drivers

Bidirectional linear stepper motors (Yeaple, 1988) or X-Y positioning tables can also be used to move the lower end of a limb on the base. However, such devices do not provide any increase in the mechanical advantage of a minimanipulator. Note that bidirectional linear stepper motors act as X-Y positioning tables, but

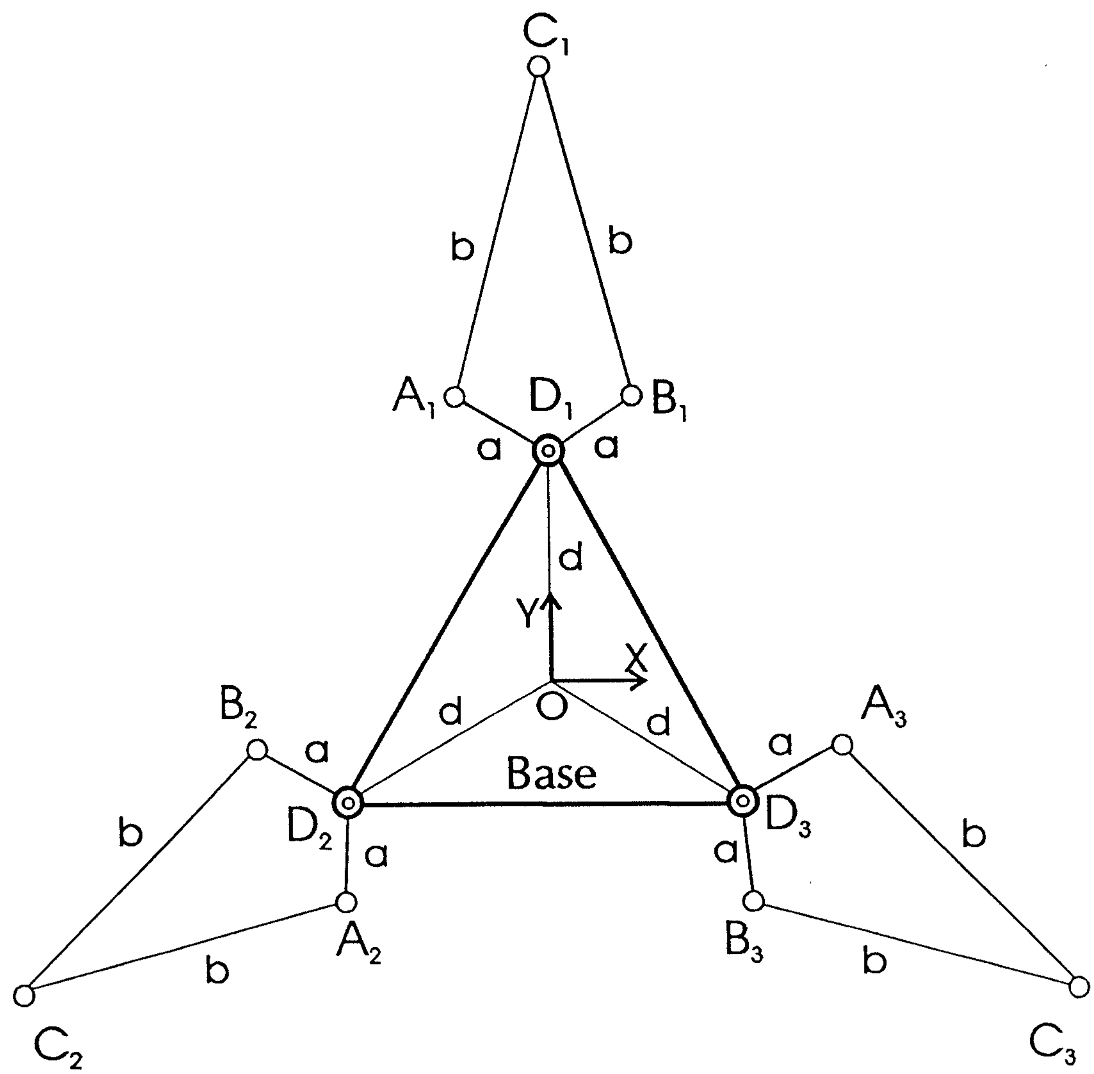

Figure 2.6: Simplified five-bar linkages as drivers.

their stators are base-mounted.

2.3 Recommended Minimanipulator Configurations

In this dissertation, we analyze the following two types of minimanipulators in detail. The difference between the two types of minimanipulators is in their two-DOF drivers.

2.3.1 Type 1 Minimanipulator

If bidirectional linear stepper motors are used as drivers, we have a Type 1 minimanipulator. *Such a minimanipulator is studied in detail, because its kinematic structure represents the primary portion (platform and limbs) of other types of minimanipulators. If a minimanipulator has five-bar linkage or pantograph drivers, we can analyze it by combining the effect of its drivers with the results of analysis for the Type 1 minimanipulator.*

2.3.2 Type 2 Minimanipulator

If simplified five-bar linkages are used as drivers, we have a Type 2 minimanipulator. The reason for concentrating on simplified five-bar linkage drivers is given below.

A five-bar linkage has fewer links than a pantograph. In addition, all of the joints in a five-bar linkage are revolute which can be designed and maintained easier than prismatic joints. As mentioned earlier, a five-bar linkage can be designed to provide a higher speed reduction than a pantograph. On the other hand, the decoupling feature of a pantograph results in better coordination control and energy efficiency. However, the simplified five-bar driver shown in Figure 2.6 can also provide simple coordination control. Hence, it may be more suitable than those drivers shown in Figures 2.4 and 2.5 for many applications.

2.4 Other Applications

The two-DOF drivers can be designed to obtain larger workspace with reduced resolution and stiffness. For example, if simplified five-bar drivers are used (see Figure 2.6), the workspace can be maximized by making D_iB_i equal to B_iC_i and D_iA_i equal to A_iC_i. A parallel mechanism with the same structure as a minimanipulator and with a larger workspace can be used as a motion simulator. In addition, a minimanipulator can be used as a passive compliant device or a force/torque sensor, if its actuators are replaced by rotational displacement transducers.

Chapter 3

Inverse Kinematics

3.1 Introduction

In general, the fewer the number of loops in the structure of a parallel manipulator, the easier its direct kinematic analysis, and the harder its inverse kinematic analysis. In the limiting case of a manipulator with zero structural loops (serial manipulator), inverse kinematic analysis becomes much harder than direct kinematic analysis. Inverse kinematics of a three-limbed minimanipulator is more difficult than that of a six-limbed parallel mechanism. Therefore, in this chapter, closed-form inverse kinematic solutions for the Type 1 and Type 2 minimanipulators (see section 2.3, page 21) are presented.

3.2 Derivation of the Inverse Kinematic Solutions

Figure 3.1 shows a parallel mechanism whose limbs are kinematically equivalent to those of an actual minimanipulator. The equivalent limb configuration will be used for analysis, because the spherical-and-revolute limb (Figure 2.2) is easier to analyze than the universal-and-universal limb (Figure 2.1). The lower ends of the limbs (points R_1, R_2, and R_3) are connected to two-DOF drivers. The upper end of the limbs (points P_1, P_2, and P_3) are connected to the platform through revolute joints. Note that the joint axes at points P_1, P_2, and P_3 are parallel to lines P_2P_3, P_1P_3, and P_1P_2, respectively.

Let us define the fixed base reference frame (XYZ) and the moving platform reference frame (UVW) in detail.

For analysis of the Type 1 minimanipulator, origin of the base reference frame (point O) as well as the X and Y-axes can be placed anywhere on the base plane. The Z-axis is defined by the right-hand-rule.

The base reference frame used for the analysis of the Type 2 minimanipulator is shown in Figures 2.6 and 3.2. The origin of the base reference frame (point O) is placed at the centroid of triangle $D_1D_2D_3$ (actuators are mounted on both sides of the base plate at points D_1, D_2, and D_3). The positive X-axis is parallel to and points in the direction of vector $\overline{D_2D_3}$. The positive Y-axis points from point O to point D_1. The Z-axis is defined by the right-hand-rule.

Next, let us describe the platform reference frame which is used for anal-

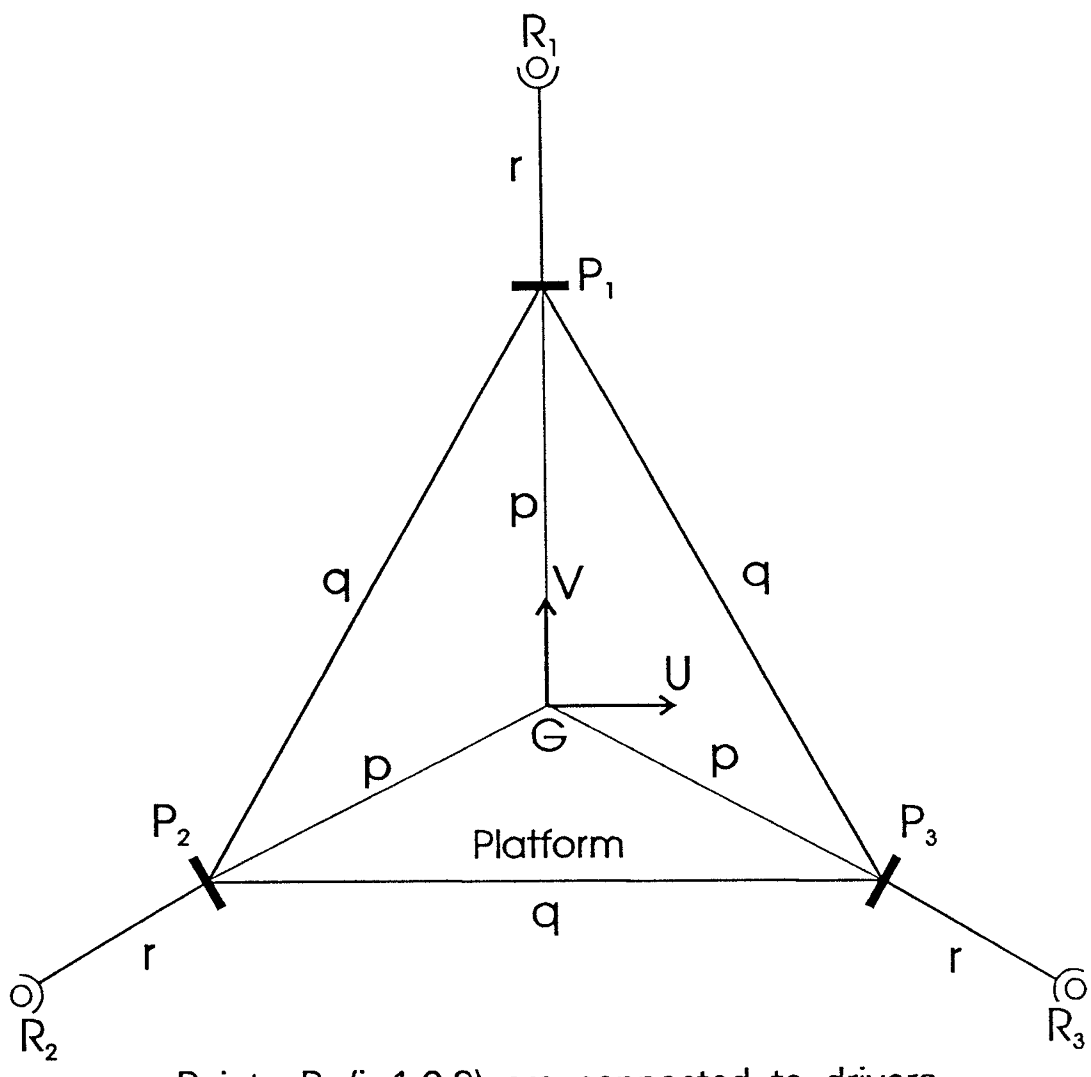

Points R_i (i=1,2,3) are connected to drivers.

Figure 3.1: Kinematic equivalent of a minimanipulator.

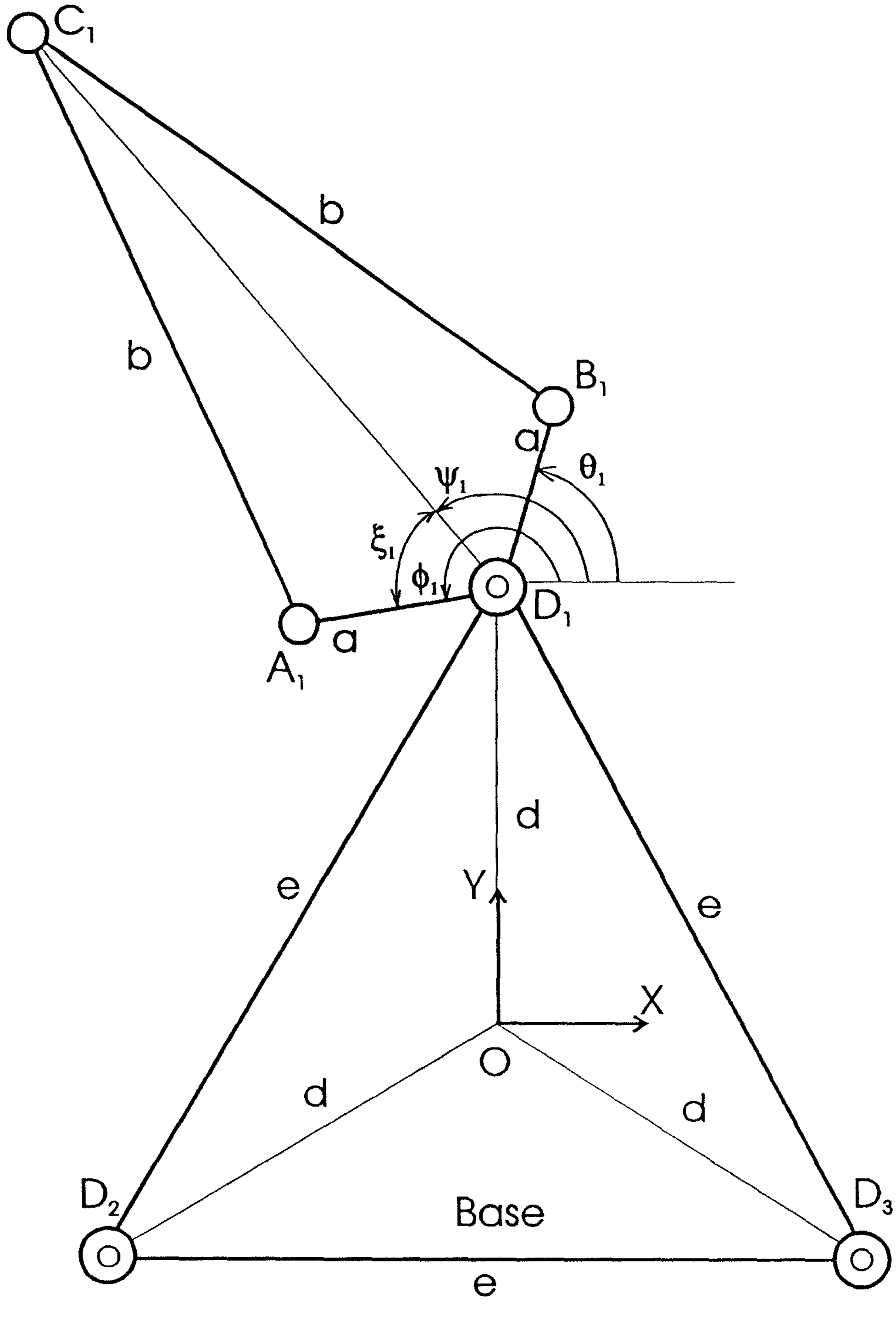

Figure 3.2: Analysis of a simplified five-bar driver.

ysis of both Type 1 and Type 2 minimanipulators. The origin of the platform reference frame (point G) is placed at the centroid of triangle $P_1P_2P_3$ (see Figure 3.1). The positive U-axis is parallel to and points in the direction of vector $\overline{P_2P_3}$. The positive V-axis points from point O to point P_1. The W-axis is defined by the right-hand-rule.

Note that we have attached only one coordinate system to each reference frame, and we use the terms reference frame and coordinate system interchangeably.

Also note that, to keep the minimanipulators symmetric, both triangles $D_1D_2D_3$ (see Figures 2.6 and 3.2) and $P_1P_2P_3$ (see Figure 3.1) are made equilateral.

In the inverse kinematics problem, the coordinates of point G in the base reference frame and the platform orientation are known. For the Type 1 minimanipulator, the coordinates of point C_i (see Figure 2.1) are the unknowns. For the Type 2 minimanipulator, input angles of the simplified five-bar drivers are also to be found.

3.2.1 Type 1 Minimanipulator

In the first step, the coordinates of points P_1, P_2, and P_3 in the base reference frame are found.

Let the length of each side of triangle $P_1P_2P_3$ be equal to q. Then the distance from point G to each one of points P_1, P_2, and P_3 (p) can be found using the law of cosines. The result is given below.

$$p = \frac{q}{\sqrt{3}} \tag{3.1}$$

Let $\mathbf{A}$ be the 4×4 homogeneous transformation matrix from the platform reference frame to the base reference frame. The elements of $\mathbf{A}$ are functions of the platform orientation and the XYZ coordinates of point G. Specifically, matrix $\mathbf{A}$ can be expressed as

$$\mathbf{A} = \begin{bmatrix} \bar{n}_u \cdot \bar{n}_x & \bar{n}_v \cdot \bar{n}_x & \bar{n}_w \cdot \bar{n}_x & X_G \\ \bar{n}_u \cdot \bar{n}_y & \bar{n}_v \cdot \bar{n}_y & \bar{n}_w \cdot \bar{n}_y & Y_G \\ \bar{n}_u \cdot \bar{n}_z & \bar{n}_v \cdot \bar{n}_z & \bar{n}_w \cdot \bar{n}_z & Z_G \\ 0 & 0 & 0 & 1 \end{bmatrix} \tag{3.2}$$

where $\bar{n}_x, \bar{n}_y, \bar{n}_z, \bar{n}_u, \bar{n}_v$, and $\bar{n}_w$ are unit vectors pointing in the X, Y, Z, U, V, and W directions, respectively.

The Coordinates of point P_i in the base reference frame can be found from the following equation.

$$\begin{bmatrix} X_{P,i} \\ Y_{P,i} \\ Z_{P,i} \\ 1 \end{bmatrix} = \mathbf{A} \begin{bmatrix} p\cos\alpha_i \\ p\sin\alpha_i \\ 0 \\ 1 \end{bmatrix} \tag{3.3}$$

where the column vector in the right hand side of the above equation is the homogeneous coordinates of point P_i in the platform reference frame and

$$\alpha_i = \frac{\pi}{2} + (i-1)\frac{2\pi}{3} \tag{3.4}$$

In the next step, the coordinates of points R_i (see Figure 3.1) in the base reference frame are found.

Vector $\overline{R_iP_i}$ is perpendicular to vector $\overline{P_{i+1}P_{i+2}}$.[1] Their dot product is equal to zero. Thus

$$(X_{P,i+1} - X_{P,i+2})(X_{R,i} - X_{P,i}) + (Y_{P,i+1} - Y_{P,i+2})(Y_{R,i} - Y_{P,i}) + \\ (Z_{P,i+1} - Z_{P,i+2})(Z_{R,i} - Z_{P,i}) = 0 \tag{3.5}$$

Let the length of each limb be equal to r. Then

$$(X_{R,i} - X_{P,i})^2 + (Y_{R,i} - Y_{P,i})^2 + (Z_{R,i} - Z_{P,i})^2 = r^2 \tag{3.6}$$

Note that in equations (3.5) and (3.6), $Z_{R,i}$ is a known constant, while $X_{R,i}$ and $Y_{R,i}$ are the unknowns. Equations (3.5) and (3.6) can be reduced to a quadratic equation in one unknown, $Y_{R,i}$, of the following form

$$K_{1,i}Y_{R,i}^2 + K_{2,i}Y_{R,i} + K_{3,i} = 0 \tag{3.7}$$

where

$$\begin{aligned}
K_{1,i} &= (X_{P,i+1} - X_{P,i+2})^2 + (Y_{P,i+2} - Y_{P,i+1})^2 \\
K_{2,i} &= 2(Z_{P,i+2} - Z_{P,i+1})(Z_{R,i} - Z_{P,i})(Y_{P,i+2} - Y_{P,i+1}) - 2Y_{P,i}(X_{P,i+1} - \\
&\quad X_{P,i+2})^2 - 2Y_{P,i}(Y_{P,i+2} - Y_{P,i+1})^2 \\
K_{3,i} &= (Z_{P,i+2} - Z_{P,i+1})^2(Z_{R,i} - Z_{P,i})^2 + Y_{P,i}^2(X_{P,i+1} - X_{P,i+2})^2 + Y_{P,i}^2(Y_{P,i+2} - \\
&\quad Y_{P,i+1})^2 - 2Y_{P,i}(Z_{P,i+2} - Z_{P,i+1})(Z_{R,i} - Z_{P,i})(Y_{P,i+2} - Y_{P,i+1}) + \\
&\quad (X_{P,i+1} - X_{P,i+2})^2(Z_{R,i} - Z_{P,i})^2 - (X_{P,i+1} - X_{P,i+2})^2 r^2
\end{aligned}$$

Therefore, there are two solutions for the coordinates of point R_i. Geometrically,

[1]The subscripts are cyclic. If $i = 2$, $i + 2$ represents 1. If $i = 3$, $i + 1$ and $i + 2$ represent 1 and 2, respectively.

these solutions represent intersections of a circle[2] with the plane parallel to the X-Y plane and containing the centers of the three spherical joints in the equivalent manipulator. Since each limb has two possible configurations, a total of eight minimanipulator postures are possible corresponding to each given platform position and orientation. In practice, the posture which corresponds to minimum displacements of points R_1, R_2, and R_3 from their previous positions or their reference positions can be used for real-time control of the minimanipulator.

Vector $\overline{C_iR_i}$ is perpendicular to the base plate. Once the coordinates of point R_i are known, the coordinates of point C_i can be found easily by subtracting a constant from the Z-component.

3.2.2 Type 2 Minimanipulator

For the Type 2 minimanipulator, results of inverse kinematics of the Type 1 minimanipulator should be used to find the input angles of the simplified five-bar drivers.

Let the length of each side of triangle $D_1D_2D_3$ (see Figure 3.2) be equal to e. Then the distance, d, from point O to each one of points D_1, D_2, and D_3 can be found using the law of cosines. The result is given below.

$$d = \frac{e}{\sqrt{3}} \tag{3.8}$$

[2]The circle has radius of r. Its plane is perpendicular to line $P_{i+1}P_{i+2}$ and its center is at point P_i.

The coordinates of point D_i in the base reference frame is given by

$$\begin{bmatrix} X_{D,i} \\ Y_{D,i} \\ Z_{D,i} \end{bmatrix} = \begin{bmatrix} d\cos\beta_i \\ d\sin\beta_i \\ 0 \end{bmatrix} \tag{3.9}$$

where

$$\beta_i = \frac{\pi}{2} + (i-1)\frac{2\pi}{3} \tag{3.10}$$

The angle which line D_iC_i makes with the positive X-axis (ψ_i) is equal to

$$\psi_i = Atan2(Y_{C,i} - Y_{D,i}, X_{C,i} - X_{D,i}) \tag{3.11}$$

where $Atan2$ is a single-valued function which calculates arc tangent of $(Y_{C,i} - Y_{D,i})/(X_{C,i} - X_{D,i})$ but uses the signs of both $Y_{C,i} - Y_{D,i}$ and $X_{C,i} - X_{D,i}$ to determine the quadrant in which ψ_i lies.

The angle which line D_iC_i makes with line D_iB_i or line D_iA_i (ξ_i) can be found by applying the law of cosines to the triangle $D_iB_iC_i$ or $D_iA_iC_i$. The result is given below.

$$\xi_i = \cos^{-1}\frac{a^2 + (X_{C,i} - X_{D,i})^2 + (Y_{C,i} - Y_{D,i})^2 - b^2}{2a\sqrt{(X_{C,i} - X_{D,i})^2 + (Y_{C,i} - Y_{D,i})^2}} \tag{3.12}$$

where a and b are link lengths of the simplified five-bar drivers. There are two opposite and equal answers for ξ_i. Let the angles which input links D_iB_i and D_iA_i make with the positive X-axis (θ_i and ϕ_i) be defined as the input angles of the drivers. Then

$$\theta_i = \psi_i \mp |\xi_i| \tag{3.13}$$

$$\phi_i = \psi_i \pm |\xi_i| \tag{3.14}$$

Mathematically, each driver has four possible configurations for a given position of its output point. If θ_i and ϕ_i are equal (two of the solutions), the driver will be in an indeterminate configuration from the direct kinematics point of view. Hence, this condition (i.e., $\theta_i = \phi_i$) should be avoided. Due to symmetry, the other two solutions result in identical configurations for the driver. In practice, one can reduce the number solutions to one by letting θ_i and ϕ_i to be always equal to $\psi_i - |\xi_i|$ and $\psi_i + |\xi_i|$, respectively.

3.3 Home Configuration

Let us define a "home" or reference configuration which will be used in the numerical examples of sections 3.4 and 4.5.

Let $\theta_{i,r}$ and $\phi_{i,r}$ represent driver input angles at the home configuration. These angles are defined to be

$$\theta_{i,r} = (i-1)\frac{2\pi}{3} \tag{3.15}$$

$$\phi_{i,r} = \pi + (i-1)\frac{2\pi}{3} \tag{3.16}$$

In addition, let

$$\left|\overline{C_i C_{i+1}}\right|_r = \left|\overline{P_i P_{i+1}}\right| \tag{3.17}$$

where $\left|\overline{C_i C_{i+1}}\right|_r$ is the length of vector $\overline{C_i C_{i+1}}$ at the home configuration. Equation (3.17) implies that, at the home configuration, the limbs are perpendicular to the base plane, and the platform is at its highest possible position. It can be shown that as a result of the above definition of the home configuration, the following constraint exists between the parameters of a Type 2 minimanipulator.

$$q = e + \sqrt{3(b^2 - a^2)} \tag{3.18}$$

3.4 Numerical Example

In this example, the above procedure is used to determine driver input angles of a Type 2 minimanipulator for a given platform position and orientation. Let the independent minimanipulator dimensions be

$$a = 1, b = 2, e = 2.5, r = 3, Z_{R,i} = 0.125$$

Note that only the ratios are important; therefore, a is set equal to 1. The dependent dimensions are found to be

$$d = 1.443, q = 5.5, p = 3.175$$

Let the roll, pitch, and yaw angles of the platform to be all equal to 5 degrees and the coordinates of point G to be (-1.75, 1.75, 1.75). The homogeneous transformation matrix becomes

$$\mathbf{A} = \begin{bmatrix} 0.9924 & -0.0793 & 0.0941 & -1.75 \\ 0.0868 & 0.9930 & -0.0793 & 1.75 \\ -0.0872 & 0.0868 & 0.9924 & 1.75 \\ 0 & 0 & 0 & 1 \end{bmatrix}$$

The calculated coordinates of points P_i, R_i, and C_i are given in Table 3.1. Note that there are two possible solutions for point R_i. The above results represent

Point	**X**	**Y**	**Z**
P_1	-2.0017	4.9034	2.0257
P_2	-4.3533	-0.0655	1.8518
P_3	1.1049	0.4120	1.3725
R_1	-1.9656	2.5826	0.125
R_2	-2.4604	1.4950	0.125
R_3	3.5877	-0.7192	0.125
C_1	-1.9656	2.5826	0.0
C_2	-2.4604	1.4950	0.0
C_3	3.5877	-0.7192	0.0

Table 3.1: Intermediate results of the inverse kinematics sample problem.

the solutions which correspond to minimum displacements of points R_1, R_2, and R_3 from their reference positions. Angles ψ_i and ξ_i are found to be

$$\psi_1 = 149.9031, \psi_2 = 118.6360, \psi_3 = 0.0592$$

$$\xi_1 = \pm 61.5969, \xi_2 = \pm 48.0193, \xi_3 = \pm 58.1855$$

Setting θ_i equal to $\psi_i - |\xi_i|$ and ϕ_i equal to $\psi_i + |\xi_i|$, the following results for the driver input angles are obtained.

$$\theta_1 = 88.3062, \theta_2 = 70.6167, \theta_3 = 301.8737$$

$$\phi_1 = 211.5, \phi_2 = 166.6554, \phi_3 = 58.2448$$

Chapter 4

Direct Kinematics

4.1 Introduction

As mentioned earlier, direct kinematics of a parallel manipulator is much more difficult than its inverse kinematics. Dieudonne et al. (1972) applied Newton-Raphson's method to solve the direct kinematics of a motion simulator identical to the Stewart platform. Behi (1988) used a similar technique to numerically solve the direct kinematics problem of a parallel mechanism similar to the Stewart platform. Griffis and Duffy (1989) as well as Nanua et al. (1990) studied direct kinematics of special cases of Stewart platform, in which pairs of spherical joints are concentric on either the platform or both the base and the platform. They were able to reduce the problem to an eighth-degree polynomial in the square of a single variable (total degree of sixteen). However, as mentioned by Griffis and Duffy (1989), pairs of concentric spherical joints may very well present design problems. Lin et al. (1990) solved direct kinematics of another class of Stewart platforms, in which there are two concentric spherical joints on the base and two more concentric spherical joints on the platform. The latter class of Stewart platforms suffer from lack of symmetry and concentric spherical joints are still needed in their construction. Other researcher have also been able to obtain closed-form solutions for other special forms of the Stewart platform (e.g., Innocenti and Parenti-Castelli, 1990; Parenti-Castelli and Innocenti, 1990; Zhang and Song, 1990; Zhang and Song, 1991). It is worth mentioning that, to the best of our knowledge, no one has yet been able to obtain a closed-form direct kinematics solution for the general Stewart platform with six independent limbs. Recently, Raghavan (1991) used a numerical technique known as polynomial continuation to show that there are forty solutions for the direct kinematics of the Stewart platform of general geometry. Murthy and Waldron (1990a, 1990b) have been able to relate the direct kinematics of some parallel mechanisms to the inverse kinematics of their serial dual mechanisms.

In this chapter, closed-form direct kinematic solutions for the Type 1 and Type 2 minimanipulators (see section 2.3, page 21) are presented. It will be shown that direct kinematics of the minimanipulators involves solving an eighth-degree polynomial in the square of a single variable.

4.2 Preliminaries

Figure 3.1 shows a parallel mechanism whose limbs are kinematically equivalent to those of an actual minimanipulator. The equivalent limb configuration will be used for analysis, because the spherical-and-revolute limb (Figure 2.2) is easier to analyze than the universal-and-universal limb (Figure 2.3). The lower ends of the limbs (points R_1, R_2, and R_3) are connected to two-DOF drivers. The upper end of the limbs (points P_1, P_2, and P_3) are connected to the platform through revolute joints. Note that the joint axes at points P_1, P_2, and P_3 are parallel to lines P_2P_3, P_1P_3, and P_1P_2, respectively.

Definition of the fixed reference frame (XYZ) and the moving reference frame (UVW) are given in section 3.2. The fixed reference frame (XYZ) used in the analysis of the Type 2 minimanipulator is shown in Figures 2.6 and 3.2. The moving (or platform) reference frame is shown in Figure 3.1. Note that both triangles $D_1D_2D_3$ and $P_1P_2P_3$ are equilateral.

4.3 Direct Kinematics of the Type 1 Minimanipulator

In the direct kinematics of the Type 1 minimanipulator, coordinates of point C_i (see Figure 2.1) are given. Coordinates of points P_1, P_2, and P_3 in the base reference frame are to be found. These three points completely define the platform position and orientation.

4.3.1 Coordinates of Point R_i

Vector $\overline{C_iR_i}$ is perpendicular to the base plate. Once the coordinates of point C_i are known, the coordinates of point R_i can be found easily by adding a constant to the Z-component.

4.3.2 Angles between the Limbs and the Platform

As shown in Figure 4.1, let η_i be the angle from vector $\overline{GP_i}$ to vector $\overline{P_iR_i}$ measured about the vector $\overline{\Gamma_i}$ which is collinear with the axis of the revolute joint at point P_i and points in the direction of vector $\overline{P_{i+2}P_{i+1}}$.[1] Also, let α_i be the angle from the positive U-axis to vector $\overline{GP_i}$ about the positive W-axis. Angle α_i can be found from Figure 3.1 as

$$\alpha_i = \frac{\pi}{2} + (i-1)\frac{2\pi}{3} \tag{4.1}$$

In the next step, angle η_i will be found from a kinematic inversion. If r is the length of each limb, the coordinates of point R_i in the moving reference frame UVW are

$$U_{R,i} = rC\alpha_i C\eta_i + U_{P,i} \tag{4.2}$$

$$V_{R,i} = rS\alpha_i C\eta_i + V_{P,i} \tag{4.3}$$

$$W_{R,i} = -rS\eta_i \tag{4.4}$$

where $C\alpha_i = \cos\alpha_i, S\alpha_i = \sin\alpha_i, C\eta_i = \cos\eta_i$, and $S\eta_i = \sin\eta_i$. Note that $U_{P,i}$ and $V_{P,i}$ are known quantities which can be found from

$$U_{P,i} = pC\alpha_i \tag{4.5}$$

$$V_{P,i} = pS\alpha_i \tag{4.6}$$

where p is the length of vector $\overline{GP_i}$ (see Figure 3.1).

[1]The subscripts are cyclic. If $i = 2$, $i + 2$ represents 1. If $i = 3$, $i + 1$ and $i + 2$ represent 1 and 2, respectively.

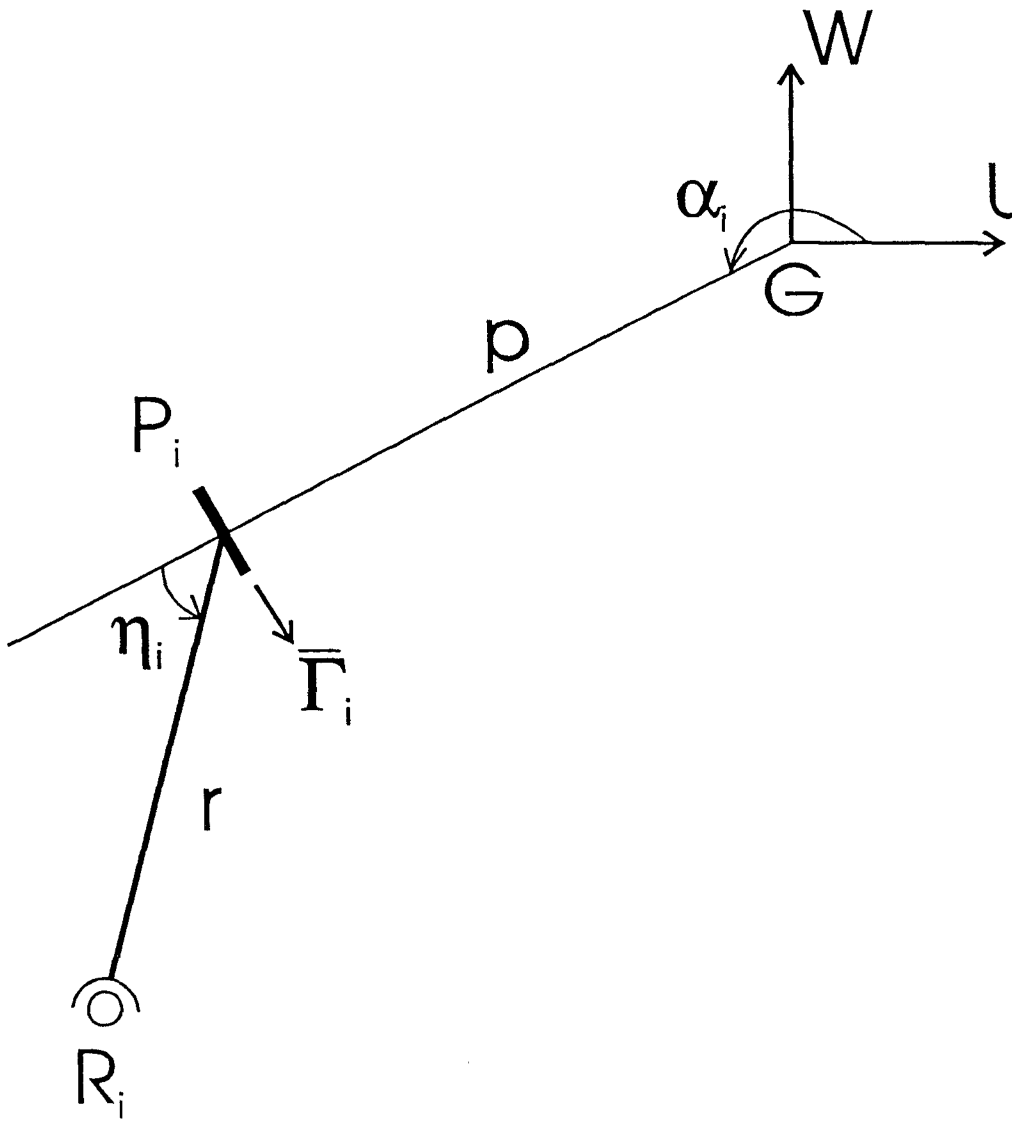

Figure 4.1: Depiction of angles α_i, and η_i.

The coordinates of point R_i in the base reference frame have already been found in the previous section. Hence, the length of vector $\overline{R_iR_{i+1}}$, denoted by l_{i+2}, is known. We can write

$$(U_{R,i} - U_{R,i+1})^2 + (V_{R,i} - V_{R,i+1})^2 + (W_{R,i} - W_{R,i+1})^2 = l_{i+2}^2 \tag{4.7}$$

Substituting equations (4.2) - (4.4) into equation (4.7) and simplifying, we get

$$A_i S\eta_i S\eta_{i+1} + B_i C\eta_i C\eta_{i+1} + D_i C\eta_i + D_i C\eta_{i+1} + E_i = 0 \tag{4.8}$$

where

$$\begin{aligned} A_i &= -2r^2 \\ B_i &= r^2 \\ D_i &= 3rp \\ E_i &= 2r^2 + 3p^2 - l_{i+2}^2 \end{aligned}$$

Let

$$t_i = \tan\left(\frac{\eta_i}{2}\right).$$

Then, we can express $\cos\eta_i$ and $\sin\eta_i$ in terms of t_i as

$$\cos\eta_i = \frac{1 - t_i^2}{1 + t_i^2} \tag{4.9}$$

$$\sin\eta_i = \frac{2t_i}{1 + t_i^2} \tag{4.10}$$

Substituting equations (4.9) and (4.10) into equation (4.8) and simplifying, we get

$$F_i t_i^2 t_{i+1}^2 + G_i t_i^2 + G_i t_{i+1}^2 + I_i t_i t_{i+1} + J_i = 0 \tag{4.11}$$

where

$$\begin{aligned}
F_i &= 3r^2 + 3p^2 - 6rp - l_{i+2}^2 \\
G_i &= r^2 + 3p^2 - l_{i+2}^2 \\
I_i &= -8r^2 \\
J_i &= 3r^2 + 3p^2 + 6rp - l_{i+2}^2
\end{aligned}$$

Equation (4.11) can be rewritten, for $i = 1, 2, 3$, in the following forms

$$(F_1 t_1^2 + G_1)t_2^2 + (I_1 t_1)t_2 + (G_1 t_1^2 + J_1) = 0 \tag{4.12}$$

$$(F_2 t_3^2 + G_2)t_2^2 + (I_2 t_3)t_2 + (G_2 t_3^2 + J_2) = 0 \tag{4.13}$$

$$(F_3 t_1^2 + G_3)t_3^2 + (I_3 t_1)t_3 + (G_3 t_1^2 + J_3) = 0 \tag{4.14}$$

We can think of equations (4.12) and (4.13) as two equations in the variable t_2. Vanishing of their eliminant results in the following equation (Salmon, 1964). Refer to Appendix B for details.

$$N_1 t_3^4 + N_2 t_3^3 + N_3 t_3^2 + N_4 t_3 + N_5 = 0 \tag{4.15}$$

where

$$\begin{aligned}
N_1 &= Q_1 t_1^4 + Q_2 t_1^2 + Q_3 \\
N_2 &= Q_4 t_1^3 + Q_5 t_1 \\
N_3 &= Q_6 t_1^4 + Q_7 t_1^2 + Q_8 \\
N_4 &= Q_9 t_1^3 + Q_{10} t_1 \\
N_5 &= Q_{11} t_1^4 + Q_{12} t_1^2 + Q_{13}
\end{aligned}$$

where Q's are constants which can be found[2] from the following relationships.

$$
\begin{aligned}
Q_1 &= F_1^2 G_2^2 - 2F_1F_2G_1G_2 + F_2^2 G_1^2 \\
Q_2 &= 2F_2^2 G_1 J_1 + F_2 G_2 I_1^2 + 2F_1 G_1 G_2^2 - 2F_1F_2G_2J_1 - 2F_2G_1^2G_2 \\
Q_3 &= F_2^2 J_1^2 + G_1^2 G_2^2 - 2F_2 G_1 G_2 J_1 \\
Q_4 &= -F_1 G_2 I_1 I_2 - F_2 G_1 I_1 I_2 \\
Q_5 &= -F_2 I_1 I_2 J_1 - G_1 G_2 I_1 I_2 \\
Q_6 &= 2F_1^2 G_2 J_2 + F_1 G_1 I_2^2 + 2F_2 G_1^2 G_2 - 2F_1 F_2 G_1 J_2 - 2F_1 G_1 G_2^2 \\
Q_7 &= F_2 I_1^2 J_2 + 4F_1 G_1 G_2 J_2 + F_1 I_2^2 J_1 + 4F_2 G_1 G_2 J_1 + G_1^2 I_2^2 + G_2^2 I_1^2 - \\
&\quad 2F_1 F_2 J_1 J_2 - 2F_2 G_1^2 J_2 - 2F_1 G_2^2 J_1 - 2G_1^2 G_2^2 \\
Q_8 &= 2G_1^2 G_2 J_2 + 2F_2 G_2 J_1^2 + G_1 I_2^2 J_1 - 2F_2 G_1 J_1 J_2 - 2G_1 G_2^2 J_1 \\
Q_9 &= -F_1 I_1 I_2 J_2 - G_1 G_2 I_1 I_2 \\
Q_{10} &= -G_1 I_1 I_2 J_2 - G_2 I_1 I_2 J_1 \\
Q_{11} &= F_1^2 J_2^2 + G_1^2 G_2^2 - 2F_1 G_1 G_2 J_2 \\
Q_{12} &= 2F_1 G_1 J_2^2 + G_2 I_1^2 J_2 + 2G_1 G_2^2 J_1 - 2F_1 G_2 J_1 J_2 - 2G_1^2 G_2 J_2 \\
Q_{13} &= G_1^2 J_2^2 + G_2^2 J_1^2 - 2G_2 G_1 J_1 J_2
\end{aligned}
$$

Similarly, we can think of equations (4.14) and (4.15) as two equations in the variable t_3. Vanishing of their eliminant results in (Salmon, 1964)

$$
\begin{aligned}
&-N_5 S_1[(N_3 S_1 - N_1 S_3)(S_2^2 - S_1 S_3) - S_1 S_2(-N_2 S_3 + N_3 S_2 + N_4 S_1) + \\
&S_1^2(N_4 S_2 + N_5 S_1)] + (N_2 S_1 - N_1 S_2)[N_5 S_2(S_2^2 - S_1 S_3) + \\
&S_3^2(-N_2 S_3 + N_3 S_2 + N_4 S_1) - S_2(N_4 S_2 + N_5 S_1) S_3] +
\end{aligned}
$$

[2]Macsyma (1988) was used here and in other portions of this work for symbolic calculations.

$$N_4S_1[-S_1S_3(-N_2S_3 + N_3S_2 + N_4S_1) + S_2S_3(N_3S_1 - N_1S_3) + N_5S_1^2S_2] -$$

$$(N_3S_1 - N_1S_3)[S_3^2(N_3S_1 - N_1S_3) - S_1(N_4S_2 + N_5S_1)S_3 + N_5S_1S_2^2] = 0 \quad (4.16)$$

where S's are the coefficients of equation (4.14). Namely,

$$\begin{aligned} S_1 &= F_3t_1^2 + G_3 \\ S_2 &= I_3t_1 \\ S_3 &= G_3t_1^2 + J_3 \end{aligned}$$

Equation (4.16) is an eighth-degree polynomial in square of t_1 (see Appendix C for details). It follows that there are sixteen possible solutions for each angle η_i and therefore sixteen solutions for the direct kinematics of the minimanipulator. The elimination procedure described above is similar to those used by Nanua et al. (1990), Griffis and Duffy (1989), and Innocenti and Parenti-Castelli (1990) for solving direct kinematics of special forms of the Stewart platform.

4.3.3 Coordinates of Point G

In the next step, the coordinates of point G in the base reference frame will be found. Let h_i be the length of vector $\overline{GR_i}$. Using equations (4.2) - (4.4), we can write h_i^2 in terms of the UVW coordinates of points G and R_i as

$$h_i^2 = (rC\alpha_iC\eta_i + U_{P,i})^2 + (rS\alpha_iC\eta_i + V_{P,i})^2 + r^2S\eta_i^2 \quad (4.17)$$

We observe that sixteen values of η_i result in only eight values for h_i^2. Writing h_i^2 in terms of the XYZ coordinates of points G and R_i, we get

$$(X_G - X_{R,i})^2 + (Y_G - Y_{R,i})^2 + (Z_G - k)^2 = h_i^2 \quad (4.18)$$

where k is the Z-coordinate of point R_i. If equation (4.18) is written for $i = 1$ and $i = 2$ and the latter equation is subtracted from the former one, the following relation is obtained.

$$2(X_{R,2}-X_{R,1})X_G+2(Y_{R,2}-Y_{R,1})Y_G = h_1^2-h_2^2-X_{R,1}^2-Y_{R,1}^2+X_{R,2}^2+Y_{R,2}^2 \quad (4.19)$$

Similarly, If equation (4.18) is written for $i = 1$ and $i = 3$ and the latter equation is subtracted from the former one, the following relation is obtained.

$$2(X_{R,3}-X_{R,1})X_G+2(Y_{R,3}-Y_{R,1})Y_G = h_1^2-h_3^2-X_{R,1}^2-Y_{R,1}^2+X_{R,3}^2+Y_{R,3}^2 \quad (4.20)$$

The above two equations can be solved for X_G and Y_G. Eight h_i^2 values result in eight solutions for (X_G, Y_G). These solutions can be substituted back in equation (4.18) to find Z_G. For each (X_G, Y_G) solution, two values for Z_G are obtained. Therefore, there are eight pairs of (sixteen) solutions for point G. In each pair, one element is the mirror image of the other element with respect to the plane passing through points R_1, R_2, and R_3 ($Z = k$ plane).

4.3.4 Coordinates of Point $\mathbf{P_i}$

In the final step, the coordinates of point P_i in the base reference frame are found. Referring to Figure 4.1, we can write

$$(X_{P,i} - X_{R,i})^2 + (Y_{P,i} - Y_{R,i})^2 + (Z_{P,i} - k)^2 = r^2 \quad (4.21)$$

$$(X_{P,i} - X_G)^2 + (Y_{P,i} - Y_G)^2 + (Z_{P,i} - Z_G)^2 = p^2 \quad (4.22)$$

Subtracting equation (4.22) from equation (4.21) results in

$$(X_G - X_{R,i})X_{P,i} + (Y_G - Y_{R,i})Y_{P,i} + (Z_G - k)Z_{P,i} =$$
$$(r^2 - p^2 + X_G^2 + Y_G^2 + Z_G^2 - X_{R,i}^2 - Y_{R,i}^2 - k^2)/2 \quad (4.23)$$

Referring to Figure 3.1, we obtain the following geometric relations. Vector $\overline{P_i R_i}$ is perpendicular to vector $\overline{P_{i+1} P_{i+2}}$. Hence

$$(X_{P,i} - X_{R,i})(X_{P,i+1} - X_{P,i+2}) + (Y_{P,i} - Y_{R,i})(Y_{P,i+1} - Y_{P,i+2}) + (Z_{P,i} - k)(Z_{P,i+1} - Z_{P,i+2}) = 0 \quad (4.24)$$

Also, vector $\overline{GP_i}$ is perpendicular to vector $\overline{P_{i+1} P_{i+2}}$. Thus

$$(X_{P,i} - X_G)(X_{P,i+1} - X_{P,i+2}) + (Y_{P,i} - Y_G)(Y_{P,i+1} - Y_{P,i+2}) + (Z_{P,i} - Z_G)(Z_{P,i+1} - Z_{P,i+2}) = 0 \quad (4.25)$$

Subtracting equation (4.24) from equation (4.25) results in

$$(X_{R,i} - X_G)X_{P,i+1} + (X_G - X_{R,i})X_{P,i+2} + (Y_{R,i} - Y_G)Y_{P,i+1} + (Y_G - Y_{R,i})Y_{P,i+2} + (k - Z_G)Z_{P,i+1} + (Z_G - k)Z_{P,i+2} = 0 \quad (4.26)$$

Point G is the centroid of the triangle $P_1 P_2 P_3$. Hence

$$X_{P,1} + X_{P,2} + X_{P,3} = 3X_G \quad (4.27)$$

$$Y_{P,1} + Y_{P,2} + Y_{P,3} = 3Y_G \quad (4.28)$$

$$Z_{P,1} + Z_{P,2} + Z_{P,3} = 3Z_G \quad (4.29)$$

Equations (4.23) and (4.26) can be written for $i = 1, 2, 3$. These equations plus equations (4.27), (4.28), and (4.29) represent nine linearly-independent equations in nine unknowns, $X_{P,1}$, $Y_{P,1}$, $Z_{P,1}$, $X_{P,2}$, $Y_{P,2}$, $Z_{P,2}$, $X_{P,3}$, $Y_{P,3}$, and $Z_{P,3}$. Solving this system of equations results in the following expressions for the unknowns.

$$X_{P,i} = [3(\mathrm{Y}_{\mathrm{R},i+2} - \mathrm{Y}_{\mathrm{R},i+1})(\mathrm{Z}_{\mathrm{G}} - k)^2 + 2(\mathrm{Y}_{\mathrm{R},i+2} - \mathrm{Y}_{\mathrm{R},i+1})\mathrm{Y}_{\mathrm{R},i}{}^2 + (\mathrm{Y}_{\mathrm{R},i+2}{}^2 - 6\,\mathrm{Y}_{\mathrm{G}}\,\mathrm{Y}_{\mathrm{R},i+2} - \mathrm{Y}_{\mathrm{R},i+1}{}^2 +$$

$$6\,\mathrm{Y_G}\,\mathrm{Y_{R,i+1}} + \mathrm{X_{R,i+2}}^2 - 6\,\mathrm{X_G}\,\mathrm{X_{R,i+2}} - \mathrm{X_{R,i+1}}^2 + 6\,\mathrm{X_G}\,\mathrm{X_{R,i+1}})\,\mathrm{Y_{R,i}} -$$

$$\mathrm{Y_{R,i+1}}\,\mathrm{Y_{R,i+2}}^2 + (\mathrm{Y_{R,i+1}}^2 + 3\,\mathrm{Y_G}^2 + 2\,\mathrm{X_{R,i}}^2 + \mathrm{X_{R,i+1}}^2 - 6\,\mathrm{X_G}\,\mathrm{X_{R,i+1}} +$$

$$3\,\mathrm{X_G}^2 - 3\,r^2 + 3\,p^2)\,\mathrm{Y_{R,i+2}} + (-3\,\mathrm{Y_G}^2 - 2\,\mathrm{X_{R,i}}^2 - \mathrm{X_{R,i+2}}^2 +$$

$$6\,\mathrm{X_G}\,\mathrm{X_{R,i+2}} - 3\,\mathrm{X_G}^2 + 3\,r^2 - 3\,p^2)\,\mathrm{Y_{R,i+1}} / \{4[\mathrm{X_{R,i+1}}(\mathrm{Y_{R,i}} - \mathrm{Y_{R,i+2}}) -$$

$$\mathrm{X_{R,i+2}}\,\mathrm{Y_{R,i}} + \mathrm{X_{R,i}}\,\mathrm{Y_{R,i+2}} + (\mathrm{X_{R,i+2}} - \mathrm{X_{R,i}})\,\mathrm{Y_{R,i+1}}]\} \tag{4.30}$$

$$Y_{P,i} = [3(\mathrm{X_{R,i+1}} - \mathrm{X_{R,i+2}})\,(\mathrm{Z_G} - k)^2 + 2(\mathrm{X_{R,i+1}} - \mathrm{X_{R,i+2}})\,\mathrm{Y_{R,i}}^2 +$$

$$(\mathrm{X_{R,i+1}} - \mathrm{X_{R,i}})\,\mathrm{Y_{R,i+2}}^2 + 6(\mathrm{X_{R,i}} - \mathrm{X_{R,i+1}})\,\mathrm{Y_G}\,\mathrm{Y_{R,i+2}} + (\mathrm{X_{R,i}} -$$

$$\mathrm{X_{R,i+2}})\,\mathrm{Y_{R,i+1}}^2 + 6(\mathrm{X_{R,i+2}} - \mathrm{X_{R,i}})\,\mathrm{Y_G}\,\mathrm{Y_{R,i+1}} + 3(\mathrm{X_{R,i+1}} -$$

$$\mathrm{X_{R,i+2}})\,\mathrm{Y_G}^2 + 2(\mathrm{X_{R,i+1}} - \mathrm{X_{R,i+2}})\,\mathrm{X_{R,i}}^2 + (-\mathrm{X_{R,i+2}}^2 +$$

$$6\,\mathrm{X_G}\,\mathrm{X_{R,i+2}} + \mathrm{X_{R,i+1}}^2 - 6\,\mathrm{X_G}\,\mathrm{X_{R,i+1}})\,\mathrm{X_{R,i}} + \mathrm{X_{R,i+1}}\,\mathrm{X_{R,i+2}}^2 +$$

$$(-\mathrm{X_{R,i+1}}^2 - 3\,\mathrm{X_G}^2 + 3\,r^2 - 3\,p^2)\,\mathrm{X_{R,i+2}} + 3(\mathrm{X_G}^2 - r^2 +$$

$$p^2)\,\mathrm{X_{R,i+1}}] / \{4[\mathrm{X_{R,i+1}}(\mathrm{Y_{R,i}} - \mathrm{Y_{R,i+2}}) - \mathrm{X_{R,i+2}}\,\mathrm{Y_{R,i}} + \mathrm{X_{R,i}}\,\mathrm{Y_{R,i+2}} +$$

$$(\mathrm{X_{R,i+2}} - \mathrm{X_{R,i}})\,\mathrm{Y_{R,i+1}}]\} \tag{4.31}$$

$$Z_{P,i} = \{[5(\mathrm{X_{R,i+1}} - \mathrm{X_{R,i+2}})\,\mathrm{Y_{R,i}} + (5\,\mathrm{X_{R,i}} - 2\,\mathrm{X_{R,i+1}} - 3\,\mathrm{X_G})\,\mathrm{Y_{R,i+2}} +$$

$$(-5\,\mathrm{X_{R,i}} + 2\,\mathrm{X_{R,i+2}} + 3\,\mathrm{X_G})\,\mathrm{Y_{R,i+1}} + 3(\mathrm{X_{R,i+2}} - \mathrm{X_{R,i+1}})\,\mathrm{Y_G}]\,(\mathrm{Z_G} -$$

$$k)^2 + 4k\,[(\mathrm{X_{R,i+1}} - \mathrm{X_{R,i+2}})\,\mathrm{Y_{R,i}} + (\mathrm{X_{R,i}} - \mathrm{X_{R,i+1}})\,\mathrm{Y_{R,i+2}} + (\mathrm{X_{R,i+2}} -$$

$$\mathrm{X_{R,i}})\,\mathrm{Y_{R,i+1}}]\,(\mathrm{Z_G} - k) + 2[(\mathrm{X_{R,i+1}} - \mathrm{X_G})\,\mathrm{Y_{R,i+2}} + (\mathrm{X_G} -$$

$$\mathrm{X_{R,i+2}})\,\mathrm{Y_{R,i+1}} + (\mathrm{X_{R,i+2}} - \mathrm{X_{R,i+1}})\,\mathrm{Y_G}]\,\mathrm{Y_{R,i}}^2 + [(\mathrm{X_{R,i+1}} -$$

$$\mathrm{X_G})\,\mathrm{Y_{R,i+2}}^2 + 6(\mathrm{X_G} - \mathrm{X_{R,i+1}})\,\mathrm{Y_G}\,\mathrm{Y_{R,i+2}} + (\mathrm{X_G} - \mathrm{X_{R,i+2}})\,\mathrm{Y_{R,i+1}}^2 +$$

$$6(\mathrm{X_{R,i+2}} - \mathrm{X_G})\,\mathrm{Y_G}\,\mathrm{Y_{R,i+1}} + 5(\mathrm{X_{R,i+1}} - \mathrm{X_{R,i+2}})\,\mathrm{Y_G}^2 + (\mathrm{X_{R,i+1}} -$$

$$\mathrm{X_G})\,\mathrm{X_{R,i+2}}^2 + (-\mathrm{X_{R,i+1}}^2 + \mathrm{X_G}^2 + r^2 - p^2)\,\mathrm{X_{R,i+2}} + \mathrm{X_G}\,\mathrm{X_{R,i+1}}^2 +$$

$$(-\mathrm{X_G}^2 - r^2 + p^2)\,\mathrm{X_{R,i+1}}]\,\mathrm{Y_{R,i}} + [(\mathrm{X_G} - \mathrm{X_{R,i}})\,\mathrm{Y_{R,i+1}} + (\mathrm{X_{R,i}} -$$

$$\mathrm{X_{R,i+1}})\,\mathrm{Y_G}]\,\mathrm{Y_{R,i+2}}^2+[(\mathrm{X_{R,i}}-\mathrm{X_G})\,\mathrm{Y_{R,i+1}}^2+(-\mathrm{X_{R,i}}+4\,\mathrm{X_{R,i+1}}-$$

$$3\,\mathrm{X_G})\,\mathrm{Y_G}^2+2(\mathrm{X_{R,i+1}}-\mathrm{X_G})\,\mathrm{X_{R,i}}^2+(\mathrm{X_{R,i+1}}^2-6\,\mathrm{X_G}\,\mathrm{X_{R,i+1}}+$$

$$5\,\mathrm{X_G}^2-r^2+p^2)\,\mathrm{X_{R,i}}-\mathrm{X_G}\,\mathrm{X_{R,i+1}}^2+2(2\,\mathrm{X_G}^2-r^2+p^2)\,\mathrm{X_{R,i+1}}-$$

$$3\,\mathrm{X_G}^3+3(r^2-p^2)\,\mathrm{X_G}]\,\mathrm{Y_{R,i+2}}+(\mathrm{X_{R,i+2}}-\mathrm{X_{R,i}})\,\mathrm{Y_G}\,\mathrm{Y_{R,i+1}}^2+$$

$$[(\mathrm{X_{R,i}}-4\,\mathrm{X_{R,i+2}}+3\,\mathrm{X_G})\,\mathrm{Y_G}^2+2(\mathrm{X_G}-\mathrm{X_{R,i+2}})\,\mathrm{X_{R,i}}^2+$$

$$(-\mathrm{X_{R,i+2}}^2+6\,\mathrm{X_G}\,\mathrm{X_{R,i+2}}-5\,\mathrm{X_G}^2+r^2-p^2)\,\mathrm{X_{R,i}}+\mathrm{X_G}\,\mathrm{X_{R,i+2}}^2+$$

$$2(-2\,\mathrm{X_G}^2+r^2-p^2)\,\mathrm{X_{R,i+2}}+3\,\mathrm{X_G}^3+3(p^2-r^2)\,\mathrm{X_G}]\,\mathrm{Y_{R,i+1}}+$$

$$3(\mathrm{X_{R,i+2}}-\mathrm{X_{R,i+1}})\,\mathrm{Y_G}^3+[2(\mathrm{X_{R,i+2}}-\mathrm{X_{R,i+1}})\,\mathrm{X_{R,i}}^2+(\mathrm{X_{R,i+2}}^2-$$

$$6\,\mathrm{X_G}\,\mathrm{X_{R,i+2}}-\mathrm{X_{R,i+1}}^2+6\,\mathrm{X_G}\,\mathrm{X_{R,i+1}})\,\mathrm{X_{R,i}}-\mathrm{X_{R,i+1}}\,\mathrm{X_{R,i+2}}^2+$$

$$(\mathrm{X_{R,i+1}}^2+3\,\mathrm{X_G}^2-3\,r^2+3\,p^2)\,\mathrm{X_{R,i+2}}+3(-\mathrm{X_G}^2+r^2-$$

$$p^2)\,\mathrm{X_{R,i+1}}]\,\mathrm{Y_G}\}/\{4[(\mathrm{X_{R,i+1}}-\mathrm{X_{R,i+2}})\,\mathrm{Y_{R,i}}+(\mathrm{X_{R,i}}-$$

$$\mathrm{X_{R,i+1}})\,\mathrm{Y_{R,i+2}}+(\mathrm{X_{R,i+2}}-\mathrm{X_{R,i}})\,\mathrm{Y_{R,i+1}}]\,(\mathrm{Z_G}-k)\} \tag{4.32}$$

Note that Variables $X_{P,i}$ and $Y_{P,i}$ are functions of X_G, Y_G, and $(Z_G - k)^2$. It was shown in section 4.3.3 that there are only eight values for each one of these quantities. Hence, only eight values for $(X_{P,i}, Y_{P,i})$ exist. The above equation for $Z_{P,i}$ can be rewritten as

$$Z_{P,i} = k + \Upsilon_1(Z_G - k) + \Upsilon_2(Z_G - k)^{-1} \tag{4.33}$$

where Υ_1 and Υ_2 are functions of (X_G, Y_G) and the coordinates of points R_1, R_2, and R_3. As a result, there are eight values for each variable Υ_1 and Υ_2. In section 4.3.3, we showed that there are eight pairs of opposite and equal values for $(Z_G - k)$. Therefore, equation (4.33) is equivalent to $Z_{P,i} = k \pm \Upsilon_3$ where eight values for Υ_3 exist. The preceeding discussion shows that there are eight pairs of (sixteen) solutions for $(X_{P,i}, Y_{P,i}, Z_{P,i})$. In each pair, one element is the mirror image of the other element with respect to the $Z = k$ plane.

4.4 Direct Kinematics of the Type 2 Minimanipulator

Figure 4.2 shows a simplified five-bar linkage driver for a Type 2 minimanipulator. Recall that θ_i and ϕ_i (driver input angles) are the angles from the positive X-axis to the vectors $\overline{D_iB_i}$ and $\overline{D_iA_i}$, respectively, measured about the positive Z-axis. D_iB_i and D_iA_i are the the input links of the driver and vector $\overline{D_iX_{i,1}}$ is parallel to the positive X-axis.

In the direct kinematics of the Type 2 minimanipulator, angles θ_i and ϕ_i (i=1,2,3) are given. The platform position and orientation are the unknowns.

Let us find the X and Y coordinates of point C_i in terms of the driver input angles. Recall that the distance from point O to each one of points D_1, D_2, and D_3 (see Figure 2.6) is equal to d. The X and Y coordinates of point D_i in the base reference frame are given by

$$X_{D,i} = d\cos\beta_i \tag{4.34}$$

$$Y_{D,i} = d\sin\beta_i \tag{4.35}$$

where

$$\beta_i = \frac{\pi}{2} + (i-1)\frac{2\pi}{3} \tag{4.36}$$

As shown in Figure 4.2, let the angle from the positive X-axis to vector

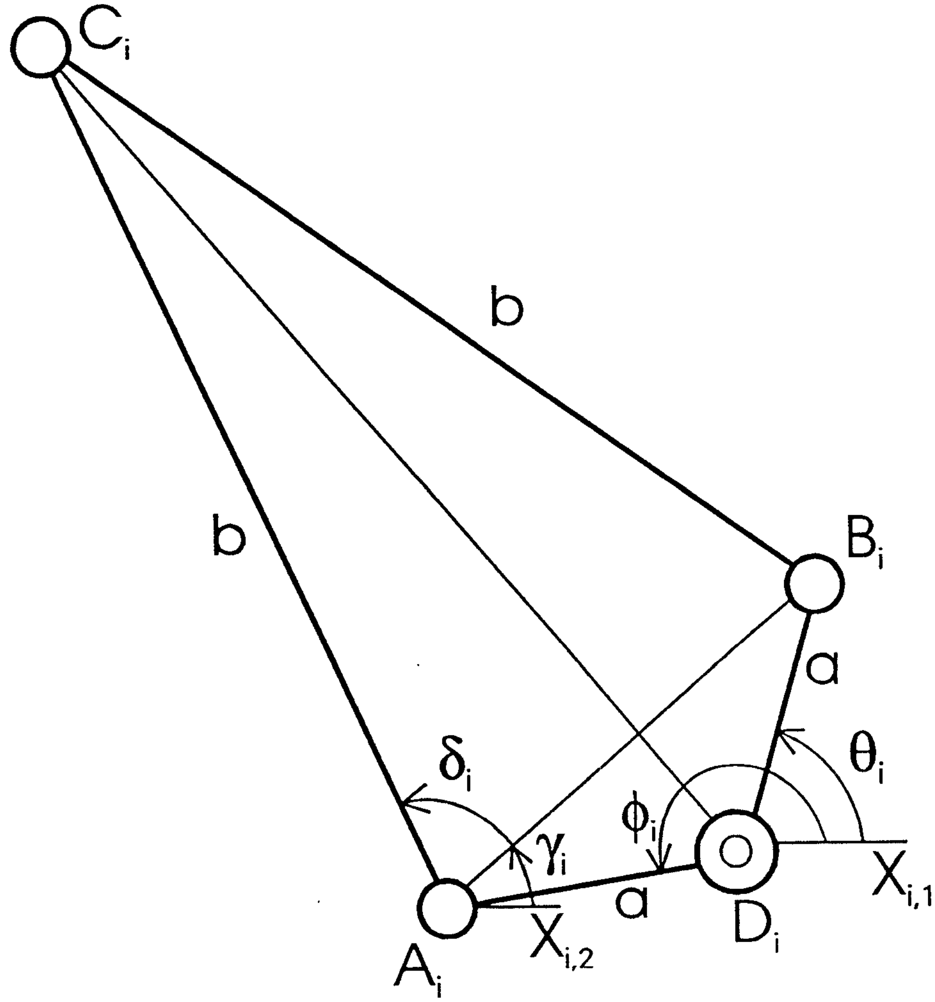

Figure 4.2: Depiction of angles $\theta_i, \phi_i, \gamma_i$, and δ_i.

$\overline{A_iB_i}$ measured about the positive Z-axis be equal to γ_i. Then

$$\gamma_i = Atan2(\sin\theta_i - \sin\phi_i, \cos\theta_i - \cos\phi_i) \tag{4.37}$$

where $Atan2$ is a single-valued function which calculates arc tangent of $(\sin\theta_i - \sin\phi_i)/(\cos\theta_i - \cos\phi_i)$ but uses the signs of both $(\sin\theta_i - \sin\phi_i)$ and $(\cos\theta_i - \cos\phi_i)$ to determine the quadrant in which γ_i lies. In addition, let the angle from vector $\overline{A_iB_i}$ to vector $\overline{A_iC_i}$ measured about the positive Z-axis be equal to δ_i. Then

$$\delta_i = \pm\left|\cos^{-1}\frac{\sqrt{2a^2 - 2a^2\cos(\phi_i - \theta_i)}}{2b}\right| \tag{4.38}$$

Note that vector $\overline{A_iX_{i,2}}$ is parallel to the positive X-axis in Figure 4.2. The X and Y coordinates of a driver output point C_i can be found from the following equations.

$$X_{C,i} = X_{D,i} + a\cos\phi_i + b\cos(\gamma_i + \delta_i) \tag{4.39}$$

$$Y_{C,i} = Y_{D,i} + a\sin\phi_i + b\sin(\gamma_i + \delta_i) \tag{4.40}$$

The above expressions for X and Y coordinates of C_i are similar to those presented by Bajpai and Roth (1986). Mathematically, there are two solutions for each output point C_i. However, only one of these solutions is feasible. The other solution can be obtained only if the simplified five-bar driver is disassembled and reassembled. A simple algorithm can be developed to determine the feasible solution for any given input angles.

The rest of direct kinematics of the Type 2 minimanipulator is identical to direct kinematics of the Type 1 minimanipulator (see section 4.3).

4.5 Numerical Example

In this example, the above procedure is used to determine the coordinates of points P_1, P_2, and P_3 for a given set of driver input angles of a Type 2 minimanipulator. The home (reference) configuration defined in section 3.3 is used in this example.

Let the minimanipulator dimensions be

$$a = 1, b = 2, d = 1.443, p = 3.175, r = 5, k = 0.125$$

In addition, let the driver input angles (in degrees) be

$$\theta_1 = 90.0, \theta_2 = 70.0, \theta_3 = 300.0$$

$$\phi_1 = 210.0, \phi_2 = 170.0, \phi_3 = 60.0$$

Then, equation (4.16) reduces to

$$t_1^{16} - 35.9507t_1^{14} + 700.3896t_1^{12} - 6635.7398t_1^{10} + 21284.2651t_1^8 - 50544.2635t_1^6 + 387426.1233t_1^4 + 524669.7298t_1^2 + 226.9895 = 0 \tag{4.41}$$

The sixteen solutions for t_1 are

$$\pm \mathrm{i}2.02797,\ \pm \mathrm{i}1.8918,\ \pm 1.6923,\ \pm 1.691,\ \pm 2.7575,\ \pm 2.8221,$$

$$3.6273 \pm \mathrm{i}2.0096,\ -3.6273 \pm \mathrm{i}2.0096$$

where $\mathrm{i}=\sqrt{-1}$. The eight real solutions yield the values shown in Tables 4.1 and 4.2 for angles η_1, η_2, and η_3 (in degrees) and the coordinates of points G, P_1, P_2, and P_3. The results of the numerical example have been verified by performing an inverse kinematics analysis. Note that pairs of solutions for point P_i are symmetric with respect to the $Z = 0.125$ plane, as predicted.

No.	1	2	3	4
η_1	118.8422	-118.8422	118.8016	-118.8016
η_2	119.7530	-119.7530	119.7972	-119.7972
η_3	55.0319	-55.0319	-156.8897	156.8897
X_G	-1.8203	-1.8203	1.5689	1.5689
Y_G	1.6418	1.6418	0.1605	0.1605
Z_G	4.4640	-4.2140	1.2035	-0.9535
$X_{P,1}$	-2.0971	-2.0971	2.9905	2.9905
$Y_{P,1}$	4.8017	4.8017	2.5909	2.5909
$Z_{P,1}$	4.6104	-4.3604	-0.2647	0.5147
$X_{P,2}$	-4.4205	-4.4205	0.6697	0.6697
$Y_{P,2}$	-0.1808	-0.1808	-2.3918	-2.3918
$Z_{P,2}$	4.4473	-4.1973	-0.4580	0.7080
$X_{P,3}$	1.0569	1.0569	1.0464	1.0464
$Y_{P,3}$	0.3044	0.3044	0.2824	0.2824
$Z_{P,3}$	4.3342	-4.0842	4.3333	-4.0833

Table 4.1: First four real solutions of the direct kinematics sample problem.

No.	5	6	7	8
η_1	140.1345	-140.1345	140.9769	-140.9769
η_2	142.3654	-142.3654	141.7002	-141.7002
η_3	44.1586	-44.1586	-140.1406	140.1406
X_G	-2.8656	-2.8656	0.5987	0.5987
Y_G	1.9494	1.9494	0.6790	0.6790
Z_G	3.2128	-2.9628	0.2659	-0.0159
$X_{P,1}$	-5.4744	-5.4744	-0.3373	-0.3373
$Y_{P,1}$	0.1892	0.1892	-1.8827	-1.8827
$Z_{P,1}$	2.7899	-2.5399	-1.3606	1.6106
$X_{P,2}$	-3.1036	-3.1036	2.0231	2.0231
$Y_{P,2}$	5.1058	5.1058	3.0836	3.0836
$Z_{P,2}$	3.4648	-3.2148	-1.2414	1.4914
$X_{P,3}$	-0.0187	-0.0187	0.1103	0.1103
$Y_{P,3}$	0.5531	0.5531	0.8359	0.8359
$Z_{P,3}$	3.3837	-3.1337	3.3996	-3.1496

Table 4.2: Last four real solutions of the direct kinematics sample problem.

Chapter 5

Jacobian Analysis

5.1 Introduction

For a serial manipulator, the Jacobian matrix is generally defined as the transformation which maps the joint rates into the Cartesian velocities (e.g., Waldron et al., 1985). In addition to singularity analysis, the Jacobian matrix has been used in defining various performance indices for serial manipulators (e.g., Salisbury and Craig, 1982; Yoshikawa, 1985; Klein and Blaho, 1987; Lee et al., 1991).

Due to dualities between parallel and serial manipulators (Waldron and Hunt, 1987), the Jacobian matrix for a parallel manipulator is generally defined as the transformation which maps the Cartesian velocities to joint rates. Gosselin and Angeles (1988, 1989) considered isotropy of the Jacobian matrix for the design optimization of planar and spherical three-DOF parallel manipulators. Arai et al. (1990) also used the Jacobian matrix in the optimal design of a six-DOF parallel manipulator. Mohamed and Duffy (1985) used the screw theory to formulate the Jacobian matrix of parallel manipulators.

In this chapter, expressions for the Jacobian matrices of the Type 1 and Type 2 minimanipulators (see section 2.3, page 21) are derived. The results are used later in formulating the stiffness matrices of the minimanipulators, determining singularities, and establishing design guidelines.

5.2 Jacobian Matrix of the Type 1 Minimanipulator

The fixed reference frame (XYZ) and the moving reference frame (UVW) are defined in section 3.2. The fixed reference frame (XYZ) is shown in Figures 2.6 and 3.2. The moving (or platform) reference frame is shown in Figure 3.1.

In this chapter, without loss of generality, we let $Z_{R,i} = 0$. If $Z_{R,i} > 0$ for a minimanipulator, a simple transformation should be applied to the coordinates of the points used in the following derivations.

Referring to Figure 5.1, we can write the following vector equation

$$\overline{OR_i} = \overline{OG} + \overline{GP_i} + \overline{P_iR_i} \tag{5.1}$$

Taking the time derivative of both sides of equation (5.1) with respect to the fixed reference frame yields

$${}^{B}\overline{V}^{R_i} = {}^{B}\overline{V}^{G} + {}^{B}\overline{\omega}^{P} \times \overline{GP_i} + {}^{B}\overline{\omega}^{L_i} \times \overline{P_iR_i} \tag{5.2}$$

where $\overline{V}$ and $\overline{\omega}$ denote linear and angular velocities, respectively. The right

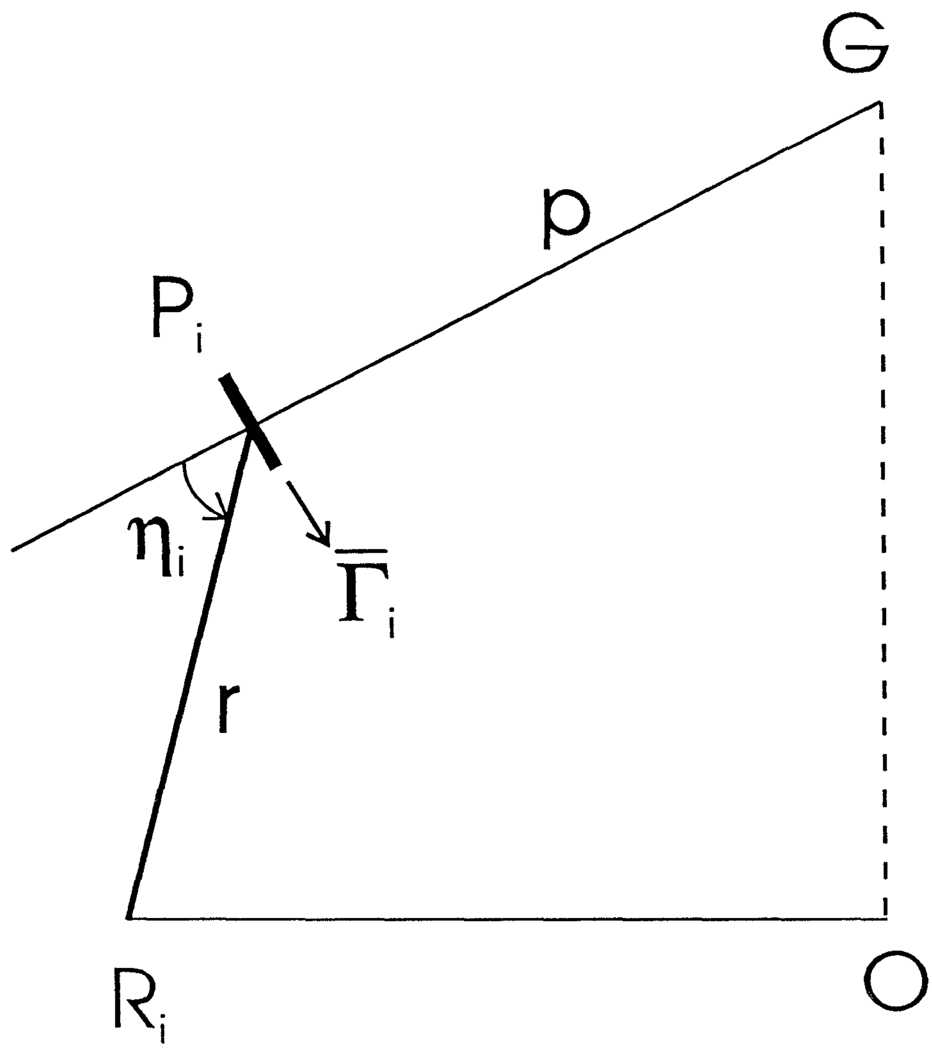

Figure 5.1: Parameters used in Jacobian analysis.

superscript for a velocity vector stands for a point or a rigid body, whereas the left superscript refers to a reference frame in which the velocity is expressed. The base, the platform, and limb $\overline{P_iR_i}$ reference frames (rigid bodies) are denoted by B, P, and L_i, respectively. The terms rigid body and reference frame are used interchangeably, because every rigid body can be used as a reference frame and every reference frame can be viewed as a massless rigid body (Kane and Levinson, 1985). Angular velocity of limb $\overline{P_iR_i}$ in the fixed reference frame can be found from

$$ {}^{B}\overline{\omega}^{L_i} = {}^{P}\overline{\omega}^{L_i} + {}^{B}\overline{\omega}^{P} \tag{5.3} $$

As shown in Figure 5.1, let η_i be the angle from vector $\overline{GP_i}$ to vector $\overline{P_iR_i}$ measured about the unit vector $\overline{\Gamma}_i$ which is collinear with the axis of the revolute joint at point P_i and points in the direction of vector $\overline{P_{i+2}P_{i+1}}$. [1] then, equation (5.3) can be converted to

$$ {}^{B}\overline{\omega}^{L_i} = \dot{\eta}_i\overline{\Gamma}_i + {}^{B}\overline{\omega}^{P} \tag{5.4} $$

where $\dot{\eta}_i$ is the time-derivative of η_i. Substituting equation (5.4) into equation (5.2), we obtain

$$ {}^{B}\overline{V}^{R_i} = {}^{B}\overline{V}^{G} + {}^{B}\overline{\omega}^{P} \times \overline{GP_i} + (\dot{\eta}_i\overline{\Gamma}_i + {}^{B}\overline{\omega}^{P}) \times \overline{P_iR_i} \tag{5.5} $$

or

$$ {}^{B}\overline{V}^{R_i} = {}^{B}\overline{V}^{G} + {}^{B}\overline{\omega}^{P} \times \overline{GR_i} + \dot{\eta}_i\overline{\Gamma}_i \times \overline{P_iR_i} \tag{5.6} $$

The Z-component of ${}^{B}\overline{V}^{R_i}$ is equal to zero. Therefore, we can conclude from the

[1]The subscripts are cyclic. If $i = 2$, $i+2$ represents 1. If $i = 3$, $i+1$ and $i+2$ represent 1 and 2, respectively.

above equation that

$$\dot{\eta}_i = -\frac{{}^B\overline{V}^G \cdot \bar{n}_z + ({}^B\overline{\omega}^P \times \overline{GR_i}) \cdot \bar{n}_z}{(\overline{\Gamma}_i \times \overline{P_iR_i}) \cdot \bar{n}_z} \tag{5.7}$$

where $\bar{n}_z$ is a unit vector in the Z-direction. Let

$$\overline{\mu}_i = \overline{\Gamma}_i \times \overline{P_iR_i} \tag{5.8}$$

then, equation (5.7) reduces to

$$\dot{\eta}_i = -\frac{\bar{n}_z \cdot {}^B\overline{V}^G + (\overline{GR_i} \times \bar{n}_z) \cdot {}^B\overline{\omega}^P}{\mu_{i,z}} \tag{5.9}$$

where $\mu_{i,z}$ is the Z-component of the vector $\overline{\mu}_i$. Also, let

$$\mu'_{i,x} = \frac{\mu_{i,x}}{\mu_{i,z}}$$

and

$$\mu'_{i,y} = \frac{\mu_{i,y}}{\mu_{i,z}}$$

where $\mu_{i,x}$ and $\mu_{i,y}$ are the X and Y-components of vector $\overline{\mu}_i$, respectively. Substituting equation (5.9) into equation (5.6), and solving for the X-component of the resulting equation, we obtain

$${}^BV_x^{R_i} = (\bar{n}_x - \mu'_{i,x}\bar{n}_z) \cdot {}^B\overline{V}^G + [(\overline{GR_i} \times \bar{n}_x) - \mu'_{i,x}(\overline{GR_i} \times \bar{n}_z)] \cdot {}^B\overline{\omega}^P \tag{5.10}$$

where ${}^BV_x^{R_i}$ is the X-component of vector ${}^B\overline{V}^{R_i}$ and $\bar{n}_x$ is a unit vector in the X-direction. Similarly, we can obtain the following equation

$${}^BV_y^{R_i} = (\bar{n}_y - \mu'_{i,y}\bar{n}_z) \cdot {}^B\overline{V}^G + [(\overline{GR_i} \times \bar{n}_y) - \mu'_{i,y}(\overline{GR_i} \times \bar{n}_z)] \cdot {}^B\overline{\omega}^P \tag{5.11}$$

where ${}^BV_y^{R_i}$ is the Y-component of vector ${}^B\overline{V}^{R_i}$ and $\bar{n}_y$ is a unit vector in the Y-direction.

Let us define the 6×1 generalized velocity vector of the platform ($\dot{\bar{x}}$) as

$$\dot{\bar{x}} = \begin{bmatrix} {}^{B}\overline{V}^{G} \\ \\ {}^{B}\overline{\omega}^{P} \end{bmatrix} \tag{5.12}$$

If the 6×1 vector of velocity components at the lower ends of the limbs ($\dot{\bar{q}}$) is given by

$$\dot{\bar{q}} = [{}^{B}\overline{V}_{x}^{R_1},\ {}^{B}\overline{V}_{y}^{R_1},\ {}^{B}\overline{V}_{x}^{R_2},\ {}^{B}\overline{V}_{y}^{R_2},\ {}^{B}\overline{V}_{x}^{R_3},\ {}^{B}\overline{V}_{y}^{R_3}]^{T} \tag{5.13}$$

then, we can define the 6×6 Jacobian matrix ($\mathbf{J}$) by

$$\dot{\bar{q}} = \mathbf{J}\dot{\bar{x}} \tag{5.14}$$

Referring to equations (5.10) and (5.11), we can express the Jacobian matrix as

$$\mathbf{J} = \begin{bmatrix} (\bar{n}_x - \mu'_{1,x}\bar{n}_z)^T & [(\overline{GR_1} \times \bar{n}_x) - \mu'_{1,x}(\overline{GR_1} \times \bar{n}_z)]^T \\ (\bar{n}_y - \mu'_{1,y}\bar{n}_z)^T & [(\overline{GR_1} \times \bar{n}_y) - \mu'_{1,y}(\overline{GR_1} \times \bar{n}_z)]^T \\ (\bar{n}_x - \mu'_{2,x}\bar{n}_z)^T & [(\overline{GR_2} \times \bar{n}_x) - \mu'_{2,x}(\overline{GR_2} \times \bar{n}_z)]^T \\ (\bar{n}_y - \mu'_{2,y}\bar{n}_z)^T & [(\overline{GR_2} \times \bar{n}_y) - \mu'_{2,y}(\overline{GR_2} \times \bar{n}_z)]^T \\ (\bar{n}_x - \mu'_{3,x}\bar{n}_z)^T & [(\overline{GR_3} \times \bar{n}_x) - \mu'_{3,x}(\overline{GR_3} \times \bar{n}_z)]^T \\ (\bar{n}_y - \mu'_{3,y}\bar{n}_z)^T & [(\overline{GR_3} \times \bar{n}_y) - \mu'_{3,y}(\overline{GR_3} \times \bar{n}_z)]^T \end{bmatrix} \tag{5.15}$$

where superscript T denotes transpose. Expanding equation (5.15), we get

$$\mathbf{J} = \begin{bmatrix} 1 & 0 & -\mu'_{1,x} & -\mu'_{1,x}\,(\mathrm{Y_{R,1}} - \mathrm{Y_G}) & -\mathrm{Z_G} - \mu'_{1,x}\,(\mathrm{X_G} - \mathrm{X_{R,1}}) & \mathrm{Y_G} - \mathrm{Y_{R,1}} \\ 0 & 1 & -\mu'_{1,y} & \mathrm{Z_G} - \mu'_{1,y}\,(\mathrm{Y_{R,1}} - \mathrm{Y_G}) & -\mu'_{1,y}\,(\mathrm{X_G} - \mathrm{X_{R,1}}) & \mathrm{X_{R,1}} - \mathrm{X_G} \\ 1 & 0 & -\mu'_{2,x} & -\mu'_{2,x}\,(\mathrm{Y_{R,2}} - \mathrm{Y_G}) & -\mathrm{Z_G} - \mu'_{2,x}\,(\mathrm{X_G} - \mathrm{X_{R,2}}) & \mathrm{Y_G} - \mathrm{Y_{R,2}} \\ 0 & 1 & -\mu'_{2,y} & \mathrm{Z_G} - \mu'_{2,y}\,(\mathrm{Y_{R,2}} - \mathrm{Y_G}) & -\mu'_{2,y}\,(\mathrm{X_G} - \mathrm{X_{R,2}}) & \mathrm{X_{R,2}} - \mathrm{X_G} \\ 1 & 0 & -\mu'_{3,x} & -\mu'_{3,x}\,(\mathrm{Y_{R,3}} - \mathrm{Y_G}) & -\mathrm{Z_G} - \mu'_{3,x}\,(\mathrm{X_G} - \mathrm{X_{R,3}}) & \mathrm{Y_G} - \mathrm{Y_{R,3}} \\ 0 & 1 & -\mu'_{3,y} & \mathrm{Z_G} - \mu'_{3,y}\,(\mathrm{Y_{R,3}} - \mathrm{Y_G}) & -\mu'_{3,y}\,(\mathrm{X_G} - \mathrm{X_{R,3}}) & \mathrm{X_{R,3}} - \mathrm{X_G} \end{bmatrix} \tag{5.16}$$

where $(X_{R,i}, Y_{R,i})$ are the (X, Y) coordinates of point R_i and (X_G, Y_G, Z_G) are the coordinates of point G. The Jacobian matrix is a function of the minimanipulator configuration and dimensions.

5.2.1 Dimensionally-Uniform Jacobian Matrix

As shown in equation (5.12), the first three elements of $\dot{\bar{x}}$ have the dimension of length/time, whereas the last three elements of $\dot{\bar{x}}$ have the dimension of radian/time. As a result, as shown in equation (5.16), elements of the first three columns of $\mathbf{J}$ are dimensionless, whereas elements of the last three columns of $\mathbf{J}$ have the dimension of length.

In this section, we define a dimensionally-uniform generalized velocity vector for the platform in order to obtain a dimensionally-uniform Jacobian matrix. The result will be used in section 6.2.1 to obtain a dimensionally-uniform stiffness matrix, which can be diagonalized by means of a principal axis transformation.

Let $\dot{\tilde{x}}$ be a dimensionally-uniform generalized velocity vector for the platform, whose elements have the dimension of length/s. We define vector $\dot{\tilde{x}}$ as

$$\dot{\tilde{x}} = \mathbf{W_v}\dot{\bar{x}} \tag{5.17}$$

where $\mathbf{W_v}$ is a 6×6 diagonal, positive definite, weighting matrix given by

$$\mathbf{W_v} = diag(1,\ 1,\ 1,\ L,\ L,\ L) \tag{5.18}$$

In equation (5.18), L is a parameter which has the dimension of length (e.g., p). Solving equation (5.17) for $\dot{\bar{x}}$ and substituting the result into equation (5.14), we obtain

$$\dot{\tilde{q}} = \tilde{\mathbf{J}}\dot{\tilde{x}} \tag{5.19}$$

where $\tilde{\mathbf{J}}$ is a dimensionally-uniform Jacobian matrix, which is given by

$$\tilde{\mathbf{J}} = \mathbf{J}\mathbf{W_v}^{-1} \tag{5.20}$$

The elements of $\tilde{\mathbf{J}}$ are all dimensionless.

5.3 Jacobian Matrix of the Type 2 Minimanipulator

Figure 5.2 shows a simplified five-bar driver. Let θ_i and ϕ_i (driver input angles) be the angles from the positive X-axis to the vectors $\overline{D_iB_i}$ and $\overline{D_iA_i}$, respectively, measured about the positive Z-axis. D_iB_i and D_iA_i are the input links of the driver and vector $\overline{D_iX_{i,1}}$ is parallel to the positive X-axis. In the following analysis, we assume that $\phi_i \geq \theta_i$ (if $\phi_i < \theta_i$, 360 degrees is added to ϕ_i). In addition, only one branch of a driver is considered, because the other branch can be realized only by disassembling and reassembling the driver. From the driver geometry, we can write

$$\left|\overline{D_iC_i}\right| = a\cos\xi_i + b\cos\vartheta_i \tag{5.21}$$

where ξ_i is the angle of line D_iC_i with line D_iB_i or line D_iA_i and ϑ_i is the angle of line C_iD_i with line C_iB_i or line C_iA_i. Applying the law of sines to the triangle $D_iA_iC_i$, we get

$$\frac{\sin\vartheta_i}{a} = \frac{\sin\xi_i}{b} \tag{5.22}$$

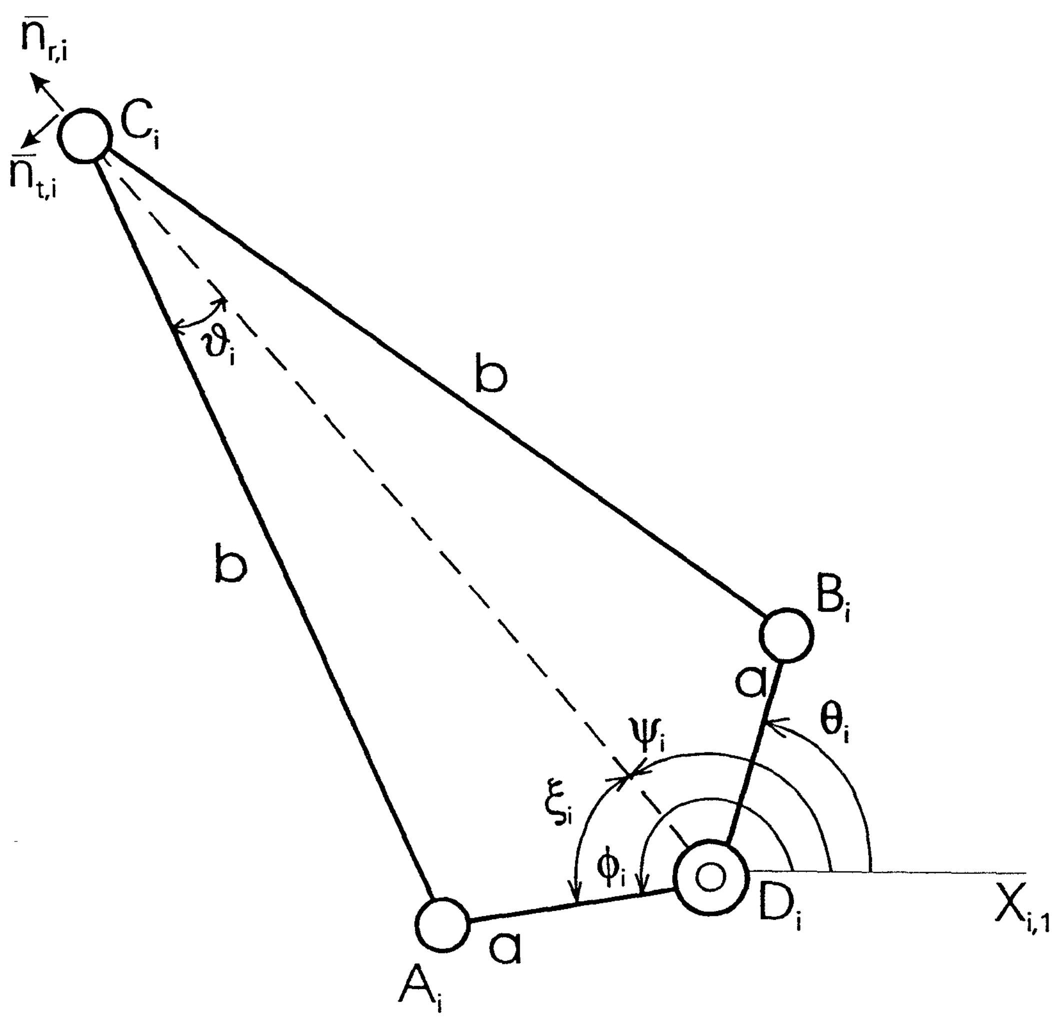

Figure 5.2: Parameters used in velocity analysis of drivers.

or

$$\cos\vartheta_i = \sqrt{1 - \left(\frac{a}{b}\right)^2 \sin^2\xi_i} \tag{5.23}$$

From equations (5.21) and (5.23), we conclude that

$$\overline{D_iC_i} = \left[a\cos\xi_i + b\sqrt{1 - \left(\frac{a}{b}\right)^2 \sin^2\xi_i}\right] \bar{n}_{r,i} \tag{5.24}$$

where $\bar{n}_{r,i}$ is a unit vector in the direction of vector $\overline{D_iC_i}$.

Let ψ_i be the angle from the positive X-axis to the vector $\overline{D_iC_i}$, measured about the positive Z-axis. Also, as shown in Figure 5.2, let the unit vector $\bar{n}_{t,i}$ be at 90 degrees to the unit vector $\bar{n}_{r,i}$, measured about the positive Z-axis. Taking the time-derivative of both sides of equation (5.24), with respect to the fixed reference frame, we obtain

$$\begin{bmatrix} {}^BV_r^{C_i} \\ {}^BV_t^{C_i} \end{bmatrix} = \mathbf{\Delta}^{(i)} \begin{bmatrix} \dot{\xi}_i \\ \dot{\psi}_i \end{bmatrix} \tag{5.25}$$

where $\mathbf{\Delta}^{(i)}$ is a 2×2 diagonal matrix whose diagonal elements are given by

$$\Delta_{1,1}^{(i)} = -b\left[\left(\frac{a}{b}\right)\sin\xi_i + \left(\frac{a}{b}\right)^2 \frac{\sin\xi_i\cos\xi_i}{\sqrt{1 - \left(\frac{a}{b}\right)^2\sin^2\xi_i}}\right] \tag{5.26}$$

$$\Delta_{2,2}^{(i)} = b\left[\left(\frac{a}{b}\right)\cos\xi_i + \sqrt{1 - \left(\frac{a}{b}\right)^2 \sin^2\xi_i}\right] \tag{5.27}$$

and $({}^BV_r^{C_i}, {}^BV_t^{C_i})$ are the radial (in the $\bar{n}_{r,i}$ direction) and tangential (in the $\bar{n}_{t,i}$ direction) components of the velocity of point C_i. In addition, $\dot{\xi}_i$ and $\dot{\psi}_i$ denote time-derivatives of angles ξ_i and ψ_i, respectively. Note that $\dot{\xi}_i$ and $\dot{\psi}_i$ are related to the input speeds ($\dot{\theta}_i$ and $\dot{\phi}_i$) by the following linear relationships.

$$\dot{\psi}_i = \frac{\dot{\phi}_i + \dot{\theta}_i}{2} \tag{5.28}$$

$$\dot{\xi}_i = \frac{\dot{\phi}_i - \dot{\theta}_i}{2} \tag{5.29}$$

Equations (5.25) - (5.29) show that for a given b, the smaller the ratio a/b, the higher the speed reduction (mechanical advantage) of the driver in the radial direction.

Substituting equations (5.28) and (5.29) into equation (5.25), we obtain

$$\frac{1}{2}\begin{bmatrix} \dot{\phi}_i - \dot{\theta}_i \\ \dot{\phi}_i + \dot{\theta}_i \end{bmatrix} = \begin{bmatrix} \frac{1}{\Delta^{(i)}_{1.1}} & 0 \\ 0 & \frac{1}{\Delta^{(i)}_{2.2}} \end{bmatrix} \begin{bmatrix} {}^B V_r^{C_i} \\ {}^B V_t^{C_i} \end{bmatrix} \tag{5.30}$$

Manipulation the above equation, we obtain

$$\begin{bmatrix} \dot{\theta}_i \\ \dot{\phi}_i \end{bmatrix} = \begin{bmatrix} -\frac{1}{\Delta^{(i)}_{1.1}} & \frac{1}{\Delta^{(i)}_{2.2}} \\ \frac{1}{\Delta^{(i)}_{1.1}} & \frac{1}{\Delta^{(i)}_{2.2}} \end{bmatrix} \begin{bmatrix} {}^B V_r^{C_i} \\ {}^B V_t^{C_i} \end{bmatrix} \tag{5.31}$$

We can also write

$$\begin{bmatrix} {}^B V_r^{C_i} \\ {}^B V_t^{C_i} \end{bmatrix} = \begin{bmatrix} C\psi_i & S\psi_i \\ -S\psi_i & C\psi_i \end{bmatrix} \begin{bmatrix} {}^B V_x^{C_i} \\ {}^B V_y^{C_i} \end{bmatrix} \tag{5.32}$$

where $({}^B V_x^{C_i},\ {}^B V_y^{C_i})$ are the components of the velocity of point C_i in the X and Y directions, respectively; $C\psi_i = \cos\psi_i$; and $S\psi_i = \sin\psi_i$. Equations (5.31) and (5.32) imply that

$$\begin{bmatrix} \dot{\theta}_i \\ \dot{\phi}_i \end{bmatrix} = \mathbf{J_d}^{(i)} \begin{bmatrix} {}^B V_x^{C_i} \\ {}^B V_y^{C_i} \end{bmatrix} \tag{5.33}$$

where

$$\mathbf{J_d}^{(i)} = \begin{bmatrix} -\frac{C\psi_i}{\Delta^{(i)}_{1.1}} - \frac{S\psi_i}{\Delta^{(i)}_{2.2}} & -\frac{S\psi_i}{\Delta^{(i)}_{1.1}} + \frac{C\psi_i}{\Delta^{(i)}_{2.2}} \\ \frac{C\psi_i}{\Delta^{(i)}_{1.1}} - \frac{S\psi_i}{\Delta^{(i)}_{2.2}} & \frac{S\psi_i}{\Delta^{(i)}_{1.1}} + \frac{C\psi_i}{\Delta^{(i)}_{2.2}} \end{bmatrix} \tag{5.34}$$

Let $\dot{\vec{\theta}}$ be the 6×1 vector of input joint rates, i.e.

$$\dot{\vec{\theta}} = [\dot{\theta}_1,\ \dot{\phi}_1,\ \dot{\theta}_2,\ \dot{\phi}_2,\ \dot{\theta}_3,\ \dot{\phi}_3]^T \tag{5.35}$$

Since ${}^{B}V_{x}^{R_i} = {}^{B}V_{x}^{C_i}$ and ${}^{B}V_{y}^{R_i} = {}^{B}V_{y}^{C_i}$, we can write

$$\dot{\bar{\theta}} = \mathbf{J_d}\dot{\bar{q}} \tag{5.36}$$

where $\dot{\bar{q}}$ is defined in equation (5.13) and $\mathbf{J_d}$ is the 6×6 Jacobian for the drivers which is given by

$$\mathbf{J_d} = \begin{bmatrix} \mathbf{J_d}^{(1)} & & \mathbf{0} \\ & \mathbf{J_d}^{(2)} & \\ \mathbf{0} & & \mathbf{J_d}^{(3)} \end{bmatrix} \tag{5.37}$$

The overall Jacobian for a Type 2 minimanipulator ($\widehat{\mathbf{J}}$) is defined by

$$\dot{\bar{\theta}} = \widehat{\mathbf{J}}\dot{\bar{x}} \tag{5.38}$$

where $\dot{\bar{x}}$ is defined in equation (5.12). Referring to equations (5.14) and (5.36), we can see that

$$\widehat{\mathbf{J}} = \mathbf{J_d}\mathbf{J} \tag{5.39}$$

where $\mathbf{J}$, which can be found from equation (5.15), represents the Jacobian for the primary portion (platform and limbs) of the minimanipulator.

5.3.1 Dimensionally-Uniform Jacobian Matrix

Elements of the first three columns of $\widehat{\mathbf{J}}$ have the dimension of $(\text{length})^{-1}$, whereas elements of the last three columns of $\widehat{\mathbf{J}}$ are dimensionless.

Following the same procedure used in section 5.2.1, we can obtain

$$\dot{\bar{\theta}} = \grave{\mathbf{J}}\dot{\bar{x}} \tag{5.40}$$

where $\grave{\mathbf{J}}$ is a dimensionally-uniform Jacobian matrix for the Type 2 minimanipulator. All of the elements of $\grave{\mathbf{J}}$ have the dimension of $(\text{length})^{-1}$. Matrices $\grave{\mathbf{J}}$ and $\widehat{\mathbf{J}}$ are related by

$$\grave{\mathbf{J}} = \widehat{\mathbf{J}}\mathbf{W_v}^{-1} \tag{5.41}$$

Results of this section are used in Chapter 9 to establish guidelines for design of the simplified five-bar drivers of the Type 2 minimanipulator.

Chapter 6

Stiffness Analysis

6.1 Introduction

The stiffness matrix of a manipulator is generally defined as the transformation which relates the generalized force (force and torque) applied to the end-effector and its resulting displacement (Asade and Slotine, 1986). In a parallel manipulator, the platform plays the role of the end-effector. Stiffness matrices of parallel manipulators, which are closely related to their Jacobian matrices, have been studied by Kerr (1989) and Gosselin (1990a).

In this chapter, the results of the previous chapter are used to formulate the stiffness matrices of the Type 1 and Type 2 minimanipulators (see section 2.3, page 21).

6.2 Stiffness Matrix of the Type 1 Minimanipulator

From equation (5.14), we can conclude that

$$\overline{\delta q} = \mathbf{J}\overline{\delta x} \tag{6.1}$$

where $\overline{\delta q}$ and $\overline{\delta x}$ represent infinitesimal displacements at the lower ends of the limbs and at the center of the platform, respectively. Equation (5.14) and the principle of virtual work can be used to derive the following equation (Asada and Slotine, 1986).

$$\overline{\mathcal{F}} = \mathbf{J}^T\overline{f} \tag{6.2}$$

where

$$\overline{\mathcal{F}} = \begin{bmatrix} \overline{F}_P \\ \overline{M}_P \end{bmatrix} \tag{6.3}$$

and

$$\overline{f} = [f_{1,x},\ \ f_{1,y},\ \ f_{2,x},\ \ f_{2,y},\ \ f_{3,x},\ \ f_{3,y}]^T \tag{6.4}$$

Vectors $\overline{F}_P$ and $\overline{M}_P$ in equation (6.3) represent the force and moment applied to the platform. Also, $f_{i,x}$ and $f_{i,y}$ in equation (6.4) are the X and Y-components of the actuator force applied at point R_i. The actuator forces and displacements at the lower ends of the limbs can be related by the following equation.

$$\overline{f} = \mathbf{k}\overline{\delta q} \tag{6.5}$$

where $\mathbf{k}$ is a 6×6 diagonal matrix whose elements have the dimension of force/length. Substituting equation (6.1) into equation (6.5) and the resulting equation into equation (6.2), yields

$$\overline{\mathcal{F}} = \mathbf{J}^T\mathbf{k}\mathbf{J}\overline{\delta x} \tag{6.6}$$

If κ represents the stiffness of each bidirectional linear stepper motor in the X and Y directions, then the diagonal elements of $\mathbf{k}$ are all equal to κ. Therefore, the stiffness matrix for the platform (K) can be expressed as

$$\mathrm{K} = \kappa\mathbf{J}^T\mathbf{J} \tag{6.7}$$

It can be shown that $\mathbf{K}$ is a symmetric, positive semidefinite matrix. Elements of the lower triangular portion of K/κ, denoted as $\check{\mathbf{K}}$, are given in Appendix D.

6.2.1 Dimensionally-Uniform Stiffness Matrix and Its Principal Axis Transformation

As mentioned in section 5.2.1, matrix $\mathbf{J}$ is not dimensionally uniform. As a result, the stiffness matrix $\mathbf{K}$, which is defined by equation (6.7), is not dimensionally uniform either.

The upper left 3×3 portion of $\mathbf{K}$ represents the direct or translatory stiffness, and consists of elements which have the dimension of force/length. The lower right 3×3 portion of K represents the torsional stiffness, and consists of elements which have the dimension of force-length. The other 3×3 portions of $\mathbf{K}$ consist of cross-coupling elements which have the dimension of force.

We can ask ourselves if $\mathbf{K}$ can be diagonalized by means of a coordinate transformation. To diagonalize the matrix $\mathbf{K}$, its eigenvalue problem should be solved. Let us examine if such an eigenvalue problem makes sense physically.

Referring to equations (6.6) and (6.7), we note that the eigenvalue problem for $\mathbf{K}$ involves solving the following equation.

$$\overline{\mathcal{F}} = \mathbf{K}\overline{\delta x} = \lambda\overline{\delta x} \tag{6.8}$$

where λ is the eigenvalue of $\mathbf{K}$. In other words, we are looking for certain directions of $\overline{\delta x}$ which are identical to the corresponding directions of $\overline{\mathcal{F}}$. The first three elements of $\overline{\mathcal{F}}$ have the dimension of force and the first three elements of $\overline{\delta x}$ have the dimension of length. Therefore, the dimension of λ has to be force/length. However, the last three elements of $\overline{\mathcal{F}}$ have the dimension of force-length and the last three elements of $\overline{\delta x}$ have the dimension of radians. As a result, the dimension of λ should also be equal to force-length. Since the dimension of λ can not be both force/length and force-length, the eigenvalue problem for $\mathbf{K}$ is dimensionally inconsistent and does not make sense physically. This is due to the fact that $\mathbf{K}$, $\overline{\mathcal{F}}$, and $\overline{\delta x}$ are not dimensionally uniform.

Let us define a dimensionally-uniform generalized force applied to the platform ($\tilde{\mathcal{F}}$) and use it in connection with the definitions of $\dot{\tilde{x}}$ and $\tilde{\mathbf{J}}$ (see section 5.2.1) to obtain a dimensionally-uniform stiffness matrix ($\widetilde{\mathbf{K}}$).

Let the elements of $\tilde{\mathcal{F}}$ have the dimension of force, and let $\tilde{\mathcal{F}}$ be defined as

$$\tilde{\mathcal{F}} = \mathbf{W_f}\overline{\mathcal{F}} \tag{6.9}$$

where $\mathbf{W_f}$ is a 6×6 diagonal, positive definite, weighting matrix given by

$$\mathbf{W_f} = diag(1,\ 1,\ 1,\ L^{-1},\ L^{-1},\ L^{-1}) \tag{6.10}$$

In equation (6.10), L is a parameter with the dimension of length (e.g., p).

Comparing equations (6.10) and (5.18), we note that

$$\mathbf{W_f W_v} = \mathbf{I} \tag{6.11}$$

where $\mathbf{I}$ is the 6×6 identity matrix. Substituting equation (6.2) into equation (6.9) yields

$$\tilde{\mathcal{F}} = \mathbf{W_f J}^T \overline{f} \tag{6.12}$$

Following the same procedure used for the derivation of equations (6.6) and (6.7) and using equation (6.11), we obtain

$$\tilde{\mathcal{F}} = \widetilde{\mathbf{K}}\widetilde{\delta x} \tag{6.13}$$

where

$$\widetilde{\mathbf{K}} = \kappa \mathbf{W_f J}^T \mathbf{J W_f} \tag{6.14}$$

Note that $\widetilde{\mathbf{K}}$ is the dimensionally-uniform stiffness matrix and $\widetilde{\delta x}$ represents the dimensionally-uniform infinitesimal displacement of the platform. The elements of $\widetilde{\delta x}$ have the dimension of length and the elements of $\widetilde{\mathbf{K}}$ have the dimension of force/length. It can be shown that $\widetilde{\mathbf{K}}$ is symmetric and positive semidefinite. Comparison of equations (6.14) and (6.7) shows that

$$\widetilde{\mathbf{K}} = \mathbf{W_f K W_f} \tag{6.15}$$

Matrix $\widetilde{\mathbf{K}}$ can be diagonalized by means of a principal axis transformation. Since $\widetilde{\mathbf{K}}$ is symmetric, it has a complete set of orthonormal eigenvectors (Strang, 1988). Let $\mathbf{E}$ be an orthogonal matrix whose columns represent orthonormal eigenvalues of $\widetilde{\mathbf{K}}$. Also, let Λ be a diagonal matrix, with the eigenvalues of $\widetilde{\mathbf{K}}$ along its diagonal. Then,

$$\widetilde{\mathbf{K}} = \mathbf{E}\Lambda\mathbf{E}^T \tag{6.16}$$

Substituting equation (6.16) into equation (6.13), and modifying the resulting equation, we get

$$\mathbf{E}^T\tilde{\mathcal{F}} = \mathbf{\Lambda}\mathbf{E}^T\widetilde{\delta x} \tag{6.17}$$

Matrix $\mathbf{E}^T$ represents the principal axis transformation and the elements of $\mathbf{E}^T\tilde{\mathcal{F}}$ point in the same directions as the corresponding elements of $\mathbf{E}^T\widetilde{\delta x}$. These directions, which are determined by the orthonormal eigenvectors, are the principal axes of $\widetilde{\mathbf{K}}$.

To gain more insight into the physical meaning of the principal axes of $\widetilde{\mathbf{K}}$, let us examine $\widetilde{\delta x}$ when a dimensionally-uniform generalized force of unit magnitude is applied to the platform, i.e.

$$\tilde{\mathcal{F}}^T\tilde{\mathcal{F}} = 1 \tag{6.18}$$

Substituting equation (6.13) into equation (6.18), we get

$$\widetilde{\delta x}^T\widetilde{\mathbf{K}}^T\widetilde{\mathbf{K}}\widetilde{\delta x} = 1 \tag{6.19}$$

Since $\widetilde{\mathbf{K}}$ is symmetric, equation (6.19) reduces to

$$\widetilde{\delta x}^T\widetilde{\mathbf{K}}^2\widetilde{\delta x} = 1 \tag{6.20}$$

Equation (6.20) represents a six-dimensional ellipsoid whose axes point along the eigenvectors of $\widetilde{\mathbf{K}}$ (principal directions). The axes lengths are $1/\lambda_1, \ldots, 1/\lambda_6$, where $\lambda_1, \ldots, \lambda_6$ are the eigenvalues of $\widetilde{\mathbf{K}}$ (Strang, 1988).[1]

[1]Note that eigenvectors of $\widetilde{\mathbf{K}}^2$ are the same as those of $\widetilde{\mathbf{K}}$ and eigenvalues of $\widetilde{\mathbf{K}}^2$ are $\lambda_1^2, \ldots, \lambda_6^2$.

6.2.2 Central Stiffness Matrix

Since $\widetilde{\mathbf{K}}$ is symmetric, its norm is equal to its largest eigenvalue. Theoretically, the norm of $\widetilde{\mathbf{K}}$ can be used to measure and/or to compare the stiffness levels of different minimanipulators. However, to find the norm of $\widetilde{\mathbf{K}}$, its eigenvalue problem, which is a sixth order polynomial, should be solved. In general, there are no analytical expressions for the solutions of such a polynomial. Also, $\widetilde{\mathbf{K}}$ is configuration-dependent. Therefore, finding the eigenvalues and the norm of $\widetilde{\mathbf{K}}$ at all of the minimanipulator configurations becomes impractical. Even if we try to use the norm of $\widetilde{\mathbf{K}}$ at a specific configuration as a measure of stiffness, no analytical expression for such a measure can be obtained. As a result, establishing design guidelines for obtaining high stiffness becomes difficult.

In what follows, we define a central configuration for the minimanipulator and study the stiffness of the minimanipulator at the central configuration. Since the minimanipulator is intended for fine manipulation around such a designated posture, the stiffness will not deviate significantly from that corresponding to the central configuration. Hence, it is important that we understand fully the minimanipulator stiffness at the central configuration.

Let us define the "central configuration" of the minimanipulator workspace as the configuration where

1. The platform is not rotated with respect to the base.
2. The centroid of triangle $P_1P_2P_3$ (platform) is directly on top of the origin of the base reference frame.

3. The platform is positioned at a designated elevation, i.e., $Z_G = \zeta$ (a design value).

Note that the central configuration defined in this section is different from the "home configuration" defined in section 3.3.

Next, the stiffness matrix at the central configuration of the minimanipulator (central stiffness matrix) will be derived. It will be shown that, if proper minimanipulator dimensions are used, the central stiffness matrix can be diagonalized (decoupled) without any coordinate transformations. The diagonalized central stiffness matrix will be used to obtain a simple measure of stiffness and to establish design guidelines for the minimanipulators. As mentioned before, a minimanipulator will be operated at or near the central configuration during most of its operations. Therefore, establishing design guidelines based on the central stiffness matrix is justified. The results of this section will also be used to compare the minimanipulator stiffness with that of the Stewart platform (see section 6.2.3).

Recall that $\left|\overline{GP_i}\right| = p$, and $Z_G = \zeta$ at the central configuration. Also, let $\left|\overline{OR_i}\right| = \nu$ at the central configuration. Using equations (5.16) and (6.7), the central stiffness matrix ($\mathbf{K}^+$) is found to be

$$\mathbf{K}^+ = 3\kappa \begin{bmatrix} 1 & 0 & 0 & 0 & \frac{(2p-\nu)\zeta}{2(\nu-p)} & 0 \\ 0 & 1 & 0 & \frac{(\nu-2p)\zeta}{2(\nu-p)} & 0 & 0 \\ 0 & 0 & \frac{\zeta^2}{(\nu-p)^2} & 0 & 0 & 0 \\ 0 & \frac{(\nu-2p)\zeta}{2(\nu-p)} & 0 & \frac{(\nu^2-2p\nu+2p^2)\zeta^2}{2(\nu-p)^2} & 0 & 0 \\ \frac{(2p-\nu)\zeta}{2(\nu-p)} & 0 & 0 & 0 & \frac{(\nu^2-2p\nu+2p^2)\zeta^2}{2(\nu-p)^2} & 0 \\ 0 & 0 & 0 & 0 & 0 & \nu^2 \end{bmatrix} \tag{6.21}$$

It is desirable to eliminate the off-diagonal terms which couple the forces (moments) applied along (about) the X and Y axes to the rotations (translations) about (along) the Y and X axes, respectively. Fortunately, this can be easily accomplished by choosing

$$p = \frac{\nu}{2} \tag{6.22}$$

as a design condition. In other words, the platform (triangle $P_1P_2P_3$) should be equal to one-half of the triangle $R_1R_2R_3$ at the central configuration. The above result is similar to that obtained by Kerr (1989) in designing a Stewart-platform-based force/torque transducer. If the condition expressed in equation (6.22) is satisfied, then

$$\zeta^2 = r^2 - p^2 \tag{6.23}$$

where r is the limb length. If equations (6.22) and (6.23) are used to substitute for ν and ζ in equation (6.21), matrix $\mathbf{K}^+$ reduces to

$$\mathbf{K}^* = 3\kappa \begin{bmatrix} 1 & & & & & \mathbf{0} \\ & 1 & & & & \\ & & (r^2 - p^2)/p^2 & & & \\ & & & r^2 - p^2 & & \\ & & & & r^2 - p^2 & \\ & \mathbf{0} & & & & 4p^2 \end{bmatrix} \tag{6.24}$$

We shall refer to matrix $\mathbf{K}^*$ as the decoupled central stiffness matrix. The first three diagonal elements of $\mathbf{K}^*$ have the dimension of force/length, whereas its last three diagonal elements have the dimension of force-length.

Using equation (6.15), and setting $L = p$ in $\mathbf{W_f}$, we obtain the following expression for the dimensionally-uniform decoupled central stiffness matrix

$$\widetilde{\mathbf{K}}^* = 3\kappa \begin{bmatrix} 1 & & & & & \mathbf{0} \\ & 1 & & & & \\ & & (r/p)^2 - 1 & & & \\ & & & (r/p)^2 - 1 & & \\ & & & & (r/p)^2 - 1 & \\ & \mathbf{0} & & & & 4 \end{bmatrix} \tag{6.25}$$

Equation (6.25) can be used to determine the relative dimensions of the mini-manipulator so that desirable characteristics are obtained.

Note that parameter ν in equation (6.22) can be determined from other design considerations such as the upper bound on the base plate size.

To move the platform in the X or Y-direction, the lower ends of all three limbs should also move in the X or Y-direction. As a result, elements $\widetilde{K}^*_{1,1}$ and $\widetilde{K}^*_{2,2}$ are constants. From the statics point of view, external forces in the X and Y directions are shared equally among the three actuators. Element $\widetilde{K}^*_{6,6}$ is also a constant. This is related to the fact that in order to rotate the platform about the Z-axis, the lower ends of the limbs should move on a circle, which passes through them, in the same direction and by an equal amount. Note that we can not increase the values of $\widetilde{K}^*_{1,1}$, $\widetilde{K}^*_{2,2}$, and $\widetilde{K}^*_{6,6}$ by changing the minimanipulator parameters r and p.

The other three non-zero elements $\widetilde{K}^*_{3,3}$, $\widetilde{K}^*_{4,4}$, and $\widetilde{K}^*_{5,5}$ are functions of minimanipulator dimensions and are equal to each other. Therefore, we can use any of these terms as the stiffness measure ($S.M.$) of the minimanipulator. Namely, we can define

$$S.M. = 3\kappa \left[\left(\frac{r}{p} \right)^2 - 1 \right] \tag{6.26}$$

The higher the value of r/p, the higher the stiffness of the minimanipulator. Another way to interpret the $S.M.$ is to note that $S.M.$ is proportional to tangent-squared of the angle between any of the limbs and the base plane at the central configuration. The closer this angle to 90 degrees, the higher the stiffness of the minimanipulator.

The first three diagonal elements of $\widetilde{\mathbf{K}}^*$ are the direct stiffness terms. Equation (6.25) shows that if $r = \sqrt{2}p$, we obtain equal direct stiffness values in the X, Y, and Z directions. At this configuration, the angle between any of the limbs and the base plane becomes equal to 45 degrees.

The last three diagonal elements of $\widetilde{\mathbf{K}}^*$ are the torsional stiffness terms.

Referring to equation (6.25), we notice that if $r = \sqrt{5}p$, we obtain equal torsional stiffness values in the X, Y, and Z directions. At this configuration, the angle between any of the limbs and the base plane becomes equal to 63.43 degrees.

6.2.3 Comparison to the Stewart Platform

In this section, the results of Kerr (1989) are used to compare the minimanipulator stiffness with that of the Stewart platform.

Duplicating Kerr's model, let us consider a Stewart platform with its linkage parameters identical to those of the minimanipulator. As shown in Figure 6.1, the six limbs connect three points on the base to three points on the platform. The three points on the platform form an equilateral triangle whose circumradius is equal to p. Similarly, The three points on the base form an equilateral triangle whose circumradius is equal to ν. Kerr (1989) showed that the stiffness matrix of the Stewart platform is decoupled, when all of the limb lengths are equal, and $p = \nu/2$. When all of the limb lengths are equal, the platform is not rotated with respect to the base, and the centroid of the platform (point G) is right on top of the centroid of the base (point O). Therefore, the conditions under which the Stewart platform has a decoupled stiffness matrix are identical to those which decouple the stiffness matrix of the minimanipulator (see section 6.2.2). When the limb lengths are equal, we refer to the common limb length as r. The axial (actuator) stiffness of each limb, κ, is taken to be the same as the stiffness of each bidirectional linear stepper motor in the X and Y directions (see section 6.2).

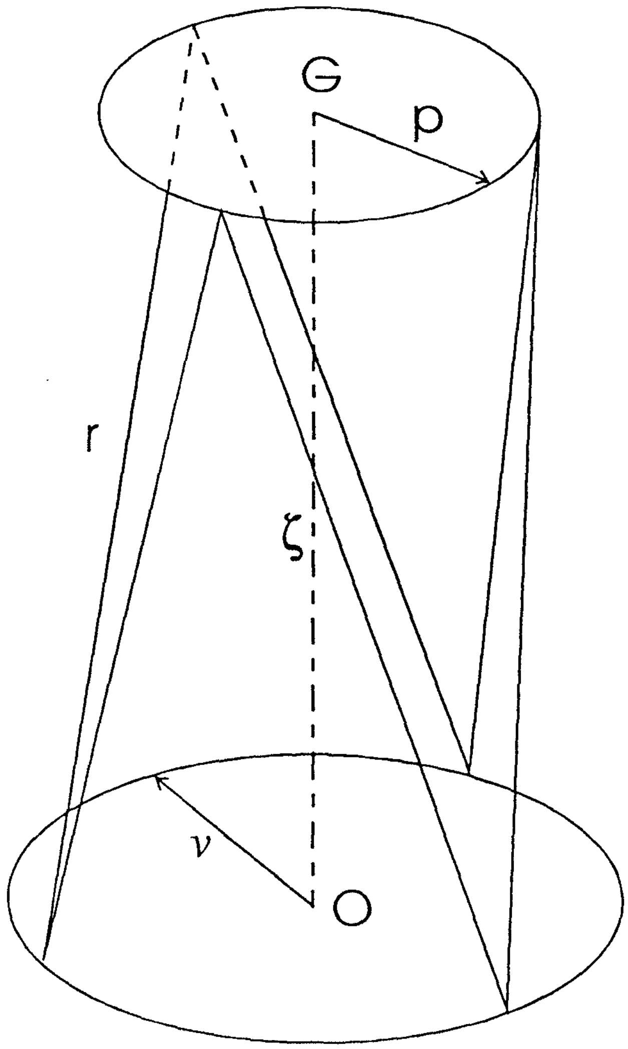

Figure 6.1: A Stewart platform configuration in which the limb lengths are equal.

Kerr's expression for the decoupled stiffness matrix ($\mathbf{K}^{\#}$) is not dimensionally uniform and its elements have the same dimensions as the corresponding elements of $\mathbf{K}^{*}$. Using the same procedure used in section 6.2.2 for obtaining $\widetilde{\mathbf{K}}^{*}$, we find the following dimensionally-uniform decoupled stiffness matrix for the Stewart platform.

$$\widetilde{\mathbf{K}}^{\#} = 3\kappa \begin{bmatrix} 3\left(\frac{p}{r}\right)^2 & & & & & \mathbf{0} \\ & 3\left(\frac{p}{r}\right)^2 & & & & \\ & & 2\left[1-3\left(\frac{p}{r}\right)^2\right] & & & \\ & & & \left[1-3\left(\frac{p}{r}\right)^2\right] & & \\ & & & & \left[1-3\left(\frac{p}{r}\right)^2\right] & \\ & & \mathbf{0} & & & 6\left(\frac{p}{r}\right)^2 \end{bmatrix} \tag{6.27}$$

The coordinate system, configuration, and parameters used for derivation of $\widetilde{\mathbf{K}}^{*}$ in section 6.2.2 are identical to those used for obtaining $\widetilde{\mathbf{K}}^{\#}$. Therefore, the diagonal elements of these two matrices can be used to compare the stiffness of the minimanipulator to that of the Stewart platform.

Equation (6.27) shows that decreasing p/r results in higher values for $\widetilde{K}^{\#}_{3,3}$, $\widetilde{K}^{\#}_{4,4}$, and $\widetilde{K}^{\#}_{5,5}$, and lower values for $\widetilde{K}^{\#}_{1,1}$, $\widetilde{K}^{\#}_{2,2}$, and $\widetilde{K}^{\#}_{6,6}$. To avoid having a negative or a zero value for any of the diagonal elements of $\widetilde{\mathbf{K}}^{\#}$, p/r should be constrained as shown below.

$$\frac{1}{\sqrt{3}} > \frac{p}{r} > 0 \tag{6.28}$$

Due to the constraints expressed in equation (6.28), the diagonal elements of $\widetilde{\mathbf{K}}^{\#}$ are bounded, as shown below.

$$\widetilde{K}^{\#}_{1,1} \quad < \quad 3\kappa \tag{6.29a}$$

$$\widetilde{K}^{\#}_{2,2} \quad < \quad 3\kappa \tag{6.29b}$$

$$\widetilde{K}^{\#}_{3,3} \quad < \quad 6\kappa \tag{6.29c}$$

$$\widetilde{K}^{\#}_{4,4} \quad < \quad 3\kappa \tag{6.29d}$$

$$\widetilde{K}^{\#}_{5,5} \quad < \quad 3\kappa \tag{6.29e}$$

$$\widetilde{K}^{\#}_{6,6} \quad < \quad 6\kappa \tag{6.29f}$$

Comparing equations (6.25) and (6.29), we note that

$$\widetilde{K}^{*}_{1,1} = 3\kappa \quad > \quad \widetilde{K}^{\#}_{1,1} \tag{6.30a}$$

$$\widetilde{K}^{*}_{2,2} = 3\kappa \quad > \quad \widetilde{K}^{\#}_{2,2} \tag{6.30b}$$

$$\widetilde{K}^{*}_{6,6} = 12\kappa \quad > \quad \widetilde{K}^{\#}_{6,6} \tag{6.30c}$$

The other three non-zero elements of $\widetilde{\mathbf{K}}^{*}$ ($\widetilde{K}^{*}_{3,3}$, $\widetilde{K}^{*}_{4,4}$, and $\widetilde{K}^{*}_{5,5}$) are all functions of r/p. Writing equation (6.28) in terms of r/p, we obtain

$$\infty > \frac{r}{p} > \sqrt{3} \tag{6.31}$$

For comparison purposes, let us apply the lower limit of r/p in equation (6.31) to $\widetilde{K}^{*}_{3,3}$, $\widetilde{K}^{*}_{4,4}$, and $\widetilde{K}^{*}_{5,5}$. We find out that

$$\widetilde{K}^{*}_{3,3} = \widetilde{K}^{*}_{4,4} = \widetilde{K}^{*}_{5,5} > 6\kappa \tag{6.32}$$

Comparing equations (6.29) and (6.32), we note the

$$\widetilde{K}^{*}_{3,3} \quad > \quad \widetilde{K}^{\#}_{3,3} \tag{6.33a}$$

$$\widetilde{K}^{*}_{4,4} \quad > \quad \widetilde{K}^{\#}_{4,4} \tag{6.33b}$$

$$\widetilde{K}^{*}_{5,5} \quad > \quad \widetilde{K}^{\#}_{5,5} \tag{6.33c}$$

r/p	1.75	2.0	2.5
$\widetilde{K}^*_{1,1} = \widetilde{K}^*_{2,2}$	3κ	3κ	3κ
$\widetilde{K}^\#_{1,1} = \widetilde{K}^\#_{2,2}$	2.9388κ	2.25κ	1.44κ
$\widetilde{K}^*_{3,3}$	6.1875κ	9κ	15.75κ
$\widetilde{K}^\#_{3,3}$	0.1224κ	1.5κ	3.12κ
$\widetilde{K}^*_{4,4} = \widetilde{K}^*_{5,5}$	6.1875κ	9κ	15.75κ
$\widetilde{K}^\#_{4,4} = \widetilde{K}^\#_{5,5}$	0.0612κ	0.75κ	1.56κ
$\widetilde{K}^*_{6,6}$	12κ	12κ	12κ
$\widetilde{K}^\#_{6,6}$	5.8776κ	4.5κ	2.88κ

Table 6.1: Sample values for the diagonal elements of $\widetilde{\mathbf{K}}^*$ and $\widetilde{\mathbf{K}}^\#$.

Table 6.1 shows the values for the diagonal elements of $\widetilde{\mathbf{K}}^*$ and $\widetilde{\mathbf{K}}^\#$ corresponding to three typical values of r/p, which satisfy the constraints imposed by equation (6.31).

The above results confirm that, due to the use of inextensible limbs, the Type 1 minimanipulator has higher stiffness than the Stewart platform. In particular, direct stiffness in the Z direction, and torsional stiffness in the X and Y directions can be increased drastically by making the ratio of r to p large.

The simplified five-bar drivers of the Type 2 minimanipulator can be designed to cause further displacement reduction and force/torque amplification. Therefore, even higher stiffness can be obtained for the Type 2 minimanipulator.

6.3 Stiffness Matrix of the Type 2 Minimanipulator

Equation (5.38) implies that

$$\overline{\delta\theta} = \widehat{\mathbf{J}}\overline{\delta x} \tag{6.34}$$

where $\overline{\delta\theta}$ and $\overline{\delta x}$ represent infinitesimal displacements of the actuated joints and the platform, respectively. Let $\overline{\tau}$ be the 6×1 vector of input joint torques. Similar to equation (6.2), we can write

$$\overline{\mathcal{F}} = \widehat{\mathbf{J}}^T\overline{\tau} \tag{6.35}$$

where $\overline{\mathcal{F}}$ is defined in equation (6.3). Input actuator torques and displacements are related by

$$\overline{\tau} = \widehat{\mathbf{k}}\overline{\delta\theta} \tag{6.36}$$

where $\widehat{\mathbf{k}}$ is a 6×6 diagonal matrix whose elements represent stiffness of the actuators. Substituting equation (6.34) into equation (6.36) and the resulting equation into equation (6.35), yields

$$\overline{\mathcal{F}} = \widehat{\mathbf{J}}^T\widehat{\mathbf{k}}\widehat{\mathbf{J}}\overline{\delta x} \tag{6.37}$$

The above equation and equation (5.39) show that the stiffness matrix for the platform ($\widehat{\mathrm{K}}$) is given by

$$\widehat{\mathrm{K}} = \widehat{\mathrm{J}}^T\widehat{\mathrm{k}}\widehat{\mathrm{J}} = \mathrm{J}^T{\mathrm{J_d}}^T\widehat{\mathrm{k}}\mathrm{J_d}\mathrm{J} \tag{6.38}$$

6.3.1 Dimensionally-Uniform Stiffness Matrix

The upper left 3×3 portion of $\widehat{\mathrm{K}}$ represents direct or translatory stiffness, and consists of elements which have the dimension of force/length. The lower right 3×3 portion of $\widehat{\mathrm{K}}$ represents torsional stiffness, and consists of elements which have the dimension of force-length. The other 3×3 portions of $\widehat{\mathrm{K}}$ consist of cross-coupling elements which have the dimension of force.

Following the same procedure used in section 6.2.1, we obtain

$$\tilde{\mathcal{F}} = \grave{\mathrm{K}}\widetilde{\delta x} \tag{6.39}$$

where $\grave{\mathrm{K}}$ is the dimensionally-uniform stiffness matrix for the Type 2 minimanipulator. All of the elements of $\grave{\mathrm{K}}$ have the dimension of force/length. Matrices $\grave{\mathrm{K}}$ and $\widehat{\mathrm{K}}$ are related by

$$\grave{\mathrm{K}} = \mathbf{W_f}\widehat{\mathrm{K}}\mathbf{W_f} \tag{6.40}$$

The discussions in sections 6.2.1 and 6.2.2 about diagonalization and eigenvalue problem of matrix $\widetilde{\mathrm{K}}$ can also be applied to the $\grave{\mathrm{K}}$ matrix.

Chapter 7

Workspace Analysis

7.1 Introduction

As mentioned before, the major disadvantage of parallel manipulators is their limited workspace. Therefore, developing an efficient method for determining the workspace of the minimanipulators is very important.

Considerable research has been performed in determining both reachable and dexterous workspaces of serial manipulators (e.g., Kumar and Waldron, 1981; Gupta and Roth, 1982; Yang and Lee, 1983). Most of the reported work on workspace of parallel manipulators deal with two-DOF and three-DOF planar or spherical mechanisms. Bajpai and Roth (1986) studied the workspace of a two-DOF parallel manipulator based on a five-bar linkage. Gosselin and Angeles (1988, 1989) studied the workspaces of planar and spherical three-DOF parallel manipulators. Few researchers have studied the workspace of six-DOF parallel manipulators. In all cases, the workspace is determined for a given orientation of the output link. Most of the reported work in this area involves developing algorithms based on discretization for determining the workspace of Stewart-platform-based manipulators (e.g., Merlet, 1987; Cleary and Arai, 1991; Yang and Haug, 1991). Gosselin (1990b) used geometric properties to introduce another algorithm for determining the workspace of the Stewart platform. He showed that the workspace is the intersection of six annular regions.

In this chapter, a discretization algorithm is used to determine the minimanipulator workspace for any given platform orientation. Note that to represent the six-dimensional minimanipulator workspace in three dimensions, three of the six variables should be fixed. Therefore, determining the workspace using the platform orientation as the fixed parameter is justifiable.

7.2 Algorithm for Determination of Workspace

Again, without loss of generality, we let $Z_{R,i} = 0$. It was shown in section 6.2.2 that the central stiffness matrix of a minimanipulator can be diagonalized (decoupled), if the length of vector $\overline{GP_i}$ is half of the length of vector $\overline{OR_i}$ ($p = \nu/2$). We use this condition in determining the minimanipulator dimensions for workspace analysis. Also, to normalize the dimensions, we let $p = 1$. As a result, ν becomes equal to 2 (see Figure 7.1). At the central configuration corresponding to $p = \nu/2$, let the angle between any one of the limbs and the base plane be equal to ϖ. It was shown in section 6.2.2 that ϖ has to be equal to 45 degrees to obtain equal direct stiffness values in the X, Y, and Z directions. It was also shown that ϖ value of 63.43 degrees results in equal torsional stiffness values

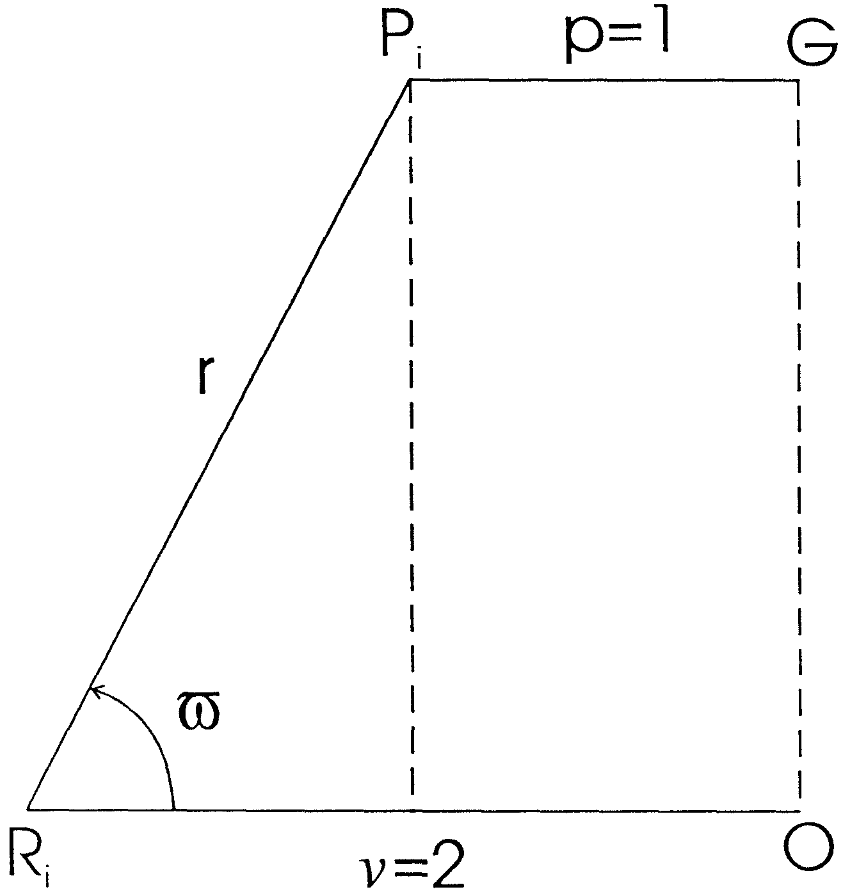

Figure 7.1: Parameters used in workspace analysis.

in the X, Y, and Z directions. These two values are used for ϖ in workspace analysis of the minimanipulators. Referring to Figure 7.1, we see that the limb length (r) can be found from

$$r = \frac{1}{\cos \varpi} \tag{7.1}$$

In addition, as shown in Figure 7.2, when the minimanipulator is at the central configuration corresponding to $p = \nu/2$, we define the position of the lower end of a limb as the central point ($R_{i,c}$) of its operating area. Furthermore, we let the operating area of point R_i to be constrained to within a circle of unit radius around the central point $R_{i,c}$. Such a circular area can be generated by a two-DOF driver.

Given a platform orientation, directions of the axes of topmost revolute joints at points P_1, P_2, and P_3 are known. These directions determine normals to the planes in which limbs P_1R_1, P_2R_2, and P_3R_3 can move. Given these normals, and the operating areas of points R_1, R_2, and R_3, operating volumes of points P_1, P_2, and P_3 can be obtained. For a given platform orientation, vector $\overline{P_iG}$ is also known. If operating volumes of points P_1, P_2, and P_3 are translated by vectors $\overline{P_1G}, \overline{P_2G}$, and $\overline{P_3G}$, respectively; the intersection of such translated volumes is the workspace. However, the above approach is not efficient, because the operating volume of point P_i is not a well-defined geometric object and changes with the platform orientation. Besides, finding the intersection of three such volumes can not be easily accomplished analytically or numerically. Therefore, the following discretization algorithm is developed for finding the minimanipulator workspace.

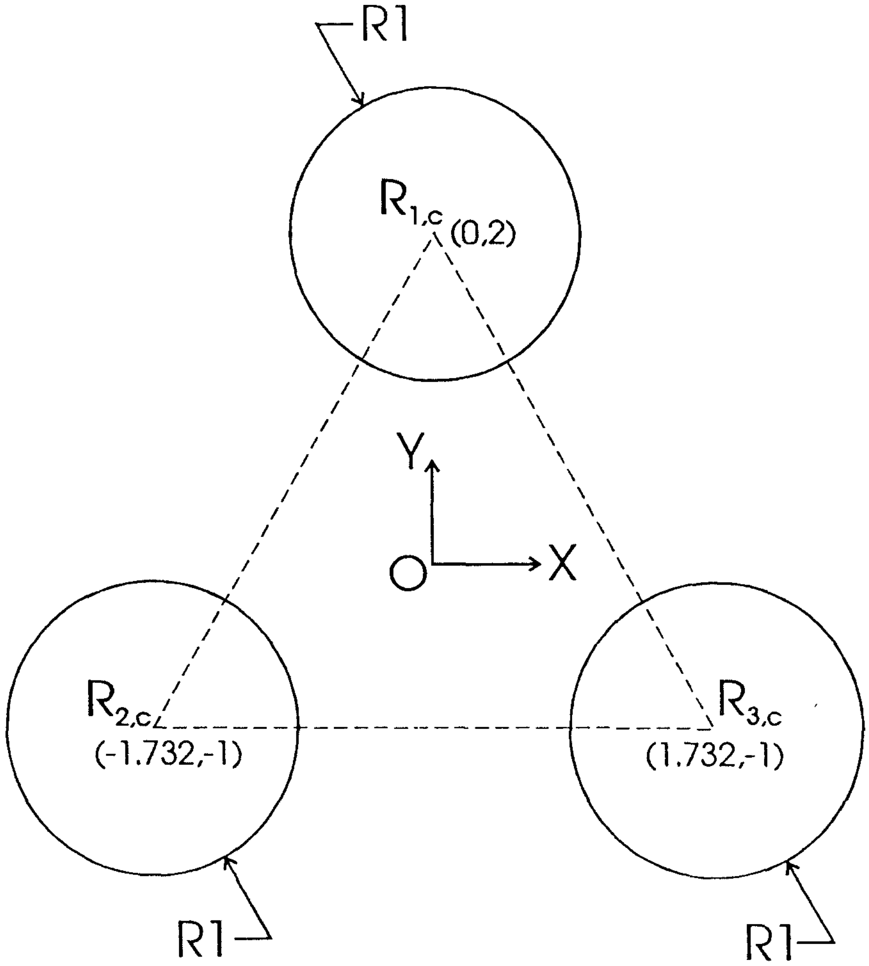

Figure 7.2: Circular operating areas of points R_1, R_2, and R_3.

For any given set of minimanipulator dimensions and platform orientation, the following steps are taken:

1. Find minimum and maximum values for Z_G. This is accomplished by making $X_G = Y_G = 0$, and using the bisection (binary-search) method to find the Z_G values at which transition between "no solution" and "acceptable solution" occurs for the inverse kinematics problem.

2. Define the increment for Z_G as the difference between maximum and minimum values of Z_G divided by a finite integer. To make the workspace plots (see step 4 below) appropriately dense, integer value of 25 was used.

3. Vary Z_G incrementally from its minimum value to its maximum value. For each Z_G, move out and around and find points on the cross-sectional boundary of the workspace. Moving out in the radial direction, the bisection method is used to find the workspace boundary point at which transition between "acceptable solution" and "no solution" occurs for the inverse kinematics problem. Moving around in the tangential direction, a resolution of 5 degrees is used.

4. Write out the points obtained in the previous step to a file and plot them using Mathematica (Wolfram, 1991).

The bisection method is used because of its speed of convergence. However, in a given direction (Z or radial), this method works if there is only one transition between "acceptable solution" and "no solution" for the inverse kinematics problem. This is true, if there are no voids (holes) within the workspace.

Therefore, another program was written to detect voids inside of the workspace. This program, which is much slower than the main algorithm, works in the following manner. Similar to the main algorithm, Z_G is varied incrementally. But, for a given Z_G, it marches out in the radial direction with very small steps and looks for regions where transition between "acceptable solution" and "no solution" (and vice versa) occurs for the inverse kinematics problem. It was found that, unless there are discontinuities within the operating area of point R_i, no voids exist inside of the minimanipulator workspace. Since no holes are allowed inside of the circular operating areas, using the bisection method is acceptable.

Let θ_x, θ_y, and θ_z represent rotations of the platform about the X, Y, and Z axes, respectively. These rotations are called yaw, pitch, and roll, respectively. In what follows, we demonstrate the minimanipulator workspace algorithm by presenting examples based on ϖ values of 63.43 and 45 degrees and different platform orientations $(\theta_x, \theta_y, \theta_z)$. Ten degrees is chosen for roll, pitch, and/or yaw values in the examples, because a minimanipulator is expected to handle such rotations in fine manipulation of its end-effector (platform).

7.3 Examples (ϖ=63.43)

Equation (7.1) shows that $r = \sqrt{5}$ for the examples in this section.

Example 1a - Let us begin with

$$\theta_x = 0, \quad \theta_y = 0, \quad \theta_z = 0$$

Perspective, front, side, and top views of the workspace are shown in Figures 7.3, 7.4, 7.5, and 7.6, respectively. As shown in Figure 7.2, point $R_{1,c}$ is on the Y axis, and points $R_{2,c}$, and $R_{3,c}$ are symmetric with respect to the Y axis. Therefore, as expected, the front view of the workspace is symmetric with respect to the Z axis. However, since distance of points $R_{2,c}$, and $R_{3,c}$ from the X axis is different from that of point $R_{1,c}$, the side view of the workspace is not symmetric with respect to the Z axis. When points R_1, R_2, and R_3 are at the centers of their circular operating areas, the Z cross-section of the workspace is circular. At this configuration, $Z_G = \tan(63.43) = 2$ and the area of the Z cross-section is larger than that of any other Z cross-section, as shown in Figures 7.3 and 7.6. For a given $Z_G > 2$, if we keep X_G constant and move away from the corresponding central configuration in the positive Y direction, points R_2 and R_3 get closer to the boundaries of their circular operating areas. As a result the width of the Z cross-section (in the X direction) becomes smaller. If $Z_G < 2$, the same thing happens when we move in the negative Y direction.■

Workspace plots for the rest of examples in this section are shown in Appendix E.

Example 1b - In this example, let us allow only a rotation of 10 degrees about the X axis. That is

$$\theta_x = 10, \quad \theta_y = 0, \quad \theta_z = 0$$

Perspective, front, and side views of the workspace are shown in Figures E.1, E.2, and E.3, respectively.

Example 1c - Next, let us consider only a rotation of 10 degrees about the Y axis. That is

$$\theta_x = 0, \quad \theta_y = 10, \quad \theta_z = 0$$

Perspective, front, and side views of the workspace are shown in Figures E.4, E.5, and E.6, respectively.

Example 1d - Here, we consider only a rotation of 10 degrees about the Z axis. That is

$$\theta_x = 0, \quad \theta_y = 0, \quad \theta_z = 10$$

Perspective, front, and side views of the workspace are shown in Figures E.7, E.8, and E.9, respectively.

Example 1e - Finally, let us consider 10 degrees of rotation about all three axes. Namely,

$$\theta_x = 10, \quad \theta_y = 10, \quad \theta_z = 10$$

Perspective, front, and side views of the workspace are shown in Figures E.10, E.11, and E.12, respectively.

7.4 Examples (ϖ=45)

Equation (7.1) shows that $r = \sqrt{2}$ for the examples in this section.

Example 2a - Again, we start with the following values (in degrees) for the yaw, pitch, and roll angles:

$$\theta_x = 0, \quad \theta_y = 0, \quad \theta_z = 0$$

Perspective, front, side, and top views of the workspace are shown in Figures 7.7, 7.8, 7.9, and 7.10, respectively.

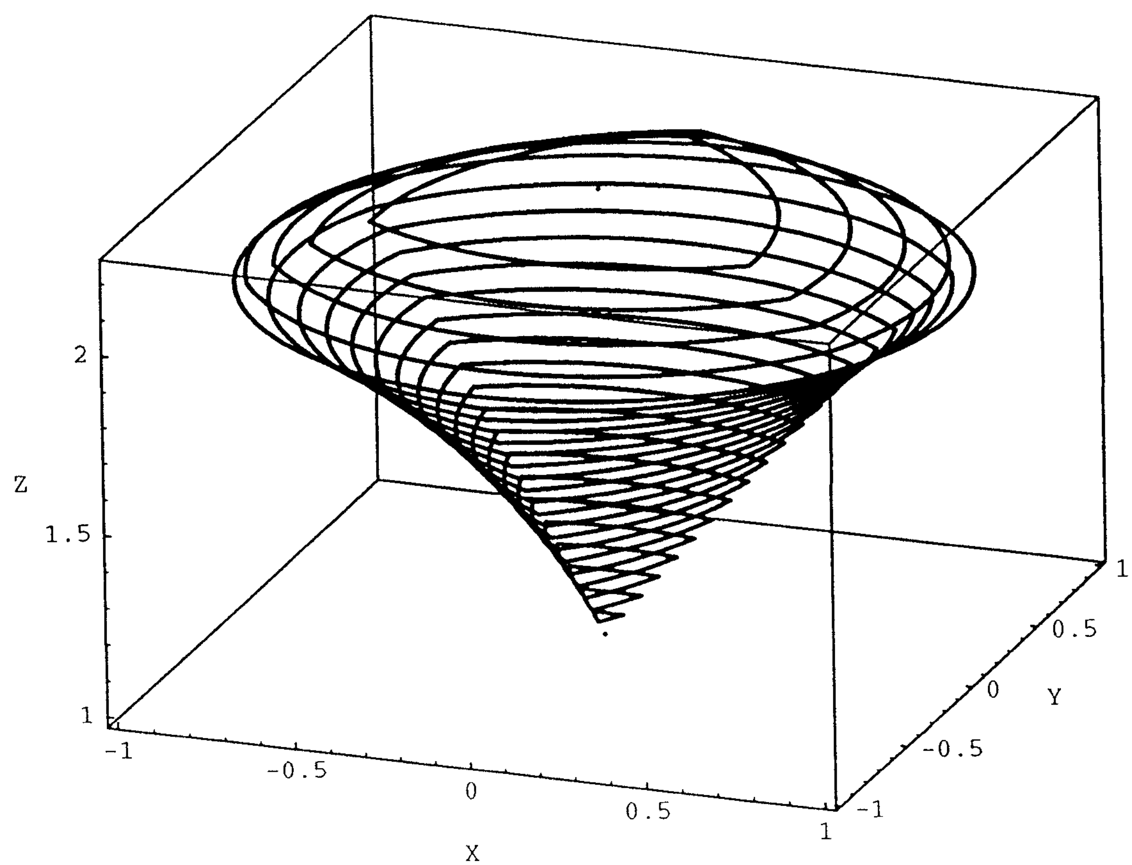

Figure 7.3: Perspective view of workspace for ϖ=63.43, θ_x=0, θ_y=0, and θ_z=0.

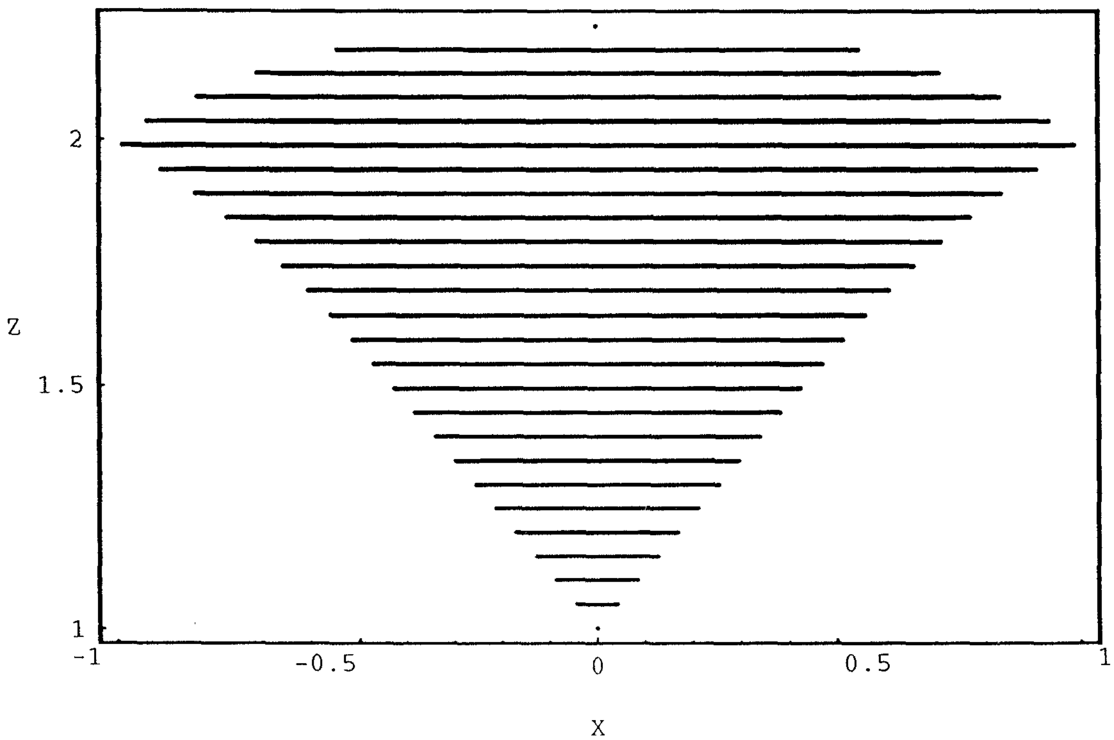

Figure 7.4: Front view of workspace for ϖ=63.43, θ_x=0, θ_y=0, and θ_z=0.

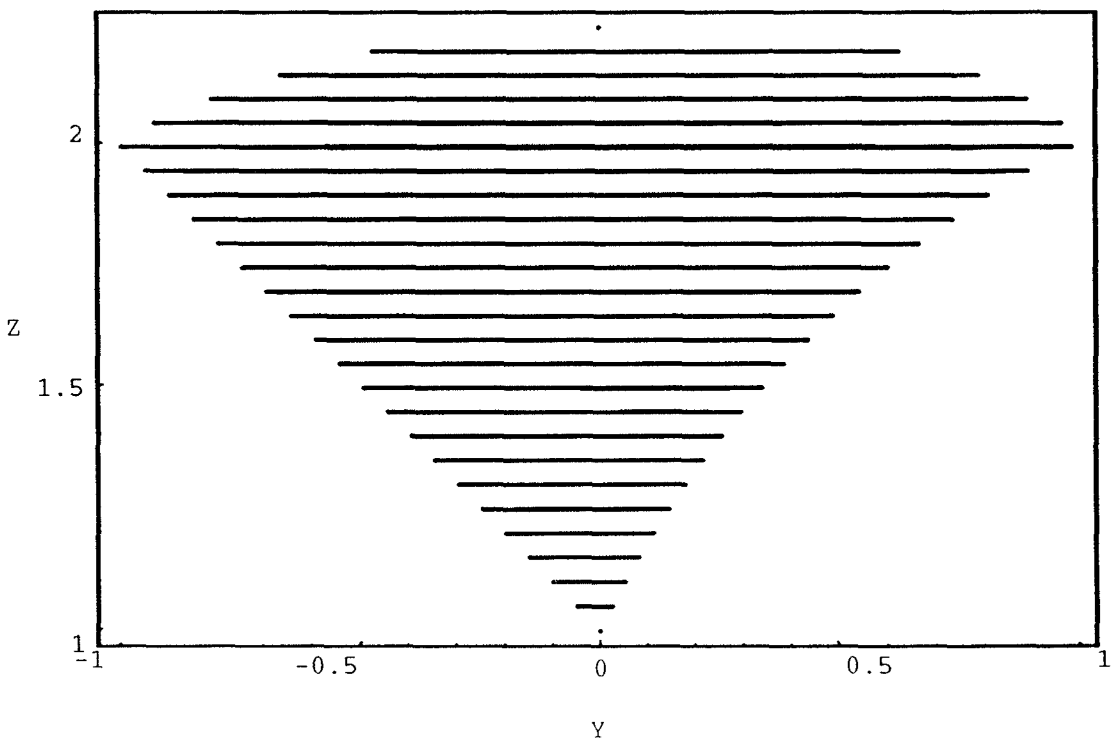

Figure 7.5: Side view of workspace for ϖ=63.43, θ_x=0, θ_y=0, and θ_z=0.

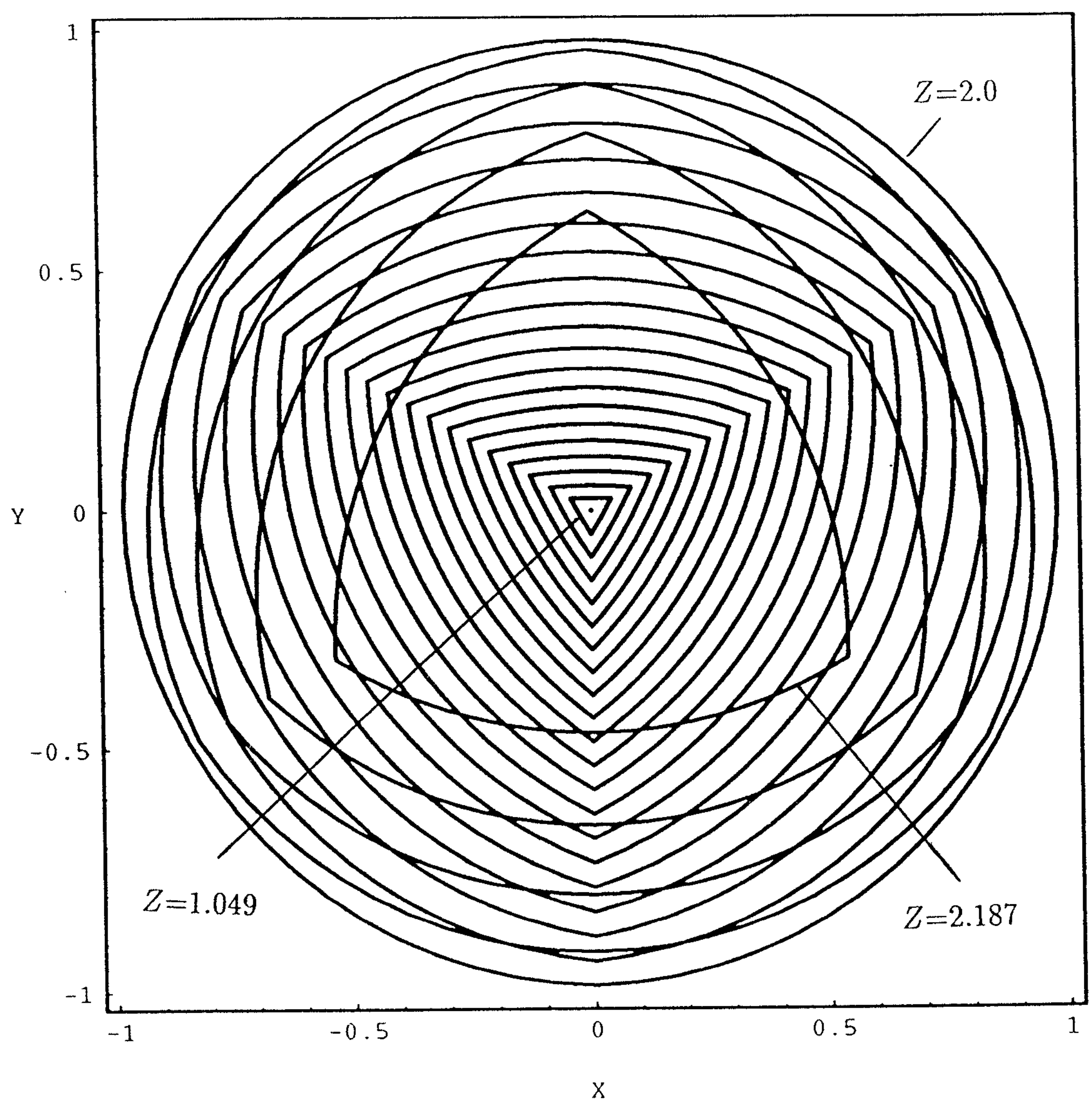

Figure 7.6: Top view of workspace for ϖ=63.43, θ_x=0, θ_y=0, and θ_z=0.

The discussion about symmetry and shape of Z cross-sections in Example 1a can also be applied to this example, except that $Z_G = \tan(45) = 1$ when points R_1, R_2, and R_3 are at the centers of their circular operating areas. ■

Workspace plots for the rest of examples in this section are shown in Appendix F.

Example 2b - Next, let us consider only a rotation of 10 degrees about the X axis. That is

$$\theta_x = 10, \ \ \theta_y = 0, \ \ \theta_z = 0$$

Perspective, front, and side views of the workspace are shown in Figures F.1, F.2, and F.3, respectively.

Example 2c - In this example, we consider only a rotation of 10 degrees about the Y axis. That is

$$\theta_x = 0, \ \ \theta_y = 10, \ \ \theta_z = 0$$

Perspective, front, and side views of the workspace are shown in Figures F.4, F.5, and F.6, respectively.

Example 2d - Here, we allow only a rotation of 10 degrees about the Z axis. Namely

$$\theta_x = 0, \ \ \theta_y = 0, \ \ \theta_z = 10$$

Perspective, front, and side views of the workspace are shown in Figures F.7, F.8, and F.9, respectively.

Example 2e - Finally, we allow 10 degrees of rotation about all three axes. Namely

$$\theta_x = 10, \ \ \theta_y = 10, \ \ \theta_z = 10$$

Perspective, front, and side views of the workspace are shown in Figures F.10, F.11, and F.12, respectively.■

The workspace of the output point of a simplified five-bar linkage driver (point C_i in Figure 2.6) is a ring with inner radius of $|b-a|$ and outer radius of $b+a$. If simplified five-bar linkage drivers are used, only continuous sectors (or circular portions) of such rings must be used to move the lower ends of the limbs. Thus, possibility of workspace discontinuities can be eliminated.

Increasing the workspace size is not a design goal for the minimanipulators. However, let us discuss briefly the relationships between a minimanipulator workspace size and its parameters. For a given displacement of point R_i on the $R_1R_2R_3$ plane, the smaller the value of r, the larger the displacement of point P_i.[1] Similarly, for a given displacement of point P_i, the smaller the value of p, the larger the displacement of point G.[2] Therefore, the smaller the values of r and/or p, the larger the size of the workspace. As mentioned before, for ϖ values of 63.43 and 45 degrees, r values are equal to $\sqrt{5}$ and $\sqrt{2}$, respectively. Therefore, for a given set of variables (p, ν, platform orientation, and operating area of point R_i), ϖ value of 45 degrees yields a larger workspace than ϖ value of 63.43 degrees. Also, it is obvious that the larger the size of the operating area for point R_i, the larger the size of the workspace.

---

[1] As $r \longrightarrow \infty$, displacement of point P_i approaches zero.

[2] As $p \longrightarrow \infty$, displacement of point G approaches zero.

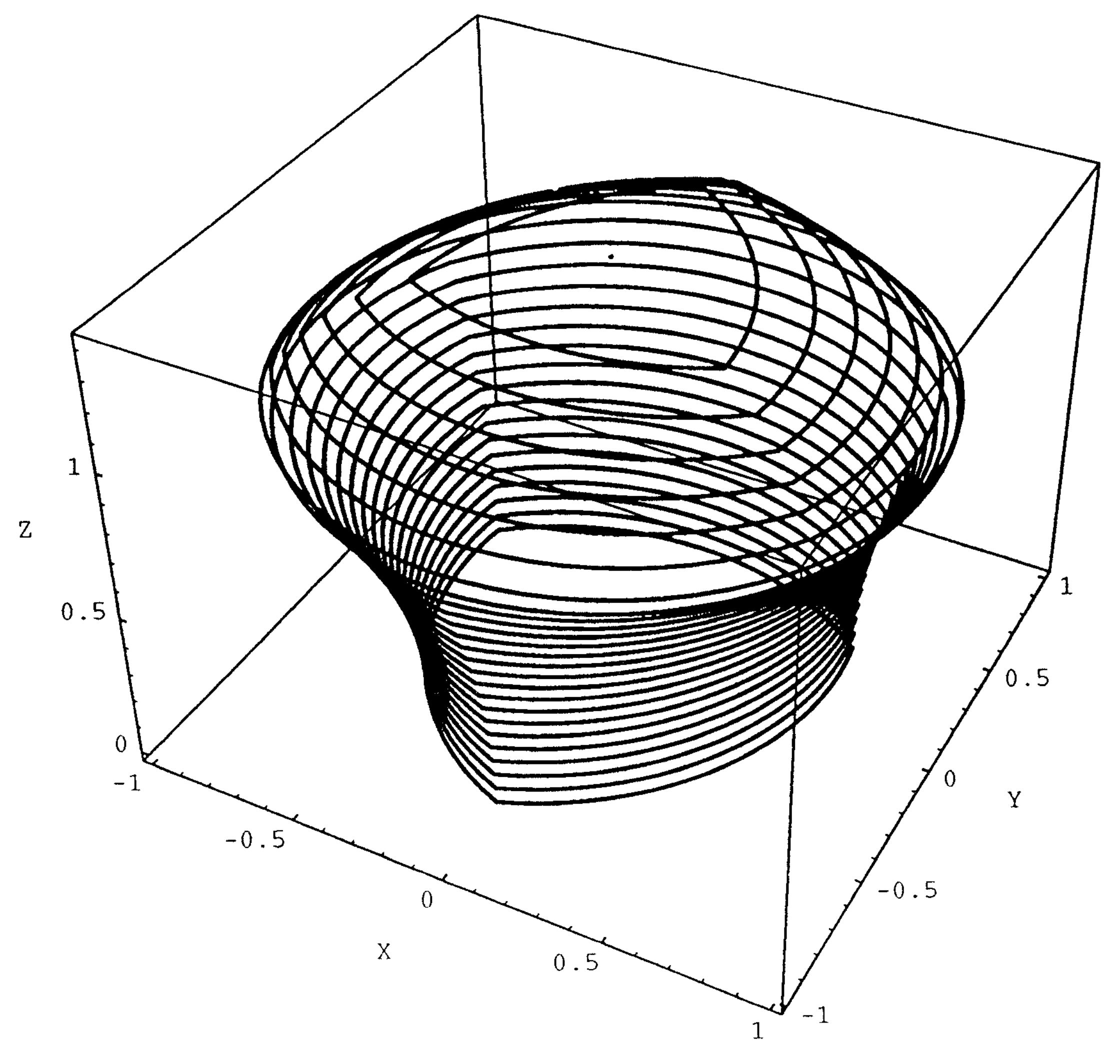

Figure 7.7: Perspective view of workspace for ϖ=45, θ_x=0, θ_y=0, and θ_z=0.

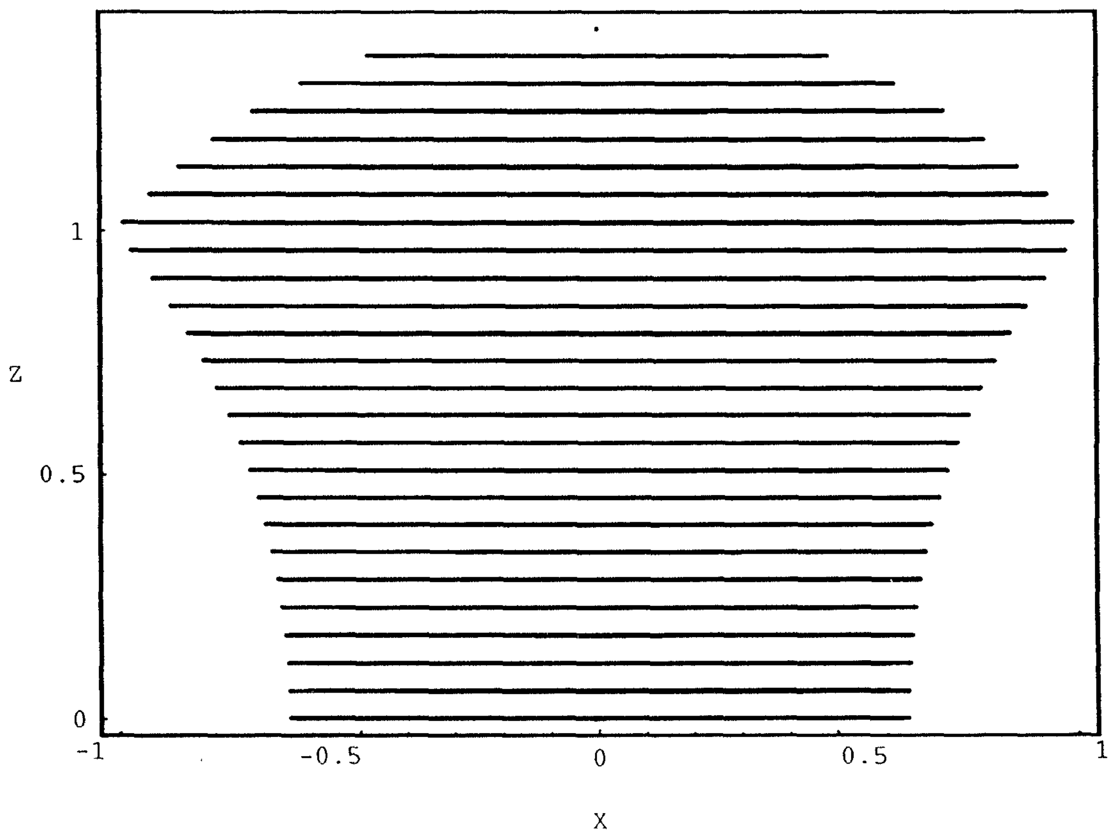

Figure 7.8: Front view of workspace for ϖ=45, θ_x=0, θ_y=0, and θ_z=0.

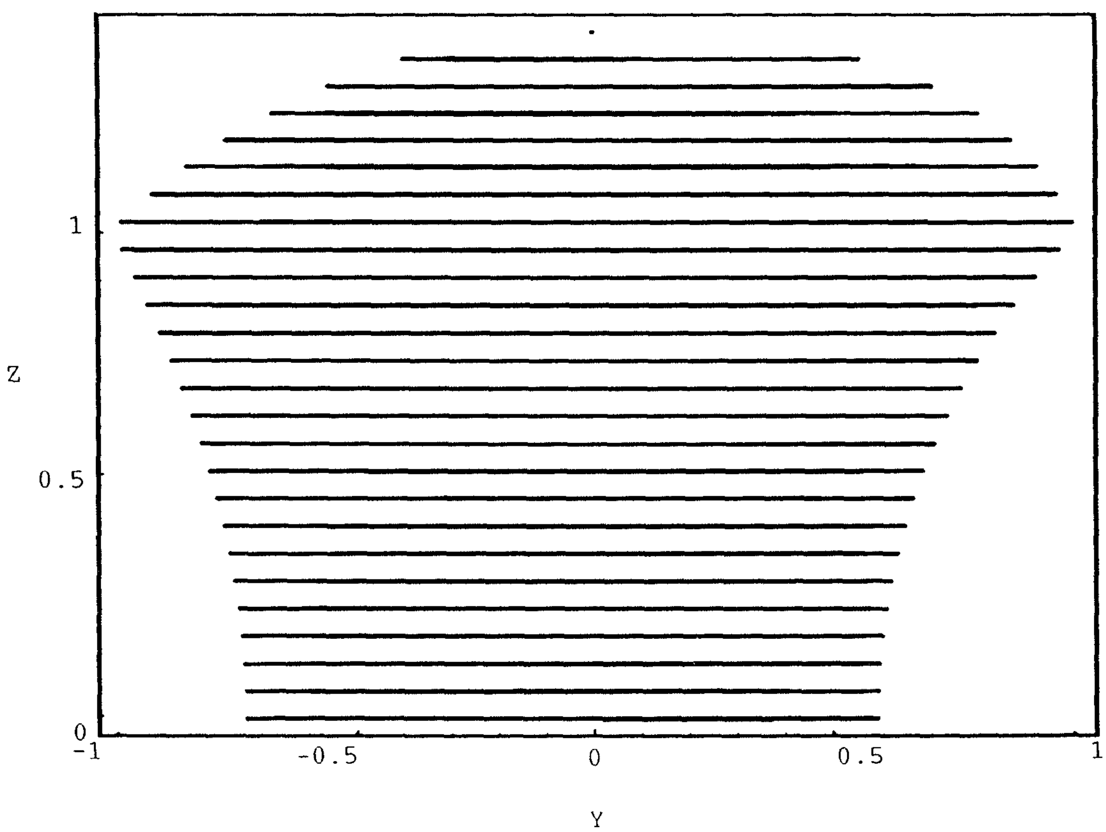

Figure 7.9: Side view of workspace for ϖ=45, θ_x=0, θ_y=0, and θ_z=0.

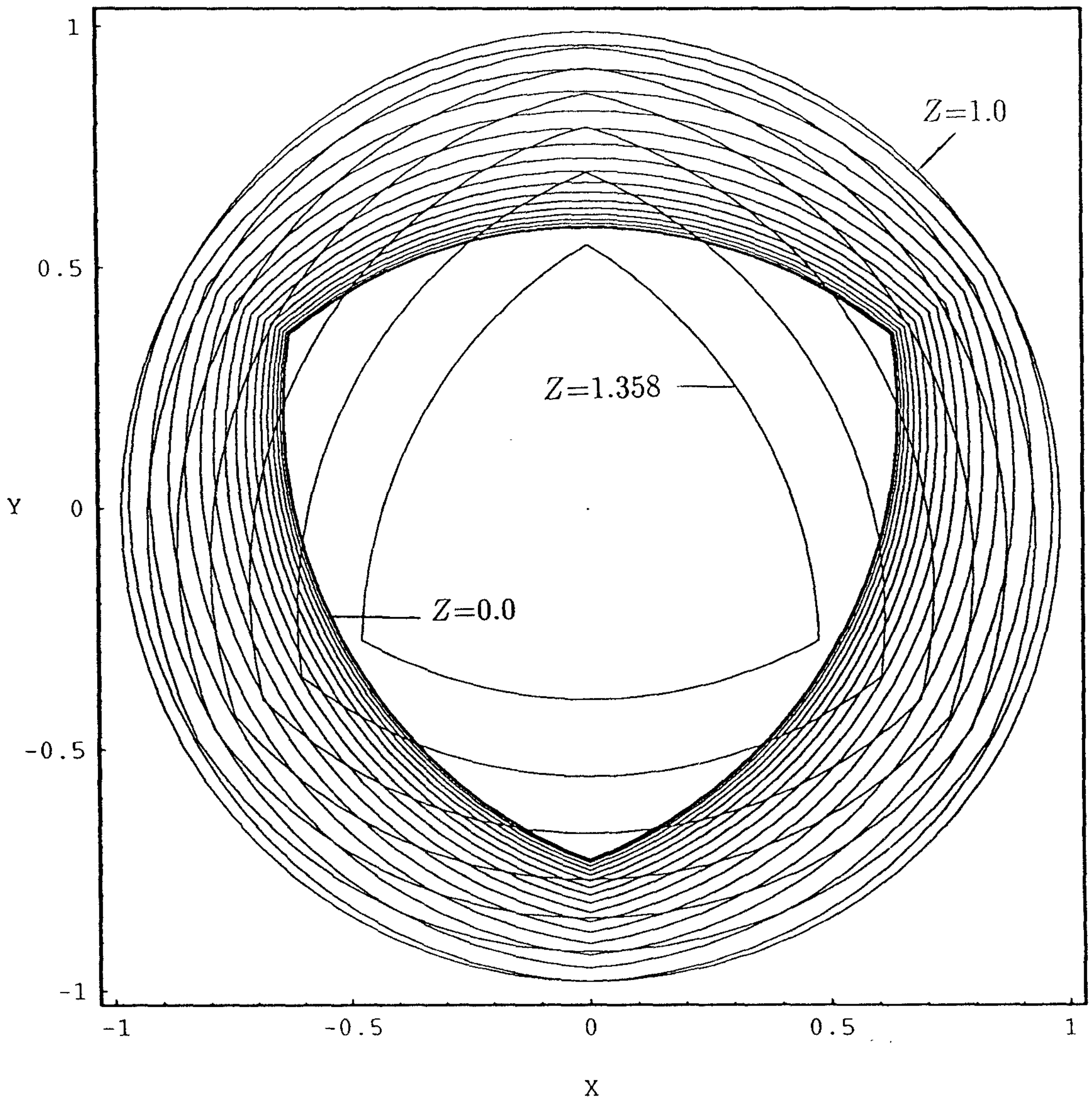

Figure 7.10: Top view of workspace for ϖ=45, θ_x=0, θ_y=0, and θ_z=0.

Chapter 8

Singularity Analysis

8.1 Introduction

In a serial manipulator, singularities occur when different branches of the inverse kinematics problem converge. Singularities take place at the workspace boundary or an internal boundary which separates regions with different degrees of accessibility. At a singular point, the manipulator loses one or more degrees of freedom and the output link can not be moved in one or more directions. From the statics point of view, one or more forces (or moments) applied at the output link can be resisted without exerting any forces (or torques) at the actuated joints. Most researchers have used Jacobian matrices to study singularities of serial manipulators (e.g., Wang and Waldron, 1987; Lipkin and Pohl, 1991). Kohli and Spanos (1985) have used discriminants of inverse kinematics polynomials to determine singularities of serial manipulators.

In a parallel manipulator, in addition to the inverse kinematics singularities described above, another type of singularity occurs when different branches of the direct kinematics problem converge. At such a singular point, which lies within the workspace, the parallel manipulator gains one or more degrees of freedom. In other words, with the actuators locked, the manipulator can move in one or more directions and one or more applied forces (or moments) at the output link can not be resisted by the input forces (or torques).

For the first time, Hunt (1983) discussed one of the direct kinematics singular configurations of the Stewart platform. Fichter (1986) discovered another such configuration. Merlet (1989) used Grassman geometry to enumerate all of the direct kinematics singular configurations of a special kind of Stewart platform in which pairs of spherical joints on the platform are concentric. Gosselin and Angeles (1990) classified singularities of parallel manipulators and discussed all singularities of some planar and spherical mechanisms. Ma and Angeles (1991) introduced architecture singularities of the Stewart platform. Direct kinematics singularities of six-DOF parallel manipulators which are not based on the Stewart platform have also been studied by researchers (e.g., Behi, 1988; Mouly and Merlet, 1992).

In this chapter, both inverse kinematics and direct kinematics singularities of the Type 1 and Type 2 minimanipulators (see section 2.3, page 21) are discussed. Once again, without loss of generality, we let $Z_{R,i} = 0$.

8.2 Inverse Kinematics Singularities of the Type 1 Minimanipulator

In the inverse kinematics problem, the position and orientation of the platform are known. Coordinates of the lower ends of the limbs (points R_1, R_2, and R_3) in the base reference frame are to be found. As shown in equation (3.7), the problem can be reduced to solving a quadratic equation in the unknown $Y_{R,i}$.

Recall from Chapter 4 that $\overline{\Gamma_i}$ is a unit vector which is collinear with the axis of the topmost revolute joint at point P_i and points in the direction of vector $\overline{P_{i+2}P_{i+1}}$ (see Figure 4.1). Let Π_i be the plane passing through P_i and perpendicular to vector $\overline{\Gamma_i}$. Also, let Λ_i be the intersection of the base plane with plane Π_i. As discussed in Chapter 3, the two solutions for point R_i represent intersections of a circle with line Λ_i. The circle is centered at P_i, has radius of r, and lies in the plane Π_i. The two intersections represent two branches of the inverse kinematics problem and when they converge, the minimanipulator is in a singular configuration. At such a singularity, limb P_iR_i is perpendicular to Λ_i. In Chapter 5, we defined vector $\overline{\mu}_i$ by

$$\overline{\mu}_i = \overline{\Gamma}_i \times \overline{P_iR_i} \tag{8.1}$$

When $P_iR_i \perp \Lambda_i$, $\overline{\mu}_i$ is parallel to the base plane and $\mu_{i,z}$ (Z component of vector $\overline{\mu_i}$) becomes equal to zero.

Note that in the above discussion i can be equal to 1 and/or 2 and/or 3. If the singularity condition is satisfied only for one of the i's (one of the limbs), the number of inverse kinematics solutions reduces from 8 to 4. Similarly, if the singularity condition is satisfied for two of the limbs, the number of inverse kinematics solutions reduces to 2. Finally, if the singularity condition is satisfied for all three limbs, the number of solutions for the inverse kinematics problem reduces to 1. For a given platform orientation, when the singularity condition is satisfied, the platform is at its highest possible Z value and point G (centroid of the platform) is at the top boundary of its workspace (as defined in Chapter 7).

At this point, let us relate the inverse kinematics singularities to the minimanipulator Jacobian matrix. In Chapter 5, we defined the Jacobian matrix ($\mathbf{J}$) by

$$\dot{\bar{q}} = \mathbf{J}\dot{\bar{x}}$$

where $\dot{\bar{x}}$ is the 6×1 generalized velocity vector of the platform and $\dot{\bar{q}}$ is the 6×1 vector of velocity components at the lower ends of the limbs. Solving the above equation for $\dot{\bar{x}}$, we get

$$\dot{\bar{x}} = \mathbf{J}^{-1}\dot{\bar{q}} = \frac{adj(\mathbf{J})}{|\mathbf{J}|}\dot{\bar{q}} \tag{8.2}$$

where $adj(\mathbf{J})$ and $|\mathbf{J}|$ denote adjoint and determinant of $\mathbf{J}$, respectively. At an inverse kinematics singularity, regardless of the value of $\dot{\bar{q}}$, one or more elements of $\dot{\bar{x}}$ are equal to zero, i.e.

$$|\mathbf{J}| \rightarrow \infty \tag{8.3}$$

Let us verify the geometric interpretation of the inverse kinematics singularities ($P_iR_i \perp \Lambda_i$ and $\mu_{i,z} = 0$) by examining $|\mathbf{J}|$. In Chapter 5, we showed that the Jacobian matrix is given by

$$\mathbf{J} = \begin{bmatrix} 1 & 0 & -\mu'_{1,x} & -\mu'_{1,x}\,(Y_{R,1} - Y_G) & -Z_G - \mu'_{1,x}\,(X_G - X_{R,1}) & Y_G - Y_{R,1} \\ 0 & 1 & -\mu'_{1,y} & Z_G - \mu'_{1,y}\,(Y_{R,1} - Y_G) & -\mu'_{1,y}\,(X_G - X_{R,1}) & X_{R,1} - X_G \\ 1 & 0 & -\mu'_{2,x} & -\mu'_{2,x}\,(Y_{R,2} - Y_G) & -Z_G - \mu'_{2,x}\,(X_G - X_{R,2}) & Y_G - Y_{R,2} \\ 0 & 1 & -\mu'_{2,y} & Z_G - \mu'_{2,y}\,(Y_{R,2} - Y_G) & -\mu'_{2,y}\,(X_G - X_{R,2}) & X_{R,2} - X_G \\ 1 & 0 & -\mu'_{3,x} & -\mu'_{3,x}\,(Y_{R,3} - Y_G) & -Z_G - \mu'_{3,x}\,(X_G - X_{R,3}) & Y_G - Y_{R,3} \\ 0 & 1 & -\mu'_{3,y} & Z_G - \mu'_{3,y}\,(Y_{R,3} - Y_G) & -\mu'_{3,y}\,(X_G - X_{R,3}) & X_{R,3} - X_G \end{bmatrix} \tag{8.4}$$

The third, fourth, and fifth columns of **J** involve the terms $\mu'_{i,x}$ and $\mu'_{i,y}$ which are defined by

$$\mu'_{i,x} = \frac{\mu_{i,x}}{\mu_{i,z}} \tag{8.5}$$

and

$$\mu'_{i,y} = \frac{\mu_{i,y}}{\mu_{i,z}} \tag{8.6}$$

where $\mu_{i,x}$ and $\mu_{i,y}$ are the X and Y-components of vector $\overline{\mu}_i$, respectively. Since $\mu_{i,z}$ is equal to zero (for i=1 and/or 2 and/or 3) at an inverse kinematics singularity, $\mu'_{i,x} \to \infty$ and $\mu'_{i,y} \to \infty$ (for i=1 and/or 2 and/or 3) and indeed $|\mathbf{J}| \to \infty$. This verifies the geometric interpretation of the inverse kinematics singularities.

8.3 Inverse Kinematics Singularities of the Type 2 Minimanipulator

For the Type 2 minimanipulator, in addition to the inverse kinematics singularities of the Type 1 minimanipulator, we also have to consider inverse kinematics singularities of the simplified five-bar drivers. As discussed in Chapter 3, in the inverse kinematics problem of a driver, coordinates of the output point (C_i) are known and the input angles (θ_i, and ϕ_i) are to be found. Singularity occurs when the branches of the inverse kinematics problem for a driver converge. At such a configuration, point C_i is at the boundary of its operating area and points A_i, and B_i fall on line D_iC_i (see Figure 2.6).

8.4 Direct Kinematics Singularities of the Type 1 Minimanipulator

Referring to equation (8.2), we see that if

$$|\mathbf{J}| = 0 \tag{8.7}$$

direct kinematics singularity occurs and even if all the elements of $\dot{\bar{q}}$ are equal to zero, one or more elements of $\dot{\bar{x}}$ can have non-zero values. As shown in equation (8.4), the expression for $\mathbf{J}$ is rather complicated. To simplify the task of obtaining $|\mathbf{J}|$, let us perform some elementary column operations and obtain another matrix ($\mathbf{J}^*$) such that

$$|\mathbf{J}| = |\mathbf{J}^*| \tag{8.8}$$

The goal is to make $\mathbf{J}^*$ independent of X_G, Y_G, and Z_G. Let $\bar{J}_1, \bar{J}_2, \ldots, \bar{J}_6$ be the column vectors of $\mathbf{J}$. Also, let $\bar{J}_1^*, \bar{J}_2^*, \ldots, \bar{J}_6^*$ be the column vectors of $\mathbf{J}^*$. The first three columns of $\mathbf{J}$ are independent of X_G, Y_G, and Z_G, therefore we let

$$\bar{J}_1^* = \bar{J}_1, \quad \bar{J}_2^* = \bar{J}_2, \quad \bar{J}_3^* = \bar{J}_3$$

To eliminate Y_G and Z_G from $\bar{J}_4$ and obtain $\bar{J}_4^*$, the following combination of column operations is performed.

$$\bar{J}_4^* = \bar{J}_4 + Y_G \bar{J}_3 - Z_G \bar{J}_2$$

Similarly, to eliminate X_G and Z_G from $\bar{J}_5$ and obtain $\bar{J}_5^*$, the following combination of column operations is performed.

$$\bar{J}_5^* = \bar{J}_5 - X_G \bar{J}_3 + Z_G \bar{J}_1$$

Finally, to eliminate X_G and Y_G from $\bar{J}_6$ and obtain $\bar{J}_6^*$, the following combination of column operations is performed.

$$\bar{J}_6^* = \bar{J}_6 + X_G \bar{J}_2 - Y_G \bar{J}_1$$

The end result is

$$\mathbf{J}^* = \begin{bmatrix} 1 & 0 & -\mu'_{1,x} & -\mu'_{1,x}\,\mathrm{Y}_{\mathrm{R},1} & \mu'_{1,x}\,\mathrm{X}_{\mathrm{R},1} & -\mathrm{Y}_{\mathrm{R},1} \\ 0 & 1 & -\mu'_{1,y} & -\mu'_{1,y}\,\mathrm{Y}_{\mathrm{R},1} & \mu'_{1,y}\,\mathrm{X}_{\mathrm{R},1} & \mathrm{X}_{\mathrm{R},1} \\ 1 & 0 & -\mu'_{2,x} & -\mu'_{2,x}\,\mathrm{Y}_{\mathrm{R},2} & \mu'_{2,x}\,\mathrm{X}_{\mathrm{R},2} & -\mathrm{Y}_{\mathrm{R},2} \\ 0 & 1 & -\mu'_{2,y} & -\mu'_{2,y}\,\mathrm{Y}_{\mathrm{R},2} & \mu'_{2,y}\,\mathrm{X}_{\mathrm{R},2} & \mathrm{X}_{\mathrm{R},2} \\ 1 & 0 & -\mu'_{3,x} & -\mu'_{3,x}\,\mathrm{Y}_{\mathrm{R},3} & \mu'_{3,x}\,\mathrm{X}_{\mathrm{R},3} & -\mathrm{Y}_{\mathrm{R},3} \\ 0 & 1 & -\mu'_{3,y} & -\mu'_{3,y}\,\mathrm{Y}_{\mathrm{R},3} & \mu'_{3,y}\,\mathrm{X}_{\mathrm{R},3} & \mathrm{X}_{\mathrm{R},3} \end{bmatrix} \tag{8.9}$$

Using equations (8.8) and (8.9), we find out that

$$\begin{aligned} |\mathbf{J}| = {} & [(\mu'_{1,x}\,\mu'_{2,y} - \mu'_{1,y}\,\mu'_{2,x})\,\mu'_{3,y}\,\mathrm{Y}_{\mathrm{R},3} + (\mu'_{1,y}\,\mu'_{3,x} - \mu'_{1,x}\,\mu'_{3,y})\,\mu'_{2,y}\,\mathrm{Y}_{\mathrm{R},2} + \\ & (\mu'_{2,x}\,\mu'_{3,y} - \mu'_{2,y}\,\mu'_{3,x})\,\mu'_{1,y}\,\mathrm{Y}_{\mathrm{R},1} + (\mu'_{1,x}\,\mu'_{2,y} - \mu'_{1,y}\,\mu'_{2,x})\,\mu'_{3,x}\,\mathrm{X}_{\mathrm{R},3} + \\ & (\mu'_{1,y}\,\mu'_{3,x} - \mu'_{1,x}\,\mu'_{3,y})\,\mu'_{2,x}\,\mathrm{X}_{\mathrm{R},2} + (\mu'_{2,x}\,\mu'_{3,y} - \mu'_{2,y}\,\mu'_{3,x})\,\mu'_{1,x}\,\mathrm{X}_{\mathrm{R},1}] \times \\ & [(\mathrm{X}_{\mathrm{R},2} - \mathrm{X}_{\mathrm{R},1})\,\mathrm{Y}_{\mathrm{R},3} + (\mathrm{X}_{\mathrm{R},1} - \mathrm{X}_{\mathrm{R},3})\,\mathrm{Y}_{\mathrm{R},2} + (\mathrm{X}_{\mathrm{R},3} - \mathrm{X}_{\mathrm{R},2})\,\mathrm{Y}_{\mathrm{R},1}] \end{aligned} \tag{8.10}$$

At a singular configuration, if all of the joints at points P_1, P_2, and P_3 are locked and the minimanipulator is translated and rotated as a rigid body until point R_1 is coincident with point O (origin of the base reference frame) and point R_2 lies on the positive Y axis, the singularity condition is preserved. Therefore, without loss of generality, we can set

$$X_{R,1} = Y_{R,1} = X_{R,2} = 0$$

in equation (8.10). Then, we get

$$\begin{aligned} |\mathrm{J}| \;=\; & -[(\mu'_{1,x}\,\mu'_{2,y} - \mu'_{1,y}\,\mu'_{2,x})\,\mu'_{3,y}\,\mathrm{Y}_{R,3} + (\mu'_{1,y}\,\mu'_{3,x} - \mu'_{1,x}\,\mu'_{3,y})\,\mu'_{2,y}\,\mathrm{Y}_{R,2} + \\ & (\mu'_{1,x}\,\mu'_{2,y} - \mu'_{1,y}\,\mu'_{2,x})\,\mu'_{3,x}\,\mathrm{X}_{R,3}]\,\mathrm{X}_{R,3}\,\mathrm{Y}_{R,2} \end{aligned} \tag{8.11}$$

Equation (8.11) is the necessary and sufficient condition for the existence of singularities. In what follows, we discuss several special singularity conditions under which Equation (8.11) is satisfied.

Condition A1:

$$X_{R,3} = 0$$

Under this condition, since

$$X_{R,1} = X_{R,2} = X_{R,3} = 0,$$

points R_1, R_2, and R_3 are collinear. This means that the minimanipulator can rotate freely about the line which passes through points R_1, R_2, and R_3 (the Y axis) even if these points are not being moved by the actuators. In other words, the minimanipulator has gained one degree of freedom.

Condition A2:

$$Y_{R,2} = 0$$

In this case, since

$$X_{R,1} = Y_{R,1} = X_{R,2} = Y_{R,2} = 0,$$

points R_1 and R_2 are coincident. Again, the minimanipulator can rotate freely about the line which passes through points R_1 (or R_2) and R_3 even if these points are not being moved by the actuators. One additional degree of freedom is gained by the minimanipulator. Note that if both $Y_{R,2} = 0$ and $X_{R,3} = 0$, we still have the same kind of singularity. In general singularity occurs, if two of the three points R_1, R_2, and R_3 coincide.

Condition A3:

$$Y_{R,2} = X_{R,3} = Y_{R,3} = 0$$

Under this condition, since

$$X_{R,1} = Y_{R,1} = X_{R,2} = Y_{R,2} = X_{R,3} = Y_{R,3} = 0,$$

points R_1, R_2, and R_3 are coincident. Two rotational degrees of freedom are gained by the minimanipulator. These degrees of freedom consist of rotations about two perpendicular lines in the $R_1R_2R_3$ plane which pass through points R_1, R_2, and R_3.

Condition A4:

$$\begin{aligned}&(\mu'_{1,\mathrm{x}}\,\mu'_{2,\mathrm{y}} - \mu'_{1,\mathrm{y}}\,\mu'_{2,\mathrm{x}})\,\mu'_{3,\mathrm{y}}\,\mathrm{Y}_{\mathrm{R},3} + (\mu'_{1,\mathrm{y}}\,\mu'_{3,\mathrm{x}} - \mu'_{1,\mathrm{x}}\,\mu'_{3,\mathrm{y}})\,\mu'_{2,\mathrm{y}}\,\mathrm{Y}_{\mathrm{R},2} + \\ &(\mu'_{1,\mathrm{x}}\,\mu'_{2,\mathrm{y}} - \mu'_{1,\mathrm{y}}\,\mu'_{2,\mathrm{x}})\,\mu'_{3,\mathrm{x}}\,\mathrm{X}_{\mathrm{R},3} = 0 \qquad (8.12)\end{aligned}$$

Let us find some mathematical conditions under which equation (8.12) is satisfied and discuss their physical meaning.

Condition A4.1:

$$\frac{\mu'_{1,x}}{\mu'_{1,y}} = \frac{\mu'_{2,x}}{\mu'_{2,y}} = \frac{\mu'_{3,x}}{\mu'_{3,y}}$$

If the above equalities are satisfied, the quantities inside parentheses on the left hand side of equation (8.12) vanish. Referring to equations (8.5) and (8.6), we see that this condition is the same as

$$\frac{\mu_{1,x}}{\mu_{1,y}} = \frac{\mu_{2,x}}{\mu_{2,y}} = \frac{\mu_{3,x}}{\mu_{3,y}} \tag{8.13}$$

The condition expressed in equation (8.13) can be satisfied only if the projections of vectors $\overline{\mu}_1$, $\overline{\mu}_2$, and $\overline{\mu}_3$ onto the base plane are parallel to each other. This is possible only if the three limbs lie on the base plane.[1] As a result, the platform and base are coincident. Even if points R_1, R_2, and R_3 are fixed, the platform can perform infinitesimal motion with respect to the base.

Condition A4.2:

$$\mu'_{i,x} = \mu'_{i,y} = 0 \quad \text{for} \quad i = 1 \ \text{and/or} \ 2 \ \text{and/or} \ 3$$

Again, referring to equations (8.5) and (8.6), we see that this condition is the same as

$$\mu_{i,x} = \mu_{i,y} = 0 \quad \text{for} \quad i = 1 \ \text{and/or} \ 2 \ \text{and/or} \ 3 \tag{8.14}$$

This condition can be satisfied only if limb P_iR_i and vector $\overline{\Gamma}_i$ (see Figure 5.1) lie on the base plane. Since vector $\overline{\Gamma}_i$ is parallel to vector $\overline{P_{i+2}P_{i+1}}$, points P_{i+1} and P_{i+2} have the same Z coordinates. Again, The platform instantaneously gains a degree of freedom.

Condition A4.3:

$$\mu'_{1,y} = \mu'_{2,y} = 0$$

[1]Under this condition, projections of vectors $\overline{\mu}_1$, $\overline{\mu}_2$, and $\overline{\mu}_3$ onto the base plane are equal to zero.

Once again, referring to equations (8.5) and (8.6), we see that this condition is the same as

$$\mu_{1,y} = \mu_{2,y} = 0 \tag{8.15}$$

This conditions can be satisfied only if the three limbs lie on the base plane. An instantaneous degree of freedom is gained by the platform.∎

Each row of matrix $\mathbf{J}^*$ is the Plücker coordinates (Bottema and Roth, 1979) of a line. The first, second, and third pairs of rows specify three pairs of lines which pass through points R_1, R_2, and R_3, respectively.[2] Hence, to determine the singularities, one can determine the conditions under which these lines become dependent. However, as shown in equation (8.9), the Plücker coordinates are related to components of vectors $\overline{\mu}_1$, $\overline{\mu}_2$, and $\overline{\mu}_3$, which do not physically exist. Therefore, geometric interpretation of the dependencies of the six lines becomes very difficult. This is precisely why we can not physically interpret equation (8.11), as a whole. In what follows, we present another approach for determining additional direct kinematics singularity conditions.

8.4.1 An Alternative Approach

When points R_1, R_2, and R_3 fall on a line or meet at a point, the minimanipulator can move even if angles η_1, η_2, and η_3 (see Figure 5.1) are not changing. To explore other singularity conditions under which points R_1, R_2, and R_3 do not

[2]The first three elements of each row represent coordinates of a vector passing through point R_i. The last three elements of each row represent cross-product of vector $\overline{OR_i}$ with the vector which is defined by the first three elements of the row.

move but one or more of angles η_1, η_2, and η_3 change, let us express the singularity condition in terms of these angles and minimanipulator dimensions (r and p). Note that when the minimanipulator performs a pure translation in the X or Y direction and when it undergoes a pure rotation about the Z axis, angles η_1, η_2, and η_3 do not change. Only three of the six degrees of freedom (translation in the Z direction and rotations about the X and Y axes) require changes in angles η_1, η_2, and η_3. Therefore, it is expected that the desired singularity condition can be obtained by setting the determinant of a 3×3 matrix equal to zero.

As defined in Chapter 4, let l_{i+2} be the length of vector $\overline{R_i R_{i+1}}$. The same kinematic inversion scheme, which was applied in section 4.3.2 to obtain equation (4.7), can be used to show that

$$l_{i+2}^2 = -2r^2 s_i s_{i+1} + r^2 c_i c_{i+1} + 3prc_i + 3prc_{i+1} + 3p^2 + 2r^2 \tag{8.16}$$

where $s_i = \sin \eta_i$ and $c_i = \cos \eta_i$. Taking the time derivative of both sides of equation (8.16) and simplifying, we get

$$\dot{l_{i+2}^2} = (-2r^2 c_i s_{i+1} - r^2 c_{i+1} s_i - 3prs_i)\dot{\eta}_i + (-2r^2 c_{i+1} s_i - r^2 c_i s_{i+1} - 3prs_{i+1})\dot{\eta}_{i+1} \tag{8.17}$$

where $\dot{l_{i+2}^2}$ and $\dot{\eta}_i$ denote time-derivatives of l_{i+2}^2 and η_i, respectively. Let

$$\dot{\overline{l^2}} = [\dot{l_1^2}, \;\; \dot{l_2^2}, \;\; \dot{l_3^2}]^T \tag{8.18}$$

and

$$\dot{\overline{\eta}} = [\dot{\eta}_1, \;\; \dot{\eta}_2, \;\; \dot{\eta}_3]^T \tag{8.19}$$

If we write equation (8.17) for i=1,2,3; then we obtain

$$\dot{\overline{l^2}} = -r\Omega\dot{\overline{\eta}} \tag{8.20}$$

where

$$
\Omega = \begin{bmatrix} 0 & 2rc_2s_3 + rc_3s_2 + 3ps_2 & 2rc_3s_2 + rc_2s_3 + 3ps_3 \\ 2rc_1s_3 + rc_3s_1 + 3ps_1 & 0 & 2rc_3s_1 + rc_1s_3 + 3ps_3 \\ 2rc_1s_2 + rc_2s_1 + 3ps_1 & 2rc_2s_1 + rc_1s_2 + 3ps_2 & 0 \end{bmatrix} \tag{8.21}
$$

Solving equation (8.20) for $\dot{\bar{\eta}}$, we get

$$
\dot{\bar{\eta}} = -\frac{1}{r}\frac{adj(\Omega)}{|\Omega|}\dot{\overline{l^2}} \tag{8.22}
$$

If points R_1, R_2, and R_3 are not moving, then

$$
\dot{\overline{l^2}} = [0, \;\; 0, \;\; 0]^T \tag{8.23}
$$

Direct kinematics singularities occur when equation (8.23) is satisfied but $\dot{\bar{\eta}}$ has a non-zero value. Equation (8.22) shows that since $r \neq 0$, such a singularity occurs if

$$
|\Omega| = 0 \tag{8.24}
$$

or

$$
\begin{aligned}
&(2rc_2s_3 + rc_3s_2 + 3ps_2)(2rc_3s_1 + rc_1s_3 + 3ps_3)(2rc_1s_2 + rc_2s_1 + 3ps_1) + \\
&(2rc_3s_2 + rc_2s_3 + 3ps_3)(2rc_1s_3 + rc_3s_1 + 3ps_1)(2rc_2s_1 + rc_1s_2 + 3ps_2) = 0
\end{aligned} \tag{8.25}
$$

Equation (8.25) provides the singularity condition in terms of the physical parameters of the minimanipulator. In what follows, several special conditions, for which equation (8.25) is satisfied, will be discussed.

The left hand side of equation (8.25) consists of the sum of two terms. Each term is the product of three expressions. If one expression in the first term and one expression in the second term vanish, then equation (8.25) is satisfied. Theoretically, there are nine possibilities for such a thing to occur, which result in nine pairs of equations. However, only three of the pairs of equations are useful. The other six pairs can be obtained by permuting the indices in the first three pairs of equations. Let us discuss singularity conditions which are related to such possibilities in more detail.

Condition B1:

$$2rc_1s_2 + rc_2s_1 + 3ps_1 = 0 \tag{8.26}$$

$$2rc_2s_1 + rc_1s_2 + 3ps_2 = 0 \tag{8.27}$$

Proposition 1: If equations (8.26) and (8.27) are satisfied, then $\eta_2 = \pm\eta_1$.

Proof: See Appendix G

Proposition 1 can be used to divide the singularity condition B1 into two subcases (conditions B1.1 and B1.2), as discussed below.

Condition B1.1: If

$$\eta_2 = \eta_1 \tag{8.28}$$

then equations (8.26) and (8.27) both reduce to

$$s_1(rc_1 + p) = 0 \tag{8.29}$$

Equations (8.28) and (8.29) imply that singularity occurs if

$$\eta_2 = \eta_1 = \begin{cases} 0 \\ \pi \end{cases} \tag{8.30}$$

or

$$\eta_2 = \eta_1 = \cos^{-1}\left(-\frac{p}{r}\right) \tag{8.31}$$

We shall refer to equations (8.30) and (8.31) as singularity **Conditions B1.1.1** and **B1.1.2**, respectively.

Proposition 2: If equation (8.31) is satisfied, then points R_1 and R_2 are coincident.

Proof: See Appendix G

Proposition 2 shows that singularity condition B1.1.2 is the same as singularity condition A2.

Condition B1.2: If

$$\eta_2 = -\eta_1 \tag{8.32}$$

then equations (8.26) and (8.27) both reduce to

$$s_1(rc_1 - 3p) = 0 \tag{8.33}$$

Equations (8.32) and (8.33) imply that singularity occurs if

$$\eta_1 = -\eta_2 = \begin{cases} 0 \\ \pi \end{cases} \tag{8.34}$$

or

$$\eta_1 = -\eta_2 = \cos^{-1}\left(\frac{3p}{r}\right) \tag{8.35}$$

We shall refer to equations (8.34) and (8.35) as singularity **Conditions B1.2.1** and **B1.2.2**, respectively.

Condition B2:

$$2rc_1s_2 + rc_2s_1 + 3ps_1 = 0 \tag{8.36}$$

$$2rc_1s_3 + rc_3s_1 + 3ps_1 = 0 \tag{8.37}$$

Equations (8.36) and (8.37) represent two linear and homogeneous equations in c_1 and s_1. The trivial solution for this system of equations ($c_1 = s_1 = 0$) is impossible. Non-trivial solutions exist when eliminant of equations (8.36) and (8.37) vanishes, i.e.

$$\begin{vmatrix} 2rs_2 & rc_2 + 3p \\ 2rs_3 & rc_3 + 3p \end{vmatrix} = 0 \tag{8.38}$$

Simplifying equation (8.38), we get

$$\varepsilon_1 s_2 - \varepsilon_2 c_2 = \varepsilon_3 \tag{8.39}$$

where

$$\varepsilon_1 = rc_3 + 3p$$

$$\varepsilon_2 = rs_3$$

$$\varepsilon_3 = 3ps_3$$

Variables ε_1, ε_2, and ε_3 are functions of η_3. For every value of η_3, equation (8.39) yields two values for η_2. One of these two values has to be equal to the given η_3 value, because $\eta_2 = \eta_3$ satisfy equation (8.38).

Let us discuss the geometric meaning of this condition using the following proposition.

Proposition 3: If equation (8.36) is satisfied, then $Z_{P,1} = 0$, $Z_{P,2} = Z_{P,3}$, and $\mu_{1,x} = \mu_{1,y} = 0$.

Proof: See Appendix G

Proposition 3 shows that singularity condition B2 is the same as singularity condition A4.2.

Condition B3:

$$2rc_1 s_2 + rc_2 s_1 + 3ps_1 = 0 \tag{8.40}$$

$$2rc_3 s_2 + rc_2 s_3 + 3ps_3 = 0 \tag{8.41}$$

Equations (8.40) and (8.41) represent two linear equations in c_2 and s_2. Solving for these two variables, we obtain

$$s_2 = 0 \tag{8.42}$$

$$c_2 = -\frac{3p}{r} \tag{8.43}$$

Since $r > 0$ and $p > 0$, equations (8.42) and (8.43) can be satisfied simultaneously only if

$$\eta_2 = \pi \tag{8.44}$$

and

$$r = 3p \tag{8.45}$$

It follows that this singularity condition can be satisfied if and only if equations (8.44) and (8.45) are both satisfied.

8.5 Direct Kinematics Singularities of the Type 2 Minimanipulator

For the Type 2 minimanipulator, in addition to the direct kinematics singularities of the Type 1 minimanipulator, we also have to consider direct kinematics singularities of the simplified five-bar drivers. As discussed in Chapter 4, in the direct kinematics problem of a driver, the input angles (θ_i, and ϕ_i) are known and coordinates of the output point (C_i) are to be found (see Figure 4.2). The following two singularity conditions can exist for a simplified five-bar linkage driver.

Condition C1:

One type of direct kinematics singularity occurs when points C_i and D_i fall on line A_iB_i (see Figure 4.2). This is possible only if the input link length of a driver is equal to its output link length (i.e., $a = b$). At such a configuration, the difference between the two driver input angles is equal to 180 degrees.

Condition C2:

Another type of direct kinematics singularity occurs when points A_i and B_i are coincident. At such a configuration, the output links A_iC_i and B_iC_i can rotate freely about point A_i (or B_i), even if the input links D_iA_i and D_iB_i are not moving. Note that if points A_i and B_i are coincident and they fall on line D_iC_i, we have both direct and inverse kinematics singularities.

Chapter 9

Design Guidelines

9.1 Stiffness Considerations

Based on the results of section 6.2.2, the following design guidelines can be established for the Type 1 minimanipulator.

- The central stiffness matrix can be diagonalized (decoupled) by making the platform (triangle $P_1P_2P_3$) one-half the size of the triangle passing through the lower ends of the limbs, i.e. $p = \nu/2$.
- If the central stiffness matrix is decoupled, then
  - The larger the ratio of the limb length to the platform circumradius (r/p), the larger the direct stiffness in the Z-direction, and the larger the torsional stiffness values in the X and Y-directions.

As mentioned earlier, a minimanipulator will be at or near the center of its workspace during most of its operations. Therefore, establishing design guidelines based on the central stiffness matrix is justified.

The primary portion (platform and limbs) of any other type of minimanipulator is the same as that of the Type 1 minimanipulator. Therefore, the above design guidelines can also be applied to other types of minimanipulator. In addition, based on the results of section 5.3, the following design guideline can be established for the five-bar drivers of the Type 2 minimanipulator.

- The smaller the ratio of the input link length to the output link length of a driver (a/b), the higher the stiffness of the minimanipulator.

9.2 Singularity and Workspace Considerations

Based on the results of Chapters 7 and 8, the following additional design guidelines can be established.

- To avoid direct kinematics singularities, the operating areas of the limbs' lower ends should be limited such that
  - The lower ends of the three limbs can not fall on a straight line. This takes care of singularity conditions A1, A2, A3, and B1.1.2.
  - The angle between any limb and the platform (η_i) is greater than 0 degrees and less than 180 degrees.[1] This takes care of singularity

[1] To keep the stiffness of the minimanipulators high, η_i should not be allowed to get too close to 0 or 180 degrees. A good operating range for η_i is 40 to 140 degrees. To operate only on one of the inverse kinematics branches, η_i should be further restricted to be between 40 and 90 degrees or between 90 and 140 degrees.

conditions A4.1, A4.2, A4.3, B1.1.1, B1.2.1, B2, and B3. Note that if line P_iR_i and its corresponding joint axis $\overline{\Gamma_i}$ lie on the base plane (singularity conditions A4.2 and B2), then $\eta_i \leq 0$.

- To avoid direct kinematics singularities (condition B1.2.2), ratio of the limb length to platform circumradius should be less than 3, i.e., $r/p < 3$.

- If a simplified five-bar linkage driver is used and its input link length is equal to its output link length (i.e., $a = b$), then direct kinematics singularity condition C1 can be avoided by making sure that the difference between the two driver input angles (θ_i and ϕ_i) is not equal to 180 degrees.

- If a simplified five-bar linkage driver is used, then direct kinematics singularity condition C2 can be avoided by making sure that the two input angles are not equal.

- To avoid having any discontinuities in the workspace, the operating areas of the lower ends of the limbs must contain no holes. In particular, if a simplified five-bar linkage driver is used, only a continuous sector or a circular portion of its ring-shaped workspace should be used to move the lower end of a limb.

Normally, there is a trade-off between the stiffness and workspace size of a mechanism. The minimanipulators are intended to provide high stiffness. Therefore, as mentioned before, increasing the workspace size is not a design goal for them. Nevertheless, the following observations can be made about the relationships between the workspace size and the parameters of a minimanipulator.

- With all of the other variables fixed, the smaller the limb length (r), the larger the workspace.
- With all of the other variables fixed, the smaller the circumradius of the platform (p), the larger the workspace.
- With all of the other variables fixed, the larger the size of the operating area of a limb's lower end, the larger the workspace.

Chapter 10

Concluding Remarks

10.1 Summary

In this dissertation, the design and analysis of a new class of high-resolution and high-stiffness six-DOF parallel minimanipulators are presented. Topological synthesis techniques are used in the design of the minimanipulators. Inverse kinematics, direct kinematics, Jacobian, stiffness, workspace, and singularity analyses are discussed. Analytical results are used in establishing dimensional synthesis guidelines for the minimanipulators. The major results are summarized below.

10.1.1 Conceptual Design

To achieve high stiffness and resolution, the limbs are made inextensible and their lower ends are connected to two-DOF drivers (e.g., bidirectional linear stepper motors, pantographs, five-bar linkages). For most applications, simplified five-bar linkages were found to be the most suitable drivers for the minimanipulators. The drivers are designed so that all of the actuators are base-mounted. Therefore, higher payload capacity, smaller actuator sizes, and lower power dissipation can be obtained. It is shown that each limb of a minimanipulator, or any other symmetric six-DOF parallel manipulator, must have six degrees of freedom in its joints. To minimize the number of loops in the structure of a minimanipulator, only three limbs are used in its synthesis. As a result, benefits such as simpler direct kinematics and lower possibility of mechanical interference between the limbs can be realized.

The two-DOF drivers can be designed to obtain larger workspace with reduced stiffness and resolution. The resulting mechanism can be used as a motion simulator. A minimanipulator can also be used as a passive compliant device or a force/torque sensor, if its actuators are replaced by rotational displacement transducers.

10.1.2 Inverse and Direct Kinematics

The inverse kinematics problem for the Type 1 minimanipulator, which represents the primary portion (platform and limbs) of any other type of minimanipulator, is reduced to solving three independent quadratic equation. Therefore, a maximum of eight solutions exist for the inverse kinematics of the Type 1 minimanipulator.

Kinematic inversion was used to obtain closed-form solution for the direct kinematics problem of the minimanipulators. It is shown that the maximum number of solutions for direct kinematics of the minimanipulator is sixteen. To obtain these solutions, only an eighth-degree polynomial in the square of a single variable has to be solved. It is also proved that the sixteen solutions are eight pairs of reflected configurations with respect to the plane passing through the lower ends of the three limbs. The results of a numerical example are verified by an inverse kinematics analysis.

10.1.3 Jacobian and Stiffness Analysis

Expressions for the Jacobian and stiffness matrices of the Type 1 (driven by bidirectional linear stepper motors) and Type 2 (driven by simplified five-bar linkages) minimanipulators are derived. It is shown that the central stiffness matrix of a Type 1 minimanipulator can be decoupled, if the platform size is made half of the size of the triangle passing through the lower ends of the limbs. Results of the Jacobian and stiffness analysis are used to establish guidelines for obtaining high stiffness values and for designing the drivers of the Type 2 minimanipulator. Moreover, it is shown that the stiffness of the minimanipulators is higher than that of the Stewart platform.

10.1.4 Workspace and Singularity Analysis

An algorithm is developed to determine the workspace of the minimanipulators. The workspace is six-dimensional in nature. To display it in three-dimensions, three variables must be held constant. Therefore, the algorithm finds the minimanipulator workspace for any given platform orientation. Guidelines for avoiding discontinuities inside of the workspace are established.

Necessary and sufficient conditions for both inverse kinematics singularities and direct kinematics singularities are obtained. The later which could occur within the minimanipulator workspace is discussed in more detail. It is found that a minimanipulator is in a direct kinematics singular configuration if

- Lower ends of the three limbs fall on a straight line. This includes the conditions under which two or all three of the limbs' lower ends coincide.
- One of the limbs lie on the base plane and the top ends of the other two limbs are at the same distance from the base plane.
- The angles between two of the limbs and the platform are equal to zero or 180 degrees.
- The angle between one of the limbs and the platform is equal to 180 degrees and the ratio of limb length to platform circumradius is equal to 3, i.e., $r/p = 3$.
- The angles between two of the limbs and the platform are equal in magnitude and opposite in sign, and the magnitude is equal to arc-cosine of $3p/r$.

If a simplified five-bar linkage drivers is used, then additional direct kinematics singularities occur when

- The driver input angles (θ_i and ϕ_i) are equal.

- The difference between the driver input angles is equal to 180 degrees and the input link length is equal to the output link length (i.e., $a = b$).

10.2 Recommendations for Future Research

In what follows, we suggest some ideas for further work related to the minimanipulators.

Wood and plastic models of the minimanipulators have been built by the author. These models have been invaluable in understanding singularities of the minimanipulators. However, due to high tolerances in manufacture of the parts used in the models, they are not rigid enough. Also, since they were built much earlier, their dimensions are not based on the guidelines obtained in this research. Therefore, the dimensional synthesis guidelines (Chapter 9) should be used in building more rigid (perhaps metal) prototypes for the minimanipulators. This can be followed by making a complete minimanipulator system with sensors and actuators.

Equation (8.25) gives the direct kinematics singularity condition in terms of the angles between the limbs and the platform. It would be interesting if one could transform this equation to another one involving only input displacements and minimanipulator dimensions. This is a very challenging problem, because as shown in Chapter 4, the mapping from the input displacements to the angle between a limb and the platform involves an eighth-order polynomial.

Elimination of direct kinematics singularities through introduction of redundant actuators can be studied.

The workspace algorithm can be expanded to calculate the workspace volume so that comparison between different workspace sizes can be performed more quickly.

Dynamic behavior of the minimanipulators should be studied so that appropriate control schemes could be devised for their operations. Lots of interesting work can be performed in position, and force control of the minimanipulators.

Path planning problem of the minimanipulators should also be considered, so that an optimality condition (e.g., minimization of energy) is satisfied and/or collisions are avoided.

References

- Arai, T., Cleary, K., Nakamura, T., Adachi, H., and Homma, K., 1990, "Design, Analysis and Construction of a Prototype Parallel Link Manipulator," *Proc. of the IEEE International Workshop on Intelligent Robots and Systems (IROS '90)*, pp. 205-212.

- Asada, H., and Youcef-Toumi, K., 1984, "Analysis and Design of a Direct-Drive Arm with a Five-Bar-Link Parallel Drive Mechanism," *Trans. ASME, J. of Dynamic Systems, Measurement, and Control*, Vol. 106, pp. 225-230.

- Asada, H., and Ro, I.H., 1985, " A Linkage Design for Direct-Drive Arms," *Trans. ASME, J. of Mech., Transmis., and Auto. in Design*, Vol. 107, pp. 536-540.

- Asada, H., and Slotine, J.-J.E., 1986, *Robot Analysis and Control*, John Wiley and Sons, New York.

- Bajpai, A., and Roth, B., 1986, "Workspace and Mobility of a Closed-Loop Manipulator," *The International J. of Robotics Research*, Vol. 5, pp. 131-142.

- Behi, F., 1988, "Kinematic Analysis for a Six-Degree-of-Freedom 3-PRPS

Parallel Mechanism," *IEEE J. of Robotics and Automation*, Vol. 4, pp. 561-565.

- Bottema, O., and Roth, B., 1979, *Theoretical Kinematics*, North-Holland, Netherlands.

- Cleary, K., and Arai, T., 1991, "A Prototype Parallel Manipulator: Kinematics, Construction, Software, Workspace Results, and Singularity Analysis," *Proc. of the IEEE International Conference on Robotics and Automation*, pp. 566-571.

- Dieudonne, J.E., Parrish, R.V., and Bardusch, R.E., 1972, "An Actuator Extension Transformation for a Motion Simulator and an Inverse Transformation Applying Newton-Raphson's Method," *NASA Technical Report D-7076*, NASA/LRC, Hampton, VA.

- Fichter, E.F., and MacDowell, E.D., 1980, "A Novel Design for a Robot Arm," *Proc. Int. Computer Technology*, ASME, New York, pp. 250-256.

- Fichter, E.F., 1986, "A Stewart Platform-based Manipulator: General Theory and Practical Construction," *Int. J. of Robotics Research*, Vol. 5, pp. 157-182.

- Gosselin, C., 1990a, "Stiffness Mapping of Parallel Manipulators," *IEEE Transactions on Robotics and Automation*, Vol. 6, pp. 377-382.

- Gosselin, C., 1990b, "Determination of the Workspace of 6-DOF Parallel Manipulators," *Trans. ASME, J. of Mechanical Design*, Vol. 112, pp. 331-336.

- Gosselin, C., and Angeles, J., 1988, "The Optimum Kinematic Design of a Planar Three-Degree-of-Freedom Parallel Manipulator," *Trans. ASME, J. of Mech., Transmis., and Auto. in Design*, Vol. 110, pp. 35-41.

- Gosselin, C., and Angeles, J., 1989, "The Optimum Kinematic Design of a Spherical Three-Degree-of-Freedom Parallel Manipulator," *Trans. ASME, J. of Mech., Transmis., and Auto. in Design*, Vol. 111, pp. 202-207.

- Gosselin, C., and Angeles, J., 1990, "Singularity Analysis of Closed-Loop Kinematic Chains," *IEEE Transactions on Robotics and Automation*, Vol. 6, pp. 281-290.

- Griffis, M., and Duffy, J., 1989, "A Forward Displacement Analysis of a Class of Stewart Platforms," *J. of Robotic Systems*, Vol. 6, pp. 703-720.

- Gupta, K.C., and Roth, B., 1982, "Design Considerations for Manipulator Workspace," *Trans. ASME, J. of Mechanical Design*, Vol. 104, pp. 704-711.

- Hudgens, J.C., and Tesar, D., 1988, "A Fully-Parallel Six Degree-of-Freedom Micromanipulator: Kinematic Analysis and Dynamic Model," *Trends and Developments in Mechanisms, Machines, and Robotics - Proc. of the 20th Biennial Mechanisms Conference*, ASME, New York, DE-Vol. 15-3, pp. 29-37.

- Hunt, K.H., 1983, "Structural Kinematics of In-Parallel-Actuated Robot-Arms," *Trans. ASME, J. of Mech., Transmis., and Auto. in Design*, Vol. 105, pp. 705-712.

- Hunt, K.H., 1990, *Kinematic Geometry of Mechanisms*, Clarendon Press, Oxford.

- Innocenti, C., and Parenti-Castelli, V., 1990, "Direct Position Analysis of the Stewart Platform Mechanism," *Mechanism and Machine Theory*, Vol. 25, pp. 611-612.

- Kane, T.R., and Levinson, D.A., 1985, *Dynamics: Theory and Applications*, McGraw-Hill, New York.

- Kerr, D.R., 1989, "Analysis, Properties, and Design of a Stewart-Platform Transducer," *Trans. ASME, J. of Mech., Transmis., and Auto. in Design*, Vol. 111, pp. 25-28.

- Klein, C.A., and Blaho, B.E., 1987, "Dexterity Measures for the Design and Control of Kinematically Redundant Manipulators," *Int. J. of Robotics Research*, Vol. 6, pp. 72-83.

- Kohli, D., Lee, S.H., Tsai, K.Y., and Sandor, G.N., 1988, "Manipulator Configurations Based on Rotary-Linear (R-L) Actuators and Their Direct and Inverse Kinematics," *Trans. ASME, J. of Mech., Transmis., and Auto. in Design*, Vol. 110, pp. 397-404.

- Kohli, D., and Spanos, J., 1985, "Workspace Analysis of Mechanical Manipulators Using Polynomial Discriminants," *Trans. ASME. J. of Mech., Transmis., and Auto. in Design*, Vol. 107, pp. 209-215.

- Kumar, A., and Waldron, K.J., 1981, "The Workspace of a Mechanical

Manipulator," *Trans. ASME, J. of Mechanical Design*, Vol. 112, pp. 665-672.

- Lee, M.Y., Erdman, A.G., and Gutman, Yevsey, 1991, "Development of Kinematic/Kinetic Performance Tools in Synthesis of Multi-D.O.F. Mechanisms," *Proc. of the Design Automation Conference*, ASME, New York, DE-Vol. 32-2, pp. 291-300.

- Lin, W., Duffy, J., and Griffis, M., 1990, "Forward Displacement Analyses of the 4-4 Stewart Platforms," *Proc. of the 21st Biennial Mechanisms Conference*, ASME, New York, DE-Vol. 25, pp. 263-269.

- Lipkin, H., and Pohl, E., 1991, "Enumeration of Singular Configurations for Robotic Manipulators," *Trans. ASME, J. of Mechanical Design*, Vol. 113, pp. 272-279.

- Ma, O., and Angeles, J., 1991, "Architecture Singularities of Platform Manipulators," *Proc. of the IEEE International Conference on Robotics and Automation*, pp. 1542-1547.

- Macsyma, 1988, *Reference Manual Version 13*, Symbolics, Inc., Burlington, MA.

- Merlet, J.P., 1987, "Parallel Manipulators, Part I: Theory, Design, Kinematics, Dynamics and Control," *Technical Report 646*, INRIA, France.

- Merlet, J.P., 1989, "Singular Configurations of Parallel Manipulators and Grassman Geometry," *Int. J. of Robotics Research*, Vol. 8, pp. 45-56.

- Mohamed, M.G., and Duffy, J., 1985, "A Direct Determination of the Instantaneous Kinematics of Fully Parallel Robot Manipulators," *Trans. ASME, J. of Mech., Transmis., and Auto. in Design*, Vol. 107, pp. 226-229.

- Mouly, N., and Merlet, J.P., 1992, "Singular Configurations and Direct Kinematics of a New Parallel Manipulator," *Proc. of the IEEE International Conference on Robotics and Automation*, pp. 338-343.

- Murthy, V., and Waldron, K.J., 1990a, "The Parallel Dual of the Stanford Arm," *Proc. of the 21st Biennial Mechanisms Conference*, ASME, New York, DE-Vol. 25, pp. 141-145.

- Murthy, V., and Waldron, K.J., 1990b, "Position Kinematics of the Generalized Lobster Arm and its Series-Parallel Dual," *Proc. of the 21st Biennial Mechanisms Conference*, ASME, New York, DE-Vol. 25, pp. 253-261.

- Nanua, P., Waldron, K.J., and Murthy, V., 1990, "Direct Kinematic Solution of a Stewart Platform," *IEEE Transactions on Robotics and Automation*, Vol. 6, pp. 438-444.

- Nguyen, C.C., and Pooran, F.J., 1989, "Kinematic Analysis and Workspace Determination of a 6 DOF CKCM Robot End-Effector," *J. of Mechanical Working Technology* (Netherlands), Vol. 20, pp. 283-294.

- Parenti-Castelli, V., and Innocenti, C., 1990, "Forward Displacement Analysis of Parallel Mechanisms: Closed Form Solution of PRR-3S and PPR-3S

Structures," *Proc. of the 21st Biennial Mechanisms Conference*, ASME, New York, DE-Vol. 25, pp. 111-116.

- Premack, T., Strempek, F.M., Solis, L.A., Brodd, S.S., Cutler, E.P., and Purves, L.P., 1984, "Design and Implementation of a Compliant Robot with Force Feedback and Strategy Planning Software," *NASA Technical Memorandum 86111*, NASA/GSFC, Greenbelt, MD.

- Raghavan, M., 1991, "The Stewart Platform of General Geometry Has 40 Configurations," *Advances in Design Automation - Vol. 2*, ASME, New York, DE-Vol. 32-2, pp. 397-402.

- Salisbury, J.K., and Craig, J.J., 1982, "Articulated Hands: Force Control and Kinematic Issues," *Int. J. of Robotics Research*, Vol. 1, pp. 4-17.

- Salmon, G., 1964, *Lessons Introductory to the Modern Higher Algebra* (Fifth Edition), Chelsea, New York, pp. 76-83.

- Song, S.M., Waldron, K.J., and Kinzel, G.L., 1985, "Computer-Aided Geometric Design of Legs for a Walking Vehicle," *Mechanism and Machine Theory*, Vol. 20, pp. 587-596.

- Stewart, D., 1965, "A Platform with Six Degrees of Freedom," *Proc. Institute of Mechanical Engr.*, London, England, Vol. 180, pp. 371-386.

- Strang, G., 1988, *Linear Algebra and Its Applications* (Third Edition), Harcourt Brace Jovanovich, San Diego.

- Sugimoto, K., 1987, "Kinematic and Dynamic Analysis of Parallel Manipulators by Means of Motor Algebra," *Trans. ASME, J. of Mech., Transmis., and Auto. in Design*, Vol. 109, pp. 3-7.

- Tahmasebi, F., and Tsai, L.W., 1992a, "Closed-Form Direct Kinematics Solution of a New Parallel Minimanipulator," *Proc. of the Japan-U.S.A. Symposium on Flexible Automation*, ASME, New York, pp. 117-124.

- Tahmasebi, F., and Tsai, L.W., 1992b, "Jacobian and Stiffness Analysis of a Novel Class of Six-DOF Parallel Minimanipulators," *Proc. of the 22nd Biennial Mechanisms Conference*, ASME, New York, DE-Vol. 47, pp. 95-102.

- Tsai, L.W., and Tahmasebi, F., 1991, "Design and Analysis of a New Six-Degree-of-Freedom Parallel Minimanipulator," *Proc. of the 6th International Conference on CAD/CAM, Robotics, and Factories of the Future*, South Bank Press, London, UK, pp. 568-575.

- Tsai, L.W., and Tahmasebi, F., 1992, "Synthesis and Analysis of a New Class of Six-Degree-of-Freedom Parallel Minimanipulators," Accepted for publication in *J. of Robotic Systems.*

- Wang, S.L., and Waldron, K.J., 1987, "A Study of Singular Configurations of Serial Manipulators," *Trans. ASME, J. of Mech., Transmis.. and Auto. in Design*, Vol. 109, pp. 14-20.

- Waldron, K.J., and Hunt, K.H., 1987, "Series-Parallel Dualities in Actively Coordinated Mechanisms," *Proc. of the 4th Int. Symp. on Robotic*

Research, MIT press, Cambridge, MA, pp. 175-181.

- Waldron, K.J., Raghavan, M., and Roth, B., 1989, "Kinematics of a Hybrid Series-Parallel Manipulation System," *Trans. ASME, J. of Dynamic Systems, Measurement, and Control*, Vol. 111, pp. 211-221.

- Waldron, K.J., Wang, S.L., Bolin, S.J., 1985, "A Study of the Jacobian Matrix of Serial Manipulators," *Trans. ASME, J. of Mech., Transmis., and Auto. in Design*, Vol. 107, pp. 230-238.

- Wolfram, S., 1991, *Mathematica, A System for Doing Mathematics by Computer* (Second Edition), Addison-Wesley, New York.

- Yang, D.C., and Lee, T.W., 1983, "On the Workspace of Mechanical Manipulators," *Trans. ASME, J. of Mech., Transmis., and Auto. in Design*, Vol. 105, pp. 62-69.

- Yang, D.C., and Lee, T.W., 1984, "Feasibility Study of a Platform Type of Robotic Manipulator from a Kinematic Viewpoint," *Trans. ASME, J. of Mech., Transmis., and Auto. in Design*, Vol. 106, pp. 191-198.

- Yang, F.C., and Haug, E.J., 1991, "Numerical Analysis of the Kinematic Dexterity of Mechanisms," *Advances in Design Automation - Vol. 2*, ASME, New York, DE-Vol. 32-2, pp. 301-310.

- Yeaple, F., 1988, "Choreographed Robots Insert Automotive Parts," *Design News*, Vol. 44, No. 21, pp. 134-135.

- Yoshikawa, T., 1985, "Manipulability of Robotic Mechanisms," *Int. J. of Robotics Research*, Vol. 4, pp. 3-9.

- Zhang, C., and Song, S.M., 1990, "Kinematics of Parallel Manipulators with a Positional Subchain," *Proc. of the 21st Biennial Mechanisms Conference*, ASME, New York, pp. 271-278.

- Zhang, C., and Song, S.M., 1991, "Forward Kinematics of a Class of Parallel (Stewart) Platforms with Closed-Form Solutions," *Proc. of the IEEE International Conference on Robotics and Automation*, pp. 2676-2681.

Appendix A

Theorem 1

A symmetric six-DOF parallel manipulator can have any number of limbs and each limb must have six degrees of freedom in its joints.

Proof:

Definition of a symmetric parallel manipulator is given in section 2.2. Symbols used in the proof are described in Table A.1. Each limb is an open kinematic chain which connects the base to the platform. Let $\jmath$ include the top and bottom joints which connect a limb to the platform and the base. Then

$$\jmath = n + 1 \tag{A.1}$$

Total number of links and joints in a parallel manipulator are related to number of links and joints in each limb by the following relationships.

$$N = mn + 2 \tag{A.2}$$

$$J = m\jmath \tag{A.3}$$

Number of DOF of a mechanism can be obtained from the following mobility

Symbol	**Description**
f_l	degrees of freedom of joint l
F	degrees of freedom of a parallel manipulator
$\jmath$	number of joints in each limb
J	total number of joints in a parallel manipulator
l	index
m	number of limbs in a parallel manipulator
n	number of links in each limb
N	total number of links in a parallel manipulator
λ'	3 for planar and spherical mechanisms, 6 for spatial mechanisms
σ	total degrees of freedom in joints of each limb

Table A.1: Description of symbols used in proof of Theorem 1.

F	m	σ
1	5	5
2	2	4
2	4	5
3	3	5
4	2	5
6	any number	6

Table A.2: Acceptable values of F, m, and σ $(1 \leq F \leq 6, m \geq 2)$.

equation (Hunt, 1990).

$$F = \lambda'(N - J - 1) + \sum_{l=1}^{J} f_l \tag{A.4}$$

For a symmetric spatial parallel manipulator, $\lambda' = 6$, and

$$\sum_{l=1}^{J} f_l = m\sigma \tag{A.5}$$

Therefore, the mobility equation reduces to

$$F = 6[mn + 2 - m(n + 1) - 1] + m\sigma$$

or

$$\sigma = 6 - \frac{6 - F}{m} \tag{A.6}$$

For $1 \leq F \leq 6$, the values of σ and m which satisfy equation (A.6) are given in Table A.2. Note that we consider m to be greater than or equal to two, because we are only interested in parallel manipulators. If $F = 6$, equation (A.6) reduces to

$$\sigma = 6$$

Since the number of limbs (m) does not appear in the above result, any number of limbs can be used.

Appendix B

Derivation of Equation (4.15)

Let

$$K_1 = F_1 t_1^2 + G_1, L_1 = I_1 t_1, M_1 = G_1 t_1^2 + J_1$$

and

$$K_2 = F_2 t_3^2 + G_2, L_2 = I_2 t_3, M_2 = G_2 t_3^2 + J_2$$

then equations (4.12) and (4.13) can be written as

$$K_1 t_2^2 + L_1 t_2 + M_1 = 0 \tag{B.1}$$

and

$$K_2 t_2^2 + L_2 t_2 + M_2 = 0 \tag{B.2}$$

Multiplying equation (B.1) by K_2 and equation (B.2) by K_1, and subtracting, we get

$$(L_1 K_2 - L_2 K_1) t_2 + (M_1 K_2 - M_2 K_1) = 0 \tag{B.3}$$

Multiplying equation (B.1) by M_2 and equation (B.2) by M_1, subtracting, and dividing by t_2, we get

$$(K_1 M_2 - K_2 M_1) t_2 + (L_1 M_2 - L_2 M_1) = 0 \tag{B.4}$$

Equations (B.3) and (B.4) represent two linear equations in one unknown. Vanishing of their eliminant[1] means

$$\begin{vmatrix} L_1K_2 - L_2K_1 & M_1K_2 - M_2K_1 \\ K_1M_2 - K_2M_1 & L_1M_2 - L_2M_1 \end{vmatrix} = 0 \tag{B.5}$$

Expanding equation (B.5) and substituting the expressions for K_1, L_1, M_1, K_2, L_2, and M_2 into the resulting equation, we get

$$\begin{aligned}
&F_1^2 G_2^2 t_1^4 t_3^4 - 2 F_1 F_2 G_1 G_2 t_1^4 t_3^4 + F_2^2 G_1^2 t_1^4 t_3^4 - 2 F_1 F_2 G_2 J_1 t_1^2 t_3^4 + \\
&2 F_2^2 G_1 J_1 t_1^2 t_3^4 + F_2 G_2 I_1^2 t_1^2 t_3^4 + 2 F_1 G_1 G_2^2 t_1^2 t_3^4 - 2 F_2 G_1^2 G_2 t_1^2 t_3^4 + \\
&F_2^2 J_1^2 t_3^4 - 2 F_2 G_1 G_2 J_1 t_3^4 + G_1^2 G_2^2 t_3^4 - F_1 G_2 I_1 I_2 t_1^3 t_3^3 - \\
&F_2 G_1 I_1 I_2 t_1^3 t_3^3 - F_2 I_1 I_2 J_1 t_1 t_3^3 - G_1 G_2 I_1 I_2 t_1 t_3^3 + 2 F_1^2 G_2 J_2 t_1^4 t_3^2 - \\
&2 F_1 F_2 G_1 J_2 t_1^4 t_3^2 + F_1 G_1 I_2^2 t_1^4 t_3^2 - 2 F_1 G_1 G_2^2 t_1^4 t_3^2 + 2 F_2 G_1^2 G_2 t_1^4 t_3^2 - \\
&2 F_1 F_2 J_1 J_2 t_1^2 t_3^2 + F_2 I_1^2 J_2 t_1^2 t_3^2 + 4 F_1 G_1 G_2 J_2 t_1^2 t_3^2 - 2 F_2 G_1^2 J_2 t_1^2 t_3^2 + \\
&F_1 I_2^2 J_1 t_1^2 t_3^2 - 2 F_1 G_2^2 J_1 t_1^2 t_3^2 + 4 F_2 G_1 G_2 J_1 t_1^2 t_3^2 + G_1^2 I_2^2 t_1^2 t_3^2 + \\
&G_2^2 I_1^2 t_1^2 t_3^2 - 2 G_1^2 G_2^2 t_1^2 t_3^2 - 2 F_2 G_1 J_1 J_2 t_3^2 + 2 G_1^2 G_2 J_2 t_3^2 + \\
&2 F_2 G_2 J_1^2 t_3^2 + G_1 I_2^2 J_1 t_3^2 - 2 G_1 G_2^2 J_1 t_3^2 - F_1 I_1 I_2 J_2 t_1^3 t_3 - \\
&G_1 G_2 I_1 I_2 t_1^3 t_3 - G_1 I_1 I_2 J_2 t_1 t_3 - G_2 I_1 I_2 J_1 t_1 t_3 + F_1^2 J_2^2 t_1^4 - \\
&2 F_1 G_1 G_2 J_2 t_1^4 + G_1^2 G_2^2 t_1^4 + 2 F_1 G_1 J_2^2 t_1^2 - 2 F_1 G_2 J_1 J_2 t_1^2 + \\
&G_2 I_1^2 J_2 t_1^2 - 2 G_1^2 G_2 J_2 t_1^2 + 2 G_1 G_2^2 J_1 t_1^2 + G_1^2 J_2^2 - \\
&2 G_1 G_2 J_1 J_2 + G_2^2 J_1^2 = 0
\end{aligned} \tag{B.6}$$

[1]Given n+1 linear equations in n unknowns, the determinant of the coefficients is called the eliminant of the equations. Such a determinant must vanish, if the system of equations is to have a solution.

Factoring the above equation results in equation (4.15). The above method is introduced by Salmon (1964).

Appendix C

Derivation and Expansion of Equation (4.16)

Equations (4.15) and (4.14) can be rewritten in the following forms

$$N_1 t_3^4 + N_2 t_3^3 + N_3 t_3^2 + N_4 t_3 + N_5 = 0 \tag{C.1}$$

$$S_1 t_3^2 + S_2 t_3 + S_3 = 0 \tag{C.2}$$

Multiplying equation (C.1) by S_1 and equation (C.2) by $N_1 t_3^2$, and subtracting, we get

$$(N_2 S_1 - N_1 S_2) t_3^3 + (N_3 S_1 - N_1 S_3) t_3^2 + N_4 S_1 t_3 + N_5 S_1 = 0 \tag{C.3}$$

Multiplying equation (C.1) by $S_1 t_3 + S_2$ and equation (C.2) by $N_1 t_3^3 + N_2 t_3^2$, and subtracting, we get

$$(N_3 S_1 - N_1 S_3) t_3^3 + (N_4 S_1 + N_3 S_2 - N_2 S_3) t_3^2 + (N_5 S_1 + N_4 S_2) t_3 + N_5 S_2 = 0 \tag{C.4}$$

Multiplying equation (C.2) by t_3, we get

$$S_1 t_3^3 + S_2 t_3^2 + S_3 t_3 = 0 \tag{C.5}$$

We can think of equations (C.3), (C.4), (C.5), and (C.2) as four linear equations in three unknowns t_3^3, t_3^2, and t_3. Vanishing of their eliminant[1] means

$$\begin{vmatrix} N_2S_1 - N_1S_2 & N_3S_1 - N_1S_3 & N_4S_1 & N_5S_1 \\ N_3S_1 - N_1S_3 & N_4S_1 + N_3S_2 - N_2S_3 & N_5S_1 + N_4S_2 & N_5S_2 \\ S_1 & S_2 & S_3 & 0 \\ 0 & S_1 & S_2 & S_3 \end{vmatrix} = 0 \qquad \text{(C.6)}$$

Expansion of equation (C.6) results in equation (4.16). If we substitute the expressions given in section 4.3.2 for $S_1, S_2, S_3, N_1, N_2, N_3, N_4$, and N_5 and expand equation (4.16), we get

$$\Xi_1 t_1^{16} + \Xi_2 t_1^{14} + \Xi_3 t_1^{12} + \Xi_4 t_1^{10} + \Xi_5 t_1^8 + \Xi_6 t_1^6 + \Xi_7 t_1^4 + \Xi_8 t_1^2 + \Xi_9 = 0 \qquad \text{(C.7)}$$

where

$$\Xi_1 = -F_3^2\,G_3^2\,Q_6^2 + 2\,F_3^3\,G_3\,Q_{11}\,Q_6 + 2\,F_3\,G_3^3\,Q_1\,Q_6 - F_3^4\,Q_{11}^2 - 2\,F_3^2\,G_3^2\,Q_1\,Q_{11} - G_3^4\,Q_1^2$$

$$\begin{aligned}\Xi_2 = {} & -F_3^3\,G_3\,Q_9^2 + F_3^2\,G_3\,I_3\,Q_6\,Q_9 + 2\,F_3^2\,G_3^2\,Q_4\,Q_9 + F_3^3\,I_3\,Q_{11}\,Q_9 - \\ & 3\,F_3\,G_3^2\,I_3\,Q_1\,Q_9 - 2\,F_3^2\,G_3^2\,Q_6\,Q_7 + 2\,F_3^3\,G_3\,Q_{11}\,Q_7 + 2\,F_3\,G_3^3\,Q_1\,Q_7 - \\ & 2\,F_3^2\,G_3\,J_3\,Q_6^2 - 2\,F_3\,G_3^3\,Q_6^2 + F_3\,G_3^2\,I_3\,Q_4\,Q_6 + 2\,F_3\,G_3^3\,Q_2\,Q_6 + \\ & 2\,F_3^3\,G_3\,Q_{12}\,Q_6 + 2\,F_3^3\,J_3\,Q_{11}\,Q_6 - F_3^2\,I_3^2\,Q_{11}\,Q_6 + 6\,F_3^2\,G_3^2\,Q_{11}\,Q_6 + \\ & 6\,F_3\,G_3^2\,J_3\,Q_1\,Q_6 - G_3^2\,I_3^2\,Q_1\,Q_6 + 2\,G_3^4\,Q_1\,Q_6 - F_3\,G_3^3\,Q_4^2 - \\ & 3\,F_3^2\,G_3\,I_3\,Q_{11}\,Q_4 + G_3^3\,I_3\,Q_1\,Q_4 - 2\,F_3^2\,G_3^2\,Q_{11}\,Q_2 - 2\,G_3^4\,Q_1\,Q_2 - \\ & 2\,F_3^4\,Q_{11}\,Q_{12} - 2\,F_3^2\,G_3^2\,Q_1\,Q_{12} - 4\,F_3^3\,G_3\,Q_{11}^2 - 4\,F_3^2\,G_3\,J_3\,Q_1\,Q_{11} + \\ & 4\,F_3\,G_3\,I_3^2\,Q_1\,Q_{11} - 4\,F_3\,G_3^3\,Q_1\,Q_{11} - 4\,G_3^3\,J_3\,Q_1^2\end{aligned}$$

[1]Refer to Appendix B for the definition of eliminant.

$$
\begin{aligned}
\Xi_3 = & -F_3{}^3 J_3 Q_9{}^2 - 3 F_3{}^2 G_3{}^2 Q_9{}^2 + F_3{}^2 G_3 I_3 Q_7 Q_9 + F_3{}^2 I_3 J_3 Q_6 Q_9 + \\
& 2 F_3 G_3{}^2 I_3 Q_6 Q_9 + 2 F_3{}^2 G_3{}^2 Q_5 Q_9 + 4 F_3{}^2 G_3 J_3 Q_4 Q_9 - F_3 G_3 I_3{}^2 Q_4 Q_9 + \\
& 4 F_3 G_3{}^3 Q_4 Q_9 - 3 F_3 G_3{}^2 I_3 Q_2 Q_9 + F_3{}^3 I_3 Q_{12} Q_9 + 3 F_3{}^2 G_3 I_3 Q_{11} Q_9 - \\
& 2 F_3{}^3 G_3 Q_{10} Q_9 - 6 F_3 G_3 I_3 J_3 Q_1 Q_9 + G_3 I_3{}^3 Q_1 Q_9 - 3 G_3{}^3 I_3 Q_1 Q_9 - \\
& 2 F_3{}^2 G_3{}^2 Q_6 Q_8 + 2 F_3{}^3 G_3 Q_{11} Q_8 + 2 F_3 G_3{}^3 Q_1 Q_8 - F_3{}^2 G_3{}^2 Q_7{}^2 - \\
& 4 F_3{}^2 G_3 J_3 Q_6 Q_7 - 4 F_3 G_3{}^3 Q_6 Q_7 + F_3 G_3{}^2 I_3 Q_4 Q_7 + 2 F_3 G_3{}^3 Q_2 Q_7 + \\
& 2 F_3{}^3 G_3 Q_{12} Q_7 + 2 F_3{}^3 J_3 Q_{11} Q_7 - F_3{}^2 I_3{}^2 Q_{11} Q_7 + 6 F_3{}^2 G_3{}^2 Q_{11} Q_7 + \\
& 6 F_3 G_3{}^2 J_3 Q_1 Q_7 - G_3{}^2 I_3{}^2 Q_1 Q_7 + 2 G_3{}^4 Q_1 Q_7 - F_3{}^2 J_3{}^2 Q_6{}^2 - \\
& 4 F_3 G_3{}^2 J_3 Q_6{}^2 - G_3{}^4 Q_6{}^2 + F_3 G_3{}^2 I_3 Q_5 Q_6 + 2 F_3 G_3 I_3 J_3 Q_4 Q_6 + \\
& G_3{}^3 I_3 Q_4 Q_6 + 2 F_3 G_3{}^3 Q_3 Q_6 + 6 F_3 G_3{}^2 J_3 Q_2 Q_6 - G_3{}^2 I_3{}^2 Q_2 Q_6 + \\
& 2 G_3{}^4 Q_2 Q_6 + 2 F_3{}^3 G_3 Q_{13} Q_6 + 2 F_3{}^3 J_3 Q_{12} Q_6 - F_3{}^2 I_3{}^2 Q_{12} Q_6 + \\
& 6 F_3{}^2 G_3{}^2 Q_{12} Q_6 + 6 F_3{}^2 G_3 J_3 Q_{11} Q_6 - 2 F_3 G_3 I_3{}^2 Q_{11} Q_6 + 6 F_3 G_3{}^3 Q_{11} Q_6 + \\
& F_3{}^2 G_3 I_3 Q_{10} Q_6 + 6 F_3 G_3 J_3{}^2 Q_1 Q_6 - 2 G_3 I_3{}^2 J_3 Q_1 Q_6 + 6 G_3{}^3 J_3 Q_1 Q_6 - \\
& 2 F_3 G_3{}^3 Q_4 Q_5 - 3 F_3{}^2 G_3 I_3 Q_{11} Q_5 + G_3{}^3 I_3 Q_1 Q_5 - 3 F_3 G_3{}^2 J_3 Q_4{}^2 - \\
& G_3{}^4 Q_4{}^2 + G_3{}^3 I_3 Q_2 Q_4 - 3 F_3{}^2 G_3 I_3 Q_{12} Q_4 - 3 F_3{}^2 I_3 J_3 Q_{11} Q_4 + \\
& F_3 I_3{}^3 Q_{11} Q_4 - 6 F_3 G_3{}^2 I_3 Q_{11} Q_4 + 2 F_3{}^2 G_3{}^2 Q_{10} Q_4 + 3 G_3{}^2 I_3 J_3 Q_1 Q_4 - \\
& 2 F_3{}^2 G_3{}^2 Q_{11} Q_3 - 2 G_3{}^4 Q_1 Q_3 - G_3{}^4 Q_2{}^2 - 2 F_3{}^2 G_3{}^2 Q_{12} Q_2 - \\
& 4 F_3{}^2 G_3 J_3 Q_{11} Q_2 + 4 F_3 G_3 I_3{}^2 Q_{11} Q_2 - 4 F_3 G_3{}^3 Q_{11} Q_2 - 8 G_3{}^3 J_3 Q_1 Q_2 - \\
& 2 F_3{}^4 Q_{11} Q_{13} - 2 F_3{}^2 G_3{}^2 Q_1 Q_{13} - F_3{}^4 Q_{12}{}^2 - 8 F_3{}^3 G_3 Q_{11} Q_{12} - \\
& 4 F_3{}^2 G_3 J_3 Q_1 Q_{12} + 4 F_3 G_3 I_3{}^2 Q_1 Q_{12} - 4 F_3 G_3{}^3 Q_1 Q_{12} - 6 F_3{}^2 G_3{}^2 Q_{11}{}^2 + \\
& F_3{}^3 I_3 Q_{10} Q_{11} - 2 F_3{}^2 J_3{}^2 Q_1 Q_{11} + 4 F_3 I_3{}^2 J_3 Q_1 Q_{11} - 8 F_3 G_3{}^2 J_3 Q_1 Q_{11} - \\
& I_3{}^4 Q_1 Q_{11} + 4 G_3{}^2 I_3{}^2 Q_1 Q_{11} - 2 G_3{}^4 Q_1 Q_{11} - 3 F_3 G_3{}^2 I_3 Q_1 Q_{10} -
\end{aligned}
$$

$6\,G_3{}^2\,J_3{}^2\,Q_1{}^2$

$$
\begin{aligned}
\Xi_4 = {} & -3\,F_3{}^2\,G_3\,J_3\,Q_9{}^2 - 3\,F_3\,G_3{}^3\,Q_9{}^2 + F_3{}^2\,G_3\,I_3\,Q_8\,Q_9 + F_3{}^2\,I_3\,J_3\,Q_7\,Q_9 + \\
& 2\,F_3\,G_3{}^2\,I_3\,Q_7\,Q_9 + 2\,F_3\,G_3\,I_3\,J_3\,Q_6\,Q_9 + G_3{}^3\,I_3\,Q_6\,Q_9 + 4\,F_3{}^2\,G_3\,J_3\,Q_5\,Q_9 - \\
& F_3\,G_3\,I_3{}^2\,Q_5\,Q_9 + 4\,F_3\,G_3{}^3\,Q_5\,Q_9 + 2\,F_3{}^2\,J_3{}^2\,Q_4\,Q_9 - F_3\,I_3{}^2\,J_3\,Q_4\,Q_9 + \\
& 8\,F_3\,G_3{}^2\,J_3\,Q_4\,Q_9 - G_3{}^2\,I_3{}^2\,Q_4\,Q_9 + 2\,G_3{}^4\,Q_4\,Q_9 - 3\,F_3\,G_3{}^2\,I_3\,Q_3\,Q_9 - \\
& 6\,F_3\,G_3\,I_3\,J_3\,Q_2\,Q_9 + G_3\,I_3{}^3\,Q_2\,Q_9 - 3\,G_3{}^3\,I_3\,Q_2\,Q_9 + F_3{}^3\,I_3\,Q_{13}\,Q_9 + \\
& 3\,F_3{}^2\,G_3\,I_3\,Q_{12}\,Q_9 + 3\,F_3\,G_3{}^2\,I_3\,Q_{11}\,Q_9 - 2\,F_3{}^3\,J_3\,Q_{10}\,Q_9 - 6\,F_3{}^2\,G_3{}^2\,Q_{10}\,Q_9 - \\
& 3\,F_3\,I_3\,J_3{}^2\,Q_1\,Q_9 + I_3{}^3\,J_3\,Q_1\,Q_9 - 6\,G_3{}^2\,I_3\,J_3\,Q_1\,Q_9 - 2\,F_3{}^2\,G_3{}^2\,Q_7\,Q_8 - \\
& 4\,F_3{}^2\,G_3\,J_3\,Q_6\,Q_8 - 4\,F_3\,G_3{}^3\,Q_6\,Q_8 + F_3\,G_3{}^2\,I_3\,Q_4\,Q_8 + 2\,F_3\,G_3{}^3\,Q_2\,Q_8 + \\
& 2\,F_3{}^3\,G_3\,Q_{12}\,Q_8 + 2\,F_3{}^3\,J_3\,Q_{11}\,Q_8 - F_3{}^2\,I_3{}^2\,Q_{11}\,Q_8 + 6\,F_3{}^2\,G_3{}^2\,Q_{11}\,Q_8 + \\
& 6\,F_3\,G_3{}^2\,J_3\,Q_1\,Q_8 - G_3{}^2\,I_3{}^2\,Q_1\,Q_8 + 2\,G_3{}^4\,Q_1\,Q_8 - 2\,F_3{}^2\,G_3\,J_3\,Q_7{}^2 - \\
& 2\,F_3\,G_3{}^3\,Q_7{}^2 - 2\,F_3{}^2\,J_3{}^2\,Q_6\,Q_7 - 8\,F_3\,G_3{}^2\,J_3\,Q_6\,Q_7 - 2\,G_3{}^4\,Q_6\,Q_7 + \\
& F_3\,G_3{}^2\,I_3\,Q_5\,Q_7 + 2\,F_3\,G_3\,I_3\,J_3\,Q_4\,Q_7 + G_3{}^3\,I_3\,Q_4\,Q_7 + 2\,F_3\,G_3{}^3\,Q_3\,Q_7 + \\
& 6\,F_3\,G_3{}^2\,J_3\,Q_2\,Q_7 - G_3{}^2\,I_3{}^2\,Q_2\,Q_7 + 2\,G_3{}^4\,Q_2\,Q_7 + 2\,F_3{}^3\,G_3\,Q_{13}\,Q_7 + \\
& 2\,F_3{}^3\,J_3\,Q_{12}\,Q_7 - F_3{}^2\,I_3{}^2\,Q_{12}\,Q_7 + 6\,F_3{}^2\,G_3{}^2\,Q_{12}\,Q_7 + 6\,F_3{}^2\,G_3\,J_3\,Q_{11}\,Q_7 - \\
& 2\,F_3\,G_3\,I_3{}^2\,Q_{11}\,Q_7 + 6\,F_3\,G_3{}^3\,Q_{11}\,Q_7 + F_3{}^2\,G_3\,I_3\,Q_{10}\,Q_7 + 6\,F_3\,G_3\,J_3{}^2\,Q_1\,Q_7 - \\
& 2\,G_3\,I_3{}^2\,J_3\,Q_1\,Q_7 + 6\,G_3{}^3\,J_3\,Q_1\,Q_7 - 2\,F_3\,G_3\,J_3{}^2\,Q_6{}^2 - 2\,G_3{}^3\,J_3\,Q_6{}^2 + \\
& 2\,F_3\,G_3\,I_3\,J_3\,Q_5\,Q_6 + G_3{}^3\,I_3\,Q_5\,Q_6 + F_3\,I_3\,J_3{}^2\,Q_4\,Q_6 + 2\,G_3{}^2\,I_3\,J_3\,Q_4\,Q_6 + \\
& 6\,F_3\,G_3{}^2\,J_3\,Q_3\,Q_6 - G_3{}^2\,I_3{}^2\,Q_3\,Q_6 + 2\,G_3{}^4\,Q_3\,Q_6 + 6\,F_3\,G_3\,J_3{}^2\,Q_2\,Q_6 - \\
& 2\,G_3\,I_3{}^2\,J_3\,Q_2\,Q_6 + 6\,G_3{}^3\,J_3\,Q_2\,Q_6 + 2\,F_3{}^3\,J_3\,Q_{13}\,Q_6 - F_3{}^2\,I_3{}^2\,Q_{13}\,Q_6 + \\
& 6\,F_3{}^2\,G_3{}^2\,Q_{13}\,Q_6 + 6\,F_3{}^2\,G_3\,J_3\,Q_{12}\,Q_6 - 2\,F_3\,G_3\,I_3{}^2\,Q_{12}\,Q_6 + 6\,F_3\,G_3{}^3\,Q_{12}\,Q_6 +
\end{aligned}
$$

$$
\begin{aligned}
&6\,F_3\,G_3{}^2\,J_3\,Q_{11}\,Q_6 - G_3{}^2\,I_3{}^2\,Q_{11}\,Q_6 + 2\,G_3{}^4\,Q_{11}\,Q_6 + F_3{}^2\,I_3\,J_3\,Q_{10}\,Q_6 + \\
&2\,F_3\,G_3{}^2\,I_3\,Q_{10}\,Q_6 + 2\,F_3\,J_3{}^3\,Q_1\,Q_6 - I_3{}^2\,J_3{}^2\,Q_1\,Q_6 + 6\,G_3{}^2\,J_3{}^2\,Q_1\,Q_6 - \\
&F_3\,G_3{}^3\,Q_5{}^2 - 6\,F_3\,G_3{}^2\,J_3\,Q_4\,Q_5 - 2\,G_3{}^4\,Q_4\,Q_5 + G_3{}^3\,I_3\,Q_2\,Q_5 - \\
&3\,F_3{}^2\,G_3\,I_3\,Q_{12}\,Q_5 - 3\,F_3{}^2\,I_3\,J_3\,Q_{11}\,Q_5 + F_3\,I_3{}^3\,Q_{11}\,Q_5 - 6\,F_3\,G_3{}^2\,I_3\,Q_{11}\,Q_5 + \\
&2\,F_3{}^2\,G_3{}^2\,Q_{10}\,Q_5 + 3\,G_3{}^2\,I_3\,J_3\,Q_1\,Q_5 - 3\,F_3\,G_3\,J_3{}^2\,Q_4{}^2 - 3\,G_3{}^3\,J_3\,Q_4{}^2 + \\
&G_3{}^3\,I_3\,Q_3\,Q_4 + 3\,G_3{}^2\,I_3\,J_3\,Q_2\,Q_4 - 3\,F_3{}^2\,G_3\,I_3\,Q_{13}\,Q_4 - 3\,F_3{}^2\,I_3\,J_3\,Q_{12}\,Q_4 + \\
&F_3\,I_3{}^3\,Q_{12}\,Q_4 - 6\,F_3\,G_3{}^2\,I_3\,Q_{12}\,Q_4 - 6\,F_3\,G_3\,I_3\,J_3\,Q_{11}\,Q_4 + G_3\,I_3{}^3\,Q_{11}\,Q_4 - \\
&3\,G_3{}^3\,I_3\,Q_{11}\,Q_4 + 4\,F_3{}^2\,G_3\,J_3\,Q_{10}\,Q_4 - F_3\,G_3\,I_3{}^2\,Q_{10}\,Q_4 + 4\,F_3\,G_3{}^3\,Q_{10}\,Q_4 + \\
&3\,G_3\,I_3\,J_3{}^2\,Q_1\,Q_4 - 2\,G_3{}^4\,Q_2\,Q_3 - 2\,F_3{}^2\,G_3{}^2\,Q_{12}\,Q_3 - 4\,F_3{}^2\,G_3\,J_3\,Q_{11}\,Q_3 + \\
&4\,F_3\,G_3\,I_3{}^2\,Q_{11}\,Q_3 - 4\,F_3\,G_3{}^3\,Q_{11}\,Q_3 - 8\,G_3{}^3\,J_3\,Q_1\,Q_3 - 4\,G_3{}^3\,J_3\,Q_2{}^2 - \\
&2\,F_3{}^2\,G_3{}^2\,Q_{13}\,Q_2 - 4\,F_3{}^2\,G_3\,J_3\,Q_{12}\,Q_2 + 4\,F_3\,G_3\,I_3{}^2\,Q_{12}\,Q_2 - 4\,F_3\,G_3{}^3\,Q_{12}\,Q_2 - \\
&2\,F_3{}^2\,J_3{}^2\,Q_{11}\,Q_2 + 4\,F_3\,I_3{}^2\,J_3\,Q_{11}\,Q_2 - 8\,F_3\,G_3{}^2\,J_3\,Q_{11}\,Q_2 - I_3{}^4\,Q_{11}\,Q_2 + \\
&4\,G_3{}^2\,I_3{}^2\,Q_{11}\,Q_2 - 2\,G_3{}^4\,Q_{11}\,Q_2 - 3\,F_3\,G_3{}^2\,I_3\,Q_{10}\,Q_2 - 12\,G_3{}^2\,J_3{}^2\,Q_1\,Q_2 - \\
&2\,F_3{}^4\,Q_{12}\,Q_{13} - 8\,F_3{}^3\,G_3\,Q_{11}\,Q_{13} - 4\,F_3{}^2\,G_3\,J_3\,Q_1\,Q_{13} + 4\,F_3\,G_3\,I_3{}^2\,Q_1\,Q_{13} - \\
&4\,F_3\,G_3{}^3\,Q_1\,Q_{13} - 4\,F_3{}^3\,G_3\,Q_{12}{}^2 - 12\,F_3{}^2\,G_3{}^2\,Q_{11}\,Q_{12} + F_3{}^3\,I_3\,Q_{10}\,Q_{12} - \\
&2\,F_3{}^2\,J_3{}^2\,Q_1\,Q_{12} + 4\,F_3\,I_3{}^2\,J_3\,Q_1\,Q_{12} - 8\,F_3\,G_3{}^2\,J_3\,Q_1\,Q_{12} - I_3{}^4\,Q_1\,Q_{12} + \\
&4\,G_3{}^2\,I_3{}^2\,Q_1\,Q_{12} - 2\,G_3{}^4\,Q_1\,Q_{12} - 4\,F_3\,G_3{}^3\,Q_{11}{}^2 + 3\,F_3{}^2\,G_3\,I_3\,Q_{10}\,Q_{11} - \\
&4\,F_3\,G_3\,J_3{}^2\,Q_1\,Q_{11} + 4\,G_3\,I_3{}^2\,J_3\,Q_1\,Q_{11} - 4\,G_3{}^3\,J_3\,Q_1\,Q_{11} - F_3{}^3\,G_3\,Q_{10}{}^2 - \\
&6\,F_3\,G_3\,I_3\,J_3\,Q_1\,Q_{10} + G_3\,I_3{}^3\,Q_1\,Q_{10} - 3\,G_3{}^3\,I_3\,Q_1\,Q_{10} - 4\,G_3\,J_3{}^3\,Q_1{}^2
\end{aligned}
$$

$$
\begin{aligned}
\Xi_5 = {} & -3\,F_3\,G_3{}^2\,J_3\,Q_9{}^2 - G_3{}^4\,Q_9{}^2 + F_3{}^2\,I_3\,J_3\,Q_8\,Q_9 + 2\,F_3\,G_3{}^2\,I_3\,Q_8\,Q_9 + \\
& 2\,F_3\,G_3\,I_3\,J_3\,Q_7\,Q_9 + G_3{}^3\,I_3\,Q_7\,Q_9 + G_3{}^2\,I_3\,J_3\,Q_6\,Q_9 + 2\,F_3{}^2\,J_3{}^2\,Q_5\,Q_9 - \\
& F_3\,I_3{}^2\,J_3\,Q_5\,Q_9 + 8\,F_3\,G_3{}^2\,J_3\,Q_5\,Q_9 - G_3{}^2\,I_3{}^2\,Q_5\,Q_9 + 2\,G_3{}^4\,Q_5\,Q_9 +
\end{aligned}
$$

$$4\,F_3\,G_3\,J_3^2\,Q_4\,Q_9 - G_3\,I_3^2\,J_3\,Q_4\,Q_9 + 4\,G_3^3\,J_3\,Q_4\,Q_9 - 6\,F_3\,G_3\,I_3\,J_3\,Q_3\,Q_9 +$$

$$G_3\,I_3^3\,Q_3\,Q_9 - 3\,G_3^3\,I_3\,Q_3\,Q_9 - 3\,F_3\,I_3\,J_3^2\,Q_2\,Q_9 + I_3^3\,J_3\,Q_2\,Q_9 -$$

$$6\,G_3^2\,I_3\,J_3\,Q_2\,Q_9 + 3\,F_3^2\,G_3\,I_3\,Q_{13}\,Q_9 + 3\,F_3\,G_3^2\,I_3\,Q_{12}\,Q_9 + G_3^3\,I_3\,Q_{11}\,Q_9 -$$

$$6\,F_3^2\,G_3\,J_3\,Q_{10}\,Q_9 - 6\,F_3\,G_3^3\,Q_{10}\,Q_9 - 3\,G_3\,I_3\,J_3^2\,Q_1\,Q_9 - F_3^2\,G_3^2\,Q_8^2 -$$

$$4\,F_3^2\,G_3\,J_3\,Q_7\,Q_8 - 4\,F_3\,G_3^3\,Q_7\,Q_8 - 2\,F_3^2\,J_3^2\,Q_6\,Q_8 - 8\,F_3\,G_3^2\,J_3\,Q_6\,Q_8 -$$

$$2\,G_3^4\,Q_6\,Q_8 + F_3\,G_3^2\,I_3\,Q_5\,Q_8 + 2\,F_3\,G_3\,I_3\,J_3\,Q_4\,Q_8 + G_3^3\,I_3\,Q_4\,Q_8 +$$

$$2\,F_3\,G_3^3\,Q_3\,Q_8 + 6\,F_3\,G_3^2\,J_3\,Q_2\,Q_8 - G_3^2\,I_3^2\,Q_2\,Q_8 + 2\,G_3^4\,Q_2\,Q_8 +$$

$$2\,F_3^3\,G_3\,Q_{13}\,Q_8 + 2\,F_3^3\,J_3\,Q_{12}\,Q_8 - F_3^2\,I_3^2\,Q_{12}\,Q_8 + 6\,F_3^2\,G_3^2\,Q_{12}\,Q_8 +$$

$$6\,F_3^2\,G_3\,J_3\,Q_{11}\,Q_8 - 2\,F_3\,G_3\,I_3^2\,Q_{11}\,Q_8 + 6\,F_3\,G_3^3\,Q_{11}\,Q_8 + F_3^2\,G_3\,I_3\,Q_{10}\,Q_8 +$$

$$6\,F_3\,G_3\,J_3^2\,Q_1\,Q_8 - 2\,G_3\,I_3^2\,J_3\,Q_1\,Q_8 + 6\,G_3^3\,J_3\,Q_1\,Q_8 - F_3^2\,J_3^2\,Q_7^2 -$$

$$4\,F_3\,G_3^2\,J_3\,Q_7^2 - G_3^4\,Q_7^2 - 4\,F_3\,G_3\,J_3^2\,Q_6\,Q_7 - 4\,G_3^3\,J_3\,Q_6\,Q_7 +$$

$$2\,F_3\,G_3\,I_3\,J_3\,Q_5\,Q_7 + G_3^3\,I_3\,Q_5\,Q_7 + F_3\,I_3\,J_3^2\,Q_4\,Q_7 + 2\,G_3^2\,I_3\,J_3\,Q_4\,Q_7 +$$

$$6\,F_3\,G_3^2\,J_3\,Q_3\,Q_7 - G_3^2\,I_3^2\,Q_3\,Q_7 + 2\,G_3^4\,Q_3\,Q_7 + 6\,F_3\,G_3\,J_3^2\,Q_2\,Q_7 -$$

$$2\,G_3\,I_3^2\,J_3\,Q_2\,Q_7 + 6\,G_3^3\,J_3\,Q_2\,Q_7 + 2\,F_3^3\,J_3\,Q_{13}\,Q_7 - F_3^2\,I_3^2\,Q_{13}\,Q_7 +$$

$$6\,F_3^2\,G_3^2\,Q_{13}\,Q_7 + 6\,F_3^2\,G_3\,J_3\,Q_{12}\,Q_7 - 2\,F_3\,G_3\,I_3^2\,Q_{12}\,Q_7 + 6\,F_3\,G_3^3\,Q_{12}\,Q_7 +$$

$$6\,F_3\,G_3^2\,J_3\,Q_{11}\,Q_7 - G_3^2\,I_3^2\,Q_{11}\,Q_7 + 2\,G_3^4\,Q_{11}\,Q_7 + F_3^2\,I_3\,J_3\,Q_{10}\,Q_7 +$$

$$2\,F_3\,G_3^2\,I_3\,Q_{10}\,Q_7 + 2\,F_3\,J_3^3\,Q_1\,Q_7 - I_3^2\,J_3^2\,Q_1\,Q_7 + 6\,G_3^2\,J_3^2\,Q_1\,Q_7 -$$

$$G_3^2\,J_3^2\,Q_6^2 + F_3\,I_3\,J_3^2\,Q_5\,Q_6 + 2\,G_3^2\,I_3\,J_3\,Q_5\,Q_6 + G_3\,I_3\,J_3^2\,Q_4\,Q_6 +$$

$$6\,F_3\,G_3\,J_3^2\,Q_3\,Q_6 - 2\,G_3\,I_3^2\,J_3\,Q_3\,Q_6 + 6\,G_3^3\,J_3\,Q_3\,Q_6 + 2\,F_3\,J_3^3\,Q_2\,Q_6 -$$

$$I_3^2\,J_3^2\,Q_2\,Q_6 + 6\,G_3^2\,J_3^2\,Q_2\,Q_6 + 6\,F_3^2\,G_3\,J_3\,Q_{13}\,Q_6 - 2\,F_3\,G_3\,I_3^2\,Q_{13}\,Q_6 +$$

$$6\,F_3\,G_3^3\,Q_{13}\,Q_6 + 6\,F_3\,G_3^2\,J_3\,Q_{12}\,Q_6 - G_3^2\,I_3^2\,Q_{12}\,Q_6 + 2\,G_3^4\,Q_{12}\,Q_6 +$$

$$2\,G_3^3\,J_3\,Q_{11}\,Q_6 + 2\,F_3\,G_3\,I_3\,J_3\,Q_{10}\,Q_6 + G_3^3\,I_3\,Q_{10}\,Q_6 + 2\,G_3\,J_3^3\,Q_1\,Q_6 -$$

$3\,F_3\,G_3^{\,2}\,J_3\,Q_5^{\,2} - G_3^{\,4}\,Q_5^{\,2} - 6\,F_3\,G_3\,J_3^{\,2}\,Q_4\,Q_5 - 6\,G_3^{\,3}\,J_3\,Q_4\,Q_5 +$

$G_3^{\,3}\,I_3\,Q_3\,Q_5 + 3\,G_3^{\,2}\,I_3\,J_3\,Q_2\,Q_5 - 3\,F_3^{\,2}\,G_3\,I_3\,Q_{13}\,Q_5 - 3\,F_3^{\,2}\,I_3\,J_3\,Q_{12}\,Q_5 +$

$F_3\,I_3^{\,3}\,Q_{12}\,Q_5 - 6\,F_3\,G_3^{\,2}\,I_3\,Q_{12}\,Q_5 - 6\,F_3\,G_3\,I_3\,J_3\,Q_{11}\,Q_5 + G_3\,I_3^{\,3}\,Q_{11}\,Q_5 -$

$3\,G_3^{\,3}\,I_3\,Q_{11}\,Q_5 + 4\,F_3^{\,2}\,G_3\,J_3\,Q_{10}\,Q_5 - F_3\,G_3\,I_3^{\,2}\,Q_{10}\,Q_5 + 4\,F_3\,G_3^{\,3}\,Q_{10}\,Q_5 +$

$3\,G_3\,I_3\,J_3^{\,2}\,Q_1\,Q_5 - F_3\,J_3^{\,3}\,Q_4^{\,2} - 3\,G_3^{\,2}\,J_3^{\,2}\,Q_4^{\,2} + 3\,G_3^{\,2}\,I_3\,J_3\,Q_3\,Q_4 +$

$3\,G_3\,I_3\,J_3^{\,2}\,Q_2\,Q_4 - 3\,F_3^{\,2}\,I_3\,J_3\,Q_{13}\,Q_4 + F_3\,I_3^{\,3}\,Q_{13}\,Q_4 - 6\,F_3\,G_3^{\,2}\,I_3\,Q_{13}\,Q_4 -$

$6\,F_3\,G_3\,I_3\,J_3\,Q_{12}\,Q_4 + G_3\,I_3^{\,3}\,Q_{12}\,Q_4 - 3\,G_3^{\,3}\,I_3\,Q_{12}\,Q_4 - 3\,G_3^{\,2}\,I_3\,J_3\,Q_{11}\,Q_4 +$

$2\,F_3^{\,2}\,J_3^{\,2}\,Q_{10}\,Q_4 - F_3\,I_3^{\,2}\,J_3\,Q_{10}\,Q_4 + 8\,F_3\,G_3^{\,2}\,J_3\,Q_{10}\,Q_4 - G_3^{\,2}\,I_3^{\,2}\,Q_{10}\,Q_4 +$

$2\,G_3^{\,4}\,Q_{10}\,Q_4 + I_3\,J_3^{\,3}\,Q_1\,Q_4 - G_3^{\,4}\,Q_3^{\,2} - 8\,G_3^{\,3}\,J_3\,Q_2\,Q_3 -$

$2\,F_3^{\,2}\,G_3^{\,2}\,Q_{13}\,Q_3 - 4\,F_3^{\,2}\,G_3\,J_3\,Q_{12}\,Q_3 + 4\,F_3\,G_3\,I_3^{\,2}\,Q_{12}\,Q_3 - 4\,F_3\,G_3^{\,3}\,Q_{12}\,Q_3 -$

$2\,F_3^{\,2}\,J_3^{\,2}\,Q_{11}\,Q_3 + 4\,F_3\,I_3^{\,2}\,J_3\,Q_{11}\,Q_3 - 8\,F_3\,G_3^{\,2}\,J_3\,Q_{11}\,Q_3 - I_3^{\,4}\,Q_{11}\,Q_3 +$

$4\,G_3^{\,2}\,I_3^{\,2}\,Q_{11}\,Q_3 - 2\,G_3^{\,4}\,Q_{11}\,Q_3 - 3\,F_3\,G_3^{\,2}\,I_3\,Q_{10}\,Q_3 - 12\,G_3^{\,2}\,J_3^{\,2}\,Q_1\,Q_3 -$

$6\,G_3^{\,2}\,J_3^{\,2}\,Q_2^{\,2} - 4\,F_3^{\,2}\,G_3\,J_3\,Q_{13}\,Q_2 + 4\,F_3\,G_3\,I_3^{\,2}\,Q_{13}\,Q_2 - 4\,F_3\,G_3^{\,3}\,Q_{13}\,Q_2 -$

$2\,F_3^{\,2}\,J_3^{\,2}\,Q_{12}\,Q_2 + 4\,F_3\,I_3^{\,2}\,J_3\,Q_{12}\,Q_2 - 8\,F_3\,G_3^{\,2}\,J_3\,Q_{12}\,Q_2 - I_3^{\,4}\,Q_{12}\,Q_2 +$

$4\,G_3^{\,2}\,I_3^{\,2}\,Q_{12}\,Q_2 - 2\,G_3^{\,4}\,Q_{12}\,Q_2 - 4\,F_3\,G_3\,J_3^{\,2}\,Q_{11}\,Q_2 + 4\,G_3\,I_3^{\,2}\,J_3\,Q_{11}\,Q_2 -$

$4\,G_3^{\,3}\,J_3\,Q_{11}\,Q_2 - 6\,F_3\,G_3\,I_3\,J_3\,Q_{10}\,Q_2 + G_3\,I_3^{\,3}\,Q_{10}\,Q_2 - 3\,G_3^{\,3}\,I_3\,Q_{10}\,Q_2 -$

$8\,G_3\,J_3^{\,3}\,Q_1\,Q_2 - F_3^{\,4}\,Q_{13}^{\,2} - 8\,F_3^{\,3}\,G_3\,Q_{12}\,Q_{13} - 12\,F_3^{\,2}\,G_3^{\,2}\,Q_{11}\,Q_{13} +$

$F_3^{\,3}\,I_3\,Q_{10}\,Q_{13} - 2\,F_3^{\,2}\,J_3^{\,2}\,Q_1\,Q_{13} + 4\,F_3\,I_3^{\,2}\,J_3\,Q_1\,Q_{13} - 8\,F_3\,G_3^{\,2}\,J_3\,Q_1\,Q_{13} -$

$I_3^{\,4}\,Q_1\,Q_{13} + 4\,G_3^{\,2}\,I_3^{\,2}\,Q_1\,Q_{13} - 2\,G_3^{\,4}\,Q_1\,Q_{13} - 6\,F_3^{\,2}\,G_3^{\,2}\,Q_{12}^{\,2} -$

$8\,F_3\,G_3^{\,3}\,Q_{11}\,Q_{12} + 3\,F_3^{\,2}\,G_3\,I_3\,Q_{10}\,Q_{12} - 4\,F_3\,G_3\,J_3^{\,2}\,Q_1\,Q_{12} + 4\,G_3\,I_3^{\,2}\,J_3\,Q_1\,Q_{12} -$

$4\,G_3^{\,3}\,J_3\,Q_1\,Q_{12} - G_3^{\,4}\,Q_{11}^{\,2} + 3\,F_3\,G_3^{\,2}\,I_3\,Q_{10}\,Q_{11} - 2\,G_3^{\,2}\,J_3^{\,2}\,Q_1\,Q_{11} -$

$F_3^{\,3}\,J_3\,Q_{10}^{\,2} - 3\,F_3^{\,2}\,G_3^{\,2}\,Q_{10}^{\,2} - 3\,F_3\,I_3\,J_3^{\,2}\,Q_1\,Q_{10} + I_3^{\,3}\,J_3\,Q_1\,Q_{10} -$

$$6\,G_3^2\,I_3\,J_3\,Q_1\,Q_{10}-J_3^4\,Q_1^2$$

$$\Xi_6=-G_3^3\,J_3\,Q_9^2+2\,F_3\,G_3\,I_3\,J_3\,Q_8\,Q_9+G_3^3\,I_3\,Q_8\,Q_9+G_3^2\,I_3\,J_3\,Q_7\,Q_9+$$
$$4\,F_3\,G_3\,J_3^2\,Q_5\,Q_9-G_3\,I_3^2\,J_3\,Q_5\,Q_9+4\,G_3^3\,J_3\,Q_5\,Q_9+2\,G_3^2\,J_3^2\,Q_4\,Q_9-$$
$$3\,F_3\,I_3\,J_3^2\,Q_3\,Q_9+I_3^3\,J_3\,Q_3\,Q_9-6\,G_3^2\,I_3\,J_3\,Q_3\,Q_9-3\,G_3\,I_3\,J_3^2\,Q_2\,Q_9+$$
$$3\,F_3\,G_3^2\,I_3\,Q_{13}\,Q_9+G_3^3\,I_3\,Q_{12}\,Q_9-6\,F_3\,G_3^2\,J_3\,Q_{10}\,Q_9-2\,G_3^4\,Q_{10}\,Q_9-$$
$$2\,F_3^2\,G_3\,J_3\,Q_8^2-2\,F_3\,G_3^3\,Q_8^2-2\,F_3^2\,J_3^2\,Q_7\,Q_8-8\,F_3\,G_3^2\,J_3\,Q_7\,Q_8-$$
$$2\,G_3^4\,Q_7\,Q_8-4\,F_3\,G_3\,J_3^2\,Q_6\,Q_8-4\,G_3^3\,J_3\,Q_6\,Q_8+2\,F_3\,G_3\,I_3\,J_3\,Q_5\,Q_8+$$
$$G_3^3\,I_3\,Q_5\,Q_8+F_3\,I_3\,J_3^2\,Q_4\,Q_8+2\,G_3^2\,I_3\,J_3\,Q_4\,Q_8+6\,F_3\,G_3^2\,J_3\,Q_3\,Q_8-$$
$$G_3^2\,I_3^2\,Q_3\,Q_8+2\,G_3^4\,Q_3\,Q_8+6\,F_3\,G_3\,J_3^2\,Q_2\,Q_8-2\,G_3\,I_3^2\,J_3\,Q_2\,Q_8+$$
$$6\,G_3^3\,J_3\,Q_2\,Q_8+2\,F_3^3\,J_3\,Q_{13}\,Q_8-F_3^2\,I_3^2\,Q_{13}\,Q_8+6\,F_3^2\,G_3^2\,Q_{13}\,Q_8+$$
$$6\,F_3^2\,G_3\,J_3\,Q_{12}\,Q_8-2\,F_3\,G_3\,I_3^2\,Q_{12}\,Q_8+6\,F_3\,G_3^3\,Q_{12}\,Q_8+6\,F_3\,G_3^2\,J_3\,Q_{11}\,Q_8-$$
$$G_3^2\,I_3^2\,Q_{11}\,Q_8+2\,G_3^4\,Q_{11}\,Q_8+F_3^2\,I_3\,J_3\,Q_{10}\,Q_8+2\,F_3\,G_3^2\,I_3\,Q_{10}\,Q_8+$$
$$2\,F_3\,J_3^3\,Q_1\,Q_8-I_3^2\,J_3^2\,Q_1\,Q_8+6\,G_3^2\,J_3^2\,Q_1\,Q_8-2\,F_3\,G_3\,J_3^2\,Q_7^2-$$
$$2\,G_3^3\,J_3\,Q_7^2-2\,G_3^2\,J_3^2\,Q_6\,Q_7+F_3\,I_3\,J_3^2\,Q_5\,Q_7+2\,G_3^2\,I_3\,J_3\,Q_5\,Q_7+$$
$$G_3\,I_3\,J_3^2\,Q_4\,Q_7+6\,F_3\,G_3\,J_3^2\,Q_3\,Q_7-2\,G_3\,I_3^2\,J_3\,Q_3\,Q_7+6\,G_3^3\,J_3\,Q_3\,Q_7+$$
$$2\,F_3\,J_3^3\,Q_2\,Q_7-I_3^2\,J_3^2\,Q_2\,Q_7+6\,G_3^2\,J_3^2\,Q_2\,Q_7+6\,F_3^2\,G_3\,J_3\,Q_{13}\,Q_7-$$
$$2\,F_3\,G_3\,I_3^2\,Q_{13}\,Q_7+6\,F_3\,G_3^3\,Q_{13}\,Q_7+6\,F_3\,G_3^2\,J_3\,Q_{12}\,Q_7-G_3^2\,I_3^2\,Q_{12}\,Q_7+$$
$$2\,G_3^4\,Q_{12}\,Q_7+2\,G_3^3\,J_3\,Q_{11}\,Q_7+2\,F_3\,G_3\,I_3\,J_3\,Q_{10}\,Q_7+G_3^3\,I_3\,Q_{10}\,Q_7+$$
$$2\,G_3\,J_3^3\,Q_1\,Q_7+G_3\,I_3\,J_3^2\,Q_5\,Q_6+2\,F_3\,J_3^3\,Q_3\,Q_6-I_3^2\,J_3^2\,Q_3\,Q_6+$$
$$6\,G_3^2\,J_3^2\,Q_3\,Q_6+2\,G_3\,J_3^3\,Q_2\,Q_6+6\,F_3\,G_3^2\,J_3\,Q_{13}\,Q_6-G_3^2\,I_3^2\,Q_{13}\,Q_6+$$
$$2\,G_3^4\,Q_{13}\,Q_6+2\,G_3^3\,J_3\,Q_{12}\,Q_6+G_3^2\,I_3\,J_3\,Q_{10}\,Q_6-3\,F_3\,G_3\,J_3^2\,Q_5^2-$$

$$3\,G_3^3\,J_3\,Q_5^2 - 2\,F_3\,J_3^3\,Q_4\,Q_5 - 6\,G_3^2\,J_3^2\,Q_4\,Q_5 + 3\,G_3^2\,I_3\,J_3\,Q_3\,Q_5 +$$

$$3\,G_3\,I_3\,J_3^2\,Q_2\,Q_5 - 3\,F_3^2\,I_3\,J_3\,Q_{13}\,Q_5 + F_3\,I_3^3\,Q_{13}\,Q_5 - 6\,F_3\,G_3^2\,I_3\,Q_{13}\,Q_5 -$$

$$6\,F_3\,G_3\,I_3\,J_3\,Q_{12}\,Q_5 + G_3\,I_3^3\,Q_{12}\,Q_5 - 3\,G_3^3\,I_3\,Q_{12}\,Q_5 - 3\,G_3^2\,I_3\,J_3\,Q_{11}\,Q_5 +$$

$$2\,F_3^2\,J_3^2\,Q_{10}\,Q_5 - F_3\,I_3^2\,J_3\,Q_{10}\,Q_5 + 8\,F_3\,G_3^2\,J_3\,Q_{10}\,Q_5 - G_3^2\,I_3^2\,Q_{10}\,Q_5 +$$

$$2\,G_3^4\,Q_{10}\,Q_5 + I_3\,J_3^3\,Q_1\,Q_5 - G_3\,J_3^3\,Q_4^2 + 3\,G_3\,I_3\,J_3^2\,Q_3\,Q_4 +$$

$$I_3\,J_3^3\,Q_2\,Q_4 - 6\,F_3\,G_3\,I_3\,J_3\,Q_{13}\,Q_4 + G_3\,I_3^3\,Q_{13}\,Q_4 - 3\,G_3^3\,I_3\,Q_{13}\,Q_4 -$$

$$3\,G_3^2\,I_3\,J_3\,Q_{12}\,Q_4 + 4\,F_3\,G_3\,J_3^2\,Q_{10}\,Q_4 - G_3\,I_3^2\,J_3\,Q_{10}\,Q_4 + 4\,G_3^3\,J_3\,Q_{10}\,Q_4 -$$

$$4\,G_3^3\,J_3\,Q_3^2 - 12\,G_3^2\,J_3^2\,Q_2\,Q_3 - 4\,F_3^2\,G_3\,J_3\,Q_{13}\,Q_3 + 4\,F_3\,G_3\,I_3^2\,Q_{13}\,Q_3 -$$

$$4\,F_3\,G_3^3\,Q_{13}\,Q_3 - 2\,F_3^2\,J_3^2\,Q_{12}\,Q_3 + 4\,F_3\,I_3^2\,J_3\,Q_{12}\,Q_3 - 8\,F_3\,G_3^2\,J_3\,Q_{12}\,Q_3 -$$

$$I_3^4\,Q_{12}\,Q_3 + 4\,G_3^2\,I_3^2\,Q_{12}\,Q_3 - 2\,G_3^4\,Q_{12}\,Q_3 - 4\,F_3\,G_3\,J_3^2\,Q_{11}\,Q_3 +$$

$$4\,G_3\,I_3^2\,J_3\,Q_{11}\,Q_3 - 4\,G_3^3\,J_3\,Q_{11}\,Q_3 - 6\,F_3\,G_3\,I_3\,J_3\,Q_{10}\,Q_3 + G_3\,I_3^3\,Q_{10}\,Q_3 -$$

$$3\,G_3^3\,I_3\,Q_{10}\,Q_3 - 8\,G_3\,J_3^3\,Q_1\,Q_3 - 4\,G_3\,J_3^3\,Q_2^2 - 2\,F_3^2\,J_3^2\,Q_{13}\,Q_2 +$$

$$4\,F_3\,I_3^2\,J_3\,Q_{13}\,Q_2 - 8\,F_3\,G_3^2\,J_3\,Q_{13}\,Q_2 - I_3^4\,Q_{13}\,Q_2 + 4\,G_3^2\,I_3^2\,Q_{13}\,Q_2 -$$

$$2\,G_3^4\,Q_{13}\,Q_2 - 4\,F_3\,G_3\,J_3^2\,Q_{12}\,Q_2 + 4\,G_3\,I_3^2\,J_3\,Q_{12}\,Q_2 - 4\,G_3^3\,J_3\,Q_{12}\,Q_2 -$$

$$2\,G_3^2\,J_3^2\,Q_{11}\,Q_2 - 3\,F_3\,I_3\,J_3^2\,Q_{10}\,Q_2 + I_3^3\,J_3\,Q_{10}\,Q_2 - 6\,G_3^2\,I_3\,J_3\,Q_{10}\,Q_2 -$$

$$2\,J_3^4\,Q_1\,Q_2 - 4\,F_3^3\,G_3\,Q_{13}^2 - 12\,F_3^2\,G_3^2\,Q_{12}\,Q_{13} - 8\,F_3\,G_3^3\,Q_{11}\,Q_{13} +$$

$$3\,F_3^2\,G_3\,I_3\,Q_{10}\,Q_{13} - 4\,F_3\,G_3\,J_3^2\,Q_1\,Q_{13} + 4\,G_3\,I_3^2\,J_3\,Q_1\,Q_{13} - 4\,G_3^3\,J_3\,Q_1\,Q_{13} -$$

$$4\,F_3\,G_3^3\,Q_{12}^2 - 2\,G_3^4\,Q_{11}\,Q_{12} + 3\,F_3\,G_3^2\,I_3\,Q_{10}\,Q_{12} - 2\,G_3^2\,J_3^2\,Q_1\,Q_{12} +$$

$$G_3^3\,I_3\,Q_{10}\,Q_{11} - 3\,F_3^2\,G_3\,J_3\,Q_{10}^2 - 3\,F_3\,G_3^3\,Q_{10}^2 - 3\,G_3\,I_3\,J_3^2\,Q_1\,Q_{10}$$

$$\Xi_7 = G_3^2\,I_3\,J_3\,Q_8\,Q_9 + 2\,G_3^2\,J_3^2\,Q_5\,Q_9 - 3\,G_3\,I_3\,J_3^2\,Q_3\,Q_9 + G_3^3\,I_3\,Q_{13}\,Q_9 -$$

$$2\,G_3^3\,J_3\,Q_{10}\,Q_9 - F_3^2\,J_3^2\,Q_8^2 - 4\,F_3\,G_3^2\,J_3\,Q_8^2 - G_3^4\,Q_8^2 -$$

$$4\,F_3\,G_3\,J_3^2\,Q_7\,Q_8 - 4\,G_3^3\,J_3\,Q_7\,Q_8 - 2\,G_3^2\,J_3^2\,Q_6\,Q_8 + F_3\,I_3\,J_3^2\,Q_5\,Q_8 +$$

$$2\,G_3^2\,I_3\,J_3\,Q_5\,Q_8 + G_3\,I_3\,J_3^2\,Q_4\,Q_8 + 6\,F_3\,G_3\,J_3^2\,Q_3\,Q_8 - 2\,G_3\,I_3^2\,J_3\,Q_3\,Q_8 +$$

$$6\,G_3^3\,J_3\,Q_3\,Q_8 + 2\,F_3\,J_3^3\,Q_2\,Q_8 - I_3^2\,J_3^2\,Q_2\,Q_8 + 6\,G_3^2\,J_3^2\,Q_2\,Q_8 +$$

$$6\,F_3^2\,G_3\,J_3\,Q_{13}\,Q_8 - 2\,F_3\,G_3\,I_3^2\,Q_{13}\,Q_8 + 6\,F_3\,G_3^3\,Q_{13}\,Q_8 + 6\,F_3\,G_3^2\,J_3\,Q_{12}\,Q_8 -$$

$$G_3^2\,I_3^2\,Q_{12}\,Q_8 + 2\,G_3^4\,Q_{12}\,Q_8 + 2\,G_3^3\,J_3\,Q_{11}\,Q_8 + 2\,F_3\,G_3\,I_3\,J_3\,Q_{10}\,Q_8 +$$

$$G_3^3\,I_3\,Q_{10}\,Q_8 + 2\,G_3\,J_3^3\,Q_1\,Q_8 - G_3^2\,J_3^2\,Q_7^2 + G_3\,I_3\,J_3^2\,Q_5\,Q_7 +$$

$$2\,F_3\,J_3^3\,Q_3\,Q_7 - I_3^2\,J_3^2\,Q_3\,Q_7 + 6\,G_3^2\,J_3^2\,Q_3\,Q_7 + 2\,G_3\,J_3^3\,Q_2\,Q_7 +$$

$$6\,F_3\,G_3^2\,J_3\,Q_{13}\,Q_7 - G_3^2\,I_3^2\,Q_{13}\,Q_7 + 2\,G_3^4\,Q_{13}\,Q_7 + 2\,G_3^3\,J_3\,Q_{12}\,Q_7 +$$

$$G_3^2\,I_3\,J_3\,Q_{10}\,Q_7 + 2\,G_3\,J_3^3\,Q_3\,Q_6 + 2\,G_3^3\,J_3\,Q_{13}\,Q_6 - F_3\,J_3^3\,Q_5^2 -$$

$$3\,G_3^2\,J_3^2\,Q_5^2 - 2\,G_3\,J_3^3\,Q_4\,Q_5 + 3\,G_3\,I_3\,J_3^2\,Q_3\,Q_5 + I_3\,J_3^3\,Q_2\,Q_5 -$$

$$6\,F_3\,G_3\,I_3\,J_3\,Q_{13}\,Q_5 + G_3\,I_3^3\,Q_{13}\,Q_5 - 3\,G_3^3\,I_3\,Q_{13}\,Q_5 - 3\,G_3^2\,I_3\,J_3\,Q_{12}\,Q_5 +$$

$$4\,F_3\,G_3\,J_3^2\,Q_{10}\,Q_5 - G_3\,I_3^2\,J_3\,Q_{10}\,Q_5 + 4\,G_3^3\,J_3\,Q_{10}\,Q_5 + I_3\,J_3^3\,Q_3\,Q_4 -$$

$$3\,G_3^2\,I_3\,J_3\,Q_{13}\,Q_4 + 2\,G_3^2\,J_3^2\,Q_{10}\,Q_4 - 6\,G_3^2\,J_3^2\,Q_3^2 - 8\,G_3\,J_3^3\,Q_2\,Q_3 -$$

$$2\,F_3^2\,J_3^2\,Q_{13}\,Q_3 + 4\,F_3\,I_3^2\,J_3\,Q_{13}\,Q_3 - 8\,F_3\,G_3^2\,J_3\,Q_{13}\,Q_3 - I_3^4\,Q_{13}\,Q_3 +$$

$$4\,G_3^2\,I_3^2\,Q_{13}\,Q_3 - 2\,G_3^4\,Q_{13}\,Q_3 - 4\,F_3\,G_3\,J_3^2\,Q_{12}\,Q_3 + 4\,G_3\,I_3^2\,J_3\,Q_{12}\,Q_3 -$$

$$4\,G_3^3\,J_3\,Q_{12}\,Q_3 - 2\,G_3^2\,J_3^2\,Q_{11}\,Q_3 - 3\,F_3\,I_3\,J_3^2\,Q_{10}\,Q_3 + I_3^3\,J_3\,Q_{10}\,Q_3 -$$

$$6\,G_3^2\,I_3\,J_3\,Q_{10}\,Q_3 - 2\,J_3^4\,Q_1\,Q_3 - J_3^4\,Q_2^2 - 4\,F_3\,G_3\,J_3^2\,Q_{13}\,Q_2 +$$

$$4\,G_3\,I_3^2\,J_3\,Q_{13}\,Q_2 - 4\,G_3^3\,J_3\,Q_{13}\,Q_2 - 2\,G_3^2\,J_3^2\,Q_{12}\,Q_2 - 3\,G_3\,I_3\,J_3^2\,Q_{10}\,Q_2 -$$

$$6\,F_3^2\,G_3^2\,Q_{13}^2 - 8\,F_3\,G_3^3\,Q_{12}\,Q_{13} - 2\,G_3^4\,Q_{11}\,Q_{13} + 3\,F_3\,G_3^2\,I_3\,Q_{10}\,Q_{13} -$$

$$2\,G_3^2\,J_3^2\,Q_1\,Q_{13} - G_3^4\,Q_{12}^2 + G_3^3\,I_3\,Q_{10}\,Q_{12} - 3\,F_3\,G_3^2\,J_3\,Q_{10}^2 -$$

$$G_3^4\,Q_{10}^2$$

$$\Xi_8 = -2\,F_3\,G_3\,J_3^2\,Q_8^2 - 2\,G_3^3\,J_3\,Q_8^2 - 2\,G_3^2\,J_3^2\,Q_7\,Q_8 + G_3\,I_3\,J_3^2\,Q_5\,Q_8 +$$

$$2\,F_3\,J_3^3\,Q_3\,Q_8 - I_3^2\,J_3^2\,Q_3\,Q_8 + 6\,G_3^2\,J_3^2\,Q_3\,Q_8 + 2\,G_3\,J_3^3\,Q_2\,Q_8 +$$

$$6\,F_3\,G_3^2\,J_3\,Q_{13}\,Q_8 - G_3^2\,I_3^2\,Q_{13}\,Q_8 + 2\,G_3^4\,Q_{13}\,Q_8 + 2\,G_3^3\,J_3\,Q_{12}\,Q_8 +$$

$$G_3^2\,I_3\,J_3\,Q_{10}\,Q_8 + 2\,G_3\,J_3^3\,Q_3\,Q_7 + 2\,G_3^3\,J_3\,Q_{13}\,Q_7 - G_3\,J_3^3\,Q_5^2 +$$

$$I_3\,J_3^3\,Q_3\,Q_5 - 3\,G_3^2\,I_3\,J_3\,Q_{13}\,Q_5 + 2\,G_3^2\,J_3^2\,Q_{10}\,Q_5 - 4\,G_3\,J_3^3\,Q_3^2 -$$

$$2\,J_3^4\,Q_2\,Q_3 - 4\,F_3\,G_3\,J_3^2\,Q_{13}\,Q_3 + 4\,G_3\,I_3^2\,J_3\,Q_{13}\,Q_3 - 4\,G_3^3\,J_3\,Q_{13}\,Q_3 -$$

$$2\,G_3^2\,J_3^2\,Q_{12}\,Q_3 - 3\,G_3\,I_3\,J_3^2\,Q_{10}\,Q_3 - 2\,G_3^2\,J_3^2\,Q_{13}\,Q_2 - 4\,F_3\,G_3^3\,Q_{13}^2 -$$

$$2\,G_3^4\,Q_{12}\,Q_{13} + G_3^3\,I_3\,Q_{10}\,Q_{13} - G_3^3\,J_3\,Q_{10}^2$$

$$\Xi_9 = -G_3^2\,J_3^2\,Q_8^2 + 2\,G_3\,J_3^3\,Q_3\,Q_8 + 2\,G_3^3\,J_3\,Q_{13}\,Q_8 - J_3^4\,Q_3^2 -$$

$$2\,G_3^2\,J_3^2\,Q_{13}\,Q_3 - G_3^4\,Q_{13}^2 = 0$$

The above method is introduced by Salmon (1964).

Appendix D

Lower Triangular Elements of $\breve{\mathrm{K}}$

$$\breve{K}_{1,1} = 3$$

$$\breve{K}_{2,1} = 0$$

$$\breve{K}_{2,2} = 3$$

$$\breve{K}_{3,1} = -\mu'_{3,\mathrm{x}} - \mu'_{2,\mathrm{x}} - \mu'_{1,\mathrm{x}}$$

$$\breve{K}_{3,2} = -\mu'_{3,\mathrm{y}} - \mu'_{2,\mathrm{y}} - \mu'_{1,\mathrm{y}}$$

$$\breve{K}_{3,3} = {\mu'_{3,\mathrm{y}}}^2 + {\mu'_{3,\mathrm{x}}}^2 + {\mu'_{2,\mathrm{y}}}^2 + {\mu'_{2,\mathrm{x}}}^2 + {\mu'_{1,\mathrm{y}}}^2 + {\mu'_{1,\mathrm{x}}}^2$$

$$\breve{K}_{4,1} = -\mu'_{3,\mathrm{x}}\,(\mathrm{Y}_{\mathrm{R},3} - \mathrm{Y}_{\mathrm{G}}) - \mu'_{2,\mathrm{x}}\,(\mathrm{Y}_{\mathrm{R},2} - \mathrm{Y}_{\mathrm{G}}) - \mu'_{1,\mathrm{x}}\,(\mathrm{Y}_{\mathrm{R},1} - \mathrm{Y}_{\mathrm{G}})$$

$$\breve{K}_{4,2} = 3\,\mathrm{Z}_{\mathrm{G}} - \mu'_{3,\mathrm{y}}\,(\mathrm{Y}_{\mathrm{R},3} - \mathrm{Y}_{\mathrm{G}}) - \mu'_{2,\mathrm{y}}\,(\mathrm{Y}_{\mathrm{R},2} - \mathrm{Y}_{\mathrm{G}}) - \mu'_{1,\mathrm{y}}\,(\mathrm{Y}_{\mathrm{R},1} - \mathrm{Y}_{\mathrm{G}})$$

$$\breve{K}_{4,3} = -\mu'_{3,y}\left[Z_G - \mu'_{3,y}\left(Y_{R,3} - Y_G\right)\right] - \mu'_{2,y}\left[Z_G - \mu'_{2,y}\left(Y_{R,2} - Y_G\right)\right] - \mu'_{1,y}\left[Z_G - \mu'_{1,y}\left(Y_{R,1} - Y_G\right)\right] + {\mu'_{3,x}}^2\left(Y_{R,3} - Y_G\right) + {\mu'_{2,x}}^2\left(Y_{R,2} - Y_G\right) + {\mu'_{1,x}}^2\left(Y_{R,1} - Y_G\right)$$

$$\breve{K}_{4,4} = \left[Z_G - \mu'_{3,y}\left(Y_{R,3} - Y_G\right)\right]^2 + \left[Z_G - \mu'_{2,y}\left(Y_{R,2} - Y_G\right)\right]^2 + \left[Z_G - \mu'_{1,y}\left(Y_{R,1} - Y_G\right)\right]^2 + {\mu'_{3,x}}^2\left(Y_{R,3} - Y_G\right)^2 + {\mu'_{2,x}}^2\left(Y_{R,2} - Y_G\right)^2 + {\mu'_{1,x}}^2\left(Y_{R,1} - Y_G\right)^2$$

$$\breve{K}_{5,1} = -3\,Z_G - \mu'_{3,x}\left(X_G - X_{R,3}\right) - \mu'_{2,x}\left(X_G - X_{R,2}\right) - \mu'_{1,x}\left(X_G - X_{R,1}\right)$$

$$\breve{K}_{5,2} = -\mu'_{3,y}\left(X_G - X_{R,3}\right) - \mu'_{2,y}\left(X_G - X_{R,2}\right) - \mu'_{1,y}\left(X_G - X_{R,1}\right)$$

$$\breve{K}_{5,3} = -\mu'_{3,x}\left[-Z_G - \mu'_{3,x}\left(X_G - X_{R,3}\right)\right] - \mu'_{2,x}\left[-Z_G - \mu'_{2,x}\left(X_G - X_{R,2}\right)\right] - \mu'_{1,x}\left[-Z_G - \mu'_{1,x}\left(X_G - X_{R,1}\right)\right] + {\mu'_{3,y}}^2\left(X_G - X_{R,3}\right) + {\mu'_{2,y}}^2\left(X_G - X_{R,2}\right) + {\mu'_{1,y}}^2\left(X_G - X_{R,1}\right)$$

$$\breve{K}_{5,4} = -\mu'_{3,y}\left(X_G - X_{R,3}\right)\left[Z_G - \mu'_{3,y}\left(Y_{R,3} - Y_G\right)\right] - \mu'_{2,y}\left(X_G - X_{R,2}\right)\left[Z_G - \mu'_{2,y}\left(Y_{R,2} - Y_G\right)\right] - \mu'_{1,y}\left(X_G - X_{R,1}\right)\left[Z_G - \mu'_{1,y}\left(Y_{R,1} - Y_G\right)\right] - \mu'_{3,x}\left(Y_{R,3} - Y_G\right)\left[-Z_G - \mu'_{3,x}\left(X_G - X_{R,3}\right)\right] - \mu'_{2,x}\left(Y_{R,2} - Y_G\right)\left[-Z_G - \mu'_{2,x}\left(X_G - X_{R,2}\right)\right] - \mu'_{1,x}\left(Y_{R,1} - Y_G\right)\left[-Z_G - \mu'_{1,x}\left(X_G - X_{R,1}\right)\right]$$

$$\breve{K}_{5,5} = \left[-Z_G - \mu'_{3,x}\left(X_G - X_{R,3}\right)\right]^2 + \left[-Z_G - \mu'_{2,x}\left(X_G - X_{R,2}\right)\right]^2 + \left[-Z_G - \mu'_{1,x}\left(X_G - X_{R,1}\right)\right]^2 + {\mu'_{3,y}}^2\left(X_G - X_{R,3}\right)^2 + {\mu'_{2,y}}^2\left(X_G - X_{R,2}\right)^2 + {\mu'_{1,y}}^2\left(X_G - X_{R,1}\right)^2$$

$$\breve{K}_{6,1} = -\mathrm{Y}_{\mathrm{R},3} - \mathrm{Y}_{\mathrm{R},2} - \mathrm{Y}_{\mathrm{R},1} + 3\,\mathrm{Y}_{\mathrm{G}}$$

$$\breve{K}_{6,2} = \mathrm{X}_{\mathrm{R},3} + \mathrm{X}_{\mathrm{R},2} + \mathrm{X}_{\mathrm{R},1} - 3\,\mathrm{X}_{\mathrm{G}}$$

$$\breve{K}_{6,3} = -\mu'_{3,\mathrm{x}}\,(\mathrm{Y}_{\mathrm{G}} - \mathrm{Y}_{\mathrm{R},3}) - \mu'_{2,\mathrm{x}}\,(\mathrm{Y}_{\mathrm{G}} - \mathrm{Y}_{\mathrm{R},2}) - \mu'_{1,\mathrm{x}}\,(\mathrm{Y}_{\mathrm{G}} - \mathrm{Y}_{\mathrm{R},1}) -$$
$$\mu'_{3,\mathrm{y}}\,(\mathrm{X}_{\mathrm{R},3} - \mathrm{X}_{\mathrm{G}}) - \mu'_{2,\mathrm{y}}\,(\mathrm{X}_{\mathrm{R},2} - \mathrm{X}_{\mathrm{G}}) - \mu'_{1,\mathrm{y}}\,(\mathrm{X}_{\mathrm{R},1} - \mathrm{X}_{\mathrm{G}})$$

$$\breve{K}_{6,4} = (\mathrm{X}_{\mathrm{R},3} - \mathrm{X}_{\mathrm{G}})\,[\mathrm{Z}_{\mathrm{G}} - \mu'_{3,\mathrm{y}}\,(\mathrm{Y}_{\mathrm{R},3} - \mathrm{Y}_{\mathrm{G}})] + (\mathrm{X}_{\mathrm{R},2} - \mathrm{X}_{\mathrm{G}})\,[\mathrm{Z}_{\mathrm{G}} -$$
$$\mu'_{2,\mathrm{y}}\,(\mathrm{Y}_{\mathrm{R},2} - \mathrm{Y}_{\mathrm{G}})] + (\mathrm{X}_{\mathrm{R},1} - \mathrm{X}_{\mathrm{G}})\,[\mathrm{Z}_{\mathrm{G}} - \mu'_{1,\mathrm{y}}\,(\mathrm{Y}_{\mathrm{R},1} - \mathrm{Y}_{\mathrm{G}})] -$$
$$\mu'_{3,\mathrm{x}}\,(\mathrm{Y}_{\mathrm{G}} - \mathrm{Y}_{\mathrm{R},3})\,(\mathrm{Y}_{\mathrm{R},3} - \mathrm{Y}_{\mathrm{G}}) - \mu'_{2,\mathrm{x}}\,(\mathrm{Y}_{\mathrm{G}} - \mathrm{Y}_{\mathrm{R},2})\,(\mathrm{Y}_{\mathrm{R},2} - \mathrm{Y}_{\mathrm{G}}) -$$
$$\mu'_{1,\mathrm{x}}\,(\mathrm{Y}_{\mathrm{G}} - \mathrm{Y}_{\mathrm{R},1})\,(\mathrm{Y}_{\mathrm{R},1} - \mathrm{Y}_{\mathrm{G}})$$

$$\breve{K}_{6,5} = (\mathrm{Y}_{\mathrm{G}} - \mathrm{Y}_{\mathrm{R},3})\,[-\mathrm{Z}_{\mathrm{G}} - \mu'_{3,\mathrm{x}}\,(\mathrm{X}_{\mathrm{G}} - \mathrm{X}_{\mathrm{R},3})] + (\mathrm{Y}_{\mathrm{G}} - \mathrm{Y}_{\mathrm{R},2})\,[-\mathrm{Z}_{\mathrm{G}} -$$
$$\mu'_{2,\mathrm{x}}\,(\mathrm{X}_{\mathrm{G}} - \mathrm{X}_{\mathrm{R},2})] + (\mathrm{Y}_{\mathrm{G}} - \mathrm{Y}_{\mathrm{R},1})\,[-\mathrm{Z}_{\mathrm{G}} - \mu'_{1,\mathrm{x}}\,(\mathrm{X}_{\mathrm{G}} - \mathrm{X}_{\mathrm{R},1})] -$$
$$\mu'_{3,\mathrm{y}}\,(\mathrm{X}_{\mathrm{G}} - \mathrm{X}_{\mathrm{R},3})\,(\mathrm{X}_{\mathrm{R},3} - \mathrm{X}_{\mathrm{G}}) - \mu'_{2,\mathrm{y}}\,(\mathrm{X}_{\mathrm{G}} - \mathrm{X}_{\mathrm{R},2})\,(\mathrm{X}_{\mathrm{R},2} - \mathrm{X}_{\mathrm{G}}) -$$
$$\mu'_{1,\mathrm{y}}\,(\mathrm{X}_{\mathrm{G}} - \mathrm{X}_{\mathrm{R},1})\,(\mathrm{X}_{\mathrm{R},1} - \mathrm{X}_{\mathrm{G}})$$

$$\breve{K}_{6,6} = (\mathrm{Y}_{\mathrm{G}} - \mathrm{Y}_{\mathrm{R},3})^2 + (\mathrm{Y}_{\mathrm{G}} - \mathrm{Y}_{\mathrm{R},2})^2 + (\mathrm{Y}_{\mathrm{G}} - \mathrm{Y}_{\mathrm{R},1})^2 +$$
$$(\mathrm{X}_{\mathrm{R},3} - \mathrm{X}_{\mathrm{G}})^2 + (\mathrm{X}_{\mathrm{R},2} - \mathrm{X}_{\mathrm{G}})^2 + (\mathrm{X}_{\mathrm{R},1} - \mathrm{X}_{\mathrm{G}})^2$$

Appendix E

Workspace Plots for Examples 1b, 1c, 1d, and 1e

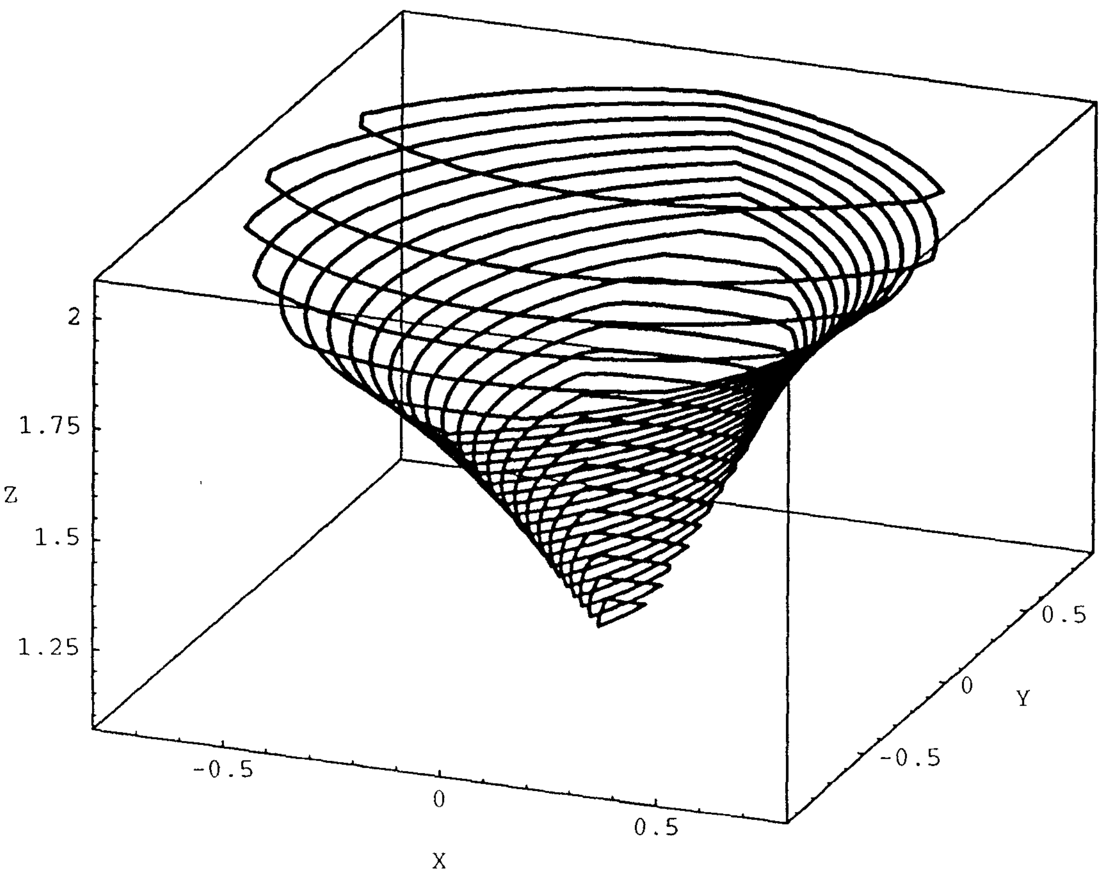

Figure E.1: Perspective view of workspace for ϖ=63.43, θ_x=10, θ_y=0, and θ_z=0.

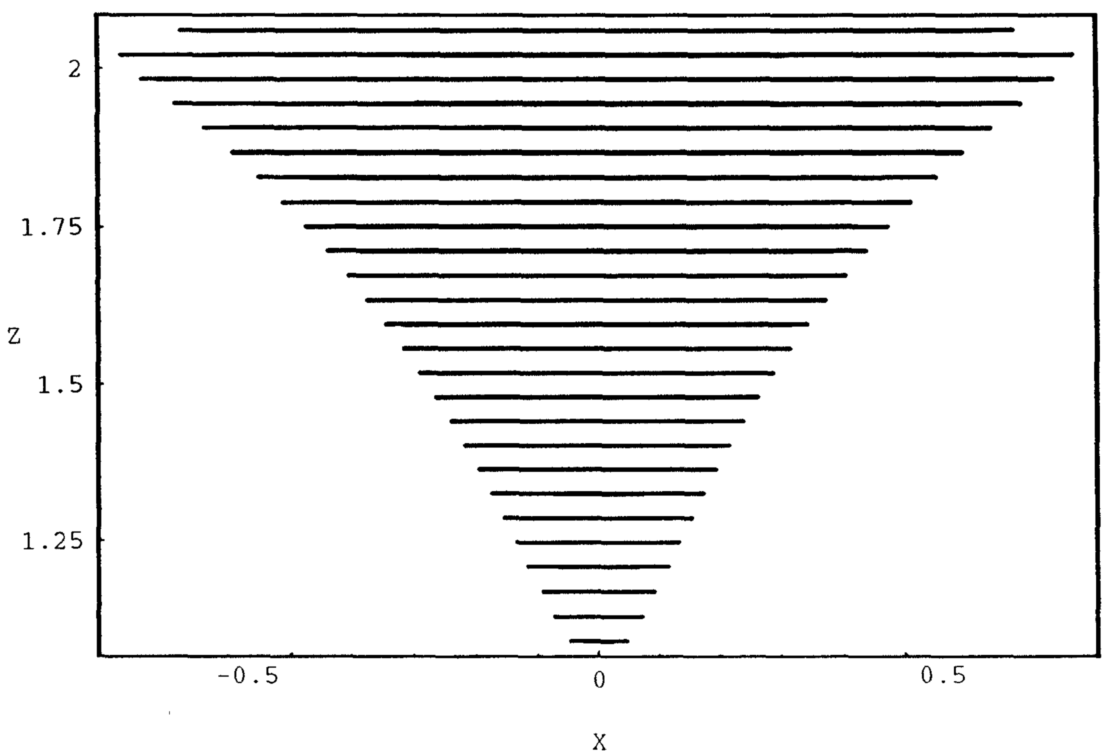

Figure E.2: Front view of workspace for ϖ=63.43, θ_x=10, θ_y=0, and θ_z=0.

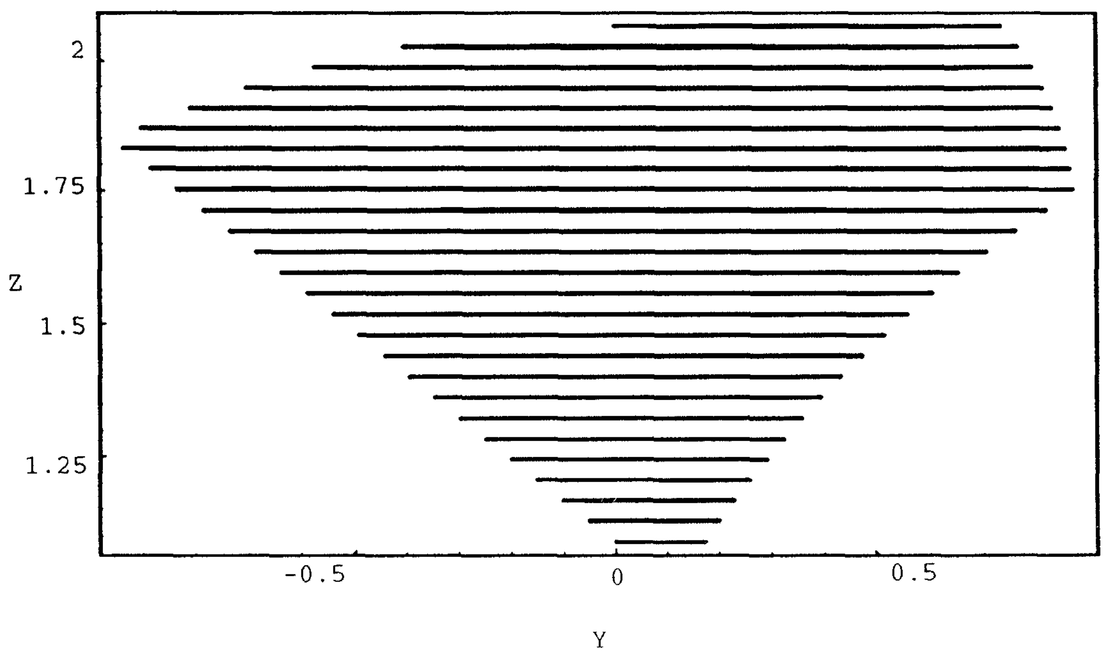

Figure E.3: Side view of workspace for ϖ=63.43, θ_x=10, θ_y=0, and θ_z=0.

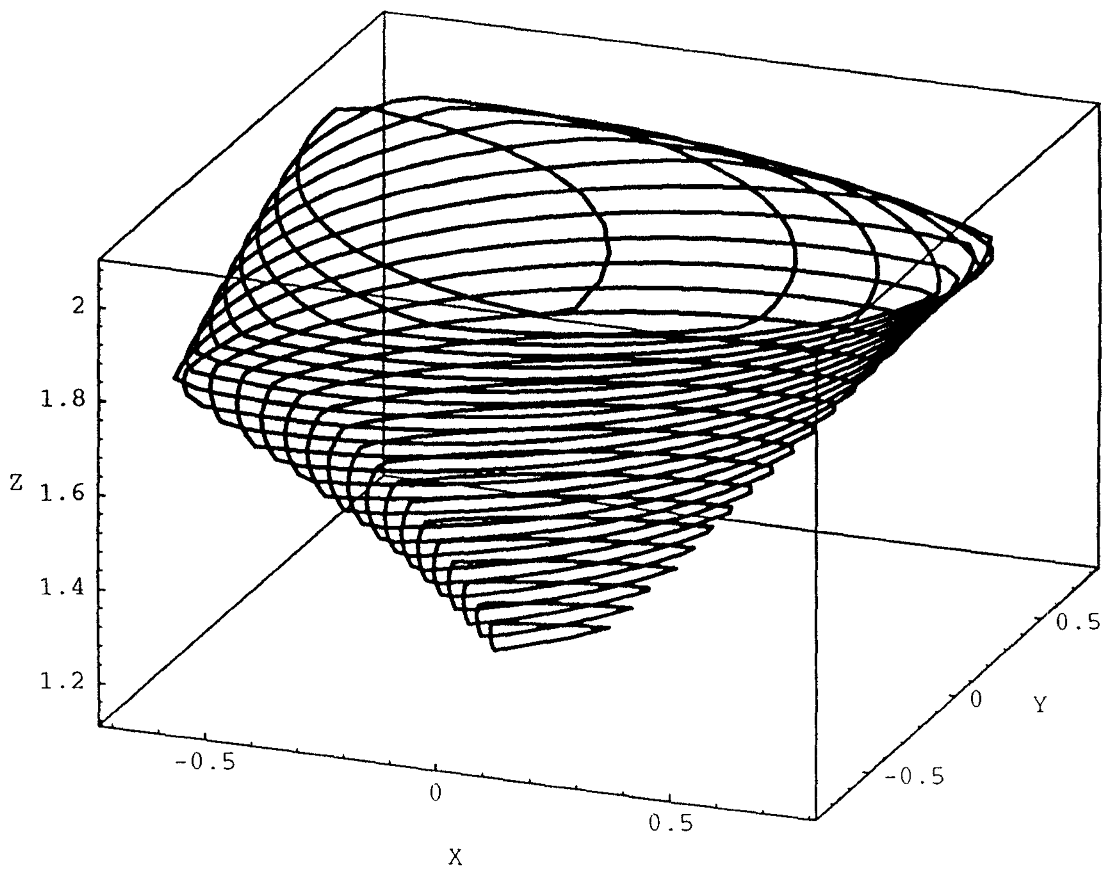

Figure E.4: Perspective view of workspace for ϖ=63.43, θ_x=0, θ_y=10, and θ_z=0.

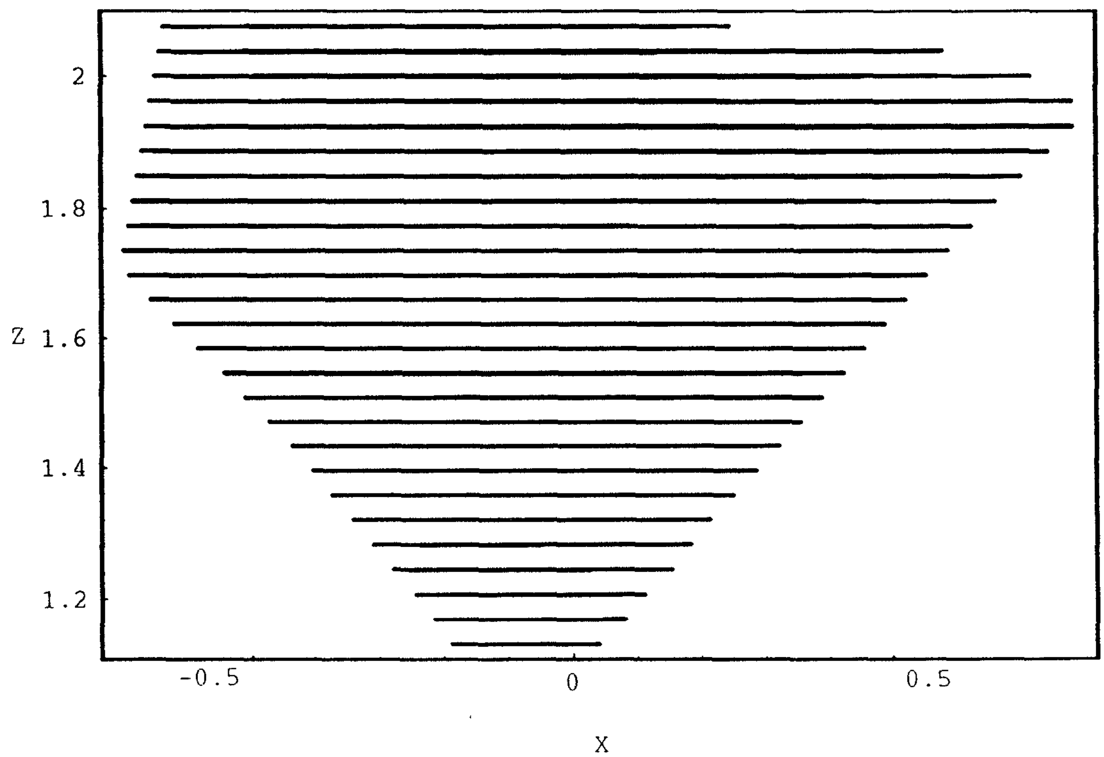

Figure E.5: Front view of workspace for ϖ=63.43, θ_x=0, θ_y=10, and θ_z=0.

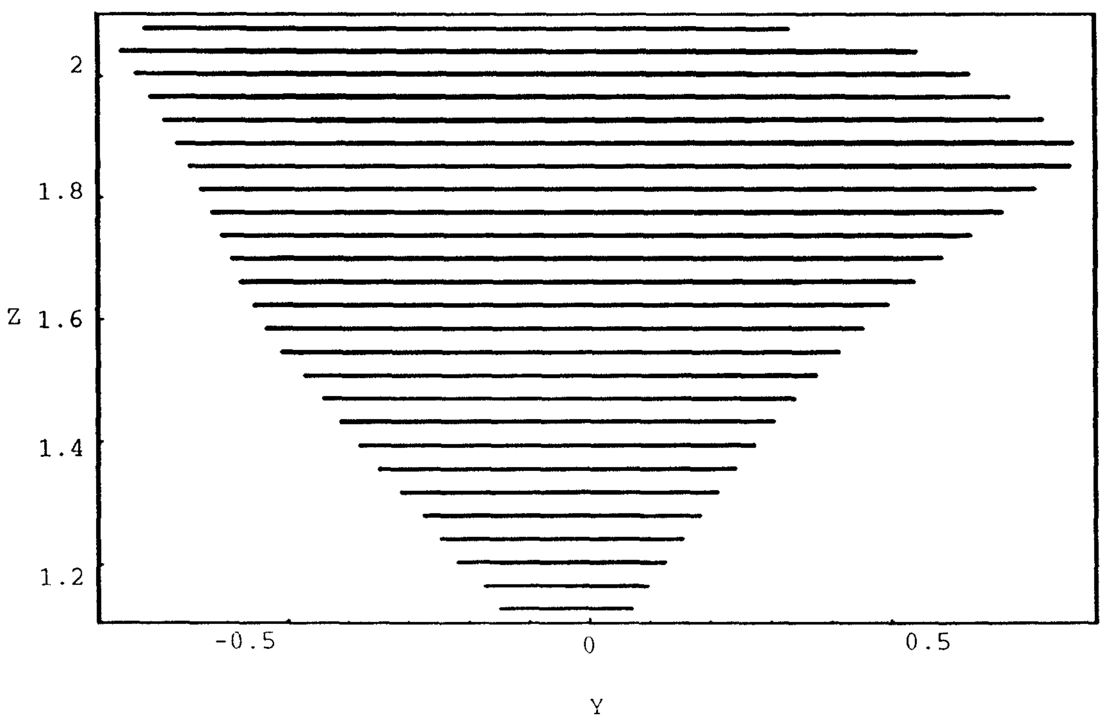

Figure E.6: Side view of workspace for ϖ=63.43, θ_x=0, θ_y=10, and θ_z=0.

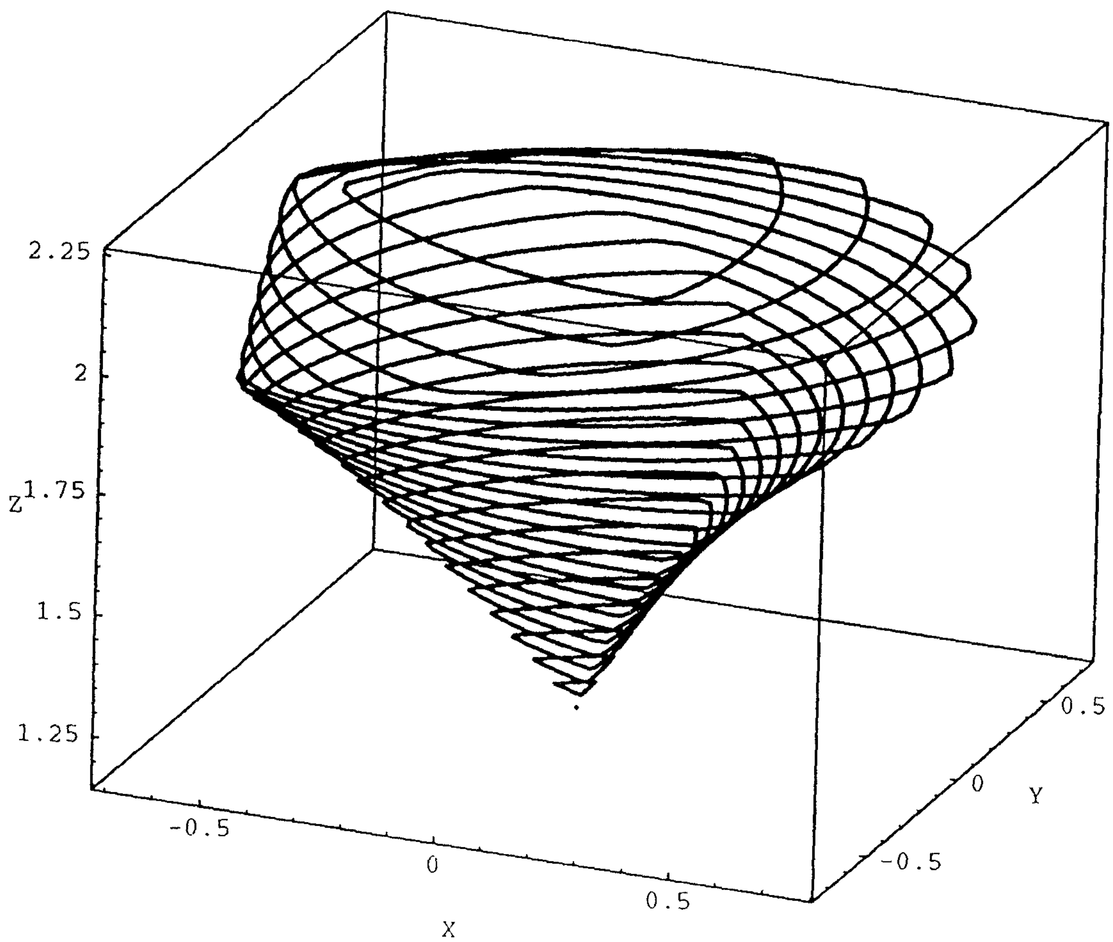

Figure E.7: Perspective view of workspace for ϖ=63.43, θ_x=0, θ_y=0, and θ_z=10.

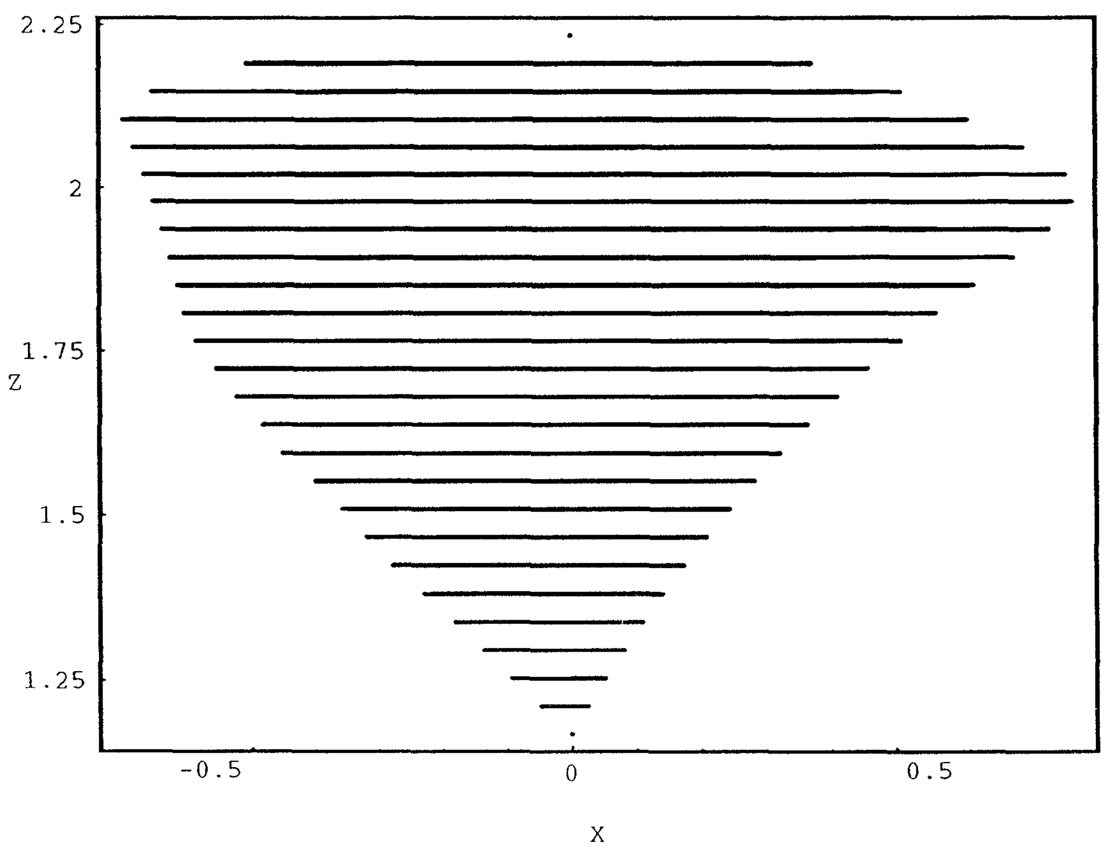

Figure E.8: Front view of workspace for ϖ=63.43, θ_x=0, θ_y=0, and θ_z=10.

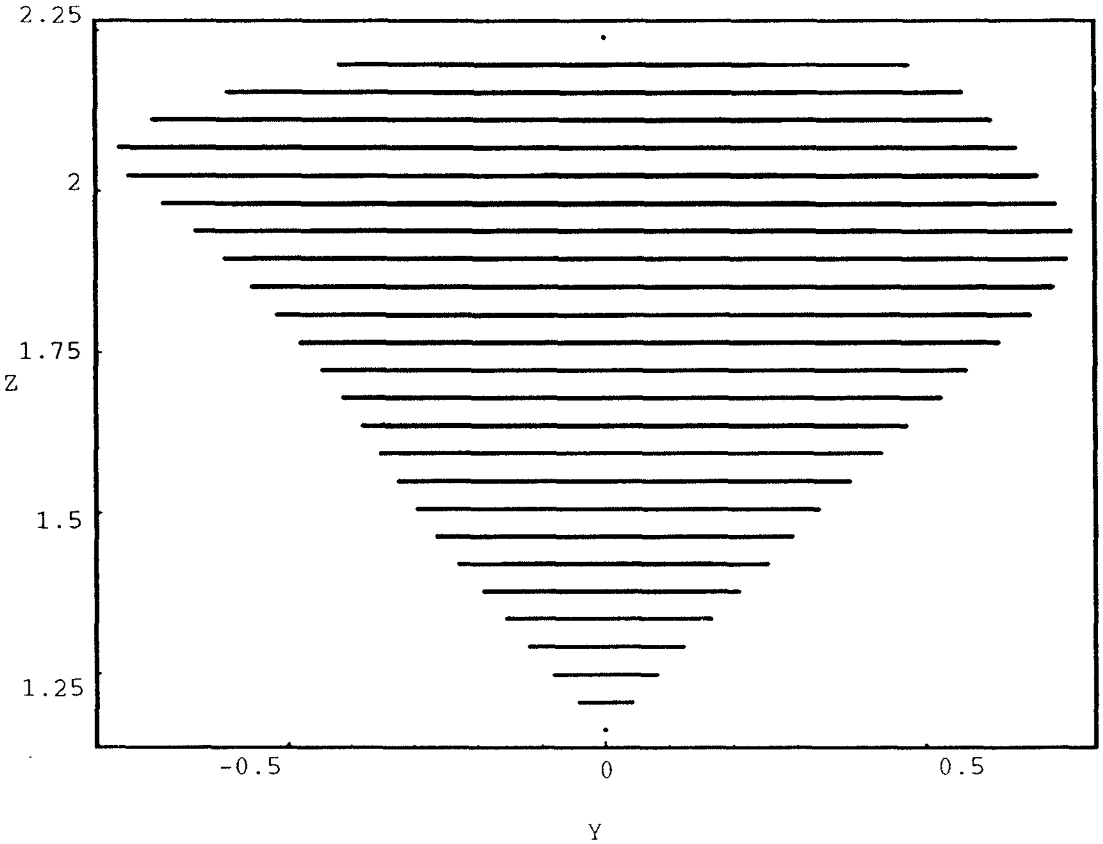

Figure E.9: Side view of workspace for ϖ=63.43, θ_x=0, θ_y=0, and θ_z=10.

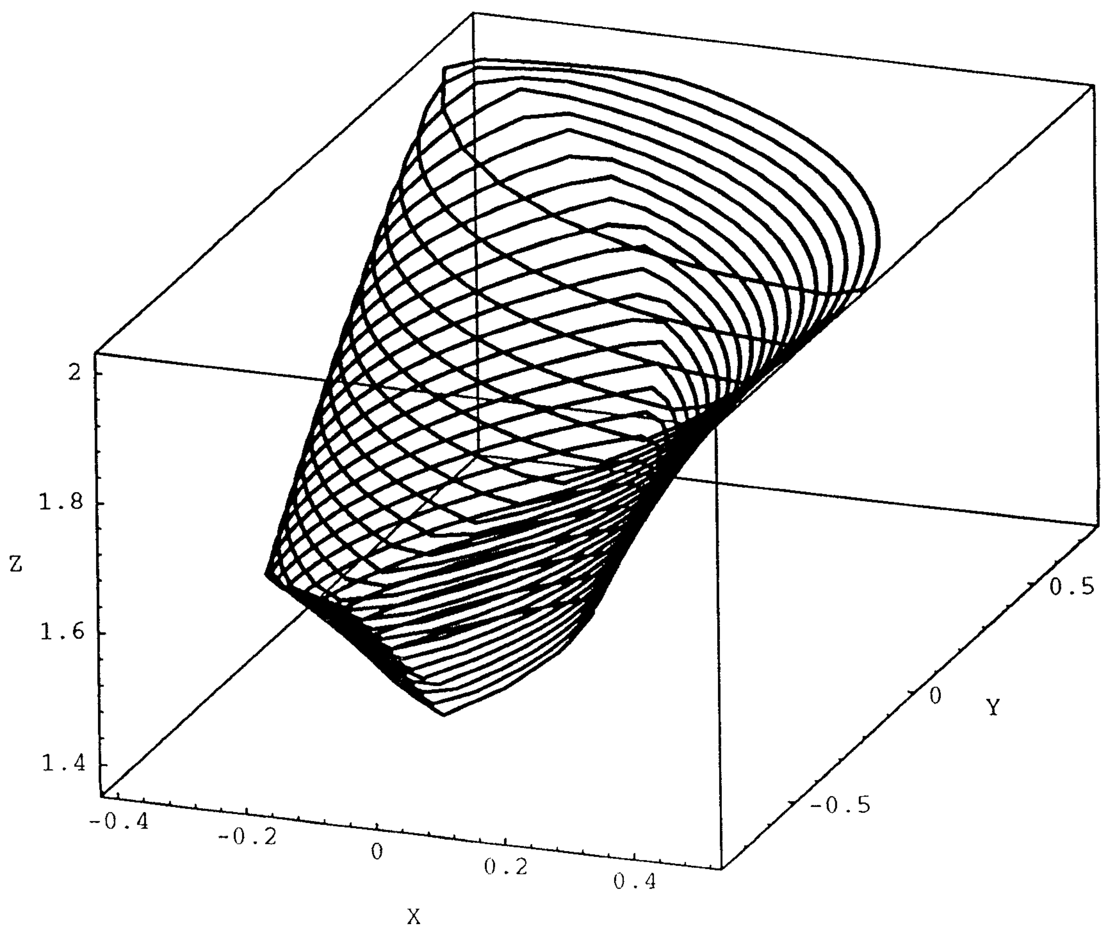

Figure E.10: Perspective view of workspace for ϖ=63.43, θ_x=10, θ_y=10, and θ_z=10.

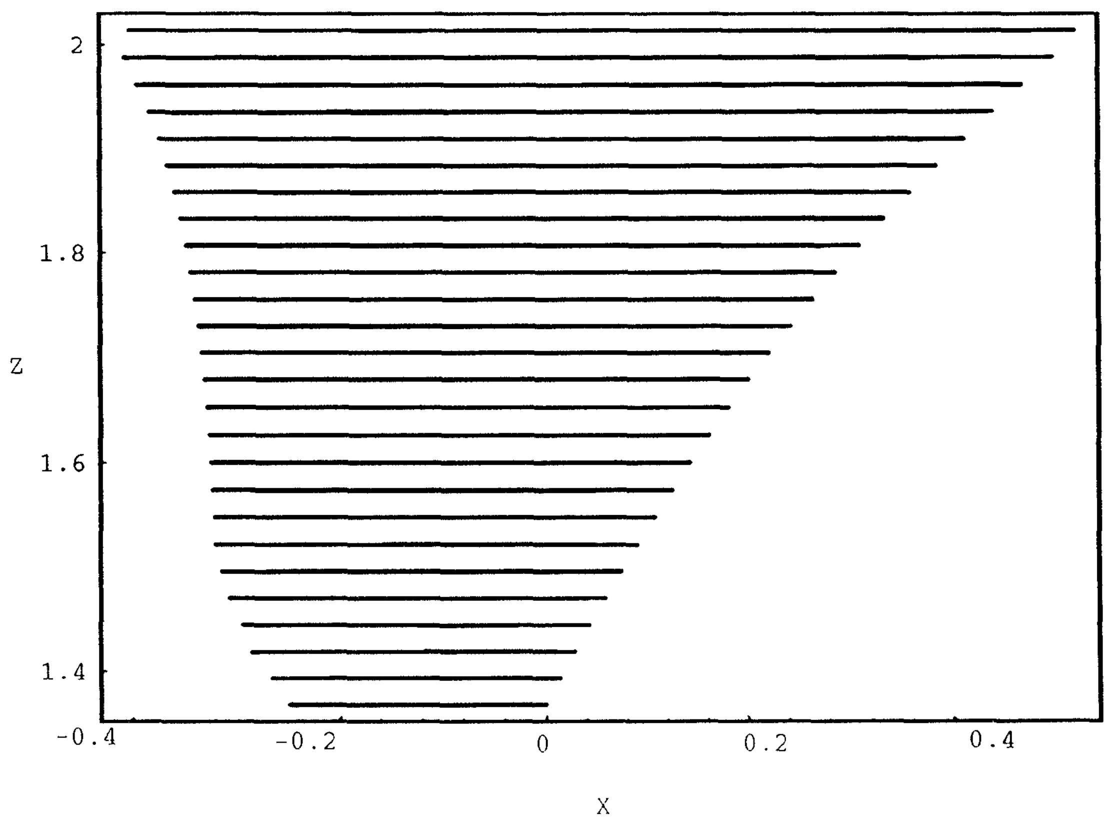

Figure E.11: Front view of workspace for ϖ=63.43, θ_x=10, θ_y=10, and θ_z=10.

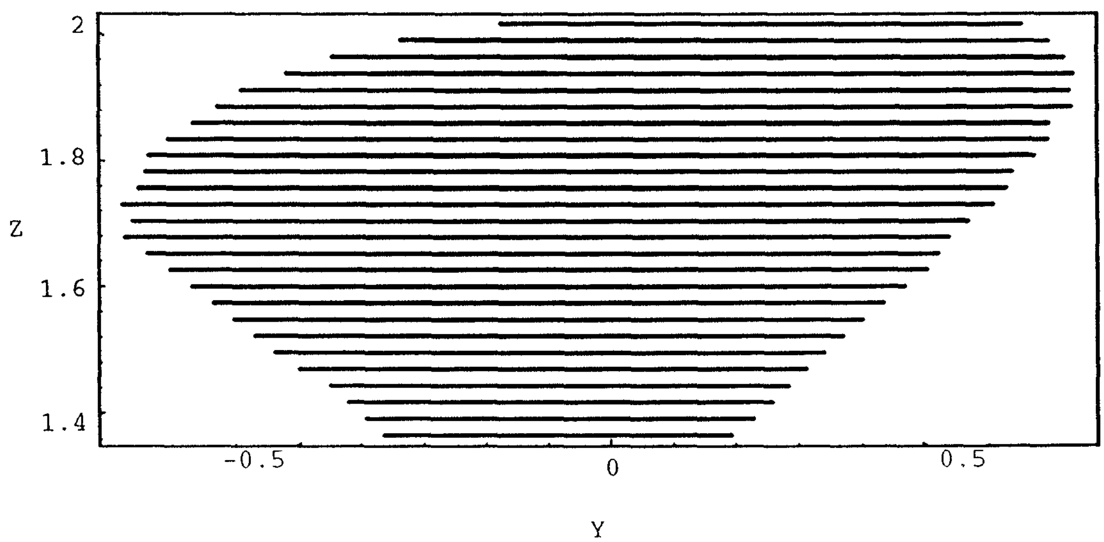

Figure E.12: Side view of workspace for ϖ=63.43, θ_x=10, θ_y=10, and θ_z=10.

Appendix F

Workspace Plots for Examples 2b, 2c, 2d, and 2e

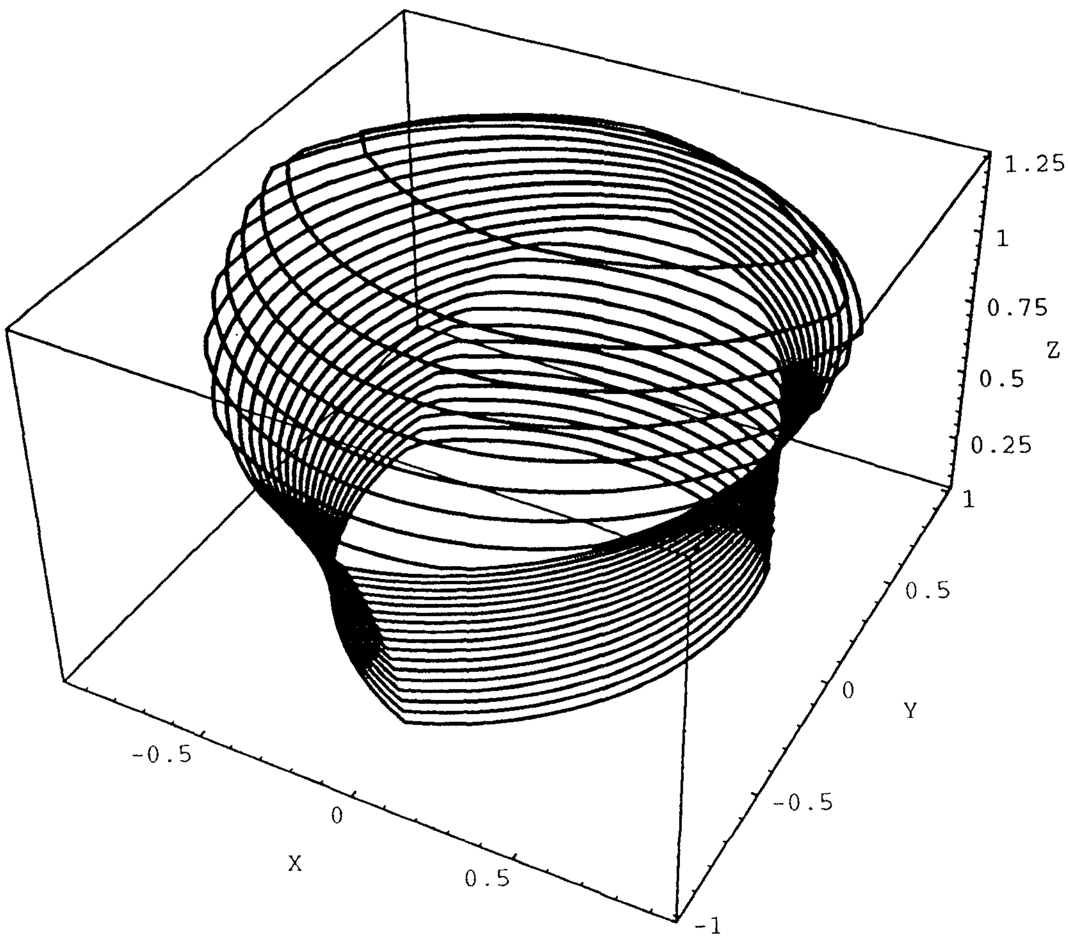

Figure F.1: Perspective view of workspace for ϖ=45, θ_x=10, θ_y=0, and θ_z=0.

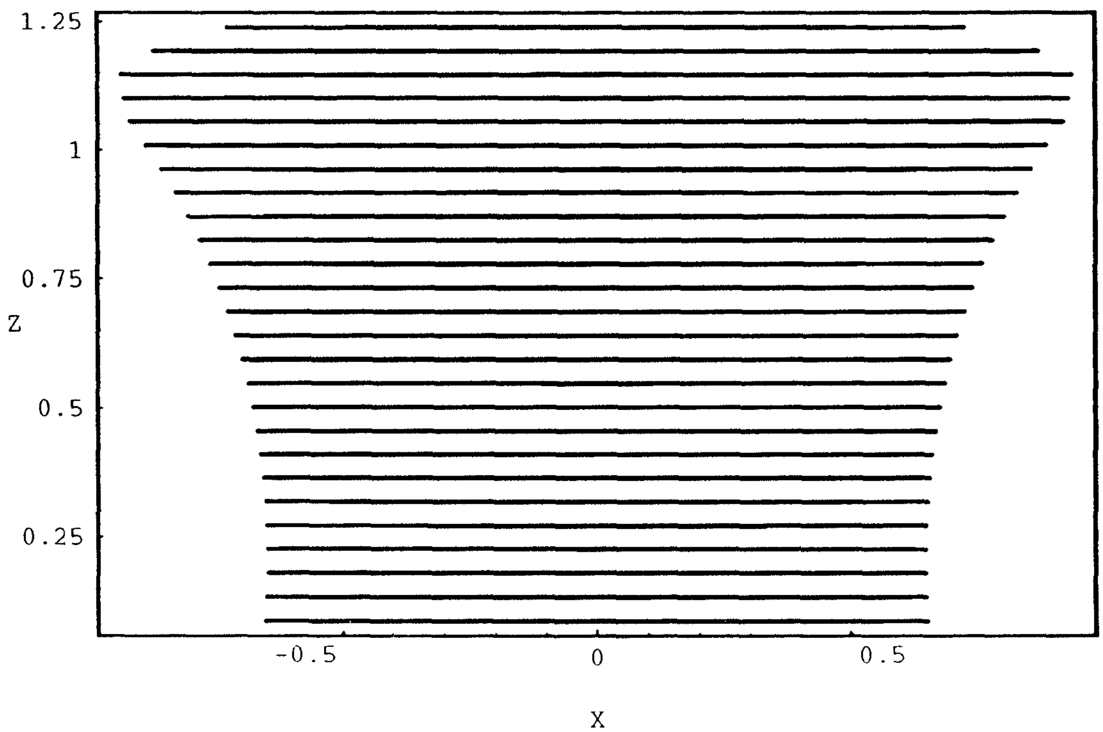

Figure F.2: Front view of workspace for ϖ=45, θ_x=10, θ_y=0, and θ_z=0.

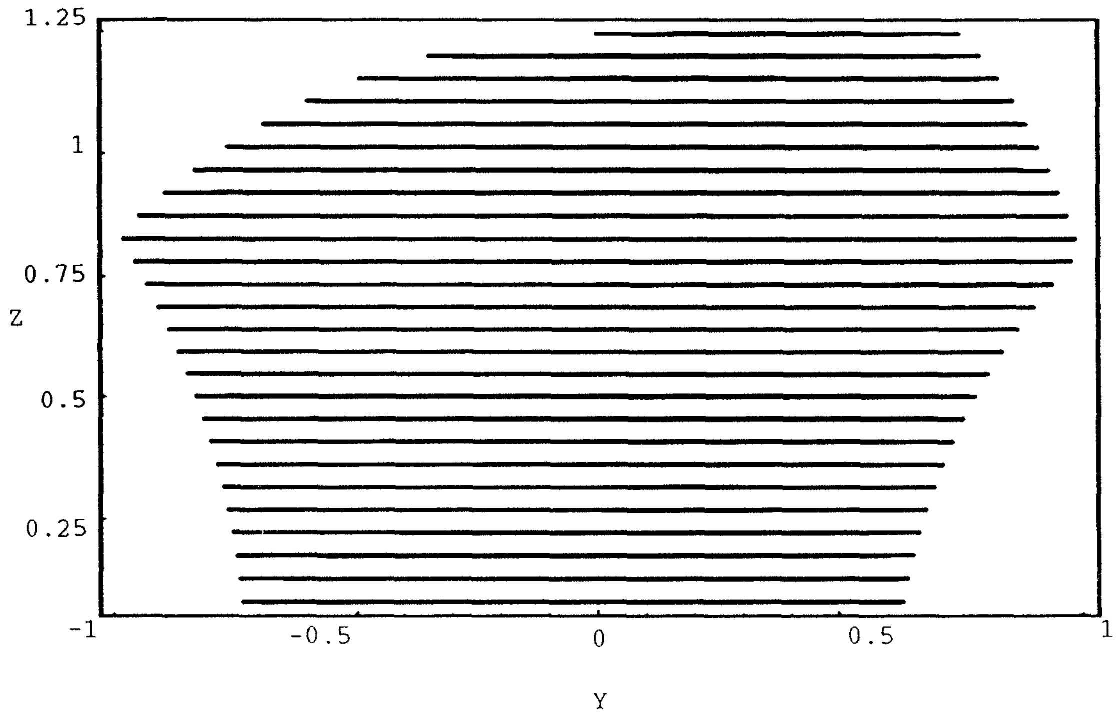

Figure F.3: Side view of workspace for ϖ=45, θ_x=10, θ_y=0, and θ_z=0.

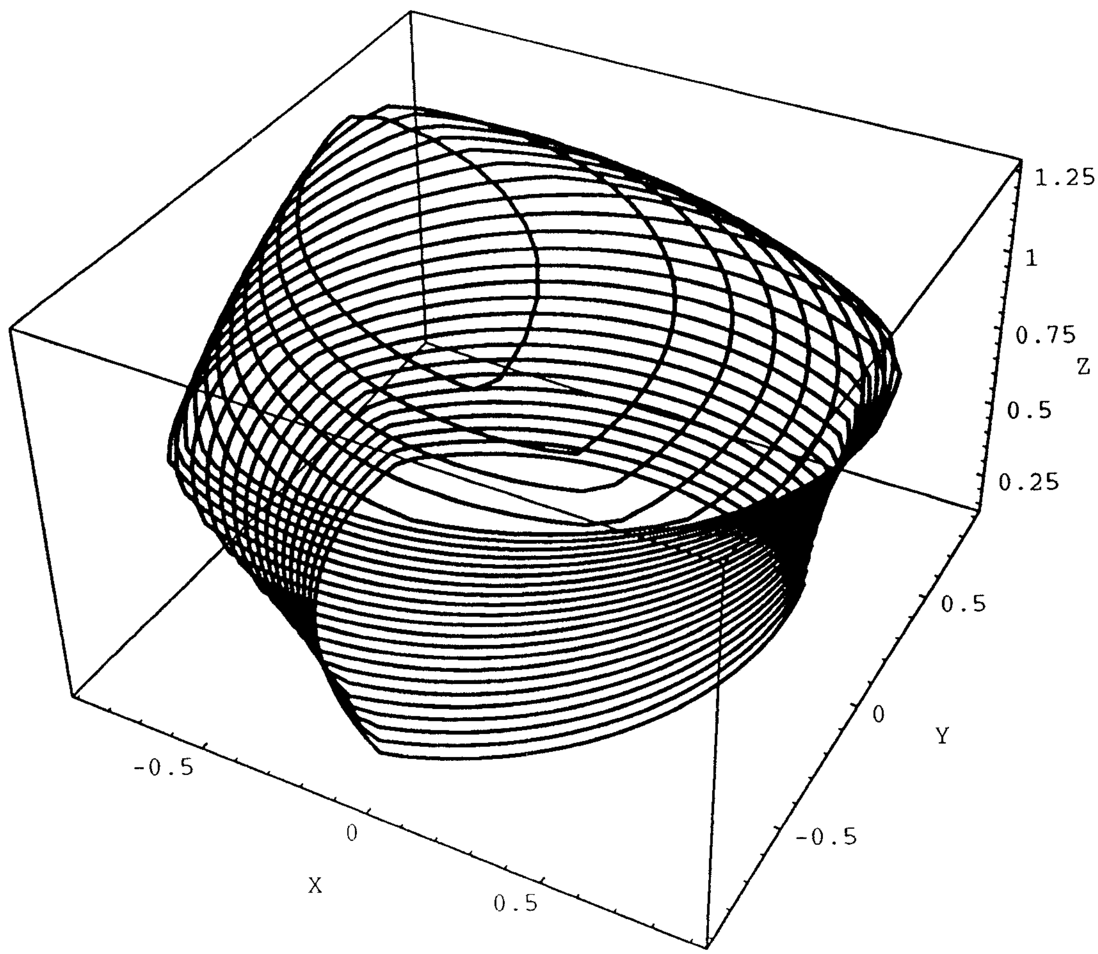

Figure F.4: Perspective view of workspace for ϖ=45, θ_x=0, θ_y=10, and θ_z=0.

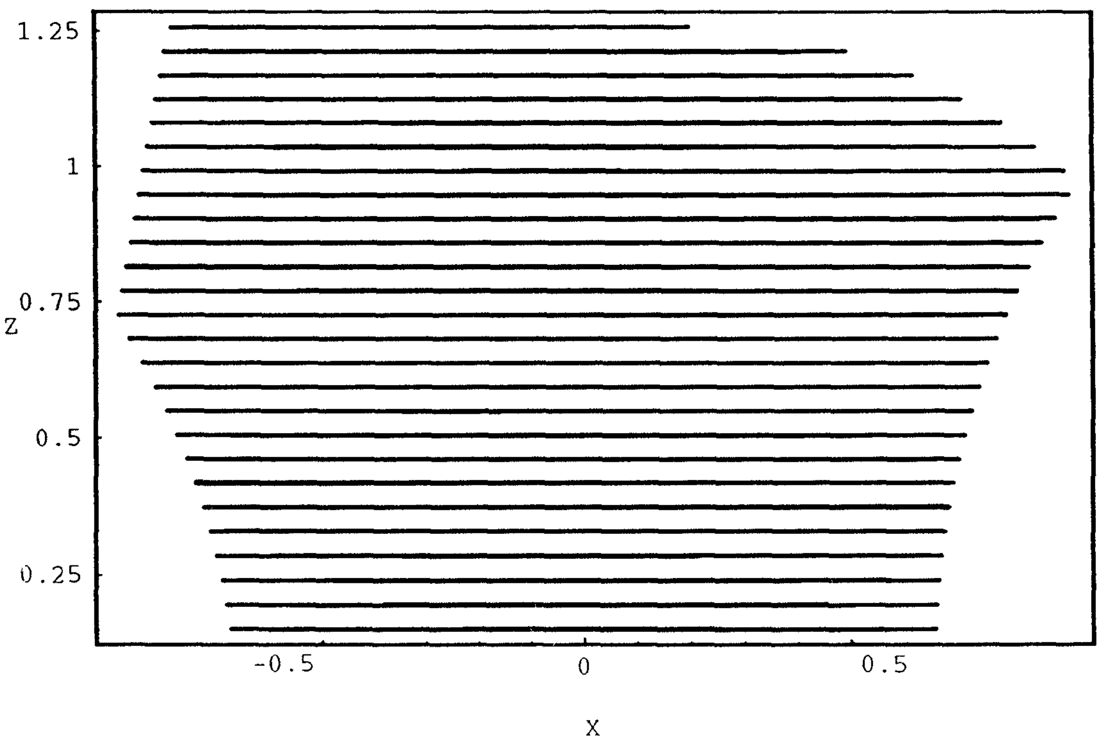

Figure F.5: Front view of workspace for ϖ=45, θ_x=0, θ_y=10, and θ_z=0.

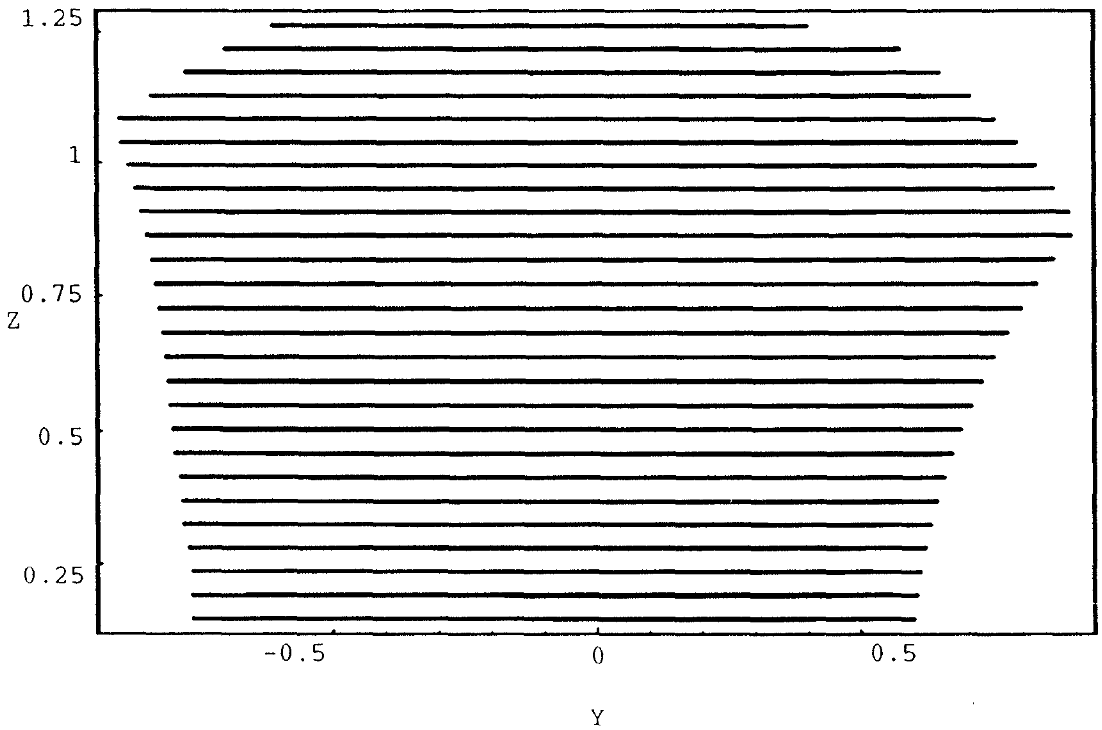

Figure F.6: Side view of workspace for ϖ=45, θ_x=0, θ_y=10, and θ_z=0.

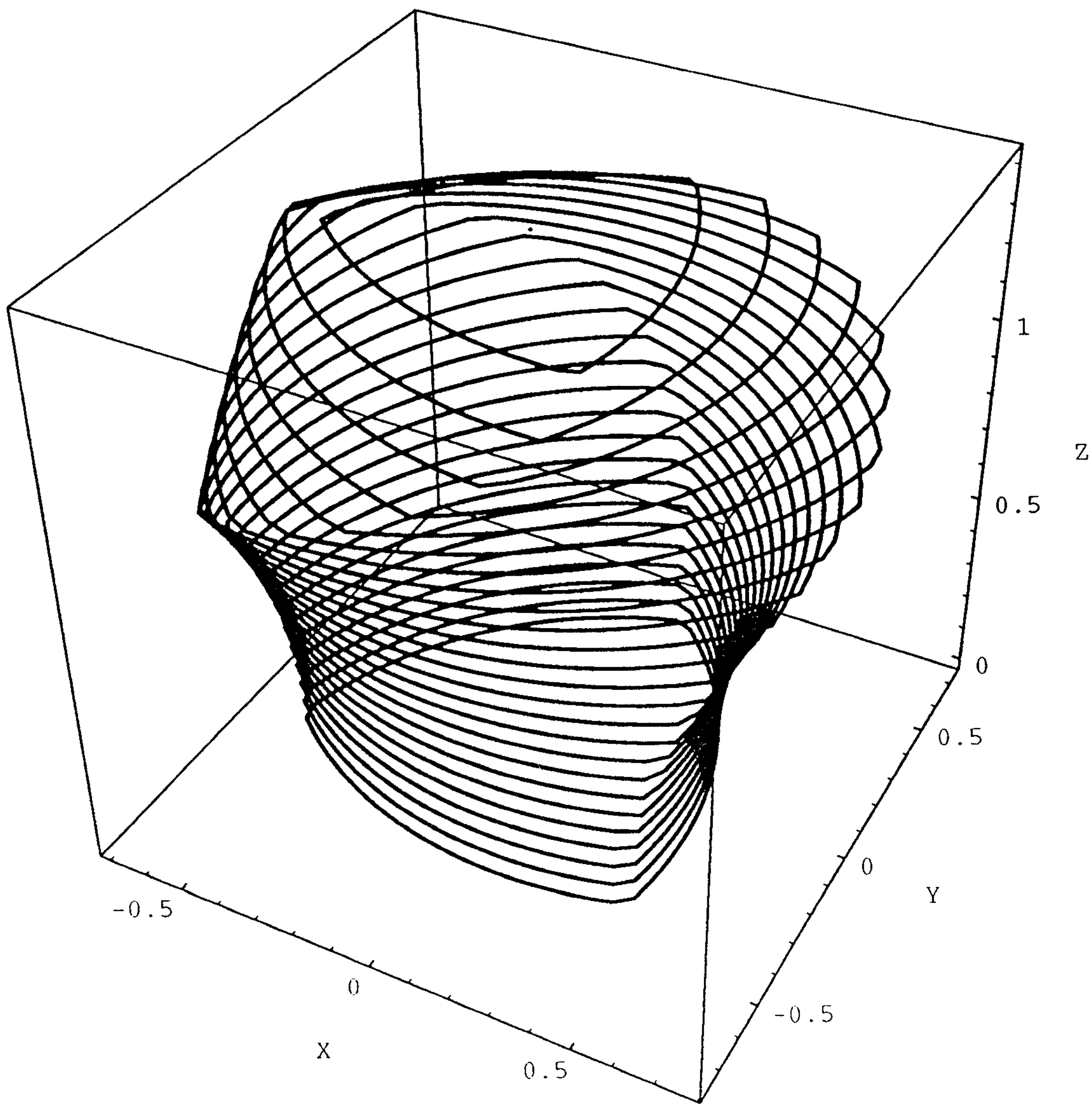

Figure F.7: Perspective view of workspace for ϖ=45, θ_x=0, θ_y=0, and θ_z=10.

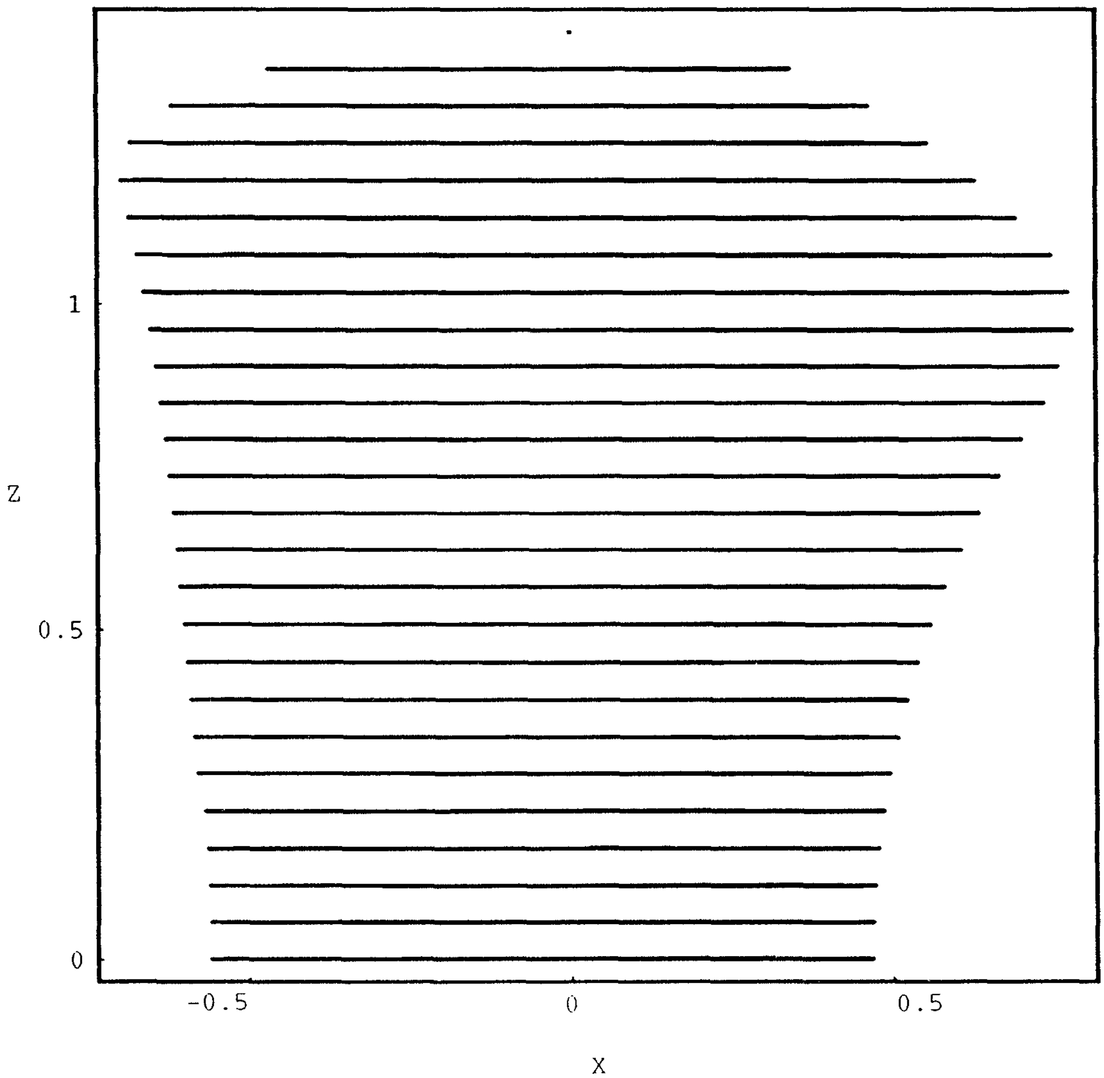

Figure F.8: Front view of workspace for ϖ=45, θ_x=0, θ_y=0, and θ_z=10.

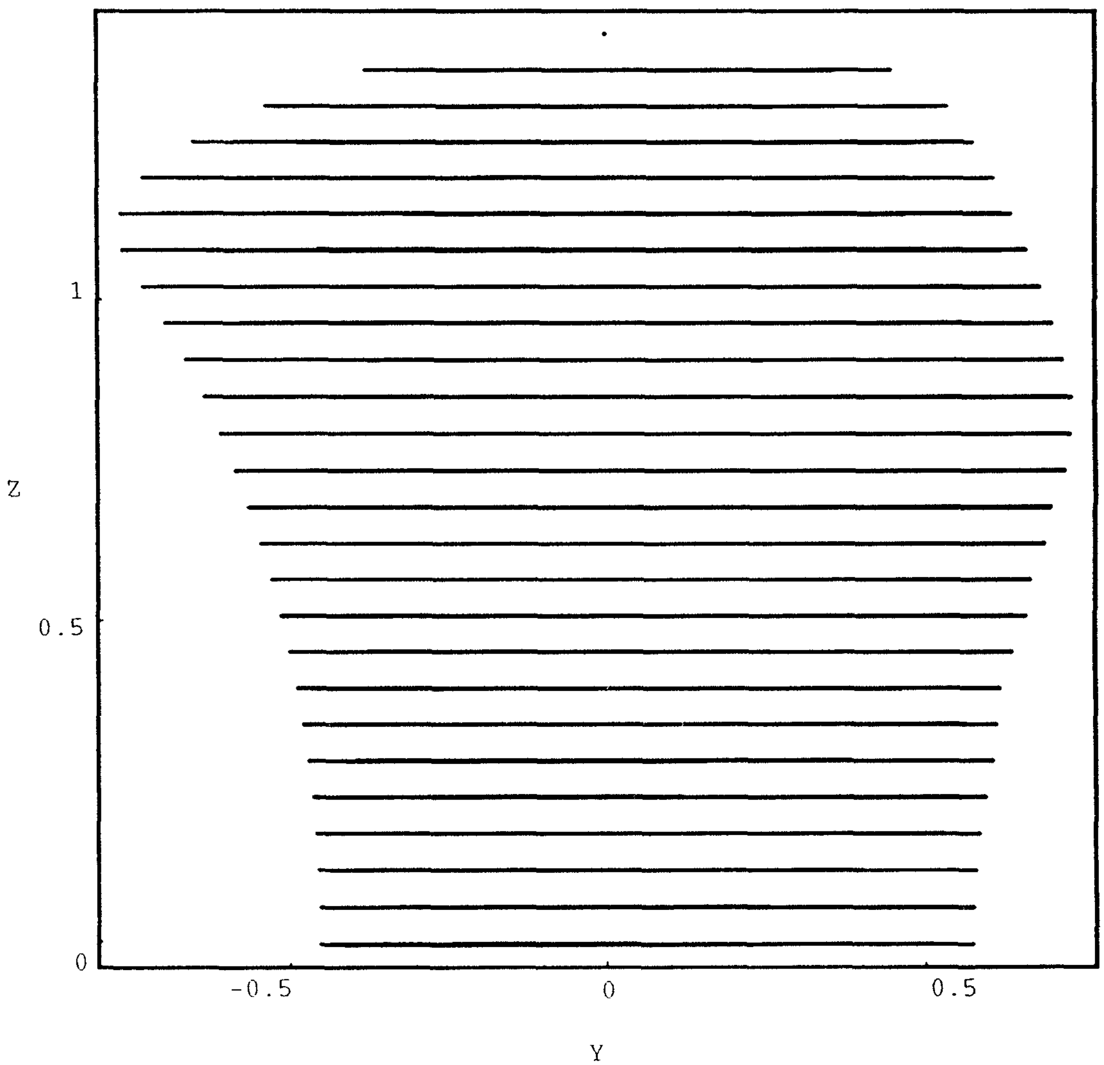

Figure F.9: Side view of workspace for ϖ=45, θ_x=0, θ_y=0, and θ_z=10.

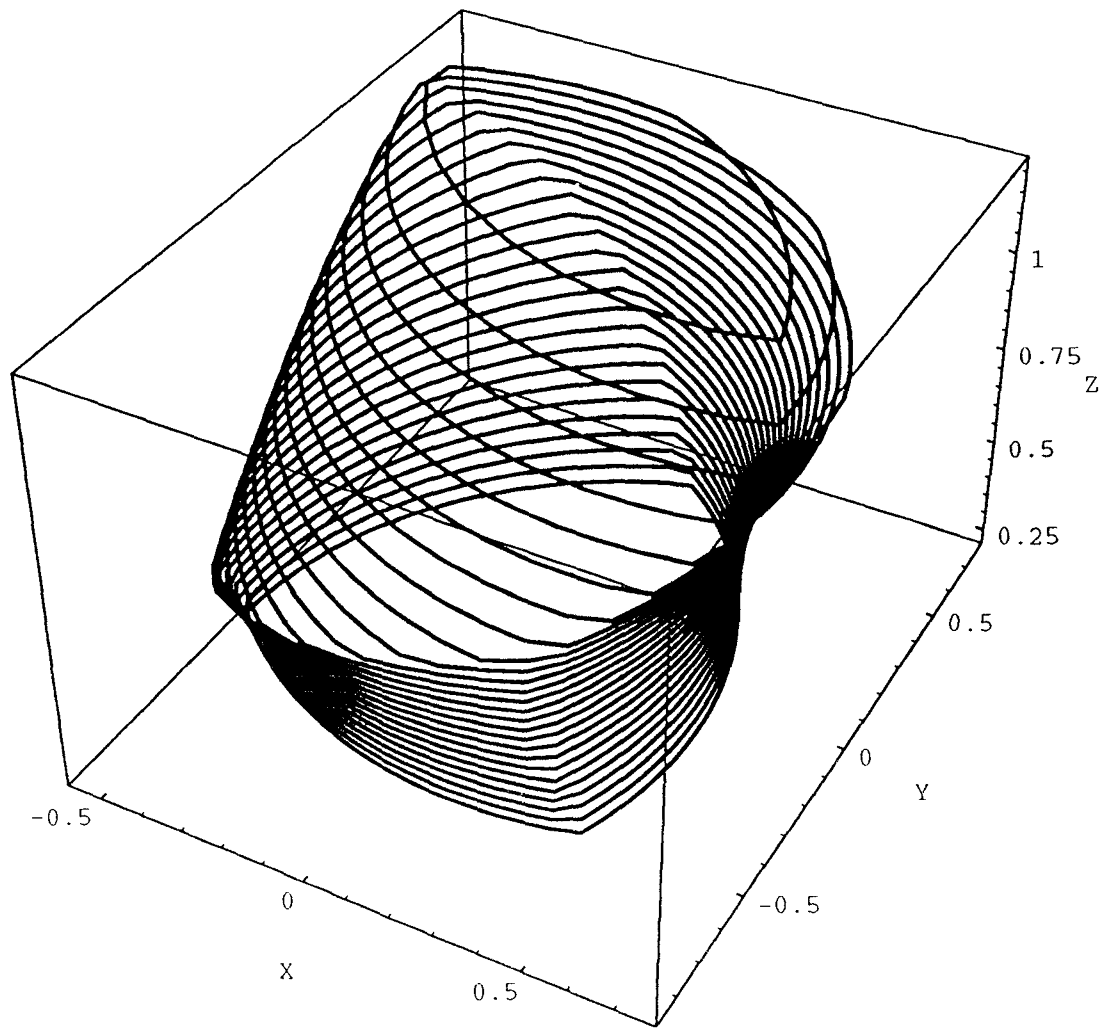

Figure F.10: Perspective view of workspace for ϖ=45, θ_x=10, θ_y=10, and θ_z=10.

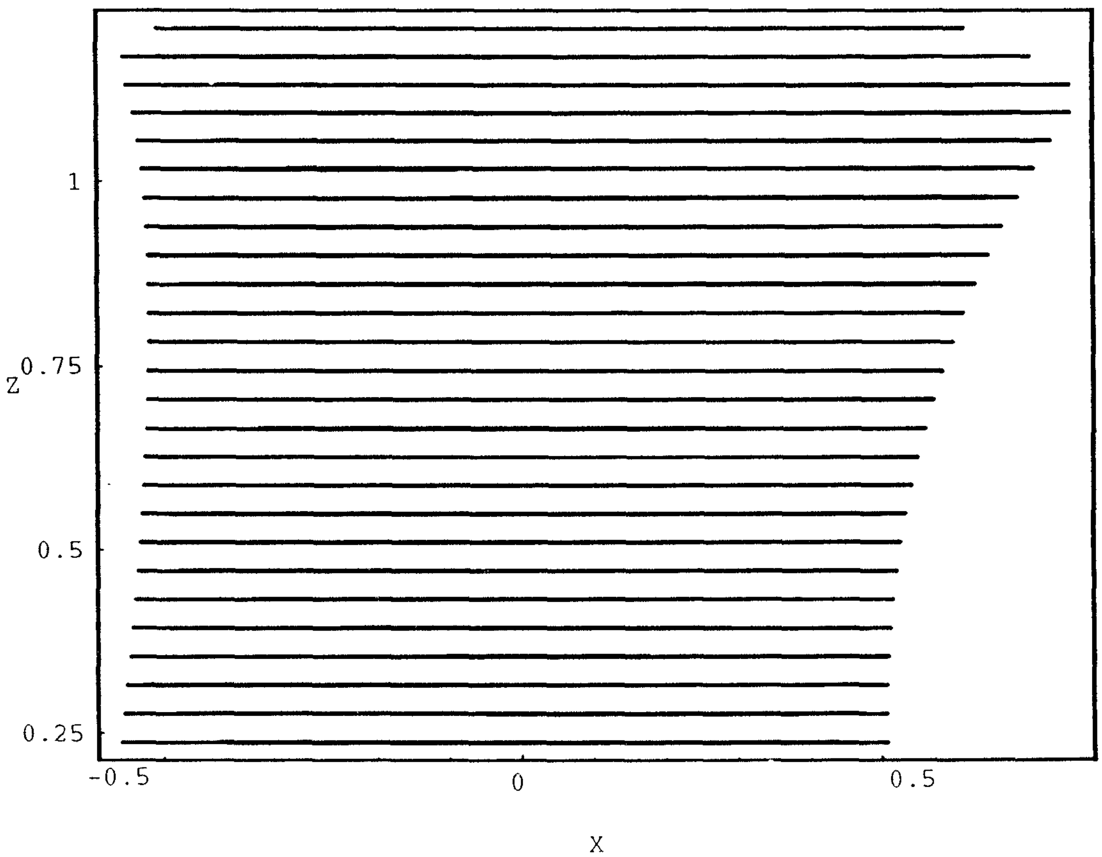

Figure F.11: Front view of workspace for ϖ=45, θ_x=10, θ_y=10, and θ_z=10.

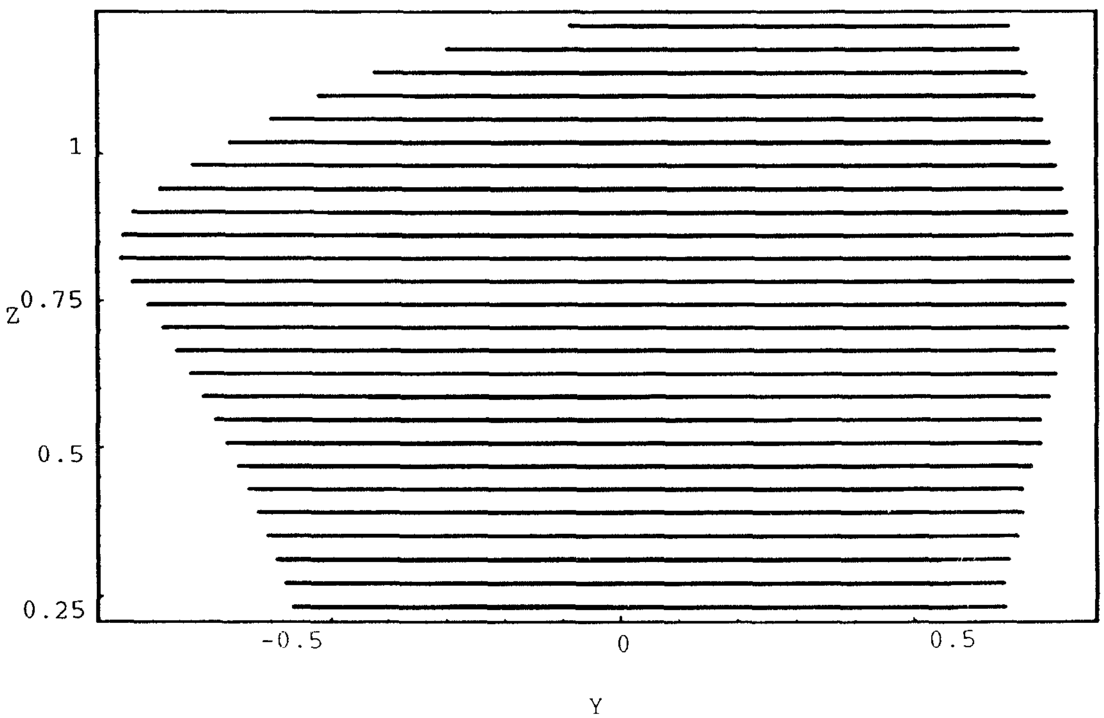

Figure F.12: Side view of workspace for ϖ=45, θ_x=10, θ_y=10, and θ_z=10.

Appendix G

Proofs of Propositions 1, 2, and 3 in Section 8.4.1

G.1 Proof of Proposition 1

Let

$$t_i = \tan\left(\frac{\eta_i}{2}\right).$$

Then

$$c_i = \frac{1 - t_i^2}{1 + t_i^2} \tag{G.1}$$

$$s_i = \frac{2t_i}{1 + t_i^2} \tag{G.2}$$

Substituting equations (G.1) and (G.2) into equations (8.26) and (8.27) and simplifying, we get

$$-2rt_1^2t_2 + (3p - r)t_2^2t_1 + (3p + r)t_1 + 2rt_2 = 0 \tag{G.3}$$

$$-2rt_2^2t_1 + (3p - r)t_1^2t_2 + (3p + r)t_2 + 2rt_1 = 0 \tag{G.4}$$

Equations (G.3) and (G.4) can be rewritten in the following forms

$$(3p-r)t_1t_2^2+2r(1-t_1^2)t_2+(3p+r)t_1 = 0 \tag{G.5}$$

$$-2rt_1t_2^2+[(3p-r)t_1^2+3p+r]t_2+2rt_1 = 0 \tag{G.6}$$

We can think of equations (G.5) and (G.6) as two quadratic equations in the unknown t_2. Applying the same elimination method used in Appendix B to derive equation (4.15), we can reduce these two equations to a polynomial equation in t_1. The result is

$$9(r^2+3p^2)t_1^2(\varrho_1t_1^4+\varrho_2t_1^2+\varrho_3)=0 \tag{G.7}$$

where

$$\varrho_1 = -(r-p)(r+3p)$$

$$\varrho_2 = 2\left(r^2+3p^2\right)$$

$$\varrho_3 = -(r+p)(r-3p)$$

Equation (G.7) has six solutions, two of which are equal to zero. The other four solutions can be found from

$$t_1^2=\frac{r+p}{r-p} \tag{G.8}$$

and

$$t_1^2=\frac{r-3p}{r+3p} \tag{G.9}$$

Equations (G.3) and (G.4) can be converted to

$$\left[(3p-r)t_2^2+3p+r\right]^2t_1^2-4r^2(t_1^2-1)^2t_2^2 = 0 \tag{G.10}$$

$$\left[(3p-r)t_1^2+3p+r\right]^2t_2^2-4r^2(t_2^2-1)^2t_1^2 = 0 \tag{G.11}$$

Substituting equation (G.8) into equation (G.10) results in a quadratic equation in the unknown t_2^2, which can be solved to obtain

$$t_2^2 = \frac{r+p}{r-p} \tag{G.12}$$

and

$$t_2^2 = \frac{(r-p)(r+3p)^2}{(r-3p)^2(r+p)} \tag{G.13}$$

Expressions for t_1^2 and t_2^2 in equations (G.8) and (G.12) satisfy equation (G.11). However, expressions for t_1^2 and t_2^2 in equations (G.8) and (G.13) do not satisfy equation (G.11). Hence, equation (G.13) is spurious. Similarly, substituting equation (G.9) into equation (G.10) and solving for t_2^2, we obtain

$$t_2^2 = \frac{r-3p}{r+3p} \tag{G.14}$$

and

$$t_2^2 = \frac{(r+3p)^3}{(r-3p)^3} \tag{G.15}$$

Using the same verification method described above, we find out that equation (G.15) is spurious. Equation (G.7) showed that t_1^2 can also be equal to zero. If so, equations (G.3) and (G.4) can be used to show that t_2^2 is also equal to zero.

The preceding discussion shows that if equations (8.26) and (8.27) are satisfied, then

$$t_2^2 = t_1^2 \tag{G.16}$$

or $\eta_2 = \pm\eta_1$.

G.2 Proof of Proposition 2

Referring to Figure G.1, we see that if equation (8.31) is satisfied, then

$$\overline{GR_i} \perp \overline{GP_i} \quad \text{for } i = 1, 2 \tag{G.17}$$

Axis of the topmost revolute joint at point P_i is parallel to $\overline{P_{i+2}P_{i+1}}$, hence

$$\overline{GP_i} \perp \overline{P_{i+2}P_{i+1}} \quad \text{for } i = 1, 2 \tag{G.18}$$

and

$$\overline{P_iR_i} \perp \overline{P_{i+2}P_{i+1}} \quad \text{for } i = 1, 2 \tag{G.19}$$

From equations (G.18) and (G.19), we can conclude that $\overline{P_{i+2}P_{i+1}}$ is perpendicular to the plane passing through points G, P_i, and R_i. As a result

$$\overline{GR_i} \perp \overline{P_{i+2}P_{i+1}} \quad \text{for } i = 1, 2 \tag{G.20}$$

Equations (G.17) and (G.20) imply that both $\overline{GR_1}$ and $\overline{GR_2}$ are perpendicular to the platform. This means that points G, R_1, and R_2 are collinear. Also, we note that since $\eta_2 = \eta_1$, points R_1 and R_2 are both on one side (above or below) of the platform. Moreover, Figure G.1 shows that

$$\left|\overline{GR_1}\right| = \left|\overline{GR_2}\right| = \sqrt{r^2 - p^2} \tag{G.21}$$

Therefore, points R_1 and R_2 are coincident.

G.3 Proof of Proposition 3

Referring to Figure G.2, we can see that vector $\overline{R_2P_2}$ can be resolved into a vector parallel to $\bar{n}_w$ (a unit vector perpendicular to the platform and parallel to

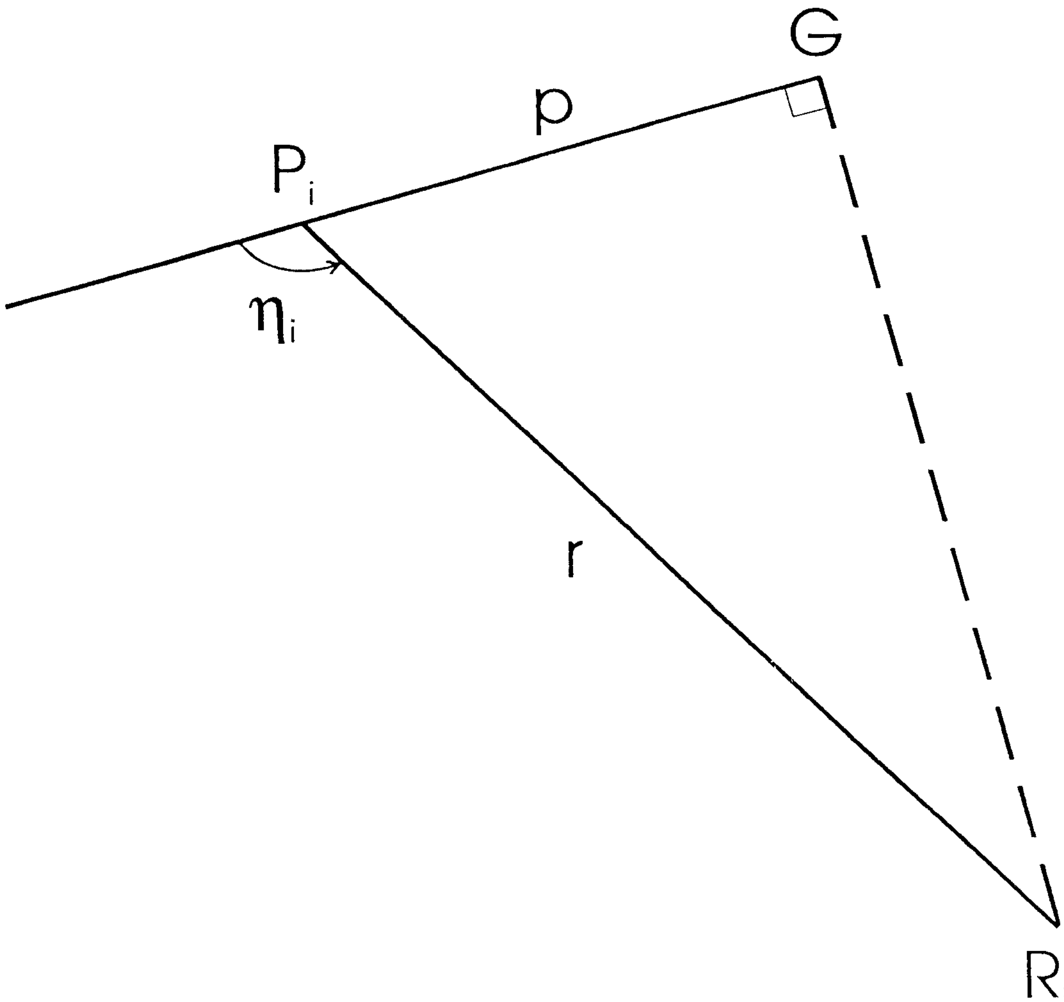

Figure G.1: Geometry of limb P_iR_i, if $\eta_i = \cos^{-1}(-p/r)$.

the W axis) and a vector parallel to $\overline{P_2G}$. Recall from Chapter 3 that $\left|\overline{GP_i}\right| = p$. Thus,

$$\overline{R_2P_2} = (rc_2)\frac{\overline{P_2G}}{p} + (rs_2)\,\bar{n}_w \tag{G.22}$$

Referring to Figure 3.1, we can see that vector $\overline{P_2G}$ can be resolved into a vector parallel to $\bar{n}_u$ (a unit vector parallel to the U axis) and a vector parallel to $\bar{n}_v$ (a unit vector parallel to the V axis). In other words

$$\overline{P_2G} = \left(\frac{\sqrt{3}}{2}\bar{n}_u + \frac{1}{2}\bar{n}_v\right)p \tag{G.23}$$

In addition, Figure 3.1 shows that

$$\overline{GP_1} = p\bar{n}_v \tag{G.24}$$

We can also write

$$\overline{R_2P_1} = \overline{R_2P_2} + \overline{P_2G} + \overline{GP_1} \tag{G.25}$$

Substituting equations (G.22), (G.23), and (G.24) into equation (G.25), and simplifying, we get

$$\overline{R_2P_1} = \frac{\sqrt{3}}{2}(rc_2 + p)\,\bar{n}_u + \frac{1}{2}(rc_2 + 3p)\,\bar{n}_v + rs_2\bar{n}_w \tag{G.26}$$

Equation (8.1) shows that $\overline{\mu_1}$ lies in the plane passing through points G, P_1, and R_1. As shown in Figure G.2, we let $\overline{\mu_1}$ pass through point P_1. Figure 3.1 shows that vector $\bar{n}_u$ is parallel to vector $\overline{\Gamma_1}$. This means that $\overline{\mu_1} \perp \bar{n}_u$. Also $|\overline{\mu_1}| = r$. Therefore, using equation (G.26), we can write

$$\overline{R_2P_1}\cdot\overline{\mu_1} = -\frac{1}{2}(rc_2 + 3p)\,rs_1 - (rs_2)rc_1 \tag{G.27}$$

further simplification results in

$$\overline{R_2P_1}\cdot\overline{\mu_1} = -\frac{r}{2}(2rc_1s_2 + rc_2s_1 + 3ps_1) \tag{G.28}$$

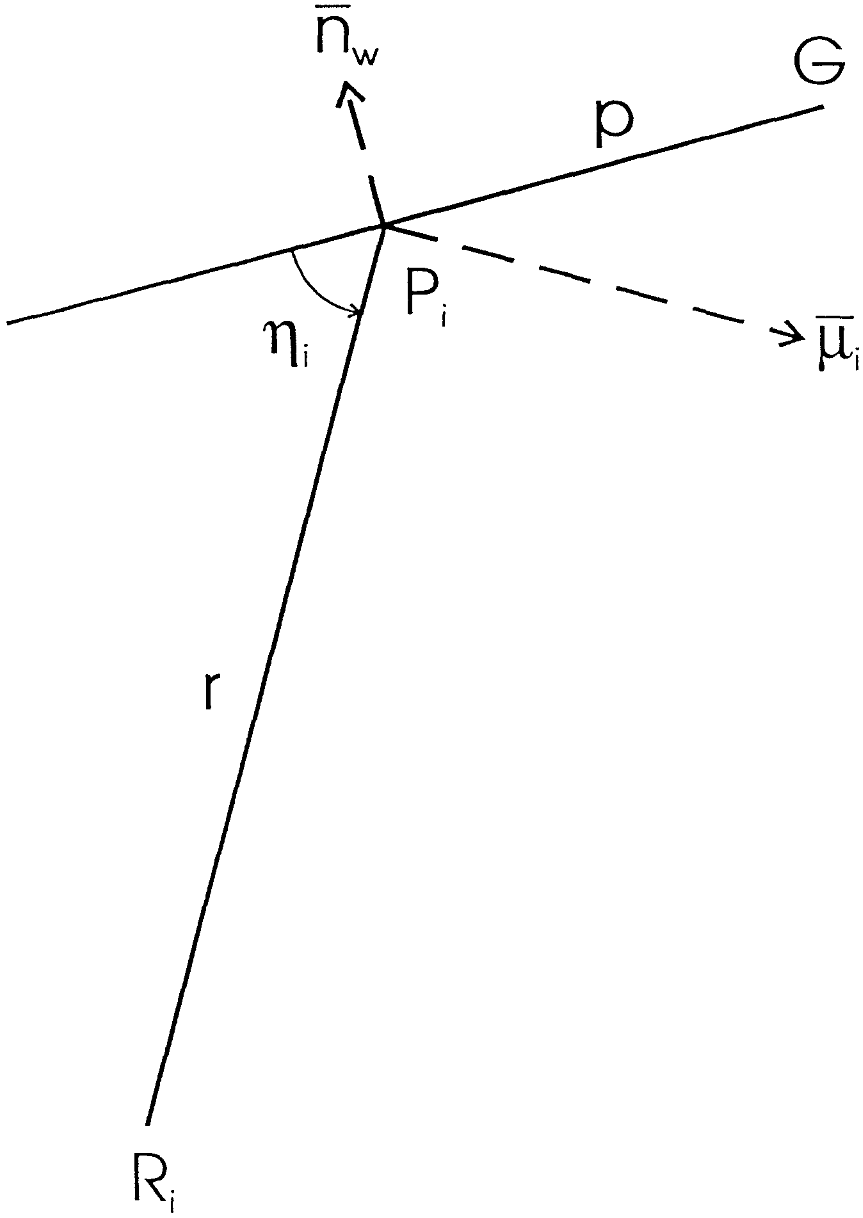

Figure G.2: Depiction of vectors $\overline{\mu_i}$ and $\bar{n}_w$.

If equation (8.36) is satisfied, then equation (G.28) reduces to

$$\overline{R_2P_1} \cdot \overline{\mu_1} = 0 \tag{G.29}$$

Equation (G.29) means that $\overline{R_2P_1}$ is perpendicular to $\overline{\mu_1}$. Vectors $\overline{\Gamma_1}$ and $\overline{P_1R_1}$ are also perpendicular to $\overline{\mu_1}$. Therefore, $\overline{R_2P_1}$ has to be parallel to the plane formed by $\overline{\Gamma_1}$ and $\overline{P_1R_1}$. This is possible only if point P_1 and vector $\overline{\Gamma_1}$ lie in the base plane. As a result, $Z_{P,1} = 0$, $\mu_{1,x} = \mu_{1,y} = 0$, and $\overline{P_2P_3}$ is parallel to the base plane (or $Z_{P,2} = Z_{P,3}$).